

2009

## Embryonic and Postnatal Development of the Neural Circuitry Involved in Motor Control

Valerie Cari Ann Siembab  
*Wright State University*

Follow this and additional works at: [https://corescholar.libraries.wright.edu/etd\\_all](https://corescholar.libraries.wright.edu/etd_all)



Part of the [Biomedical Engineering and Bioengineering Commons](#)

---

### Repository Citation

Siembab, Valerie Cari Ann, "Embryonic and Postnatal Development of the Neural Circuitry Involved in Motor Control" (2009). *Browse all Theses and Dissertations*. 944.  
[https://corescholar.libraries.wright.edu/etd\\_all/944](https://corescholar.libraries.wright.edu/etd_all/944)

This Dissertation is brought to you for free and open access by the Theses and Dissertations at CORE Scholar. It has been accepted for inclusion in Browse all Theses and Dissertations by an authorized administrator of CORE Scholar. For more information, please contact [library-corescholar@wright.edu](mailto:library-corescholar@wright.edu).

EMBRYONIC AND POSTNATAL DEVELOPMENT OF THE NEURAL  
CIRCUITRY INVOLVED IN MOTOR CONTROL

A dissertation submitted in partial fulfillment of the  
requirements for the degree of  
Doctor of Philosophy (Biomedical Sciences)

By

VALERIE CARI ANN SIEMBAB-NEFF  
B.S., Wright State University, 2003



2009  
Wright State University

WRIGHT STATE UNIVERSITY  
SCHOOL OF GRADUATE STUDIES

June 12 2009

I HEREBY RECOMMEND THAT THE DISSERTATION PREPARED UNDER MY SUPERVISION BY VALERIE CARI ANN SIEMBAB-NEFF ENTITLED EMBRYONIC AND POSTNATAL DEVELOPMENT OF THE NEURAL CIRCUITRY INVOLVED IN MOTOR CONTROL BE ACCEPTED IN PARTIAL FULFILLMENT OF THE REQUIREMENTS FOR THE DEGREE OF DOCTOR OF PHILOSOPHY.

---

Francisco Alvarez, Ph.D.  
Dissertation Director

---

Gerald Alter, Ph.D.  
Director, Biomedical Sciences Ph.D. Program

---

Joseph F. Thomas, Jr., Ph.D.  
Dean, School of Graduate Studies

Signatures of Committee  
on Final Examination

---

Francisco J. Alvarez, Ph.D.

---

Steven J. Berberich, Ph.D.

---

Timothy C. Cope, Ph.D.

---

David Ladle, Ph.D.

---

Robert W. Putnam, Ph.D.

## ABSTRACT

Siembab-Neff, Valerie Cari Ann. Ph.D., Biomedical Sciences Program, Wright State University, 2009. Embryonic and Postnatal Development of the Neural Circuitry Involved in Motor Control.

The development of locomotion is believed to result from the maturation of the spinal circuits controlling motor output, however little is known about its mechanisms. To shed some light into this process we studied the development of the synaptic connectivity of two spinal inhibitory interneurons. Adult motoneurons are controlled by inhibitory networks that include recurrent and reciprocal inhibition (Pierrot-Deseilligny & Burke, 2005). Each is modulated by different ventral horn spinal interneurons that display synaptic connectivity adapted to their function: Renshaw cells (RCs) mediate recurrent inhibition, receive excitatory inputs from motor axons and inhibit homonymous and synergistic motoneurons; while Ia inhibitory interneurons (IaINs) mediate reciprocal inhibition, receive inputs from Ia proprioceptive afferents and inhibit antagonist motor pools.

RCs and IaINs both derive from a homogenous class of embryonic ventral interneurons denominated “V1”, leading us to question whether motor axons and Ia afferents target V1 interneurons during early development, followed by postnatal de-selection of specific inputs and generation of cells with typical RC/IaIN connectivity.



Using immunohistochemistry, confocal microscopy, 3D neuronal reconstructions and transgenic animal models expressing V1-IN lineage markers, we analyzed synaptic input development on V1-derived RCs and IaINs. We found that motor axons specifically target RCs, are established in early embryo and maintained throughout development. In contrast, Ia afferents contact both IaINs and RCs in late embryo and throughout postnatal development. Ia afferent synapses are de-selected from RCs coinciding with maturation of weight-bearing locomotion. However, Ia afferent inputs on IaINs always occurred at a higher density and were more proximally located than on RCs, suggesting a stronger bias for IaINs. We concluded that there are fundamental differences between IaINs and RCs in their competence for receiving and maintaining motor and Ia afferent inputs. Finally, we investigated the possible role of “transient” Ia afferent inputs on RCs by studying RC connectivity in three genetic animal models that lack Ia afferents, or have weakened/strengthened Ia afferent inputs. We found interactions between Ia afferent strength and motor axon input density on RCs, but not with other excitatory inputs, suggesting that early Ia afferent inputs contribute to shape the organization of motor synapses on RCs.

# TABLE OF CONTENTS

	PAGE
ABSTRACT.....	iii
TABLE OF CONTENTS.....	v
LIST OF FIGURES.....	vii
LIST OF TABLES.....	xi
ACKNOWLEDGEMENTS.....	xii
DEDICATION.....	xiii
I. INTRODUCTION.....	1
II. LITERATURE REVIEW.....	4
Spinal Cord Development.....	5
Renshaw Cells and Ia Inhibitory Interneurons.....	15
Synaptogenesis and Maturation of Synaptic Connections.....	27
III. HYPOTHESIS & SPECIFIC AIMS.....	45
IV. GENERAL METHODS.....	49
Identification of V1-Derived Interneurons Using Lineage Markers.....	50
Histochemical identification of Renshaw Cells.....	53
Histochemical identification of Ia Inhibitory Interneurons.....	53
Identification of Primary Afferent Inputs.....	54
Identification of Motor Axon Inputs.....	55
Mouse Models Exhibiting Alterations of Primary Afferent Inputs into the Ventral Horn.....	57
Animals.....	58
Genotyping.....	59
Timed Pregnancies.....	61
Tissue Preparation.....	61

TABLE OF CONTENTS (CONTINUED)

	PAGE
Dorsal Root and Ventral Root Tracings in Embryonic and Neonatal Mouse Spinal Cords.....	63
Light Microscopy.....	68
Multiple Immunofluorescence.....	68
Dual Chromogen Immunofluorescence.....	70
Tyramide Signal Amplification in Embryonic Tissues.....	71
Imaging, Analysis and Statistics.....	77
3D Reconstructions of Calbindin-IR Renshaw Cells to Estimate Synaptic Densities of VGLUT1-IR and VAcHt-IR Contacts.....	78
Analysis of Synaptic Densities of VGLUT1-IR and VAcHt-IR Contacts On Distal Dendrites of Calbindin-IR Renshaw Cells in NeuroLucida.....	79
V. CHARACTERIZATION OF THE DEVELOPMENT OF THE PRIMARY AFFERENT INPUTS AND MOTOR AXON INPUTS ON RENSHAW CELLS IN THE EMBRYONIC AND POSTNATAL SPINAL CORD.....	81
VI. CHARACTERIZATION OF THE EMBRYONIC DEVELOPMENT OF THE RECURRENT INHIBITORY CIRCUIT.....	136
VII. CHARACTERIZATION OF THE DEVELOPMENT OF THE GLUTAMATERGIC PRIMARY AFFERENTS ON IA INHIBITORY INTERNEURONS IN THE POSTNATAL SPINAL CORD.....	163
VIII. ROLE OF PRIMARY AFFERENTS IN THE SPECIFICATION OF EXCITATORY SYNAPTIC INPUTS ON MATURE RENSHAW CELLS.....	208
IX. CONCLUSIONS.....	254
X. BIBLIOGRAPHY.....	257

## LIST OF FIGURES

		PAGE
FIGURE 1.	Schematic depicting the anatomy of the embryonic neural tube and the derivation of ventral spinal interneurons and motoneurons.....	9
FIGURE 2.	Schematic depicting Renshaw cell-mediated recurrent inhibition of soleus motoneurons.....	18
FIGURE 3.	Schematic depicting Ia inhibitory interneuron-mediated disinaptic reciprocal inhibition from ankle flexors to soleus.....	24
FIGURE 4.	Diversification of V1-derived interneurons from a single class of progenitors.....	44
FIGURE 5.	Conditional cre/loxP recombination system used to label V1-derived interneurons in the postnatal spinal cord.....	52
FIGURE 6.	Method utilized for cutting embryonic tissue.....	65
FIGURE 7.	Schematic depicting the tracing of sensory afferents and motor axon recurrent collaterals in the spinal cord using fluorescent dextrans.....	67
FIGURE 8.	Indirect tyramide signal amplification method.....	74
FIGURE 9.	Direct tyramide signal amplification method.....	76
FIGURE 10.	Sensory and motor axon inputs on embryonic and postnatal Renshaw cells.....	92
FIGURE 11.	Expression of Parvalbumin in the embryonic and postnatal spinal cord.....	94
FIGURE 12.	Changes in VGLUT1-IR contact density on Renshaw cells in <i>Er81</i> <sup>(-/-)</sup> knockouts.....	98
FIGURE 13.	VGLUT1-immunoreactive cluster sizes in mouse and rat during postnatal development.....	100
FIGURE 14.	Convergence of sensory and motor axon inputs on Renshaw cells in the postnatal spinal cord.....	102

LIST OF FIGURES (CONTINUED)

		PAGE
FIGURE 15.	Density of VGLUT1-IR contacts on adult cat, rat and mouse Renshaw cells.....	107
FIGURE 16.	Development of VGLUT1-IR contacts on postnatal Renshaw cells.....	110
FIGURE 17.	Density of VGLUT1-IR contacts on Renshaw cells compared to VAcHT-IR contacts.....	114
FIGURE 18.	Brightfield preparations and NeuroLucida 3D reconstructions used To analyze VGLUT1-IR and VAcHT-IR contact density on Renshaw cell distal dendritic segments.....	118
FIGURE 19.	Density and distribution of VGLUT1-IR and VAcHT-IR contacts on mature Renshaw cells.....	120
FIGURE 20.	Summary of electron microscopy data of VGLUT1-IR bouton sizes and the postsynaptic densities apposing those boutons on Calbindin-IR and non-Calbindin-IR dendrites at P15 and in the adult.....	130
FIGURE 21.	Schematic depicting developmental changes in the strength of sensory afferent (Ia afferents) and motor axon inputs on Renshaw cells.....	135
FIGURE 22.	Calbindin-IR cells in relation to EGFP+ motoneurons in the embryonic spinal cord.....	144
FIGURE 23.	Distribution of EGFP+ motor axon recurrent collaterals in the spinal cord at different embryonic ages.....	147
FIGURE 24.	VAcHT-immunoreactivity in the ventral horn during embryonic development.....	150
FIGURE 25.	Calbindin-IR in lamina IX of the spinal cord at different embryonic ages.....	153
FIGURE 26.	Synaptophysin-immunoreactivity in the embryonic spinal cord.....	155
FIGURE 27.	Synaptophysin-IR inputs on motoneurons during late embryonic development.....	157

LIST OF FIGURES (CONTINUED)

	PAGE
FIGURE 28. Distribution and labeling pattern of V1-derived neurons in <i>En1-Cre/R26-lacZ</i> , <i>En1-Cre/Tau-lacZ</i> and <i>En1-Cre/Thy1-YFP</i> P40 mice.....	173
FIGURE 29. Histochemical identification of V1-Ia inhibitory interneurons in <i>En1-Cre/Thy1-YFP</i> mice.....	177
FIGURE 30. Lineage of Parvalbumin-IR Ia inhibitory interneurons.....	179
FIGURE 31. Origin of proprioceptive sensory afferents on V1-derived Ia inhibitory interneurons and V1-derived Renshaw cells in <i>En1-Cre/Thy1-YFP</i> mice.....	183
FIGURE 32. Development of VGLUT1-IR contacts on V1-derived Ia inhibitory interneurons and Renshaw cells in postnatal <i>En1-Cre/Thy1-YFP</i> mice.....	187
FIGURE 33. Density and distribution of VGLUT1-IR contacts on V1-derived Ia inhibitory interneurons compared to Renshaw cells.....	189
FIGURE 34. Development of VAcHT-IR contacts on V1-derived Ia inhibitory interneurons and Renshaw cells in postnatal <i>En1-Cre/Thy1-YFP</i> mice.....	193
FIGURE 35. Density and distribution of VAcHT-IR contacts on V1-derived Ia inhibitory interneurons compared to Renshaw cells.....	195
FIGURE 36. Origin of VAcHT-IR boutons on V1-derived Ia inhibitory interneurons compared to Renshaw cells.....	197
FIGURE 37. Mouse models exhibiting alterations in primary afferent inputs into the ventral horn.....	212
FIGURE 38. VGLUT1-immunoreactivity in the ventral horn of wild-type, <i>EGR3<sup>(-/-)</sup></i> , <i>mlcNT3<sup>(+/-)</sup></i> and <i>Er81<sup>(-/-)</sup></i> mice at P15, P20 and in the adult.....	222
FIGURE 39. Density of VGLUT1-IR contacts on Renshaw cells in the ventral horn of control, <i>EGR3<sup>(-/-)</sup></i> and <i>mlcNT3<sup>(+/-)</sup></i> P20 mice.....	224
FIGURE 40. Density of VGLUT1-IR contacts on mature Renshaw cells in <i>EGR3<sup>(-/-)</sup></i> and <i>mlcNT3<sup>(+/-)</sup></i> mice compared to wild-type controls.....	226

LIST OF FIGURES (CONTINUED)

	PAGE
FIGURE 41. VAcHT-immunoreactivity in the ventral horn of wild-type, <i>EGR3</i> <sup>(-/-)</sup> , <i>mlcNT3</i> <sup>(+/-)</sup> and <i>Er81</i> <sup>(-/-)</sup> mice at P15, P20 and in the adult.....	231
FIGURE 42. Density of VAcHT-IR contacts on Renshaw cells in the ventral horn of control, <i>Er81</i> <sup>(-/-)</sup> , <i>EGR3</i> <sup>(-/-)</sup> and <i>mlcNT3</i> <sup>(+/-)</sup> P20 mice.....	233
FIGURE 43. VAcHT-IR contacts per 10 μm of linear dendrite of Calbindin-IR Renshaw cells in control, <i>Er81</i> <sup>(-/-)</sup> , <i>EGR3</i> <sup>(-/-)</sup> and <i>mlcNT3</i> <sup>(+/-)</sup> mice of P15, P20 and adult postnatal ages.....	235
FIGURE 44. Density of VGLUT2-IR contacts in wild-type, <i>Er81</i> <sup>(-/-)</sup> , <i>EGR3</i> <sup>(-/-)</sup> and <i>mlcNT3</i> <sup>(+/-)</sup> mice at P20.....	240
FIGURE 45. Model of homeostatic plasticity mechanisms in a mature cell.....	244
FIGURE 46. Schematic depicting a Hebbian plasticity mechanism upon complete removal of one excitatory input.....	247
FIGURE 47. Molecular hypothesis of activity-independent input selection on mature Renshaw cells in <i>Er81</i> <sup>(-/-)</sup> , <i>EGR3</i> <sup>(-/-)</sup> and <i>mlcNT3</i> <sup>(+/-)</sup> mice.....	250

LIST OF TABLES

		PAGE
TABLE 1.	Primer sequences used for polymerase chain reaction (PCR) genotyping and expected PCR size product.....	60
TABLE 2.	Primary antibodies and their sources, species raised against and dilutions.....	69
TABLE 3.	Percentage of Calbindin-IR Renshaw cells contacted by different markers of sensory afferents and motor axon recurrent collaterals in mouse versus rat.....	105
TABLE 4.	Number and density (contacts per 100 $\mu\text{m}^2$ ) of VGLUT1-IR and VAcHT-IR contacts on Calbindin-IR rat Renshaw cells during postnatal development.....	115
TABLE 5.	VGLUT1-IR bouton contact density and dendritic arbors of Renshaw cells of different ages.....	121
TABLE 6.	VAcHT-IR bouton contact density and dendritic arbors of Renshaw cells of different ages.....	122
TABLE 7.	Density of VGLUT1-IR and VAcHT-IR contacts per 10 $\mu\text{m}$ of linear dendrite of Ia inhibitory interneurons and Renshaw cells during postnatal development.....	198
TABLE 8.	Density and number of VGLUT1-IR and VAcHT-IR contacts on the somata of Ia inhibitory interneurons compared to Renshaw cells at P15 and in the adult.....	199
TABLE 9.	VGLUT1-IR contact density of Renshaw cells from P15, P20 and adult wild-type, <i>Er81</i> <sup>(-/-)</sup> , <i>EGR3</i> <sup>(-/-)</sup> and <i>mlcNT3</i> <sup>(+/-)</sup> mice.....	228
TABLE 10.	VAcHT-IR contact density of Renshaw cells from P15, P20 and adult wild-type, <i>Er81</i> <sup>(-/-)</sup> , <i>EGR3</i> <sup>(-/-)</sup> and <i>mlcNT3</i> <sup>(+/-)</sup> mice.....	238



## ACKNOWLEDGEMENTS

I would like to first thank my family and friends for all their encouragement and support, without them none of this would have been possible. I would especially like to thank my mom, Deborah Snider-Siembab for her never-ending support and for showing me that if you put your mind to it you really can accomplish anything. I would also like to thank my husband, Bob, as well as my kids, Kaitlyn and Tommy, for all their love and support. No matter what kind of day I had, it was nice knowing I had such a loving family to come home to. Next, I would like to thank Wright State University and more specifically the Biomedical Sciences Ph.D. Program for giving me the opportunity to turn a love of science into a career. I would also like to thank all lab members, both past and present, in the Alvarez and Fyffe labs for all your help and for keeping things interesting, boredom was not an option in the Alvarez/Fyffe labs. Also, thank you to all my committee members for providing me with constructive criticism, all of your suggestions were extremely helpful in shaping my project. Finally, I would like to thank my advisor Dr. Francisco Alvarez, words cannot describe how truly grateful I am for everything you have done for me throughout the years. Dr. Alvarez's enthusiasm for science is addicting to say the least. Furthermore, he always encouraged me to mold my project into what I wanted it to be and to not back down no matter what everyone else said. Dr. Alvarez is an amazing scientist who never ceases to amaze me; he is an incredible husband and father who showed me that it is possible to balance a successful career with family. As I go forth in my career, I can only attempt to mentor others with the same eagerness and interest as Dr. Alvarez has shown me.

## DEDICATION

I would like to dedicate this thesis to my mom Deborah Kay Snider-Siembab and my sisters Michelle Hopkins and Stephannie Siembab, you were always there for me whether I was right or wrong and your faith in me made me what I am today. I would also like to dedicate this thesis to my husband Robert Neff and my beautiful children Kaitlyn Marie and Thomas James for your encouragement and endless love. Finally I dedicate this thesis to my sister Nikole Beth Siembab; although we never met I know that you would have been proud of your little sister.

**CHAPTER I**  
**INTRODUCTION**

Humans are born with a multitude of immature reflexes. One such example is the stepping reflex. When a neonate or young infant is held upright, and the soles of its feet are brought in contact with a surface, the legs will extend and begin to move in an alternating sequence, as if walking (Peiper, 1966; Thelen and Fisher, 1982). It is believed that these early stepping reflexes represent an early stage in the development of locomotion. Humans are born with immature spinal circuits and appear to go through a period of “motor-learning”. It is during this “motor-learning” period that spinal circuits and reflexes mature. Little is known about how these spinal circuits in newborns develop. Understanding how these spinal circuits are formed is important because dysfunction of these networks or their development could lead to motor abnormalities in neonates.

Past research has focused on the development and characteristics of spinal motoneurons, perhaps because they are typically more accessible (Frank and Wenner, 1993; Goda and Davis 2003; Jacob et al. 2001; Shirasaki and Pfaff 2002). However, very little is known about the development of the interneuronal circuits that shape motor output. One possible reason for the scarcity of knowledge is that the ventral horn interneuronal circuitry is extremely complex and still largely unknown. A recent major advance has been the identification of four subclasses of embryonic interneurons (V1, V2, V3, V0) in the ventral horn characterized by the expression of different combinations of transcription factors and distinct genetic backgrounds (Jessell, 2000; Goulding et al., 2002). Later studies suggested that two well-known adult interneurons, Renshaw cells (RCs) and Ia inhibitory interneurons (IaINs) develop specifically from one embryonic group, named V1, which derives from just one set of progenitors. Renshaw cells mediate

recurrent inhibition, receive excitatory inputs from motor axons and inhibit homonymous and synergistic motoneurons; while Ia inhibitory interneurons mediate reciprocal inhibition, receive inputs from Ia proprioceptive afferents and inhibit antagonist motor pools.

A general conclusion for this observation is that most ventral interneuronal circuits are probably derived from few “canonical” groups of interneurons of common genetic background. The mechanisms that diversify interneuronal subclasses from each of the original four embryonic cell types (earlier denominated as a “metatype”; Sapir et al., 2004) are unknown, but clearly are important to understand the development of spinal synaptic circuits.

The purpose of this thesis is to determine what is the process of selection and maturation of the synaptic connectivity on V1-derived RCs and IaINs and what possible mechanisms or influences might be driving it.

**CHAPTER II**  
**LITERATURE REVIEW**

## **I. SPINAL CORD DEVELOPMENT**

### **Anatomy of the embryonic spinal cord**

The spinal cord emerges from the caudal part of the neural tube. During early embryonic development, the neural tube is broader at the base and appears to be shaped like a pear (Figure 1A). It can be divided into two morphological components: the alar plate (dorsal plate) which gives rise to the dorsal horn and the basal plate which is the precursor of the ventral horn. The alar and basal plates are separated by a longitudinal groove called the sulcus limitans. The ventricular zone (VZ; also known as the neuroepithelial layer or progenitor area) is located around the central canal and contains progenitor cells. These are mitotic cells that generate postmitotic neurons through successive divisions. Differentiated neurons migrate from the VZ and into the mantle layer, which contains the developing alar and basal plates. The mantle layer is the precursor of the gray matter and contains differentiated cells that will give rise to all the neurons and glial cells of the spinal cord. The axons of differentiating neurons first project to the marginal layer, which will develop in the white matter tracts that will surround the inner gray matter. In addition there are two specialized regions of the dorsal and ventral midline of the neural tube. These areas are known as the roof plate and floor plate. The roof plate is dorsal to the central canal and the floor plate ventral. They contain specialized cells that release signaling molecules to pattern the progenitor area in different dorso-ventral bands. Each of these bands generates a different class of neuron.

## **Origination of ventral spinal cord neurons involved in locomotion**

Distinct neuronal subtypes are generated in the spinal cord and topologically positioned within the spinal cord. Location of neurons within the spinal cord is important because it is a clear reflection of their function in the adult. Neurons positioned in the dorsal horn (alar plate) are responsible for processing sensory input and those neurons that coordinate motor output are found in the ventral horn (basal plate). Each spinal interneuron at specific locations develops specific characteristics and synaptic inputs and outputs that define their role in spinal circuits. Until recently, little was known about how the identity and pattern of neuronal subtypes was defined. The diversity of neuronal subtypes appears to be generated by the response of neural progenitors to graded concentration of sonic hedgehog (Shh). Shh is released from the notochord (vertebral column primordia) and the floor plate (basal cells in the neural tube). A dorso-ventral gradient is then established (Briscoe and Ericson, 1999; Briscoe and Ericson, 2001; Briscoe et al., 2000) with high Shh ventrally and low Shh dorsally. In addition, the roof plate secretes BMP-4, which alters the neural progenitor's response to Shh, resulting in a dorsalizing effect on neural progenitors (Liem et al., 2000). The concentration of Shh divides the ventricular zone (VZ) into different progenitor domains; seven domains in the dorsal portion of the spinal cord (pd0-6) give rise to eight classes of dorsal horn interneurons (Zhuang and Sockanathan, 2006) while five ventral progenitor domains (p0-p3 and pMN) will give rise to four classes of ventral horn interneurons denominated "V0, V1, V2, and V3" and motoneurons (Briscoe et al., 2000). Induction of ventral neurons involved in motor circuits requires high concentrations of Shh (Ericson et al., 1997a,b). Spinal cord ventral neurons are born, or become postmitotic, between embryonic day 9.5

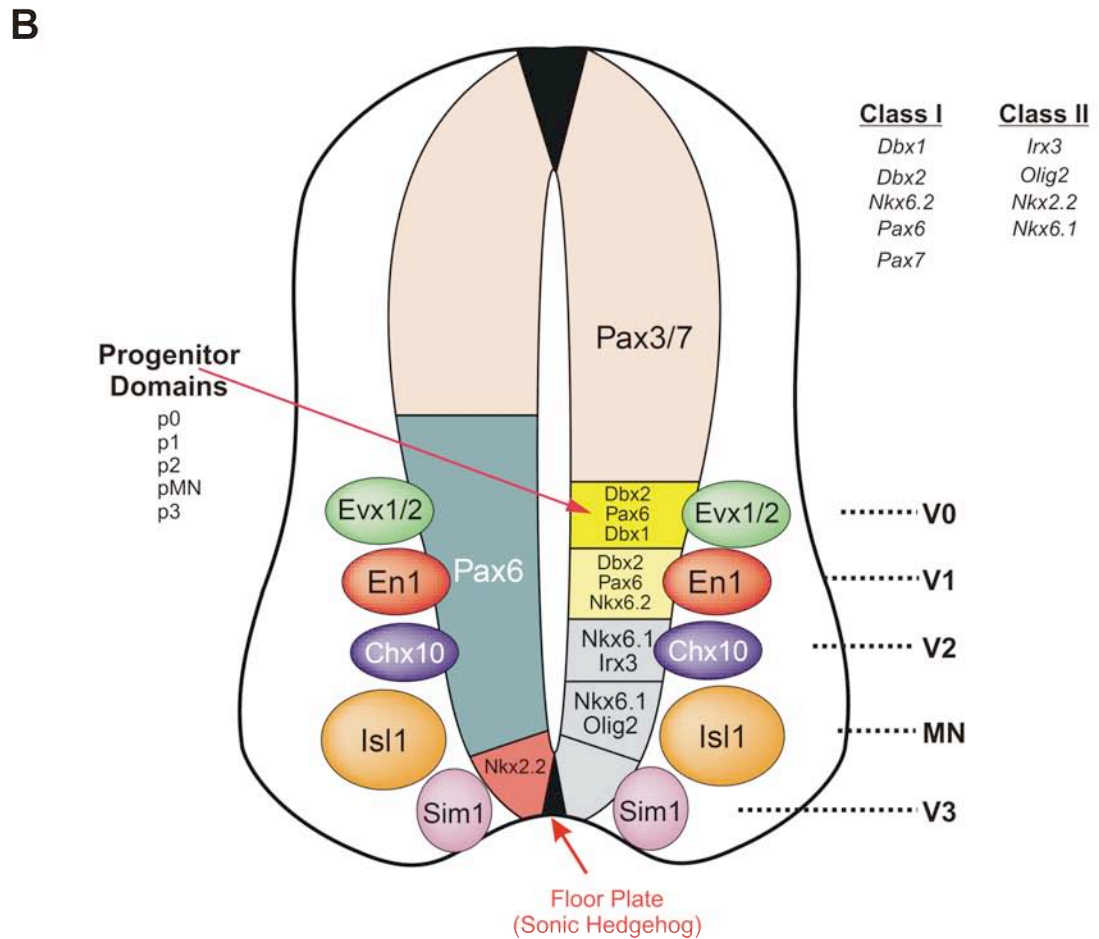
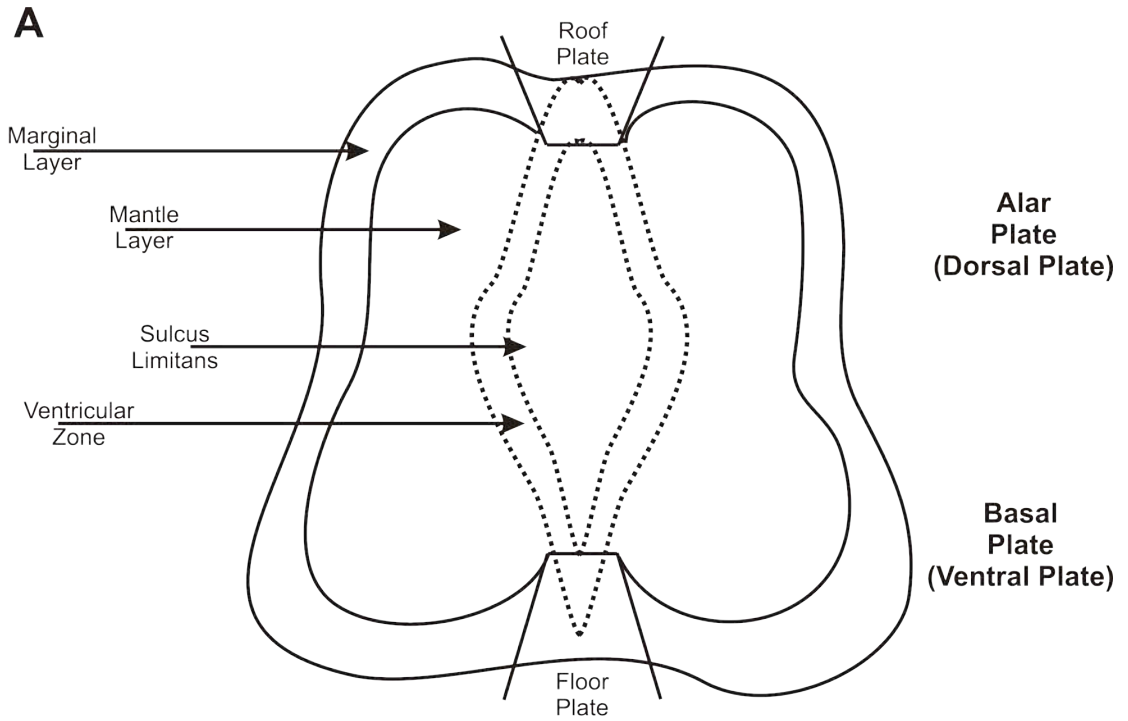


(E9.5) and E13.5 (Briscoe et al., 1999; Pierani et al., 1999; Sander et al., 2000; Moran-Rivard et al., 2001; Vallstedt et al., 2001; Smith et al., 2002; Peng et al., 2007).

Immediately after birth, spinal cord neurons migrate laterally to occupy their final anatomical positions. During migration, neurons will simultaneously begin sending out their axonal projections into specific trajectories (Saueressig et al., 1999).

How does a Shh concentration gradient cause neural progenitors to generate different neuronal subtypes at different dorso-ventral locations? Moreover, how do progenitors read and respond to differing Shh concentrations? Many believe that Shh concentration gradients control the specification of cells by establishing progenitor domains, which express distinct combinations of homeodomain transcription factors (see Figure 1B). Transcription factors expressed by ventral progenitors can be divided into Class I or Class II. Class I transcription factors such as *Dbx1* and *2*, *Nkx6.2*, and *Pax6* and *7* are repressed by Shh signaling. In contrast, Class II transcription factors like *Irx3*, *Olig2*, and *Nkx2.2* and *6.1*, are induced by Shh. The cross-repressive or inductive actions between these transcription factors create well-defined progenitor domain boundaries (Briscoe et al., 2000). The distinct transcription factor combinations are required for the generation of specific neuronal subtypes and for generating the correct number of neurons. For example, mutations of the Class II gene *Nkx6.1* results in V2 and motoneurons switching to a V1 fate (Sander et al., 2000). Similarly, deletion of the Class I gene, *Pax6* results in no V1-INs being generated (Ericson et al., 1997; Burrill et al., 1997).

**Figure 1.** Development of ventral spinal interneurons and motoneurons. **A,** Schematic depicting the anatomy of the embryonic neural tube. The neural tube is divided into the alar (dorsal) and basal (ventral) plates by the sulcus limitans. The dotted lines indicate the border of the ventricular zone (VZ) which contains the progenitor cells. Differentiating cells migrate out of the VZ into the mantle layer, which is the future gray matter. The marginal layer, which develops into the white matter, contains the axons of the differentiating neurons. The VZ is patterned by cells in the roof plate and the floor plate that release signaling molecules. The roof plate is found dorsal to the central canal and the floor plate is found ventral. **B,** Sonic hedgehog (Shh) is released from the floor plate and patterns the VZ into five ventral progenitor domains which give rise to 4 ventral interneuronal subtypes denominated “V0-V3” and also give rise to motoneurons (MNs). Each progenitor domain expresses different transcription factors (some of the transcription factors are shown here) that are repressed or induced by Shh signaling. Class I transcription factors are repressed by Shh signaling and Class II transcription factors are induced by Shh. Once a cell becomes postmitotic late transcription factors are expressed (ovals; again, only a few are shown here). Each ventral interneuron class is characterized by their genetic programs and axonal projections.



Each ventral progenitor domain gives rise to early classes of ventral interneurons characterized by specific genetic programs and axonal projections. Once a progenitor cell in a specific progenitor domain generates a postmitotic neuron it will begin expressing late transcription factors, which are believed to execute subtype-specific programs of differentiation (Figure 1B; Moran-Rivard et al., 2001). For example, *Evx1* is specifically expressed in V0 interneurons. *Evx1* mutants will generate V0 INs, which extend axons along the correct trajectory for contralateral projections to the other side of the spinal cord, but after some time these cells will begin expressing V1 markers and their axonal trajectory will change, mimicking the ipsilateral projections of V1-derived interneuron axons (Moran-Rivard et al., 2001). From these studies and those of Pierani and colleagues (2001) it was concluded that *Dbx1*, which is expressed by p0 progenitors, represses the V1 genetic program by upregulating *Evx1*. Similarly, V1-derived interneurons express *engrailed-1* (*En1*) and when it is knocked out, V1 interneurons display problems with axon pathfinding and fasciculation (Saueressig et al., 1999; discussed further in next section). In summary, the four original embryonic ventral interneuron cell types (V0-V3) give rise to a few “canonical” groups of interneurons of common genetic expression profiles that share several common features.

As mentioned previously, V0-derived interneurons express the late transcription factor *Evx1* (Pierani et al., 1999; Moran-Rivard et al., 2001; Pierani et al., 2001) and are comprised of both excitatory and inhibitory interneurons (Lanuza et al., 2004) that make contralateral projections that extend approximately one and a half segments. V1-derived interneurons (V1-INs) are ipsilaterally projecting interneurons which express *En1* postmitotically (discussed further in next section; Burrill et al., 1997; Saueressig et al.,

1999; Alvarez et al., 2005) and their projections ascend two segments at most (Sauressig et al., 1999). V2 interneurons (V2-INs) derive from a progenitor population which expresses Lhx3 (Peng et al., 2007), but are divided into excitatory and inhibitory populations. Excitatory V2-INs, denominated “V2a” express Chx10 (Hargrave et al., 2000) and inhibitory V2-INs, “V2b”, express Gata2/3 (Ericson et al., 1997b; Zhou et al., 2000; Karunaratne et al., 2002; Poh et al., 2002; Smith et al., 2002). Both V2a and V2b interneurons make ipsilateral projections that extend caudally (Lundfald et al., 2007; Sauressig et al., 1999; Lee and Pfaff, 2001). Very little research has been done on V3-derived interneurons (V3-INs), but it is known that V3-INs express the transcription factor Sim1 (Briscoe et al., 1999; Goulding et al., 2002) and are believed to be mainly excitatory interneurons that make contralateral projections (Zhang et al., 2008), although it is not known whether these projections are ascending or descending.

Recent genetic deletions of these different subclasses of ventral spinal interneurons have provided insights into their function. Lanuza and colleagues (2004) showed that V0-INs are important for left-right coordination, but not for flexor-extensor alternation. Using an *in vitro* spinal cord preparation they induced fictive locomotion with NMDA and 5-HT and recorded bursts of left L2 (lL2) and right L2 (rL2) ventral roots and found episodes of synchronous bursting between lL2 and rL2 ventral roots after genetic deletion or silencing of V0 interneurons. Similar results were observed between lL5 and rL5 ventral roots. They concluded that the loss of left-right coordination was due to a loss of V0 commissural interneurons which inhibit contralateral MNs. V1-INs appear to regulate the speed of motor output (Gosgnach et al., 2006). Using a similar *in vitro* spinal cord preparation as Lanuza, Gosgnach and colleagues studied the function of

V1-INs in *Pax6*<sup>(-/-)</sup> knockouts and in mice with selective ablation of V1-INs using *En1*<sup>Cre</sup>; *R26-lacZ*<sup>flox</sup>/*DTA* mice. They found that inducing fictive locomotion in both animals did not affect left-right coordination or flexor-extensor alternation, but the step cycle and burst duration was affected. Therefore, they concluded that V1-INs were essential for determining the speed of the locomotor rhythm. Genetic ablation of excitatory V2a-INs with *Chx10-DTA* mice demonstrated that V2a-INs, similar to V0-INs are important for left-right coordination (Crone et al., 2008). Zhang et al. (2008) assessed the function of V3-INs by blocking V3-IN neurotransmission in *Sim*<sup>Cre</sup>; *R26*<sup>floxstop-TeNT</sup> mice. They found that blocking V3-IN neurotransmission increased the variability in duration of motor bursts and the length of the step cycle. Also, these mice failed to generate normal locomotor-like oscillatory activity following either application of NMDA and 5-HT or stimulation of sensory afferents. Therefore, they concluded that V3-INs are important for stabilizing locomotor networks and maintaining rhythmicity. Although these results provide the first information on the functional roles of different classes of embryonic interneurons, these broad deletions do not capture the diversity of functional subtypes contained within each class. For that we need to understand the variety of interneuron subtypes that derive from each class and their mechanisms of differentiation. In this thesis I will examine the diversification of adult interneuron subtypes from the V1-IN class of embryonic ventral interneurons.

### **V1-derived interneurons**

Broad principles about the diversification of adult interneuronal subtypes from the five ventral interneuron classes come from studies of V1-INs. V1-derived interneurons

(V1-INs) are characterized by the expression of the *engrailed-1* transcription factor (Matisse and Joyner, 1997; Ericson et al., 1997; Sauressig et al., 1999) and derive from the ventral progenitor domain, p1, which expresses transcription factors, *Dbx2*, *Pax6*, and *Nkx6.2*. Deletion of *Nkx6.2* leads to the ventral expansion of the *Dbx1* domain (p0 progenitor domain), which leads to a loss of V1-INs and a corresponding increase in V0-derived interneurons (Vallstedt et al., 2001).

In the spinal cord, the expression of *En1* is dependent on the transcription factor *Pax6*. Deleting *Pax6* (*Small eye* mutant) results in a loss of *En1* expression in embryos (Burrill et al., 1997; Ericson et al., 1997) suggesting a loss of V1-INs without affecting V0 and motoneurons. In an elaborate set of experiments, Sauressig and colleagues (1999) identified *En1*+ cell projections using an *En1<sup>taulacZ</sup>* knock-in mouse model in which the axons originating from *En1*+ cells expressed  $\beta$ -galactosidase (Sauressig et al., 1999). They found that *En1*+ cells make ipsilateral projections to MNs. Furthermore, they showed that the ventral projection of these axons required *netrin-1*. The most interesting observation from this study was that *En1* expression does not specify cell fate, but that it is involved in regulating axonal pathfinding. Thus postnatal studies in the spinal cord show sparse connections of V1-INs with motoneurons in *En1* knockout animals (Sapir et al., 2004). In mice, *En1* expression is first observed at E9.5-10.5 in the area between the dorsal and ventral horns of the embryonic neural tube (Matisse and Joyner, 1997). Eventually, *En1*+ cells will migrate laterally and ventrally toward the area occupied by newly formed MNs. Meanwhile, as they migrate, their axons will project into the developing ventral and lateral funiculi and send collaterals that terminate on the MNs (Sauressig et al., 1999). Dextran retrograde tracings performed in E13 embryos

demonstrated that the V1-INs main axonal projection is ipsilateral and mainly ascending, but also with some descending collaterals (Sapir et al., 2004). In early embryos and postnatal spinal cord these cells express markers which suggest an inhibitory phenotype (Sapir et al., 2004; Alvarez et al., 2005). Therefore, *En1* expression defines a class of ipsilaterally projecting inhibitory spinal interneurons, which project to MNs (Saureissig et al., 1999; Sapir et al., 2004). They were denominated “V1” interneurons (Lee and Pfaff, 2001).

The purpose of this thesis is to gain insights into the process of differentiation of interneuron subclasses from these canonical embryonic ventral interneuron classes. Adult interneuron subtypes are defined by their synaptic inputs and outputs, which ultimately defines their function. We chose to focus on the V1-INs because recent studies in our lab suggested that two well-known adult inhibitory interneuron subtypes, Renshaw cells (RCs) and Ia inhibitory interneurons (IaINs) develop specifically from this class (Sapir et al., 2004; Alvarez et al., 2005). The generation of transgenic mice in Martyn Goulding’s lab (Salk Institute) in which the lineage of embryonic V1-INs can be genetically labeled (using the cre-lox system) in adult demonstrated that all RCs are V1-derived as well as IaINs (Alvarez et al., 2005) and that recurrent inhibition is absent in *Pax6* mutant mice (Sapir et al., 2004). Previous studies in the chick embryo by Wenner and colleagues (1999, 2000, 2001) showed that *En1* expressing interneurons are heterogeneous and contains a population that receives inputs from MNs and makes inhibitory projections onto MNs resembling mammalian RCs. This group of interneurons represents the avian equivalent of the mammalian RC and was denominated R-interneuron (R-IN; for recurrent inhibition). However it also displayed some



characteristics that resembled IaINs. Although the R-IN has been shown to mediate recurrent inhibition of MNs in the developing chick spinal cord, its location is similar to that of adult IaINs in the area dorsomedial to the motor pools. Similarly, R-INs receive monosynaptic inputs from muscle afferents.

*En1*-V1 interneurons are conserved through phylogeny. A class of *En1* expressing inhibitory interneurons, called circumferential ascending interneurons (CiA-INs) has recently been identified in zebrafish (Higashijima et al., 2004). Similar to mammalian V1s, CiA-INs are glycinergic and their axons project ipsilaterally to MNs. The same cell was also identified in the *Xenopus* tadpole and was shown to produce glycinergic inhibition of sensory inputs in the spinal cord (Li et al., 2002) and limits firing of MNs (Li et al., 2004). It is possible that, as chicks and mammals evolved from vertebrates with less complex locomotor programs, a wider array of interneurons with more restricted functional roles were necessary.

The strategies used during development of the mammalian spinal cord to diversify the V1 interneuron population into different functional subclasses are unknown.

## **II. RENSHAW CELLS AND IA INHIBITORY INTERNEURONS**

### **Renshaw Cells**

#### ***Physiology and Function***

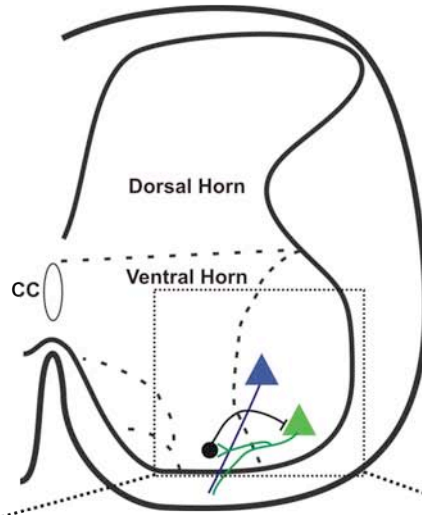
The Renshaw cell is one the most studied spinal interneurons and was the first functionally identified interneuron in the mammalian spinal cord. Birdsey Renshaw (1941) was the first to describe that antidromic volleys of motor axons in the cat decreased the excitability of motoneurons (MNs) that make projections to the same or

synergistic muscles. He called this phenomenon recurrent inhibition. Later Renshaw identified a set of spinal interneurons that fire high frequency discharges in response to a single antidromic volley in motor axons located on the same side of the spinal cord (Renshaw, 1946). Eccles and colleagues (1954) demonstrated that these spinal interneurons, which he would later denominate “Renshaw cells”, generated antidromic inhibitory postsynaptic potentials in MNs and are activated via the motor axon recurrent collaterals of MNs (Figure 2). Furthermore, they demonstrated that Renshaw cell (RC) activation via the motor axons was mediated by the neurotransmitter, acetylcholine (Eccles et al., 1954; Fyffe 1990). The addition of the glycinergic antagonist strychnine suggested that the IPSPs generated in MNs were mediated by glycine. Eccles postulated that RCs directly inhibited the same MNs they received synapses from, but it was not until almost 30 years later that van Keulen (1981) was able to record simultaneously from RCs and MNs, providing direct evidence of the connectivity between pairs of RCs and MNs. Morphological studies followed and demonstrated that most RC axon terminals were located throughout lamina IX (LIX; location of the MN pools; Lagerback and Kellerth; 1985) of the ventral horn and they contacted MN dendrites (Fyffe, 1991).

RCs will inhibit homonymous and synergistic MNs, but they also inhibit other RCs and IaINs. RCs respond to antidromic volleys in motor axons by firing high frequency discharges and this response is known as the RC early response. Curtis and Ryall (1966) found that there was a pause in RC firing following the early response. They concluded that this pause was due to desensitization of the postsynaptic membrane, but a few years later Ryall (1970) concluded that the pause was in fact the inhibition of the RCs by other RCs that were simultaneously activated by the antidromic volleys.

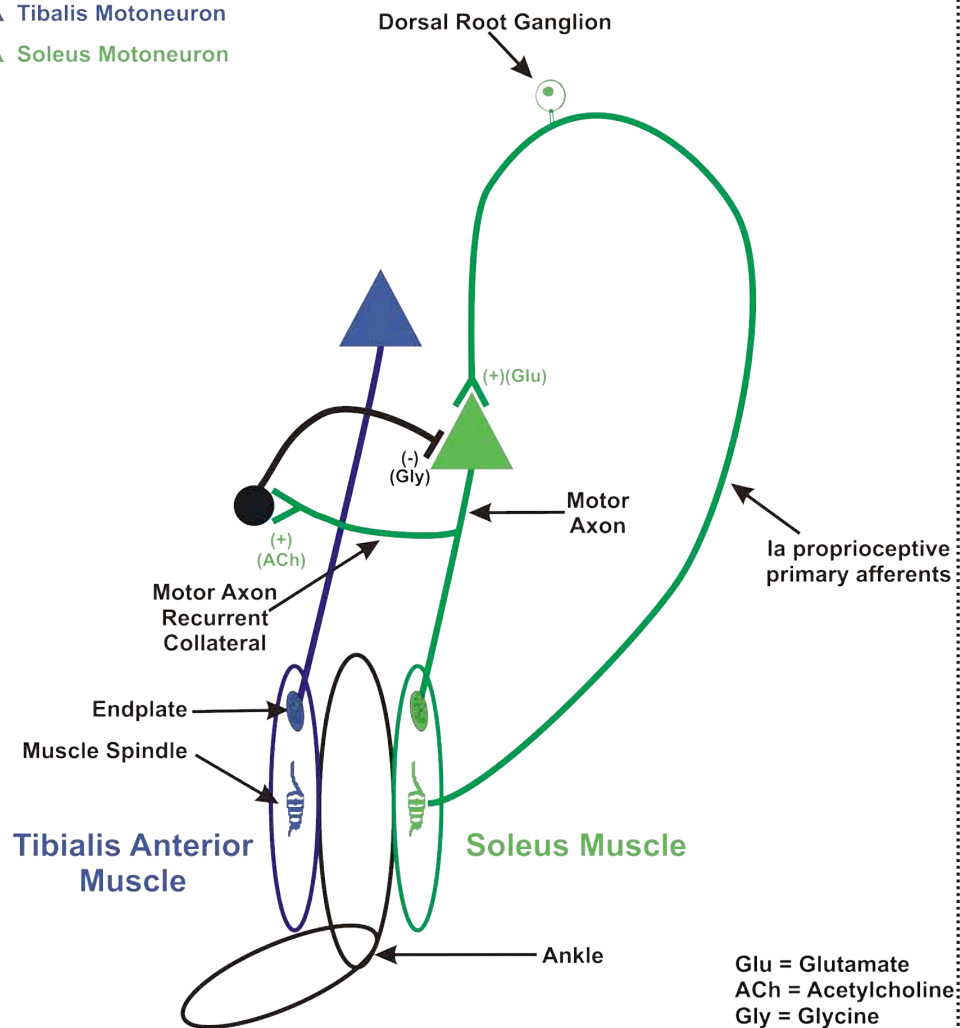
**Figure 2.** Recurrent inhibition of soleus motoneurons. **A,** Transverse hemisection of an adult spinal cord. The motoneurons (MNs) and interneurons we are interested in are located in the ventral horn of the lumbar segments of the spinal cord. The border between the dorsal and ventral horns is indicated by the dotted line above the central canal (CC). **B,** Schematic depicting the pathway of recurrent inhibition with projections of Renshaw cells to soleus MNs (S-MNs). When, in the case shown here, the soleus muscle is stretched; Ia afferents fire and excite the S-MNs. The S-MN axon recurrent collaterals project to Renshaw cells, which in turn, make glycinergic projections onto that same MN, ultimately inhibiting it. Renshaw cells also provide recurrent inhibition to Ia inhibitory interneurons (not shown here; discussed further in Figure 4). Ia afferents and motor axons use glutamate and acetylcholine, respectively, as their neurotransmitters.

A



B

- Renshaw Cell
- ▲ Tibialis Motoneuron
- ▲ Soleus Motoneuron



Following administration of DH $\beta$ E (dihydro-beta-erythroidine), which reduces significantly the early response of the RC population, they found that the pause in RC firing was attenuated, suggesting that RCs mutually inhibit other RCs. Ryall (1981) later demonstrated that RCs excited by motor axon recurrent collaterals of flexor or extensor MNs were inhibited by those RCs that are activated via motor axons of antagonist MNs. Besides mutual inhibition of other RCs, RCs also inhibit IaINs, which mediate reciprocal inhibition (Hultborn et al., 1971). Hultborn and colleagues (1971) found that the IPSPs evoked in MNs following stimulation of the nerves of the antagonist muscles were attenuated by antidromic volleys of motor axons. They concluded that the attenuation of the IPSPs were due to recurrent inhibition of IaINs. One of the characteristic features of classical IaIN identification is disynaptic recurrent inhibition via RCs from MNs that receive the same Ia excitation. Recurrent inhibition of IaINs plays an important role during regulations of co-contraction of antagonistic muscles. When co-contraction of pairs of antagonistic muscles is used to stabilize a joint (i.e., to maintain posture), recurrent inhibition will depress activation of IaIN-mediated reciprocal inhibition. Depression of reciprocal inhibition allows for the parallel activation of the two antagonistic muscles, increasing stiffness around the joint.

#### *Location, Anatomy and Morphological Identification*

Renshaw cells (RCs) are excited by motor axon recurrent collaterals and their location within the ventro-medial region of lamina VII (LVII; Thomas and Wilson, 1965) puts them near the area where motor axons exit the spinal cord. Intracellular labeling of RCs using Procion Yellow (Jankowska and Lindstrom, 1971) and horseradish peroxidase

(HRP; Lagerback and Kellerth, 1985a,b; Fyffe, 1991) confirmed that RCs were located in the ventral-most portion of LVII among the motor axons. This area was identified as the “Renshaw cell area”.

Adult cat RCs are multipolar or fusiform interneurons (Fyffe, 1990) with relatively small cell bodies (mean cell body diameter, 20-25  $\mu\text{m}$ ; Fyffe, 1990) and small dendritic arbors (dendritic lengths from soma to terminal ranges between 430 to 800  $\mu\text{m}$ ; Bui et al., 2003; Alvarez et al., 1997) and do not branch extensively. In monkeys, rat and humans, RCs are identified by their strong expression of the calcium binding proteins Calbindin (CB; Ardvisson et al., 1992; Carr et al., 1998; Fallah and Clowry, 1999; Alvarez et al., 1999; Geiman et al., 2000) and to a lesser extent, Parvalbumin and Calretinin (PV and CR; Alvarez et al., 2005). Cat RCs do not express CB (Carr et al., 1998), but are easily identified by their large Gephyrin-immunoreactive clusters (Alvarez et al., 1997). Gephyrin is a glycine receptor clustering protein (Kneussel and Betz 2000). In all mammalian species, RCs have large gephyrin-IR clusters that gradually increase in size with age after birth (Geiman et al., 2000).

### *Synaptic Inputs*

Central to interneuron identification and function is the organization of their synaptic inputs. RCs fire high frequency bursts of action potentials following stimulation of peripheral motor axons. Eccles demonstrated that this response was mediated by cholinergic motor axon recurrent collaterals (Eccles et al., 1954). As mentioned earlier, adult RCs are located in close proximity to emerging motor axons and this area contains a high density of cholinergic terminals and these terminals target RC dendrites (Alvarez et

al., 1999). RCs express the  $\alpha 2$  and  $\alpha 4$  nicotinic receptor subunits, which correlate to the RCs high sensitivity to acetylcholine (reviewed in Alvarez and Fyffe, 2007). Several studies have demonstrated that the EPSPs evoked in RCs following stimulation of the motor axons is not completely blocked by cholinergic antagonists (Eccles et al., 1954; Schneider and Fyffe, 1992; Dourado and Sargent, 2002). Mentis and colleagues (2005) recently demonstrated that some motor axon terminals on RCs activate, postsynaptically, AMPA and NMDA receptors. The physiological relevance of co-releasing excitatory amino acids and acetylcholine from motor axons terminals are still unknown, but they are actively being investigated by several different labs. Little information about the development of motor axon inputs on RCs is available. Two studies looked at the postnatal development of motor axons in the Renshaw cell area in newborn kittens (Cullheim and Ulfhake, 1982; Remahl et al., 1985). Both studies found that motor axons in newborn kittens make an excess of collaterals and synapses that were pruned during the first two postnatal weeks.

RCs receive other excitatory synaptic inputs from spinal interneurons and descending systems, but little is known about the role or development of these inputs. Synaptic inputs from spinal interneurons tend to occur at high densities, they probably facilitate descending influences on RCs via polysynaptic pathways. RCs receive few direct serotonergic, dopaminergic and noradrenergic descending inputs (reviewed in Alvarez and Fyffe, 2007). These inputs generally do not directly contact RCs and probably modulate RC activity via paracrine actions.

Inhibitory synapses are important for modulating excitatory inputs and ultimately shaping neuronal firing. RCs receive a large number of inhibitory inputs although the

source of these inputs still remains unknown. As mentioned above, RCs can be easily identified by their large gephyrin-IR clusters (Alvarez et al., 1997). RCs are unique in that gephyrin clusters are almost exclusively located on the soma and proximal dendrites (Alvarez et al., 1997; Geiman et al., 2000) and the glycinergic and GABAergic currents in RCs are much larger than those in other spinal interneurons (Gonzalez-Forero and Alvarez, 2005); suggesting inhibitory inputs in RCs can exert powerful shunting influences on excitatory potentials on dendrites.

## **Ia Inhibitory Interneurons**

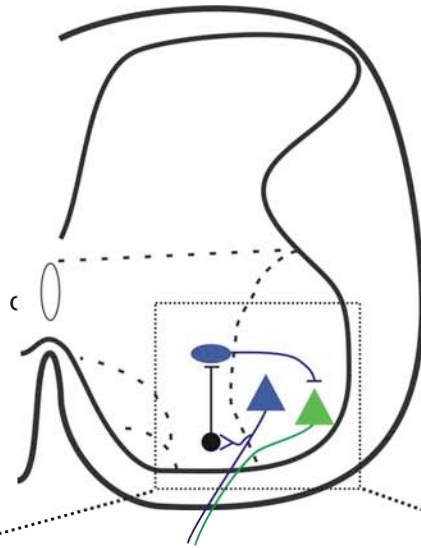
### *Physiology and Function*

Following contraction of an agonist muscle, the antagonist muscle will relax because it is inhibited from contracting (Sherrington, 1897). Inhibition of the antagonist muscle contracting is referred to as reciprocal inhibition (Figure 3). Lloyd (1941) postulated that reciprocal inhibition was mediated by Ia afferents directly effecting MNs. A few years later, Eccles and colleagues demonstrated that an interneuron must be interpolated in the reciprocal inhibitory pathway (Eccles et al., 1956). They found that when recording intracellularly from MNs, Ia afferent volleys produced an IPSP that had a longer latency than the EPSP, suggesting that Ia afferent volleys excite an intermediate interneuron, which in turn will inhibit the MNs innervating the antagonist muscle. Furthermore, Eccles and colleagues showed that the activity of this pathway inhibited the monosynaptic stretch reflex (Araki et al., 1960). This interneuron was called Ia intermediate interneuron, which eventually morphed into the now current name of Ia

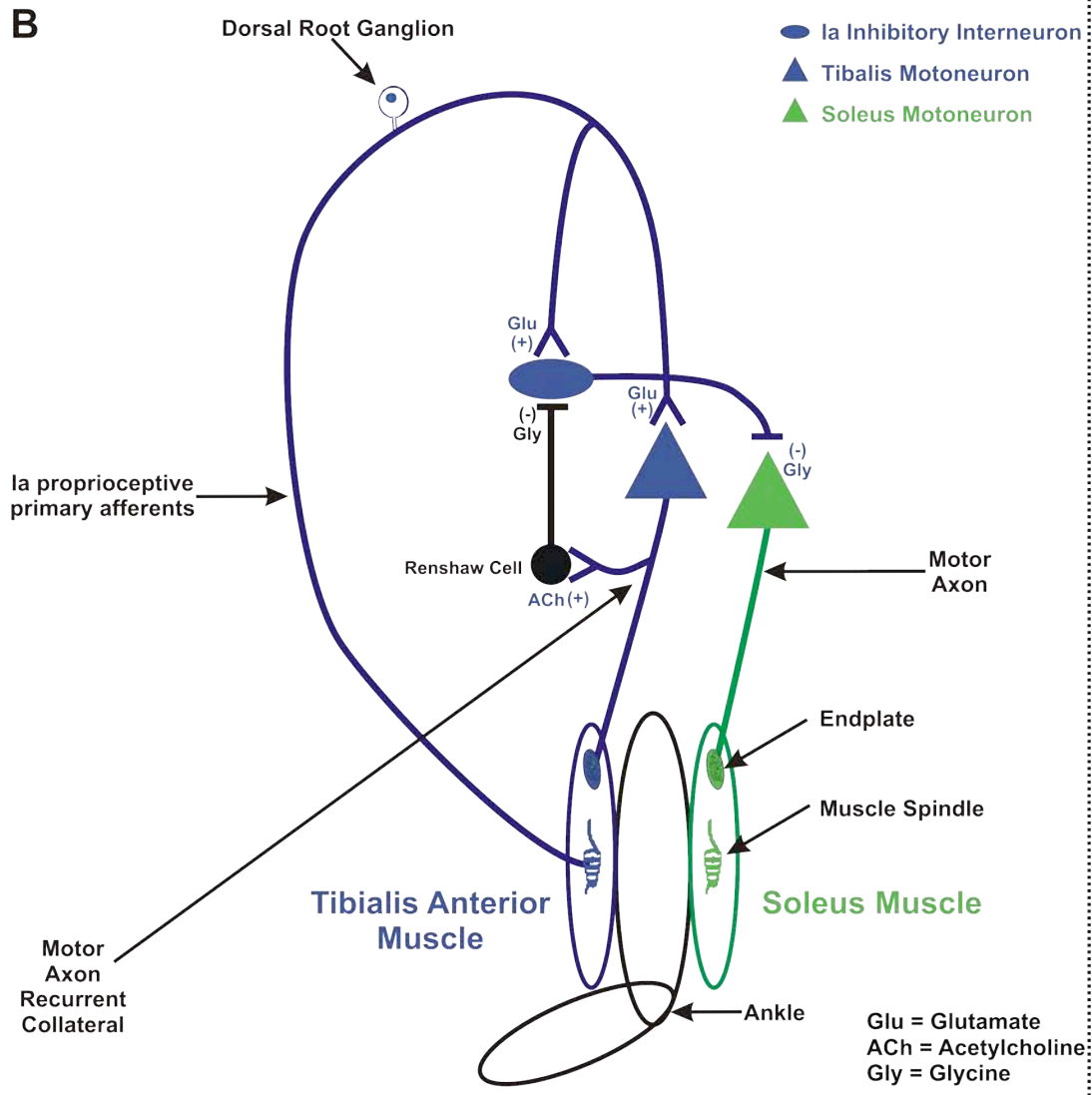


**Figure 3.** Reciprocal inhibition from ankle flexors to soleus. **A,** Transverse hemisection of an adult spinal cord. The motoneurons and interneurons involved in reciprocal inhibition that we are interested in studying in this thesis are located in the ventral horn of the spinal cord. Here the border between the ventral and dorsal horns is delineated by the dotted line above the central canal (CC). **B,** Schematic depicting the pathway of disynaptic reciprocal inhibition from tibialis anterior to soleus muscle. Ia inhibitory interneurons (IaINs) and tibialis anterior MNs (TA-MNs) receive monosynaptic inputs from Ia afferents that originate in muscle spindles in the tibialis anterior muscle (TA). When the TA is stretched, the Ia afferents will excite TA-MNs and IaINs (plus signs). Those IaINs will then make glycinergic projections to soleus MNs (S-MNs) inhibiting those MNs. This inhibition results in the soleus muscle relaxing. IaINs also receive recurrent inhibition from Renshaw cells coupled to S-MNs, depressing reciprocal inhibition on S-MNs. Ia afferents use glutamate as their neurotransmitter, while IaINs use glycine. Motor axon collaterals use acetylcholine.

A



B



inhibitory interneuron. Currently, other spinal interneuronal targets of IaINs are not known, but it has been shown that IaINs do inhibit other IaINs (Hultborn et al., 1976). Those IaINs activated by Ia afferents from one muscle inhibit IaINs activity on motor pools of the same muscle and their synergists. IaIN identification depends on three characteristics: 1) Monosynaptic activation via Ia afferents (Hultborn et al., 1970), 2) Projections to MNs innervating the antagonist muscle (Jankowska and Roberts 1971a,b) and 3) RC-mediated recurrent inhibition from the MNs that receive the same Ia excitation (Hultborn et al., 1971; Ryall 1970, 1981).

#### *Location, Anatomy and Morphological Identification*

Eccles proposed that reciprocal inhibition of MNs evoked from Ia afferents innervating antagonist muscles was mediated by interneurons in the intermediate nucleus (Eccles et al., 1956). Hultborn first suggested that the IaINs were not located in the intermediate nucleus (Hultborn et al., 1971). After recording from a physiologically identified IaIN (see criteria in the preceding paragraph), Hultborn estimated the position of these interneurons from the position of the recording electrode. He determined that the IaINs were located in the ventral horn. It was not until Jankowska and Lindstrom (1972) intracellularly labeled electrophysiologically identified IaINs with Procion Yellow that more conclusive evidence for their location and morphology was obtained. Intracellularly labeled IaINs were located in lamina VII (LVII) and dorsal or dorsomedial to lamina IX. IaIN projections to MNs target the soma and proximal dendrites (Burke et al., 1971) and IaIN inhibition of MNs is mediated by the neurotransmitter glycine (Curtis, 1959; Fyffe 1990). IaINs are located within the same

spinal cord segment as the Ia afferents that excite them. IaIN axons will project to the lateral and ventral funiculi where they ascend or descend, sending collaterals to the motor pools (Jankowska and Lindstrom, 1972).

Adult cat IaINs are fusiform interneurons whose cell bodies and dendritic arbors are larger than RCs, but smaller than alpha-MNs ( $\alpha$ MNs; Bui et al., 2003; Alvarez et al., 1997). The average dendritic length from IaIN soma to terminal ranges from approximately 660 to 1100  $\mu$ m, whereas dendritic length was shorter for RCs ( $\sim$ 430-800  $\mu$ m) and longer for  $\alpha$ MNs ( $>$ 1000  $\mu$ m). IaIN dendrites branch extensively compared to RCs, but not as extensively when compared to  $\alpha$ MNs. Histological identification of IaINs is more difficult than for RCs. In the mature rat and mouse spinal cord, IaINs can be identified as a subgroup of Parvalbumin-immunoreactive neurons (PV-IR; Alvarez et al., 2005). PV-IR cells that receive convergent inputs from VGLUT1/PV labeled primary afferents and Calbindin-immunoreactive (CB-IR) axons suggesting RC input, were previously identified as IaINs (Alvarez et al., 2005). Developing IaINs cannot be identified by histological means, because before P15, PV-IR labels very few spinal interneurons, and is found mainly in Ia sensory afferents (Smith et al., 2005), and this has hampered their study in the developing spinal cord. Aim 3 of this thesis will attempt to create new criteria in order for IaINs to be identified throughout postnatal development.

### *Synaptic Inputs*

IaIN location in LVII dorso-medial to the MNs places them in an area which is enriched in Ia afferent terminal arborizations (Brown and Fyffe, 1978). Similarly, application of glutamate activates IaIN-mediated reciprocal inhibition of MNs

(Jankowska and Roberts, 1972b). Alvarez et al. (2005) demonstrated that a group of PV-IR V1-INs in the same location as electrophysiologically identified IaINs receives a dense projection from Ia sensory afferents. Very little information is known about the distribution and development of Ia afferent inputs on IaINs.

Besides Ia afferents and IaINs (IaIN inhibition discussed in previous section), IaINs also receive projections from flexion reflex afferents (FRA), RCs, and descending inputs. The FRA is activated by high threshold afferents and in the cat and includes joint, cutaneous, and group III and IV muscle afferents (Jankowska et al., 1967). IaINs that are excited by flexors (via the ipsilateral FRA) mutually inhibit IaINs that are excited by extensors (via the contralateral side)(Hultborn et al., 1976). IaINs receive inhibitory inputs from RCs (Hultborn et al., 1971). While intracellularly recording from MNs, Hultborn and colleagues (1971) found that the IPSPs generated in MNs followed by Ia afferent volleys (mediated by IaINs) were attenuated by antidromic stimulation of motor axons (which excites RCs). Therefore, they concluded that IaINs receive recurrent inhibition from RCs that are excited by the MNs of the antagonist muscles. IaINs receive descending inputs such as corticospinal inputs. IaIN inhibition of MNs is facilitated by volleys of corticospinal axons (Hultborn and Udo, 1972). The corticospinal inputs are believed to provide reciprocal inhibition of antagonist muscles by facilitating agonists and inhibiting antagonists.

### **III. SYNAPTOGENESIS AND MATURATION OF SYNAPTIC CONNECTIONS**

Until this point, we have examined the development of the spinal cord, origin of ventral spinal interneurons and characteristics of two ventral spinal interneurons that

derive from the V1 group. The main focus of this thesis is to examine the development of the synaptic inputs of these two distinct interneuron subtypes and gain insights into the diversification of adult interneurons subtypes. It is of the utmost importance to understand the development of the specific synaptic connectivity. The synaptic inputs to any given neuron define that neurons function. The relationship and importance of these specific inputs raises the question of how does this connectivity develop? More specifically: 1) How do growing axons know to extend to the regions occupied by their target cells, 2) How do axons know which cells are their targets, 3) Once an axon encounters an attractive target, what initiates synaptogenesis and 4) How are these newly formed synapses matured and refined resulting in synaptic strengthening or elimination of specific inputs? In the next few sections I will review specific aspects of synapse development to best interpret the results on synaptic development over V1-INs.

### **Synaptic Target Selection**

Before a synapse is formed, a neuron must send out processes towards their appropriate targets. The developing nervous system contains a meshwork of axons and neurons; so how do axons navigate their way through such a complex environment and establish contact with their specific targets? An axon does not make contact with every cell it encounters, but once it approaches the appropriate synaptic target, some instructive signal tells the axon to slow its growth, make contact, and ultimately form a presynaptic terminal. Selecting the appropriate synaptic targets is a crucial first step in synapse formation and formation of neural circuits (Dickson 2002, Tessier-Lavigne & Goodman 1996).

Axons are guided through the developing embryo to their appropriate targets, which may be millimeters and sometimes centimeters away. Axon guidance is facilitated by a specialized structure found at the tip of extending axons termed growth cones (Ramon y Cajal, 1890; Harrison, 1910; Speidel, 1941). Growth cones are motile and act as surveyors of the surrounding environment, which then direct axons away from inappropriate targets and toward their appropriate targets. As the growth cone navigates its way through the embryo, it encounters repulsive and attractive signals that are used for guidance. The repellent or attractant properties of guidance proteins depend on their context (Tessier-Lavigne and Goodman, 1996).

Many families of guidance cues, including Netrins, Semaphorins, Slits and Ephrins, have been identified (Tessier-Lavigne and Goodman, 1996; Dickson, 2002; Charron and Tessier-Lavigne, 2005). They act as tropic molecules released from the target cells to guide axons towards or away from them. Netrins are chemoattractants for commissural axons in the spinal cord (axons that cross the midline; Kennedy et al., 1994; Serafini et al., 1994). Netrins attract axons ventrally toward the midline (Culotti, 1998), but in some circumstances also repel other axons away from crossing the midline (Colamarino and Tessier-Lavigne, 1995). Interestingly, the axons of V1-INs are considered pioneer axons of the ventral and lateral funiculi in the embryonic spinal cord and their navigation is affected by netrin expression despite being mainly ipsilateral projections (Saureissig et al., 1999). The characteristics of this initial navigation of V1 axons are still not well defined.

Another important signaling molecule in the spinal cord is semaphorin. Semaphorins are cell-surface and secreted proteins, which with their receptors, Plexins,

act as short-range inhibitory cues. Semaphorin/Plexin signaling guide axons through repulsive regions or deflect axons away from inappropriate regions (Tamagnone et al., 1999; Cheng et al., 2001). In the spinal cord, Ia afferent projections to the ventral horn is directed by semaphorin/plexin signaling. Ia afferent sensory neurons express the PlexA1 receptor and the areas of the dorsal horn normally devoid of Ia afferents express the PlexA1 ligand Sema6C and 6D (Yoshida et al., 2006). The binding of PlexA1 with Sema6C/6D directs Ia afferents away from these dorsal regions. Axons of Ia afferents abnormally invade the dorsal horn in PlexA1 knockouts will, suggesting that PlexA1/Sema6C-6D signaling is important for segregation of proprioceptive sensory afferents to the ventral horn.

In addition to semaphorins as major guidance molecules to establish long-tracts and projections, similar molecules are involved in establishing topographic maps within broad target regions. The interaction of cell-surface proteins Ephrins with the Eph family of receptors are responsible for the topographic mapping of retinal axons (Wilkinson, 2001). Different isoforms of Ephrins and Eph receptors are organized in a complementary gradient in the superior-colliculus and tectum respectively and this gradient is responsible for arranging retinal axons in the correct positions along the anterior-posterior and dorso-ventral axis (Rashid et al., 2005). Similar to the other guidance cues mentioned here, Ephrins act as chemoattractants or chemorepellants in the spinal cord depending on the ligand/receptor isoform combinations. When Ephrins and or their receptors are knocked out, wiring errors occur. In the spinal cord, Ephrin/Eph signaling is important for controlling whether an axon remains ipsilateral or crosses the midline and makes contralateral projections. Kullander and colleagues (2003) found that



in EphA4 and EphrinB3 null mice, bilateral ventral roots displayed synchronous rhythms instead of normal left-right alternation, ultimately leading to a rabbit-like gait. They concluded that the rabbit-like gait was due to EphA4 positive neurons aberrantly crossing the midline, suggesting that EphrinB3/EphA4 signaling is important for restricting certain axonal projections to one side of the spinal cord. Whether an axon is attracted to or repelled away from a target region, guidance cues are an important step in insuring that appropriate synaptic connections are made.

It is not known whether any of the guidance molecules mentioned above are important for the selection of synaptic targets by motor axons and Ia afferents. However it is clear that target interneurons need to be located in regions that are permissive to the growth and arborization of these two inputs.

### **Synapse Formation**

Most of what is known about synapse formation comes from synapse development at the neuromuscular junction (NMJ; Sanes and Lichtman, 1999), but recent studies have begun to elucidate the players and mechanisms responsible at central synapses. Once an axon is guided to the correct topographic position on its appropriate target a synapse forms at this contact site. The earliest contacts between an axon and its synaptic target are mediated by filopodia. Filopodia are cytoplasmic projections which extend from the growing axon (Jontes and Smith, 2000) and once the filopodia has contacted its synaptic target, it is no longer motile and becomes stabilized. Filopodia scan the environment for synaptic partners to make contact with, but what encourages loss of motility and stabilization of the filopodia? One possibility is stabilization through

adhesion. Cadherins are a family of calcium-dependent adhesion transmembrane proteins involved in cell-cell adhesion. Several cadherins exist in the nervous system (Benson and Tanaka, 1998; Tanaka et al., 2000; Salinas and Price, 2005) and are known to accumulate during early embryonic development when adhesion and synaptogenesis between neurons is taking place (Uchida, 1996). The importance of cadherins in subtype cell specification is highlighted by motor pool organization. The position of spinal motoneuron cell body in the spinal cord and the pattern of its axonal projections in the periphery is the basis of motoneuron subtype identity. MNs are aligned into motor columns which consist of MNs with common target projections. Within each motor column, MNs are further segregated into a lateral or medial division and finally, within each division, MNs are arranged into pools which innervate specific muscles. Arrangement of MNs into different motor pools is dependent on the combinatorial expression of different genes including the cadherin family (Fredette and Ranscht, 1994; Price et al., 2002; Nollet et al., 2000). It is believed that groups of cells in neural circuits express different cadherin subtypes (Fannon et al., 1996; Suzuki et al., 1997) which provide an “adhesion code” which ultimately recruits cells into specific circuits (Yagi and Takeichi, 2000; Gumbiner, 2005).

What initiates adhesion and synaptogenesis between Ia afferents and motor axons with IaINs and RCs, respectively? A first question is whether or not RCs and IaINs are both competent to receive inputs from motor axons or Ia afferents. If each input specifically targets a different interneuron we would conclude that similar ligand/receptor interactions are involved in determining specificity. One possibility is that different cadherins are expressed in the MN area and by Ia afferents. Therefore, Ia afferent and

IaIN adhesion is mediated by the expression of similar cadherin subtypes. Similarly, motor axons and RCs may express similar cadherins, mediating adhesion and synaptogenesis. Unfortunately, the cadherin subtypes expressed by RCs and IaINs are currently unknown. Therefore we can only speculate that synapse formation between the Ia afferents/IaINs and or motor axons/RCs are mediated by cadherin “adhesion codes”. Alternatively, both V1-derived interneurons might be able to establish synapses with both motor axons and primary afferents and selective inputs arise later through differential maturation and elimination.

#### *Formation of Pre- and Postsynaptic Complexes*

Synapse formation is a multi-step process that requires communication between the presynaptic axon and postsynaptic target. Following the initial cell-cell adhesion of the axon with the synaptic target, both membranes must differentiate pre- and postsynaptic specializations. Presynaptic specializations include: 1) formation of active zones, 2) restructuring the cytoskeleton and 3) clustering of the synaptic vesicles. Moreover, the presynaptic specializations must be apposed to the appropriate postsynaptic receptor clusters. So far, several presynaptic organizers have been identified in the central nervous system and include WNTs and neuroligins. WNTs are a family of secreted glycoproteins that have been found in both invertebrates and vertebrates and they participate in synapse formation. One particular family member, WNT-7A, induces axonal remodeling *in vitro* (Lucas and Salinas, 1997) and has been shown to induce increased growth cone size and synaptic vesicle clustering in pontine explants *in vitro* (Hall et al., 2000). WNT-7A might act to rearrange microtubules, ultimately shaping

presynaptic morphological development, which might facilitate the recruitment of the appropriate presynaptic organelles.

WNT3 is expressed in MNs and is important for regulating the formation of sensory-motor connections in the mouse (Krylova et al., 2002). Cultured DRG neurons from E13.5 mice were exposed to WNT3 which caused an increase in growth cone size. Similarly, in WNT3-treated cultures, there was a significant increase in the number of secondary, tertiary and higher order branches. Krylova and colleagues (2002) concluded that WNT3 expressed in MNs induces axonal branching and growth cone enlargement of Ia afferents. Furthermore, they concluded that WNT3 acts as a presynaptic organizer. When Ia afferents come in contact with their MN targets WNT3 induces the clustering of synapsin I, a presynaptic protein involved in regulating neurotransmitter release (Chin et al., 1995; Rosahl et al., 1995). These studies suggest that WNT3 plays an important role in the formation of specific sensory-motor synapses.

Neurologin (NL) is a target-derived presynaptic organizer that when expressed in nonneural cells will induce the formation of presynaptic elements in the axons that come in contact with these cells (Scheiffele et al., 2000). NL expression in nonneural cells induces the accumulation of presynaptic vesicle proteins, such as synapsin and synaptophysin, in axons (Song et al., 1999; Scheiffele et al., 2000). The synaptic varicosities formed at these “hemisynapses” (between an axon and a non-neural structure) resembled presynaptic terminals and were capable of both spontaneous and evoked neurotransmitter release as well as vesicle recycling (Scheiffele et al., 2000; Sara et al., 2005). NLs interact with neuroligins (NRXs), which are found on the presynaptic terminal, and this interaction between the two is required for synapse-formation.

Inhibiting NLs from binding NRX receptors in culture by addition of NRX fusion proteins prevents the formation of presynaptic specializations (Dean et al., 2003). Therefore, NLs, *in vitro*, induce the formation of functional presynaptic terminals, but their role in synapse formation *in vivo* is not as well understood. Triple NL knockout mice (NL1:NL2:NL3<sup>(-/-)</sup>) die shortly after birth because of respiratory failure (Varoqueaux et al., 2006). In these mice, the number and morphology of the synapses was normal, but synaptic transmission at GABAergic/glycinergic synapses was dramatically reduced. The number of postsynaptic receptors clustered and presynaptic vesicles was reduced, suggesting that *in vivo*, NLs are important more for synaptic function than formation of presynaptic terminals. Future studies are needed to confirm the function of NLs *in vivo*.

Neuroigin-1 (NL-1) has been shown to activate *Pea3*, *Er81* and *EGR3* (O'Hagen and Hassell, 1998; Bosc et al., 2001; Shepard et al., 2001; Sweeney et al., 2001) and is involved in muscle spindle differentiation. In the absence of NL-1 in DRG and MNs, muscle spindles fail to differentiate and the levels of *Pea3*, *Er81* and *EGR3* decrease significantly (Hippenmeyer et al., 2002). The lack of muscle spindle differentiation in the absence of NL-1 did not affect the central projections of proprioceptive afferents, but defects in the elaboration of the annulospiral terminals were observed. Overall, these studies suggest that NL-1 is essential for muscle spindle differentiation and the signaling cascades initiated by NL-1 are responsible for skeletal muscle differentiation.

In order for synaptic transmission to occur, the correct postsynaptic specializations need to be apposed to the correct presynaptic specializations. How do presynaptic axons ensure that the appropriate receptors are found at the postsynaptic

target? It has been suggested that, similar to postsynaptic target-derived presynaptic organizers inducing presynaptic differentiation, presynaptic-derived postsynaptic organizers induce postsynaptic differentiation. Recently, several molecules have been identified that induce postsynaptic differentiation at central synapses and include neurexins, ephrinB and NARP.

Graf and colleagues (2004) found that expression of  $\beta$ -neurexins ( $\beta$ -NRXs) alone could induce the differentiation of both glutamatergic and GABAergic postsynaptic specializations.  $\beta$ -NRXs were capable of clustering postsynaptic scaffolding proteins, such as PSD-95 and gephyrin, and neurotransmitter receptors. Most of what is known about NRXs role in postsynaptic differentiation is derived from studies investigating the formation of glutamatergic synapses. Postsynaptic density protein PSD-95 is a scaffolding protein found at glutamatergic synapses and is one of the first proteins recruited to postsynaptic sites (Friedman et al., 2000; Okabe et al., 2001; Bresler et al., 2004). NLs interact with PSD-95 and shortly after NMDA receptors are recruited to the postsynaptic membrane (Friedman et al., 2000) and stabilized by PSD-95 (Roche et al., 2001). More research needs to be done to determine how NL/NRX signaling is involved in inhibitory postsynaptic differentiation. Neuroligin-2 (NL-2) and  $\alpha$  and  $\beta$ -neurexins ( $\alpha$ -NRX and  $\beta$ '-NRX) are found at inhibitory synapses (Varoqueaux et al., 2004; Missler et al., 2003), but how signaling between the two regulates recruitment of gephyrin (inhibitory postsynaptic scaffolding protein) and inhibitory neurotransmitter receptors remains elusive.

As mentioned previously, ephrins and their receptors EphBs are important for topographical mapping of retinal axons, but both are found at excitatory synapses in

hippocampal neurons and are believed to play a role also in synapse formation (Torres et al., 1998; Buchert et al., 1999). EphB receptors are found on the postsynaptic target cell and in the presence of ephrins, interact with the NR1 subunits of NMDA receptors, ultimately clustering NMDA receptors at the postsynaptic membrane (Dalva et al., 2000).

Finally, another molecule that has been implicated in postsynaptic differentiation is neuronal activity-regulated pentraxin (NARP), which is a member of the pentraxin family of secreted lectins (Tsui et al., 1996). Initially, NARP was believed to only induce neuronal migration and neurite outgrowth, but recently studies have described its role in postsynaptic differentiation. *In vitro*, NARP is secreted from both the presynaptic axon and the postsynaptic neuron and will associate with AMPA receptors, inducing AMPA receptor clustering (O'Brien et al., 1999). In cultured spinal neurons, excitatory synapse formation increased when NARP was overexpressed suggesting that NARP is required for excitatory synapse formation (O'Brien et al., 1999). Inhibitory synapse formation was not affected suggesting that inhibitory synapse formation relies on another postsynaptic organizer. Similar to neurexins and ephrins, NARPs role *in vivo* remains elusive.

Differentiation of Ia afferent and motor axons presynaptic machinery could involve any of the above mentioned presynaptic organizers, but the actual molecules involved are currently unknown. Similarly, nothing is known about what induces differentiation of the RC and IaIN postsynaptic membrane. In aim 4 I will be discussing the possibility that the formation of specific synaptic connections between Ia afferents/IaINs and or motor axons/RCs is mediated by an activity-independent mechanism of NL and NRX induction of pre and postsynaptic apparatus respectively.

## **Synapse Elimination**

During synapse formation, an excess of synaptic connections are generated, which can be readily eliminated during circuit refinement. The dynamic nature of these early synapses is essential for the initial wiring of neural circuits and the modification of these circuits in response to environmental changes. Synapse elimination has been extensively studied in many different parts of the nervous system including Purkinje cells in the cerebellum (Ito, 1984), the NMJ (Sanes and Lichtman, 1999) and the visual cortex (Sur et al., 1984; Sretavan and Shatz, 1986; Hamos et al., 1987; Katz and Shatz, 1996), to name a few.

In the central nervous system, the innervation of Purkinje cells (PCs) by one climbing fiber in the cerebellum provides an excellent model for examining the mechanisms involved in synapse elimination in central neurons. PCs are GABAergic neurons which project to the cerebellar and vestibular nuclei and in adult, they are contacted by excitatory parallel fibers and climbing fibers, which are both excitatory. Parallel fibers are the axons of the cerebellar granule cells and in the adult they make contact with several PCs. In contrast, each PC is innervated by only one climbing fiber, whose axons originate in the inferior olivary nucleus and makes strong synaptic connections with the proximal dendrites of that PC (Eccles et al., 1966; Palay and Chan-Palay, 1974). In the developing cerebellum, each PC receives contacts from several climbing fibers and then only one is selected in the adult (Crepel, 1982; Crepel and Mariani, 1976; Lohof et al., 1996). In mice, by the third postnatal week all but one climbing fiber synapse have been eliminated (Kano et al., 1995, 1997, 1998). Several lines of evidence indicate that the elimination of excess climbing fibers is dependent on a



competitive process between parallel fibers and climbing fibers during development. Evidence for competition between parallel and climbing fibers resulting in monoinnervation comes from several mouse mutants including the *Weaver* (Crepel and Mariani, 1976; Puro and Woodward, 1977) and *Reeler* mutants (Mariani et al., 1977). In both animals, the parallel fibers are eliminated and as a result, PCs are often innervated by multiple climbing fibers that innervate a larger area of the PC dendritic tree.

How does the presence of parallel fibers mediate the elimination of excess climbing fibers during development? Several studies have begun to elucidate the mechanisms that underlie this interaction and the glutamate receptor  $\delta 2$  (GluR $\delta 2$ ), which is found exclusively in PCs (Lomeli et al., 1993; Takayama et al., 1995), has become a key player. In the absence of GluR $\delta 2$  which is located specifically at parallel fiber synapses, the spaces normally occupied by parallel fibers are now occupied by climbing fibers and multiple climbing fibers innervate each PC (Hashimoto et al., 2001; Ichikawa et al., 2002). Therefore, it appears that the weakening of parallel fibers results in multiple climbing fiber innervation on PCs. The opposite appears to be true when weakening climbing fiber synapses. In this situation more parallel fiber synapses are observed and those parallel fibers occupy the territory on the PC proximal dendrites that is normally reserved for climbing fibers (Miyazaki et al., 2004). Encroachment of parallel fiber synapses in climbing fiber territory is evident in  $\alpha 1A$  mutants;  $\alpha 1A$  is a subunit of the P/Q-type  $Ca^{2+}$  channels and differentially affects the climbing fiber synapse. In mice lacking  $\alpha 1A$ , the parallel fiber synapses occur in more proximal regions of the dendritic tree. They concluded that in these mice, the climbing fiber cannot expel other climbing

fiber and parallel fibers from its territory because of altered  $\text{Ca}^{2+}$  influx and neurotransmission.

A similar competitive process occurs at the NMJ, a synapse that is probably the most studied synapse in the nervous system because of its large size and it is easily accessible. Stimulation of presynaptic nerves with different intensities evokes an endplate potential (EPP) in mature muscle, but when the same experiments were performed in neonates, the EPPs increased in amplitude with increased stimulus strengths suggesting that, in the young animal, the NMJ is innervated by multiple motor axons that are gradually recruited by increased stimulation (Brown et al., 1976). The elimination of excess motor axons from the NMJ is an activity-dependent process. When activity is blocked by TTX during the narrow time window of synapse elimination, the NMJ will remain polyinnervated (Balice-Gordon and Lichtman, 1994). Similarly, simultaneous stimulation of two motor axons that innervate the same muscle will preserve polyinnervation (Busetto et al., 2000), but when only one motor axon is stimulated, synapse elimination is sped up resulting in monoinnervation (O'Brien et al., 1978). Focal blockade of receptor activation within a specific area of the NMJ will induce synapse elimination at these areas (Balice-Gordon and Lichtman, 1994). Therefore, it has been hypothesized that synapse elimination at the NMJ is induced by the limiting amounts of muscle-derived trophic factors and susceptibility of inactive motor axons to “punishment signals” or “synaptotoxins” which attack the competing axons (Sanes and Lichtman, 1999).

In summary, synapse elimination through synaptic competition has been amply demonstrated in the cerebellum and at the NMJ. Neonatal PCs are innervated by many

climbing fibers and in the adult only one remains. The competition between climbing fibers and parallel fibers operates heterosynaptically to select just one climbing fiber per PC in the adult. In contrast, the neonatal NMJ is polyinnervated by many motor axons, but monoinnervated in the adult. The process of selecting one motor axon over another appears to be an activity-dependent homosynaptic competitive process. In aim 4 I will investigate whether synaptic competition of all excitatory inputs on RCs operates heterosynaptically to select specific excitatory inputs.

### **Diversification of Renshaw cells and Ia inhibitory interneurons from the V1-IN class and statement of the hypothesis**

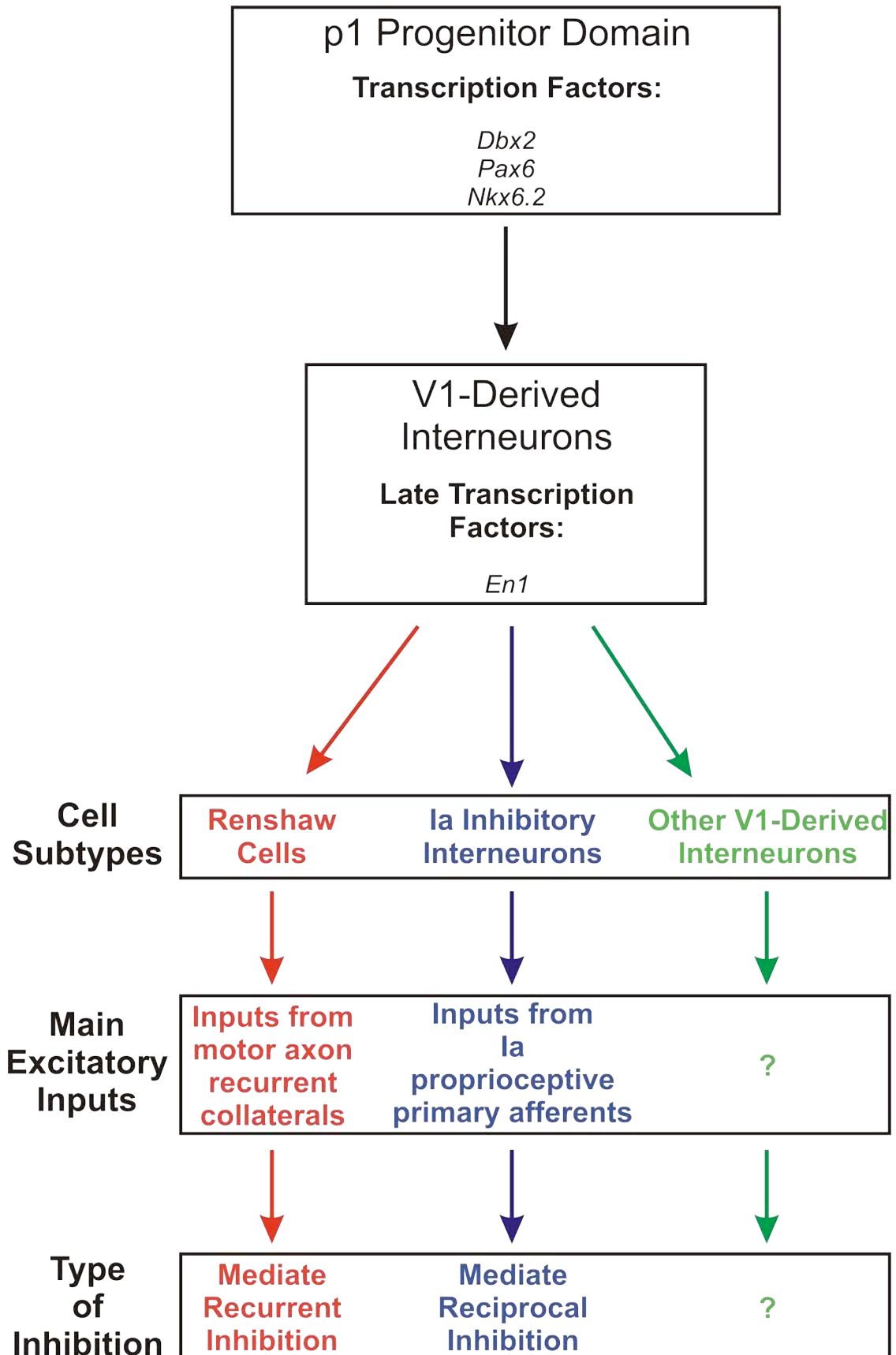
#### *The R-Interneuron and its similarities to RCs and IaINs*

How specific patterns of synaptic connectivity arise on developing spinal interneurons is unknown. The recent identification of a novel interneuron in the embryonic chick spinal cord provided us with some insights. Recently, Wenner and O'Donovan (1999) identified an inhibitory interneuron in the embryonic chick spinal cord which receives synaptic inputs from Ia sensory afferents and motor axons, thus displaying input characteristics of both IaINs and RCs. They recorded from these interneurons while stimulating the ventral root and found that a single stimulus evoked a burst of low frequency discharges, which was similar to the high frequency discharges observed in mammalian RCs following stimulation of the motor axons (see section entitled "Renshaw Cells" for more detailed explanation of this response). The difference in the frequency was probably due to the immaturity of the chick spinal cord. They denominated these cells as "R-interneurons" and dubbed them the avian equivalent to

mammalian RCs. Similar to RCs, the latency of the R-interneurons (R-IN) response to the ventral root stimulus was short and therefore they concluded that the R-IN receives monosynaptic inputs from MNs. These responses were almost completely abolished by application of the cholinergic antagonist mecamylamine. Moreover, the R-INs made monosynaptic projections to MNs and this connectivity was blocked by addition of GABAergic and glycinergic antagonists bicuculline and strychnine respectively. Finally, they demonstrated that R-INs mutually inhibit other R-INs, again similar to the mutual inhibition exhibited by RCs to other RCs and in a later study, they determined that R-INs express the transcription factor *En1* (Wenner et al., 2000).

Wenner and O'Donovan provided a seemingly flawless argument that the R-IN is the avian equivalent of the mammalian RC, but unlike mammalian RCs, the R-IN receives monosynaptic inputs from Ia sensory afferents (Wenner and O'Donovan, 1999; Ryall and Piercey, 1971). The connectivity of the adult R-IN is unknown, but the similarities between the embryonic R-IN and mammalian adult RCs raised the possibility that adult RCs and IaINs diversify from a generic interneuron class by selecting specific inputs and de-selecting others (Figure 4). Therefore we hypothesize that the common origins of adult RCs and IaINs makes them competent to receive convergent inputs from motor axons and Ia afferents, but that each input is differentially matured by each interneuron type during development in a cell-type specific manner.

**Figure 4.** Diversification of V1-derived interneurons from a single class of progenitors. V1-derived interneurons (V1-INs) derive from the p1 progenitor domain which express specific transcription factors. Once a p1 progenitor cell becomes postmitotic they express the late transcription factor *engrailed-1* (*En1*). *En1*+ V1-INs further diversify into different adult subtypes which are characterized by their synaptic inputs, which ultimately define their function.



**CHAPTER III**  
**HYPOTHESIS & SPECIFIC AIMS**

**Hypothesis: The common origins of adult Renshaw cells (RCs) and Ia inhibitory interneurons (IaINs) makes them competent to receive convergent inputs from motor axons and Ia afferents, but each input differentially matures in each interneuron type during development.**

### **Specific Aims**

In order to investigate changes in the synaptic connectivity of RCs and IaINs we pursued 4 specific aims targeting the development of the convergence of two excitatory inputs (Ia afferent inputs and motor axons inputs) on both cell types (RCs and IaINs).

**Aim 1: Characterize the development of the primary afferent inputs and motor axon inputs on Renshaw cells in the embryonic and postnatal spinal cord.**

The discovery of the R-interneuron in the chick spinal cord and its similarities to RCs led us to ask whether mammalian RCs receive inputs from Ia afferents and how these inputs compare to those from motor axons throughout development. It is hypothesized that Renshaw cells receive convergent inputs from sensory and motor axons during early development, but then de-select primary afferent inputs. Using immunohistochemical markers of primary afferents (Parvalbumin [PV] and Vesicular Glutamate Transporter1 [VGLUT1]) and motor axons (Vesicular Acetylcholine Transporter [VAcHT]) along with fluorescent dextrans to trace primary sensory afferent axons and motor axon recurrent collaterals, we investigated the convergence of both inputs on RCs at different developmental stages. The postnatal development of VGLUT1-IR and VAcHT-IR inputs on RCs was studied using immunofluorescence, confocal microscopy, brightfield preparations, and NeuroLucida 3D reconstructions.



**Aim 2: Characterize the embryonic development of the recurrent inhibitory circuit.**

Evidence gathered in aim 1 suggested that RC-like interneurons are targeted by motoneurons (MNs) synapses during very early embryonic development. Therefore, we asked when RCs are first contacted by MNs and also when are MNs first contacted by RCs leading to a functional recurrent circuit. We hypothesized that the RC recurrent inhibitory circuit is established early during embryonic development (~E11 to E12). Using an Hb9::gfp mouse model in which the motoneurons and motor axons are fluorescently labeled, we looked at when, during embryonic development, RCs are first contacted by motor axon recurrent collaterals and when motoneurons are first contacted by RC axons. The embryonic development of the recurrent inhibitory circuit was examined using immunofluorescence and confocal microscopy.

**Aim 3: Characterize the development of glutamatergic primary afferents on Ia inhibitory interneurons in the postnatal spinal cord.**

In aim 1 we found that RCs receive convergent inputs from motor axons and Ia afferents, but that the Ia afferent input is weakened after P15. We therefore investigated whether IaINs receive inputs from motor axons and how these inputs compare to those from Ia afferents throughout development. It is hypothesized that IaINs receive during development convergent inputs from motor axons and primary afferents, but they de-select the motor axon input by removal of this input. Evidence for our hypothesis comes from observations made at P20, where few, if any, VAcHT-IR contacts were seen on IaINs (Alvarez et al., 2005). Using an *En1-Cre/Thy1-YFP* mouse model, which labels the cell bodies, dendrites, and axons of V1-derived interneurons, and markers of Ia

afferents (PV and VGLUT1) and motor axons (VAcHT) we developed criteria to identify developing IaINs and investigated the convergence of these inputs on V1-derived IaINs (V1-IaINs) at different developmental stages. The postnatal development of VGLUT1-IR and VAcHT-IR inputs on V1-IaINs was studied using immunofluorescence, confocal microscopy, and NeuroLucida 3D reconstructions.

**Aim 4: Determine the role of muscle afferents in the specification of excitatory synaptic inputs on mature Renshaw cells.**

In previous aims, we found that RCs receive convergent inputs from Ia afferents and motor axons, which led us to ask whether there is a competitive interaction between these two inputs on RCs throughout development. We hypothesized that alterations in the number of sensory synapses on RCs will change synaptic densities of other inputs on RCs. Three transgenic mouse models, one with no primary afferent input in the ventral horn (VH) (*Er81*), one with a progressive degeneration of primary afferent projections after birth (*EGR3*), and one with an excess of primary afferent synapses in the VH (*mlcNT3*), were used to investigate whether there is an interaction between the motor axon collaterals and primary afferent inputs on RCs. Immunofluorescence, NeuroLucida 3D reconstructions, and confocal microscopy methods were used as described above.

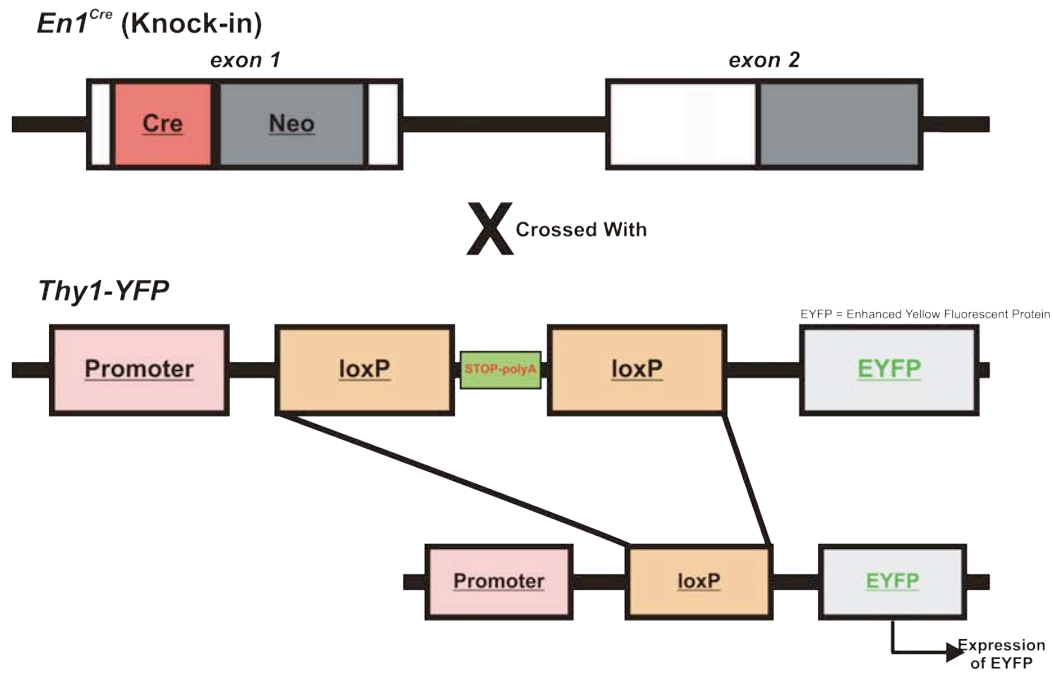
**CHAPTER IV**  
**GENERAL METHODS**

### *Identification of V1-derived interneurons using lineage markers*

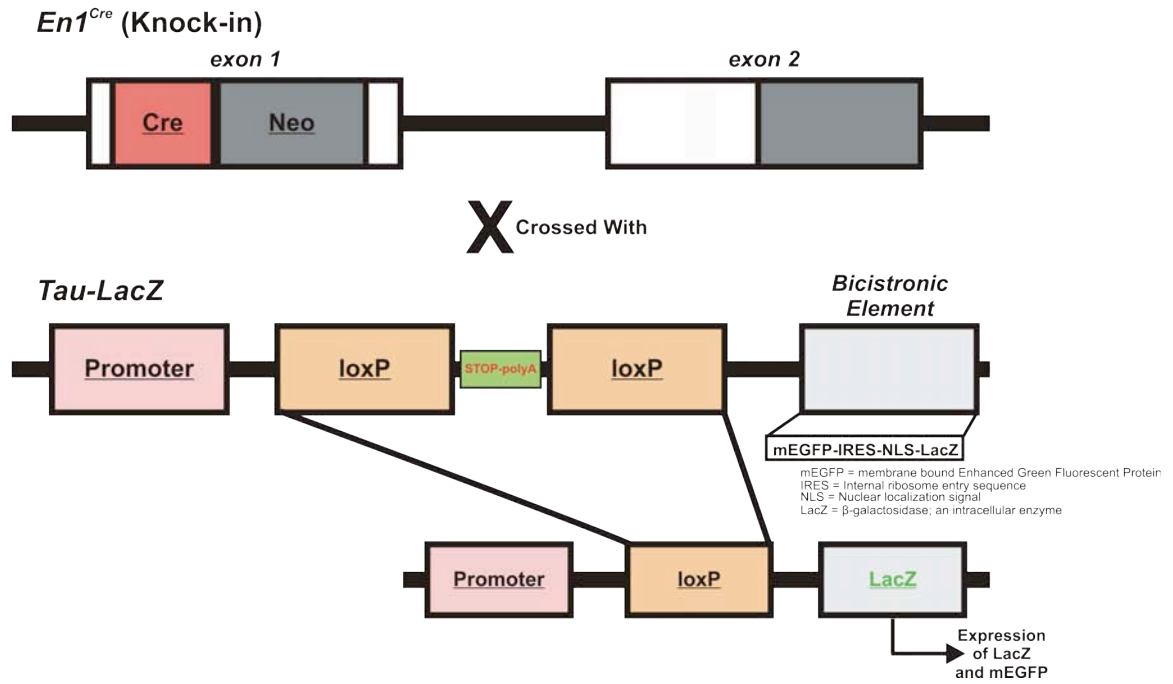
Three animal models were used in this study to identify V1-derived interneurons (V1-INs) and will be briefly explained. V1-INs were genetically labeled in *En1*<sup>Cre/+</sup> (Sapir et al., 2004) mice crossed to a *Thy1-loxP-STOP-YFP* (*Thy1-YFP*) (Buffelli et al., 2003) reporter mouse (Figure 5). In our animals a Cre insertion cassette was introduced in exon 1 of the *En1* gene, making expression of cre-recombinase dependent of *En1*, thus *En1*<sup>Cre/+</sup> heterozygotes permit targeting gene expression to V1-derived neurons in the embryonic and postnatal spinal cord using a Cre/lox strategy. *Thy1-YFP* mouse carries several copies of a transgene that expresses YFP upon removal by Cre recombination of a floxed-STOP polyA signal. Transcription is dependent on a Thy1 promoter that has been shown to result in mosaicism of expression in other targeted neuronal populations (Feng et al., 2000). Crossing the *Thy1-YFP* mice with our *En1*<sup>Cre/+</sup> mice directed Cre expression only in V1 neurons (See General Methods: *Animals*, for more information on how these crossings were made). In *En1-Cre/Thy1-YFP* mice, YFP is expressed in the cell bodies and distributed throughout the axons and dendrites of V1-derived interneurons. Similarly, *En1*<sup>Cre/+</sup> heterozygotes were also crossed with *R26-loxP-STOP-loxP-LacZ* (*R26-lacZ*; Soriano, 1999) and *Tau-loxP-STOP-loxP-mGFP-INLacZ* (*Tau-lacZ*; Hippenmeyer et al., 2005) mice. *En1-Cre/R26-LacZ* mice have been previously used and explained in full detail (Sapir et al., 2004; Alvarez et al., 2005). *En1*<sup>Cre/+</sup> mice were also crossed with *Tau-loxP-STOP-loxP-mGFP-INLacZ* mice in which reporter expression is regulated by the Tau locus (Figure 5). Upon Cre-recombination a bicistronic transcript is expressed in these animals that encodes a modified  $\beta$ -galactosidase ( $\beta$ gal) directed to the nucleus through a nuclear localization signal (nls) and a modified membrane bound

**Figure 5.** Conditional cre/loxP recombination system used to label V1-derived interneurons (V1-INs) in postnatal spinal cords. **A**, V1-INs were genetically labeled by crossing *En1*<sup>(Cre/+)</sup> heterozygotes with *Thy1-loxP-STOP-loxP-YFP* (*Thy1-YFP*; Buffelli et al., 2003) reporter mice. *En1*<sup>(Cre/+)</sup> heterozygotes permits targeting gene expression to V1-INs using a cre/lox strategy. Upon removal of the STOP-polyA signal flanked by loxP sites, V1-INs expresses EYFP. **B**, Similar to *Thy1-loxP-STOP-loxP-YFP* reporter mice, *En1*<sup>(Cre/+)</sup> heterozygotes crossed with *Tau-loxP-STOP-loxP-mEGFP-INLacZ* (*Tau-LacZ*; Hippenmeyer et al., 2005) reporter mice. Upon cre-recombination,  $\beta$ -galactosidase is directed to the nucleus via a nuclear localization signal (NLS). V1-INs also express a modified membrane-bound enhanced green fluorescent protein (mEGFP) in their axons.

A



B



EGPF (mEGFP) designed to best depict neurite morphology and cellular surfaces (De Paola et al., 2003).

#### *Histochemical identification of Renshaw cells*

Renshaw cells (RCs) were identified by several criteria, such as, location within the ventral horn and Calbindin (CB) expression. RCs are located in the ventral most region of lamina VII of the ventral horn of the spinal cord (Thomas and Wilson, 1965; Fyffe 1990). Calbindin is a calcium binding protein that was discovered in the avian intestine (Wasserman et al., 1966) and is found in many different cell types. Renshaw cells show strong CB immunoreactivity (-IR) in rodents, monkeys, and humans (Ardvisson et al., 1992; Carr et al., 1998; Fallah and Clowry, 1999), with labeling in the soma, dendrites, and axons. Calbindin expression is already present at birth in a group of ventral INs that later become adult RCs in the rodent spinal cord and is characteristically located in a ventral cluster (Geiman et al., 2000). Other ventral INs express CB at birth, but RCs are generally more brilliantly immunostained. Ventral INs with weaker expression downregulate CB postnatally, such that in the adult CB expression is largely restricted to RCs (Smith et al., 2005). Therefore, RCs will be identified as those cells with strong CB-IR in the ventral most region of lamina VII in the spinal cord.

#### *Histochemical identification of Ia inhibitory interneurons*

In this study, Ia inhibitory interneurons (IaINs) were identified as V1-derived interneurons receiving strong projections from CB-IR Renshaw cell axons and VGLUT1/Parvalbumin-IR proprioceptive sensory fibers. V1-derived IaINs (V1-IaINs)

were recognized as YFP-IR cells in *En1-Cre/Thy1-YFP* mice which receive a dense innervation from RC inputs identified as pericellular baskets of V1-derived Calbindin (CB)-IR axons. Although the percentage of IaINs with pericellular CB-IR baskets is presently unknown this criteria allows unambiguous detection of some V1 IaINs since no other interneurons are known to be targeted by strong RC inputs. In some preparations, IaINs were identified as those neurons with strong Parvalbumin-immunoreactivity (PV-IR) and densely covered by CB-IR contacts (Alvarez et al., 2005). PV-IR was only used to identify IaINs at P15, because before P10, PV labels very few if any interneurons and is contained mainly in sensory afferents (Smith et al., 2005).

#### *Identification of primary afferent inputs*

Several different anatomical methods were utilized to label primary afferents in the embryonic, postnatal, and adult spinal cord. Each approach was optimal at different developmental periods. We used *in vitro* tract tracing with fluorochrome-conjugated dextrans from the dorsal root to label primary afferents in the embryonic and early postnatal spinal cord. A problem with dextran (dxt) tracings is that the efficiency of the tracings decreases sharply at P15, probably due to the larger size of the spinal cords and the extent of myelination. This impedes oxygenation of the cord under *in vitro* conditions and during the necessary long transport times (>16 hours). Also, dxt-tracings are difficult before E16, because of the relatively small size of the spinal cord and corresponding dorsal roots. Therefore, dxt-tracings were only used in late embryonic (after E16) and early postnatal (P0, P5, and P10) spinal cords. In order to identify primary afferents in the postnatal spinal cord several immunocytochemical markers were



used. Vesicular Glutamate Transporters (VGLUTs) are proteins that package glutamate into synaptic vesicles for exocytosis. There are three known isoforms and of these three, VGLUT1 is a specific marker of large diameter primary afferents (Todd et al., 2003; Alvarez et al., 2004). Thus ventral horn synapses from proprioceptive sensory afferents express VGLUT1. This can be demonstrated by the lack of VGLUT1-immunoreactivity (VGLUT1-IR) in the ventral horns of *Er81<sup>-/-</sup>* animals (Mentis et al., 2004; see General Methods: *Mouse models exhibiting alterations of primary afferent inputs into the ventral horn*, for description of *Er81<sup>-/-</sup>* animal). VGLUT1-IR was examined in embryos and it was determined that their levels were too low for being a useful marker of sensory afferents before P0. As an alternative marker, we used Parvalbumin (PV), which is a calcium buffering protein expressed by proprioceptive primary afferents (Arber et al., 2000). PV is upregulated in sensory neurons at E14 and therefore labels sensory axons from the time they start to enter into the embryonic spinal cord and before they reach the ventral horn (Hippenmeyer et al., 2005). A problem with PV-immunoreactivity (PV-IR) as a marker of primary afferents is that by P10 spinal interneurons upregulate PV expression making it difficult to identify, with certainty, the origin of PV-immunolabeled axons. Another problem is that PV-IR is very weak at E16 perhaps because at this time it is only expressed at low levels. Therefore, PV was used as a marker only for E18 to P5.

#### *Identification of motor axon inputs*

Similar to identification of primary afferent inputs, several different anatomical methods were used to identify motor axon inputs on RCs and IaINs and each method was useful at specific developmental periods. Vesicular Acetylcholine Transporter (VACHT),

which packages acetylcholine into synaptic vesicles for exocytosis, labels motor axon collaterals specifically on RCs in the adult spinal cord (Alvarez et al., 1999). Accordingly, VAcHT-IR contacts disappear on RCs in adult superoxide dismutase 1-mutant animals undergoing motor axon degeneration (FitzSimons et al., 2006) and can be retrogradely labeled from the ventral root in neonates (Mentis et al., 2004). VAcHT-IR is a good marker of inputs from motor axons in the postnatal spinal cord and is also detectable in embryonic spinal cords using a Tyramide Signal Amplification (TSA) amplification step. TSA significantly enhances fluorescent signals (See General Methods: *Light Microscopy Immunofluorescence*, for more details about protocol used for detection using TSA method). Tract-tracing with fluorochrome-conjugated dextrans from the ventral root were used to label motor axon collaterals in late embryonic and neonatal spinal cords. As already mentioned, retrograde fills are difficult to perform in spinal cords after P10 and before E16. Therefore, alternatively we used an Hb9::gfp mouse model to label motor axons (Wichterle et al., 2002). *Hb9* is a transcription factor that is expressed in motor neurons and in these particular animals EGFP is expressed dependent on the regulatory elements of the Hb9 gene. Hb9::gfp animals not only have their motoneurons fluorescently labeled, but also the axons and dendrites, which allowed for visualization of motor axon collaterals in the embryo. Therefore, the Hb9::gfp animal, combined with VAcHT-immunohistochemistry provided a good mouse model to identify motor axons at certain embryonic stages.

*Mouse models exhibiting alterations of primary afferent inputs into the ventral horn*

We used three animal models with different genetic alterations that decrease (*Er81*<sup>-/-</sup> knockout and *EGR3*<sup>-/-</sup> knockout) or increase (*mlcNT3*<sup>+/-</sup> heterozygote) primary afferent input in the ventral horn. These animals were used to look at the distribution/density/organization of synapses on RCs, and provided insights as to whether or not sensory afferents influence the development of RC synaptic inputs.

*Er81* is a transcription factor expressed in all proprioceptive neurons and regulates the growth of Ia afferents into the ventral horn. In *Er81*<sup>-/-</sup> knockout animals, muscle afferents enter the spinal cord but do not establish arborizations in the ventral horn (Arber et al., 2000). *EGR3* is a transcription factor expressed in developing intrafusal muscle fibers and is essential for muscle spindle development (Tourtellotte et al., 2001). In *EGR3*<sup>-/-</sup> animals, spindles initially form but postnatally degenerate and do not express NT3 (Chen et al., 2002). NT3 is necessary for survival of proprioceptive sensory fibers (Ia, Ib, II afferents) and also for strengthening the central synapses of these fibers. NT3 is however expressed at low levels and downregulated from muscle postnatally, Ia afferents then become dependent on NT3 from muscle spindles. In these animals, the central synapses from proprioceptive sensory fibers on motoneurons are weakened during postnatal development most likely because of lack of NT3 (Chen et al., 2002). In *mlcNT3*<sup>+/-</sup> heterozygotes, NT3 is inserted in the genomic locus of the myosin light chain, a gene highly expressed in muscle fibers (Wright et al., 2002). Therefore, in *mlcNT3*<sup>+/-</sup> heterozygotes, NT3 expression is elevated during development and retained postnatally and in the adult. Excess of NT3 prevents normal programmed cell death of a proportion of proprioceptors and enhances the formation and development of central

arborizations from proprioceptive sensory axons. Data obtained by Courtney Smith in our laboratory with the *mlcNT3* animals demonstrates that VGLUT1-IR sensory synapses in the ventral horn are significantly increased.

### *Animals*

All animal procedures were performed according to NIH guidelines and reviewed by the local Laboratory Animal Use Committee at Wright State University under protocol numbers 736 and 738 for mice and 612 for rats.

Timed-pregnant Sprague Dawley female rats were obtained from Harlan Laboratories and the day of birth was postnatal day 0 (P0). Mice, unless noted otherwise, were C57/Black (Jackson Laboratories) wild-types and bred at Wright State University. In this thesis, we used several transgenic lines of mice breeding at Wright State, including *En1*<sup>(Cre/+)</sup>, *Thy1-YFP*, *Hb9::gfp*, and *Er81*. *mlcNT3*<sup>(+/-)</sup> heterozygotes and *EGR3*<sup>(-/-)</sup> knockouts provided to us by Dr. Neil Shneider from Columbia University, New York, NY. Our collaborator Dr. George Mentis at National Institutes of Health, Bethesda, MD, performed all dorsal and ventral root tracings in embryonic and postnatal mice using an in vitro spinal cord preparation. Maria Berrocal in our lab and Vicki Heronimus in LAR bred, tattooed, and tail clipped mice for genotyping. Animals were bred in order to generate the required genotypes for each experiment (see below). At P5, all mice (except C57/black wild-types) had their feet tattooed in different combinations (i.e., right-front paw tattooed or left-front paw tattooed) and they were assigned a litter number according to their tattoo. The tattoos and the litter numbers were for identification purposes only.

Also at P5, after tattooing, all pups had the tips of their tails clipped in order to extract DNA for genotyping using Polymerase Chain Reaction (PCR).

*Thy1-YFP* mice were crossed with *En1*<sup>Cre/+</sup> heterozygotes. We obtained two genotypic outcomes: *En1*<sup>(Cre/+)</sup>:*Thy1*<sup>YFP</sup> and *En1*<sup>(+/+)</sup>:*Thy1*<sup>YFP</sup>. PCRs were run for the following primers, Cre and GFP/YFP (Table 1). Animals that were Cre<sup>+</sup> and YFP<sup>+</sup> were used to identify V1 neurons. *Er81*<sup>(+/-)</sup> heterozygotes were also crossed and three genotypic outcomes were obtained: *Er81*<sup>(+/+)</sup> (wild-types), *Er81*<sup>(+/-)</sup> (heterozygotes), and *Er81*<sup>(-/-)</sup> (knockout). PCRs were run for the following primers, Er81 and Tau. Mice that were Er81<sup>-</sup> and Tau<sup>+</sup> were identified as *Er81*<sup>(-/-)</sup> mutants. Hb9::*gfp*<sup>(+/-)</sup> heterozygote males were crossed with C57/blk females. Hb9::*gfp*<sup>(+/+)</sup> homozygotes failed to breed as did Hb9::*gfp*<sup>(+/-)</sup> females, therefore the only breeding option was to pair Hb9::*gfp*<sup>(+/-)</sup> heterozygote males with wild-type females. Animals that were EGFP<sup>+</sup> were used to identify motoneurons, their axons, and their axon collaterals. All resulting genotypes followed closely to Mendelian proportions.

### *Genotyping*

All genotyping was carried out with help from Maria Berrocal. DNA from tail clips were extracted using Qiagen's DNeasy® kit according to manufacturer's instructions. Genotypes were determined by PCR with primers reported in table 1. The PCR was carried out using a MyCycler™ Bio Rad thermocycler with HotMaster™ Taq DNA Polymerase (Eppendorf Brinkmann Instruments, Inc) under the following condition: 5 min 95°C pre-melt step, followed by 35 cycles of 30 sec 95°C melt, 30 sec

**Table 1.** Primer sequences used for polymerase chain reaction (PCR) genotyping and expected PCR size product.

	Primer Sequence	PCR Product	Genotype
Cre	Cre 3 (5' to 3') TAA TCG CCA TCT TCC AGC AG Cre 4 (5' to 3') CAA TTT ACT GAC CGT ACA C	1 Kb	Wildtype: No Product Mutant: 1 kbp
GFP/YFP	EGFP-1 (5' to 3') GAC GTA AAC GGC CAC AAG TT EGFP-2 (5' to 3') GAA CTC CAG CAG GAC CAT GT	600 bp	Wildtype: No Product Mutant: 500-600 bp
Er81 Knockout	ER81-A (5' to 3') ATT TCA TTG CCT GGA CTG GAC GAG ER81-B (5' to 3') TTT CGC TTG GTG GTC GAA TGG G	500 bp	Wildtype: 500 bp Mutant: No Product
	Tau 253 (5') CAT GGC TGA GCC CCG CCA GGA GTT CG Tau 253 (3') CTG CGG TCC CCG GAT TTC CCA G	500 bp	Wildtype: No Product Mutant and Heterozygous: 500 bp

60°C anneal, and 7 min 72°C extension. PCR products were analyzed using 2% agarose gel electrophoresis in 1X TBE buffer with ethidium bromide staining

### *Timed Pregnancies*

In order to be certain of the embryonic ages being analyzed, the mouse pregnancies were timed using a series of hormone injections, to increase the number of ova released during ovulation. Briefly, on day 1, at 12:00 PM, female mice were injected with Pregnant Mare's Serum Gonadotropin (PMSG) (Calbiochem, LaJolla, CA, USA) which induces follicular development. Forty-eight hours later, again at 12:00 PM, on day 3, those same female mice were injected with Human Chorionic Gonadotropin (HCG) (Sigma, CG-10. St Louis, MO, USA) which induces ovulation. Ovulation occurred 12 hours after HCG injections. Therefore, females were mated later that same day (approximately 6:00 PM, which coincides with the beginning of the dark-cycle) with the males. The next morning, pregnancies were confirmed by the presence of a vaginal plug. Females were then separated from the males until they were perfused. The presence of a vaginal plug did not always signify a pregnancy just that copulation had occurred. Therefore, females were weighed before the start of hormone injections and weighed every few days until used; a steady rate of weight gain was further confirmation of successful pregnancy.

### *Tissue Preparation*

Rats and mice of different postnatal ages (P0/1, P5, P10, P15, P20, and adult, i.e. >2 months) were deeply anesthetized with Nembutal (50mg/kg, i.p.) and perfused with 4% paraformaldehyde in 0.1M PB, transcardially. After perfusion, the spinal cords were

dissected and placed in fixative for 2-4 hours or overnight and then cryoprotected in 0.1 M phosphate buffer (pH 7.4; PB) with 15% or 30% sucrose and 0.01% sodium azide until the tissue was ready to be processed. All analyses were performed in lumbar segments 4 and 5 (L4-L5), unless noted otherwise. Transverse sections were acquired using a freezing sliding microtome (50  $\mu\text{m}$ ) from L4-L5 spinal cord segments of all rat tissue and late postnatal (P10 and P20) and adult mouse tissue and processed free-floating. For neonatal (P0-P5) mouse tissue, transverse sections were obtained from L4/L5 spinal cord segments using a cryostat (20  $\mu\text{m}$ ) and processed on slides. Although processing the tissue free-floating was preferred, some of the tissue was cut using the cryostat because of the rather small size of the neonatal mouse spinal cord, and their increased chance of deterioration using free-floating sections.

Mouse and rat embryos of different ages (E11.5, E13.5, E15.5, E16, E17.5, and E18) were used for immunofluorescence. Timed-pregnant females were perfused transcardially (see above) and the uterus with embryos removed from the abdominal cavity. Embryos were then removed from the uterus and dissected free of their yolk sacs. Embryonic spinal cords are rather small and fragile; therefore, all embryos were placed in fixative *in toto* overnight and then cryoprotected in 30% sucrose. The embryos were cut below the front limbs (Figure 6) and transverse sections were obtained from the whole bottom portion including the spinal cord. Embryonic developmental stages were confirmed using the Atlas of Mouse Development (Kaufman 2005). Sections were obtained in a cryostat (20  $\mu\text{m}$ ) and picked up in subbed slides for further processing. Cut sections on slides were stored at -20 °C until used. For some studies, the vertebral columns of E16 and E18 embryos were dissected and the spinal cord exposed. The spinal



cord was postfixed overnight at 4°C inside the vertebral column and then placed in cryoprotectant until the tissue was ready to be processed. The mother's spinal cords were also dissected out, placed in postfix for 4 hours and cryoprotected. A few of the E16 and E18 spinal cords were fully dissected from the remaining vertebral columns and transverse sections (20 µm) obtained from the whole lumbar segment using a cryostat.

*Dorsal root and ventral root tracing in embryonic and neonatal mouse spinal cords*

Fluorescent dextrans (Molecular Probes) were used to trace primary sensory afferent axons and motor axon recurrent collaterals respectively from dorsal roots (anterograde tracing) and ventral roots (retrograde tracing) in neonatal and embryonic mouse spinal cords (Figure 7). Our collaborator Dr. George Mentis performed all dorsal and ventral root tracings using an in vitro spinal cord preparation. Embryos were removed from pregnant mice anesthetized with halothane, placed in cold ACSF (~4°C), decapitated and their spinal cords dissected free. Postnatal mice, ages P0, P4/5, P10, and P15 (Swiss-Webster) were also deeply anesthetized (Nembutal 50 mg/kg, i.p.) and the spinal cords quickly removed after decapitation. To facilitate neuronal survival, dissections were performed in chilled (5-10°C), modified ACSF (95%O<sub>2</sub>, 5%CO<sub>2</sub>), containing low-Ca<sup>2+</sup> (0.1 mM), high-Mg<sup>2+</sup> (2 mM) and sucrose replacement of Na<sup>+</sup>. Isolated spinal cords were pinned down in a labeling chamber with a Sylgard base and superfused with cold oxygenated ACSF (~18°C). One dorsal and one ventral root were placed inside suction electrodes and backfilled with fluorescent dextrans (30-40 mM 10,000 MW) coupled to either fluorescein (F-Dxt), Texas Red (TR-Dxt) or Cascade Blue (CB-Dxt). Sometimes the traced dorsal and ventral roots were ipsilateral, this permitted analysis of convergence

**Figure 6.** Method utilized for cutting embryonic tissue. **A**, E15.5 mouse embryo that has been removed from mother, postfixed, and cryoprotected. Yellow arrow indicates the cornea, which is still present at E15.5. The eyelids do not begin to fuse until E16. **B**, Same embryo shown in A. The white line indicates where cuts were made approximately below the front limbs. **C**, Same embryo shown in A and B. Box indicates the area that was sectioned in relation to the whole embryo.

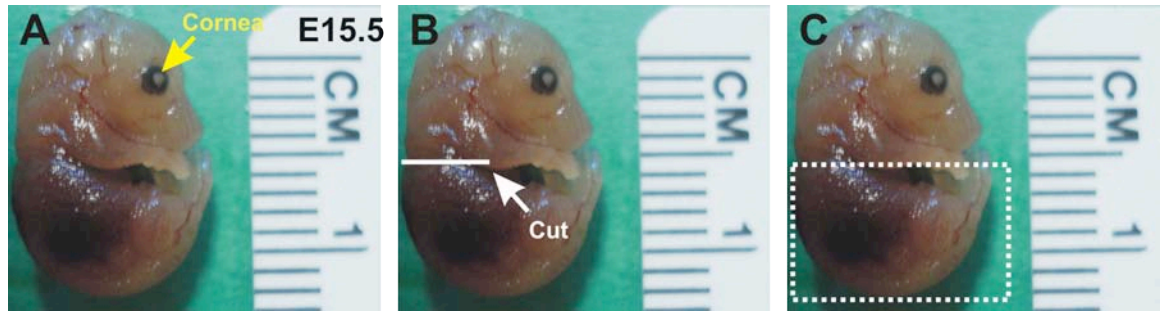
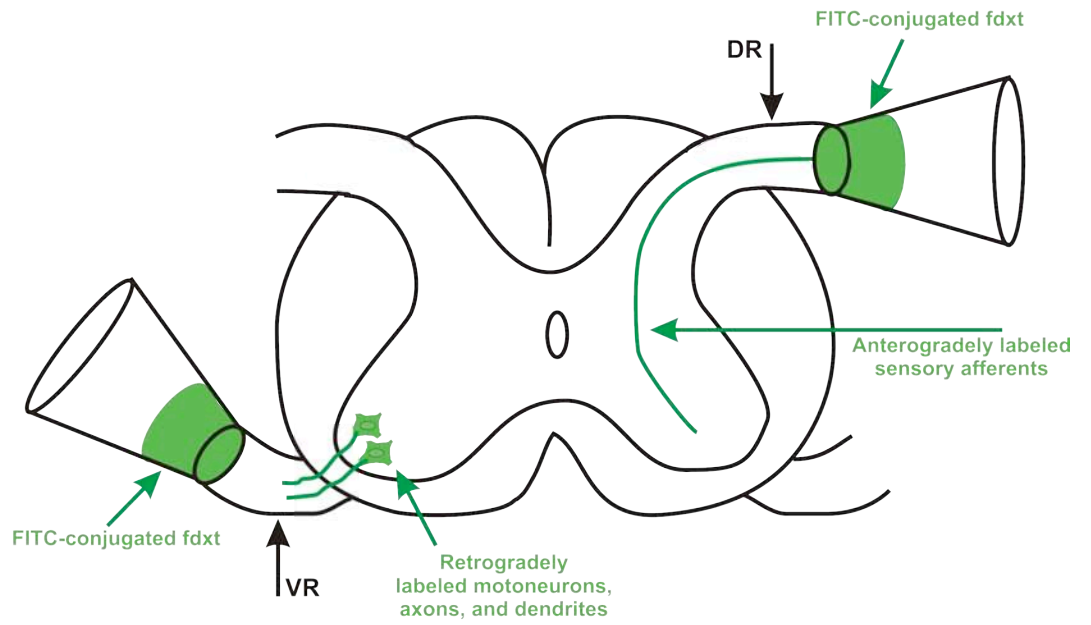


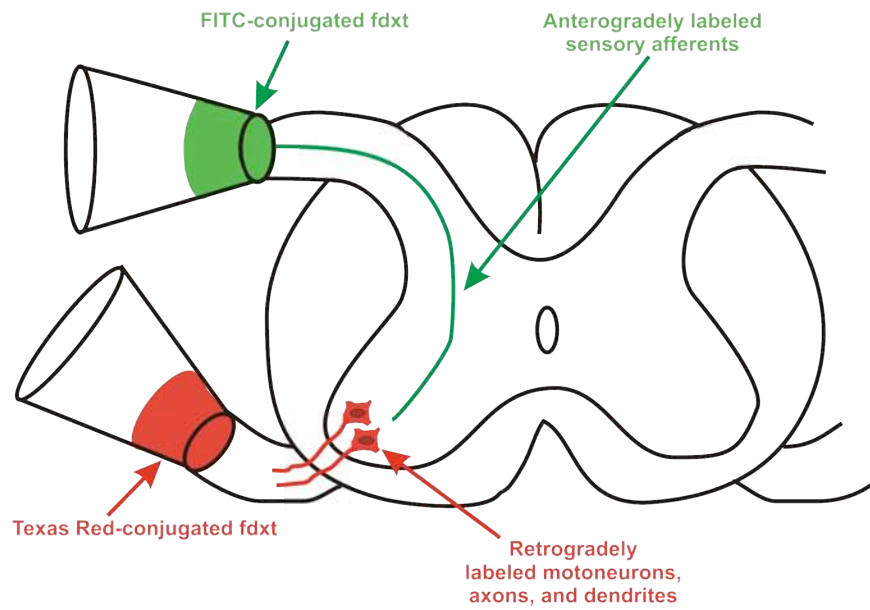
**Figure 7.** Schematic depicting tracing of sensory afferents and motor axon recurrent collaterals in the spinal cord using fluorescent dextrans (fdxts). **A,** Spinal cord section showing the dorsal and ventral roots (DR and VR, respectively). In some spinal cord sections, when many markers were used to identify one input, tracings were done with a single-fluorescent dextran dye in both DRs and VRs but on different sides of the spinal cord (contralateral tracings). In this schematic, motor axon recurrent collaterals are retrogradely labeled on the left with FITC-conjugated fdxt (green) and sensory afferents are anterogradely labeled on the right, also using FITC-conjugated fdxt (green). Retrograde tracers labeled motoneurons, their axons and their dendrites (motoneurons and motor axons are green; dendrite labeling not depicted here). **B,** In other spinal cords used for analysis of convergence of inputs on single interneurons, DR and VR were filled with different fluorochromes on the same side (ipsilateral tracings). In this schematic, on the left, motoneurons and their axons are retrogradely labeled with Texas red-conjugated fdxt (motoneurons and axons are red) and sensory afferents anterogradely labeled with FITC-conjugated fdxt (green). In some cases, only the motoneurons, their axons, and dendrites were retrogradely labeled with Cascade Blue-conjugated fdxts (not shown here).

**A**  
Contralateral Tracings



fdxt = Fluorescent Dextrans  
DR = Dorsal root  
VR = Ventral root

**B**  
Ipsilateral Tracings



in single interneurons. Alternatively when many markers were used to identify one input or interneuron class, the tracings were done with a single fluorescent-dextran dye in both ventral and dorsal roots but on different sides of the spinal cord. Labeling proceeded overnight (~16 hours) and then the spinal cord was immersion fixed in 4% paraformaldehyde (4 hours) in 0.01M phosphate buffered saline (PBS; pH 7.4) and then cryoprotected in sucrose (mentioned above). Transverse sections were obtained from L4/L5 spinal cord segments using a cryostat (20  $\mu$ m) and processed on slides as above.

### *Light Microscopy Immunohistochemistry*

#### *Multiple immunofluorescence*

Some analysis required the use of immunofluorescence with multiple fluorochromes (two, three and even four) to identify the cell types and inputs of interest. In other situations the experiments required analysis of only two markers but with brightfield microscopy analytical techniques. In this case dual-color chromogen labeling using ABC-peroxidase methods was used.

All tissue sections for immunohistochemistry were processed at room temperature. The tissue was washed in PBS 3 times for 5 minutes to rinse off the cryoprotectant. Sections were then blocked with 10% normal donkey serum diluted in 0.01M phosphate buffered saline with 0.1% Triton X-100 (PBS-T 0.1%; pH 7.4) and incubated overnight with primary antibodies. Several different combinations of primary antibodies were applied all diluted in 0.01M phosphate buffered saline with 0.3% Triton X-100 (PBS-T 0.3%; pH 7.4). Primary antibodies and their sources are listed in Table 2.

**Table 2.** Primary antibodies and their sources, species raised against, and dilutions.

<b>Antibody</b>	<b>Source</b>	<b>Species</b>	<b>Working Dilution</b>
<b><i>Calcium-Binding Proteins</i></b>			
Parvalbumin	Chemicon	Mouse/Monoclonal	1:1000
Calbindin	Swant	Rabbit/Polyclonal	1:2000
Calbindin	Swant	Mouse/Monoclonal	1:1000
<b><i>Vesicular Transporters</i></b>			
VACHT <sup>1</sup>	Chemicon	Goat/Polyclonal	1:500-1:1000
VACHT	Abcam	Goat/Polyclonal	1:500-1:1000
VACHT	Chemicon	Guinea Pig/Polyclonal	1:1000
VGLUT <sup>2</sup>	Chemicon	Guinea Pig/Polyclonal	1:1000-1:2000
VGLUT1	Synaptic Systems	Guinea Pig/Polyclonal	1:2000
VGLUT1	Synaptic Systems	Rabbit/Polyclonal	1:1000
VGLUT2	Synaptic Systems	Guinea Pig/Polyclonal	1:1000
VGLUT2	Synaptic Systems	Rabbit/Polyclonal	1:1000
<b><i>Reporters</i></b>			
EGFP <sup>3</sup>	Biogenesis	Sheep/Polyclonal	1:1000
$\beta$ -Galactosidase	Abcam	Chicken/Polyclonal	1:1000
$\beta$ -Galactosidase	Abcam	Rabbit/Polyclonal	1:10000
<b><i>Neuronal Markers</i></b>			
NeuN <sup>4</sup>	Chemicon	Mouse/Monoclonal	1:1000
<b><i>Other Markers</i></b>			
Gephyrin	Synaptic Systems	Mouse/Monoclonal	1:1000
Gephyrin	Boehringer Mannheim	Mouse/Monoclonal	1:1000
Gephyrin	Alexis Bio	Rabbit/Polyclonal	1:1000
Synaptophysin	Synaptic Systems	Guinea Pig/Polyclonal	1:1000

1. Vesicular Acetylcholine Transporter
2. Vesicular Glutamate Transporter
3. Enhance Green Fluorescent Protein
4. Neuronal Nuclear Protein

For dual and triple immunofluorescence several combinations of primary antibodies were used. These are explained in greater detail as to their purpose and selection in the appropriate sections that follow. Following an overnight incubation in primary antibodies, the tissue was washed in PBS-T 0.3%; for 3 times for 5 minutes. Immunoreactive sites were then revealed with species-specific secondary antibodies. All secondary antibodies were diluted in PBS-T 0.3% and incubated for 2 hours at room temperature. Secondary antibodies were all used at a dilution of 1:50 and were coupled to either Alexa-405 (Molecular Probes Inc, Carlsbad, CA), fluorescein isothiocyanate (FITC), cyanine3 (Cy3) or cyanine5 (Cy5) (Jackson Laboratories, West Grove, PA). Some sections required the use of 4 fluorochromes; in such instances immunoreactive sites were revealed with Streptavidin-405 (405) (Molecular Probes Inc). Preparations that used 405 required a preincubation in a biotinylated secondary antibody (diluted 1:100, Jackson Laboratories, West Grove, PA, USA) followed by Alexa-405-conjugated Streptavidin.

After incubation in secondary antibodies, the tissue was washed in 0.01 M PBS for 3 times 5 minutes. Free-floating tissue was mounted on gelatin-coated or Histobond (VWR, West Chester, PA, USA) slides and all slides were cover-slipped with Vectashield (Vector, Burlingame, CA).

#### *Dual chromogen immunohistochemistry*

Dual-chromogen immunohistochemistry for brightfield analysis was performed as in Alvarez et al. (1999). Calbindin-immunoreactivity is strongest in the cell body and



cytoplasm of RCs (Arvidsson et al., 1992; Sanna et al., 1993; Carr et al., 1998; Geiman et al., 2000; Alvarez et al., 1999), and weakens with distance from the cell body. Therefore, in order to improve labeling of more distal dendrites, we used chromogen labeling and ABC-peroxidase methods, which are more sensitive than regular immunofluorescence and results in more extensive dendritic labeling. Briefly, sections were blocked for 1 hour with normal horse serum (mentioned above) and placed in either VGLUT1 (guinea pig polyclonal, 1:5000) or VACHT antibodies (goat polyclonal, 1:2000), diluted in 0.01 M PBS with 0.3% Triton X-100, and incubated overnight at room temperature.

Immunoreactive sites were then revealed using avidin-biotin complex (ABC)-peroxidase protocols (ABC kits, Vector Laboratories). Peroxidase histochemistry was performed using diaminobenzidine (DAB) as a substrate (0.02% DAB and 0.01% H<sub>2</sub>O<sub>2</sub> diluted in 0.05M Tris buffer, pH 7.6). VGLUT1 –immunoreactivity (VGLUT1-IR) or VACHT-immunoreactivity (VACHT-IR) was revealed with silver intensification of the DAB reaction product (Sassoe-Pognetto et al., 1994). After washing the sections in 0.01 M PBS with 0.3% Triton X-100 they were incubated in Calbindin antibodies (CB, rabbit polyclonal, and 1:2000) overnight. The peroxidase labeling of antigenic sites from the second immunoreaction was developed with DAB with no silver intensification. The DAB reaction product appears brown and DAB followed by silver intensification appears dark brown/black.

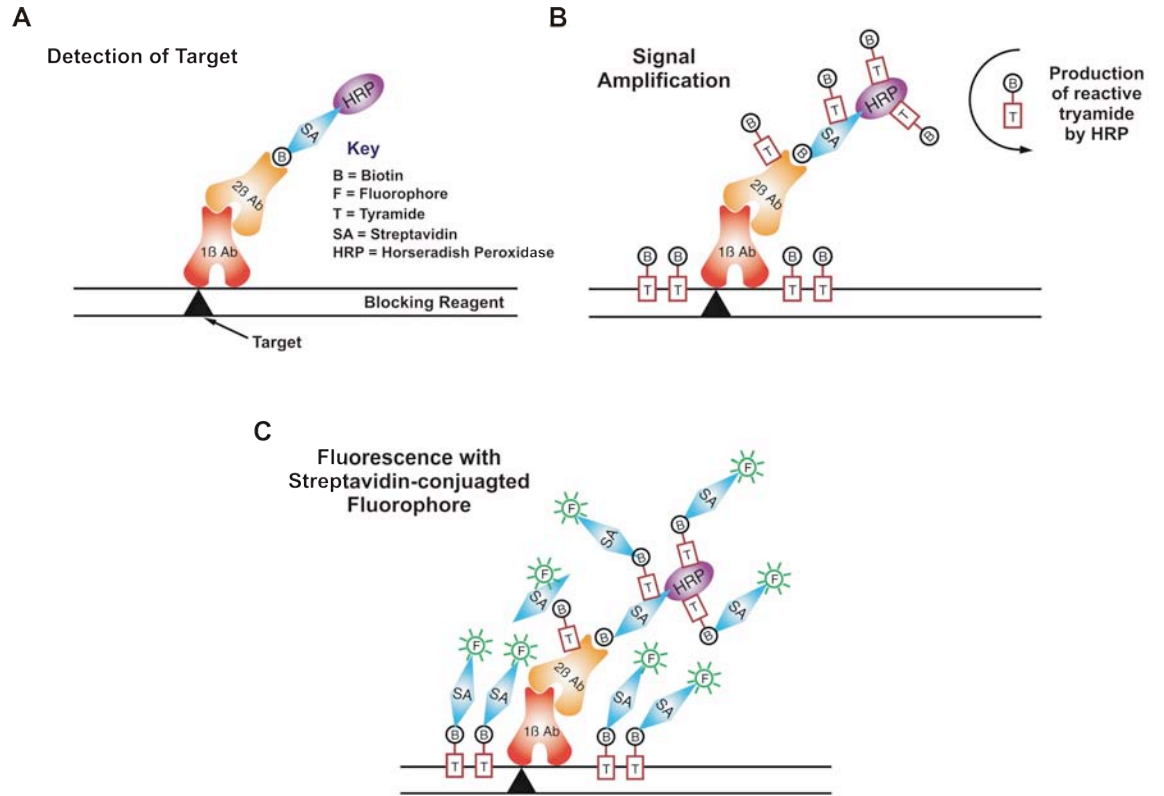
#### *Tyramide signal amplification in embryonic tissues*

Some analyses required an extra step to enhance fluorescent signals. In such cases, tyramide signal amplification (TSA) method was utilized. The TSA method

enhances sensitivity and allowed for the detection of low concentrations of antigens in embryonic tissues. Two different TSA methods were utilized in this study and will be briefly explained. In the first method, which is referred to as indirect TSA, immunoreactive sites are revealed using a fluorescent streptavidin conjugate (Figure 8). Briefly, tissue was washed with PBS-T 0.3% as before, and then incubated in 50% ethanol diluted in ddH<sub>2</sub>O. Similar to before, sections were blocked with 10% normal donkey serum for an hour and incubated in primary antibodies overnight. Following primary antibody incubation overnight, sections were washed in PBS-T 0.3% and incubated in a species-specific biotinylated secondary antibody (Jackson Laboratories, 1:100) for an hour. The biotinylated secondary introduces biotin into the sections near the primary antibody location. Sections were then incubated in ABC (avidin-biotin-peroxidase complex) (ABC kits, Vector Laboratories) for an hour, then washed with PBS-T 0.3%, and incubated with biotinylated tyramide for 10 minutes. The ABC contains biotin-peroxidase conjugates bound to avidin. These complexes bind to the biotin in the secondary antibody thus peroxidase-labeling the antigenic sites in the tissue. Biotinylated tyramide binds to these places, but in addition tyramide is a substrate for peroxidase and will be enzymatically precipitated at immunoreactive sites amplifying the original signal. Following incubation in biotinylated tyramide, immunoreactive sites were fluorochrome-tagged using streptavidin conjugated to Alexa 555 (1:100, diluted in PBS-T 0.3%).

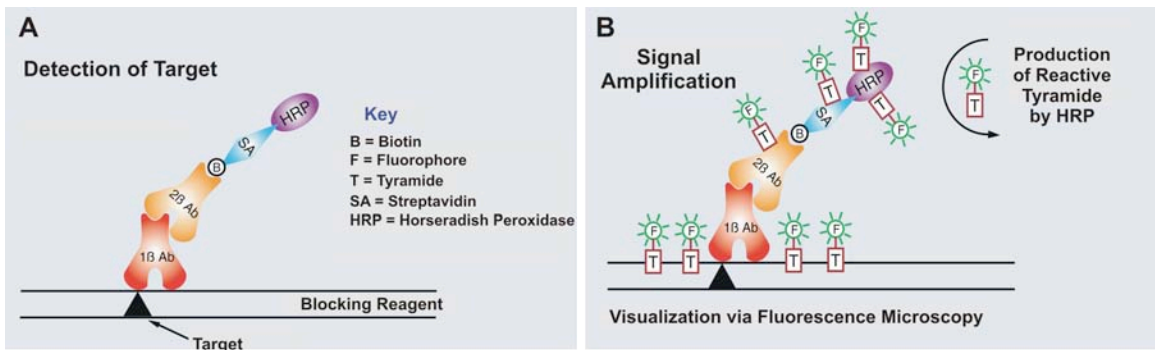
The second TSA method utilized a fluorescently conjugated tyramide and is often referred to as the direct TSA method (Figure 9). The direct TSA method allowed for immediate visualization following a short incubation with a fluorophore-conjugated

**Figure 8.** Indirect tyramide signal amplification (TSA) method. **A,** Detection of target. After overnight incubation in primary antibodies (1B Ab), sections are incubated with a species-specific biotinylated secondary antibody (2B Ab-B), which introduces biotin (B) near primary antibody locations. Next, sections are incubated in avidin-biotin complex (ABC), which contains biotin-peroxidase conjugates bound to avidin. The schematic here depicts a streptavidin-horseradish peroxidase (SA-HRP) bound to the biotinylated secondary antibody. Although we did not use SA-HRP here, the concept is the same. The peroxidase catalyzes the deposition of a labeled tyramide onto tissue sections. **B,** Signal amplification using a biotinylated tyramide. Following ABC incubation, sections were then incubated in biotinylated-tyramide (B-T). Here the HRP produces a reactive tyramide, but again we used the biotin-peroxidase in the ABC kit. **C,** Detection and visualization of the amplified signal. After signal amplification, the deposited biotin was directly visualized using a streptavidin conjugated to Alexa 555 (F).



Adapted from Perkin Elmer's Technical Literature for TSA systems  
[www.perkinelmer.com](http://www.perkinelmer.com)

**Figure 9.** Direct Tyramide signal amplification (TSA) method. **A,** Similar to the indirect TSA method, following an overnight incubation in primary antibodies (1B Ab), sections were incubated in a species-specific biotinylated secondary antibody (2B Ab-B). In contrast to the indirect TSA method, sections were then incubated in a horseradish peroxidase (HRP) conjugated to streptavidin (SA). **B,** Signal amplification with a fluorophore-conjugated tyramide (F-T). Sections were incubated with a fluorophore-conjugated tyramide, which allowed for direct visualization of the amplified signal.



Adapted from Perkin Elmer's Technical Literature for TSA systems  
[www.perkinelmer.com](http://www.perkinelmer.com)

tyramide. Slides were washed in Tris buffer saline with Tween (0.1M Tris, 0.15M NaCl, 0.05% Tween-20; Fisher Scientific) (TNT buffer, pH 7.6) 3 times for 5 minutes. Following washes, slides were incubated in TNB buffer (0.1M Tris, 0.15M NaCl, 0.5% NEN-blocking reagent) for 30 minutes and incubated in primary antibodies overnight (primary antibodies diluted in TNT buffer). Following an overnight incubation in primary antibodies, slides were washed in TNT buffer and incubated in a species-specific biotinylated secondary antibody for an hour (1:500, diluted in TNT buffer). Slides were then washed and incubated in a horseradish peroxidase conjugated to streptavidin for 30 minutes (SA-HRP, 1:2000, diluted in TNB buffer). Following SA-HRP incubation, slides were incubated in Cy3- or FITC-conjugated Tyramide for 5 minutes (1:100, diluted in Amplification diluent; TSA Plus Fluorescence Systems Kit, PerkinElmer, Street Waltham, MA). Slides were then washed in TNT buffer and coverslipped. If multiple fluorochromes were used then after the last wash, slides were incubated in species-fluorochrome-tagged specific secondary antibodies as mentioned before to reveal immunoreactivity for other primary antibodies.

#### *Imaging, Analysis, and Statistics*

Dual-immunolabeled preparations were analyzed in a Fluoview FX Olympus confocal microscope and triple- or quadruple-immunolabeled images were analyzed in a Fluoview 1000 confocal microscope. Image analysis of confocal images was done with Fluoview (Olympus), ImagePro (Media Cybernetics) and NeuroLucida software (MicroBrightfield). Brightfield preparations were analyzed in a Olympus BX51 microscope coupled to a digital camera (Microfire A/R, Optronics) and NeuroLucida, a

neuron tracing and neuron plotting stage (Neurolucida, Microbrightfield). Statistical analyses were performed with SigmaStat (version 3.1, Systat Software, Jandel) and graphing was done in SigmaPlot (version 9.0, Systat Software, Jandel).

*3D reconstructions of Calbindin-IR Renshaw cells to estimate synaptic densities of VGLUT1-IR or VAcHt-IR contacts.*

3D neuronal reconstructions were used to estimate surface area of somata and dendrites, for comparison of synaptic densities in each compartment and among cells of different ages. Immunofluorescent preparations were imaged with an Olympus Fluoview FX system confocal microscopy at 60X2.5 (oil, N.A. 1.35) magnification and a series of confocal optical sections (z-step 0.5  $\mu\text{m}$ ) obtained throughout individual randomly sampled Renshaw cells with cell bodies fully contained within the thickness of the tissue sections. The stacks of images were loaded in Image Pro Plus (ver. 5.0.) and analyzed with *3Dspace* software tools (Media Cybernetics, Burlington, VT). Calbindin immunoreactivity was threshold and segmented from the image such to isolate the Calbindin-IR soma and dendrites inside the 3D stack of confocal images. This procedure generated a 3D reconstruction of all immunolabeled processes within the field of view. All objects that were not connected to the neuron of interest were then hidden. Once a full 3D reconstruction of one Renshaw cell and its dendrites was obtained and surface rendered, we scrolled the different optical planes containing immunolabeling along this reconstruction and identified VGLUT1-IR or VAcHt-IR contacts on the Calbindin-IR Renshaw cell surface. Their placement in the cells somata or dendritic segments was noted. Then the surface of the rendered cell soma and of each dendrite was measured



using *3Dspace*. Surface densities for somata and dendrites were obtained by normalizing the number of contacts against the amount of surface sampled. One-way ANOVAs were used to determine the significance of any differences between the synaptic densities at different postnatal ages.

*Analysis of synaptic densities of VGLUT1-IR and VACHT-IR contacts on distal dendrites of Calbindin-IR Renshaw cells in NeuroLucida.*

Analysis in NeuroLucida provided a 3D reconstruction of CB-IR RCs, but unlike the *3Dspace* reconstructions, it was not limited to the small field of view of a high magnification confocal image. This system allowed the whole length of the labeled dendrite to be reconstructed. Sections processed for dual chromogen immunohistochemistry were analyzed under brightfield illumination using a 100x oil (N.A 1.35) objective lens. Only those neurons that have extensive dendritic labeling within the plane of a single 50  $\mu\text{m}$  thick section were analyzed. Their cell somas and dendritic outlines were traced using the computer-aided neuron tracing module on NeuroLucida and the locations of VGLUT1-IR or VACHT-IR contacts plotted on the reconstructions. The software generated measurements of the lengths of individual dendrites, total dendritic length, as well as the surface area of the dendrites. Using a Sholl analysis, dendrites were divided in bin segments at 50  $\mu\text{m}$  incremental distance from the cell soma. Densities of contacts were obtained by plotting the number of contacts per 10  $\mu\text{m}$  of available linear dendrite in each dendritic bin. One-way ANOVAs were used to determine any significant differences between synaptic densities at different postnatal ages in different bins.

*Confocal analysis of VGLUT1-IR and VAcHt-IR synaptic densities on Calbindin-IR Renshaw cells and Ia inhibitory interneurons in NeuroLucida.*

Multiple-color immunofluorescent preparations were imaged with a confocal microscope at 60X1.5 magnification and a series of confocal optical sections (z-step 0.5  $\mu\text{m}$ ) obtained throughout individual randomly sampled Renshaw cells or IaINs with their cell bodies fully contained within the thickness of the tissue sections. The stacks of images were loaded in NeuroLucida and analyzed using the NeuroLucida neuron tracing confocal module, which allows for reconstruction of cells from confocal stacks. VGLUT1-IR and VAcHt-IR contacts were then plotted on the reconstructed dendritic arbors. NeuroLucida provided estimates about dendritic arbors, morphology, and VGLUT1-IR and VAcHt-IR synaptic densities. Similar to analysis of brightfield preparations, a Sholl analysis was performed in 50  $\mu\text{m}$  increments from the cell soma. Densities of contacts were obtained by plotting the number of contacts per 10  $\mu\text{m}$  of surface membrane in each dendritic bin and compared across ages and genotypes using ANOVAs.

## **CHAPTER V**

### **Characterization of the development of the primary afferent inputs and motor axon inputs on Renshaw cells in the embryonic and postnatal spinal cord**

## Introduction

The development of locomotion is believed to result from the maturation of the spinal synaptic circuits controlling motor output. The spinal circuits that modulate adult motoneuron (MN) firing emerge from a dynamic set of neurons and synapses.

Unfortunately, little is known about how these circuits develop. The spinal interneurons that make up these spinal circuits are classified by their synaptic organization and their ability to modulate motor output (Jankowska, 2001). The mechanisms that select specific inputs and de-select others are unknown, but are important because they define that neurons function. One possible reason for the scarcity of knowledge is that the ventral horn interneuronal circuitry is extremely complex and still largely unknown.

Recently, it was discovered that all spinal ventral interneurons derive from four embryonic subclasses denominated “V0, V1, V2, and V3”. Each subclass is characterized by the expression of different combinations of transcription factors and distinct genetic backgrounds (Jessell, 2000; Goulding et al., 2002). Subsequent research found that both RCs and IaINs derive from the V1 subclass (Sapir et al., 2004; Alvarez et al., 2005). V1-derived interneurons, which are characterized by its expression of the postmitotic transcription factor *Engrailed-1*, are all ipsilaterally projecting inhibitory interneurons which are believed to modulate the speed of motor output (Gosgnach et al., 2006). Renshaw cells mediate recurrent inhibition of homonymous and synergistic motoneurons and their main excitation arises from cholinergic intraspinal collaterals of motor axons (Renshaw 1946; Eccles et al., 1954) and they lack monosynaptic input from primary afferents. In contrast, IaINs receive glutamatergic inputs from Ia proprioceptive primary afferents and mediate reciprocal inhibition of antagonist motor pools and are

believed to lack direct input from motoneurons (Eccles et al., 1956). The embryological origin of these interneuronal circuits that modulate MN firing is unknown.

Wenner and O'Donovan (1999) recently identified a novel inhibitory interneuron in the developing chick spinal cord that they propose is the avian equivalent of the mammalian RC. The interneuron was named the R-interneuron and receives convergent monosynaptic inputs from motoneurons and sensory afferents and provides recurrent inhibition to motoneurons. Later studies suggested that it arises from the V1 subpopulation of chick interneurons, because they express engrailed-1 transcription factor (Wenner et al., 2000). The connectivity of the adult R-IN is unknown, but the similarities between the R-IN and mammalian adult RC and IaIN connectivity raises the possibility that adult interneuron subtypes obtain their pattern of synaptic connectivity by losing/weakening and/or gaining/strengthening of specific inputs during development.

Postnatal selection of adequate inputs and numbers has been demonstrated in other systems and it has been shown to be an activity-dependent process. For example, most adult vertebrate muscle fibers are innervated by one motor axon, but during development, muscle fibers are innervated by several motor axons, a condition termed polyneuronal innervation (reviewed in Sanes and Lichtman, 1999, 2001). Polyneuronal innervation is also seen in the cerebellum with respect to the Purkinje cells. As with adult muscle fibers, adult Purkinje cells are innervated by a single climbing fiber, but during development, all inputs except one are removed in a process called synapse elimination (Ito, 1984). Synapse elimination appears to be activity-dependent. Decreased and increased synaptic activity respectively slow and speed synaptic elimination. According to Hebb's postulate (1949), inputs are strengthened by correlated

activity in the pre and postsynaptic neurons and those inputs will proliferate and mature, whereas inputs with uncorrelated activity will eventually arrest proliferation and not mature. In addition, the process is competitive in nature, such that lack of all activity prevents synapse elimination. Therefore, one possibility is that RCs and IaINs initially receive convergent inputs from motor axons and sensory afferents, but then selectively mature one or the other input throughout development via an activity dependent mechanism to obtain the input organization characteristic of their adult phenotype.

The discovery of the R-interneuron (R-IN) and its similarities to both Renshaw cells (RCs) and Ia inhibitory interneurons (IaINs) led us to investigate whether mammalian RCs receive convergent inputs from primary afferents and motor axon collaterals. We investigated the timing of synaptogenesis and developmental maturation of sensory and motor axon inputs on Renshaw cells (RCs) by counting the number of Calbindin-immunoreactive (CB-IR) RCs in the late embryonic, postnatal and adult spinal cord that receive inputs from sensory or motor axons identified using a series of markers for primary afferents (anterograde tracings from dorsal roots, Parvalbumin, Vesicular Glutamate Transporter (VGLUT1)) and motor axon collaterals (retrograde tracings from ventral roots, Vesicular Acetylcholine Transporter (VACHT)). We analyzed whether there are any differences in the developmental pattern of Ia afferent inputs on RCs compared to motor axon inputs. We then looked at the density of each input on RCs throughout postnatal development. For this purpose we used VGLUT1 as a marker for primary afferents and VACHT as a marker of motor axon collaterals. We hypothesized

that RCs receive convergent inputs from sensory and motor axons during early development, but then de-select primary afferent inputs.

Results were published as a full-length manuscript (Mentis et al., 2006) and in abstract form (Mentis et al., 2004).

## **Materials & Methods**

### *Immunohistochemistry*

Sections from lumbar spinal cord segments 4 and 5 (L4/L5) of rat and mice of various ages (E16, E18, P0, P5, P10, P15, P20, and adult) were processed for dual-color and triple-color immunofluorescence using antibodies against Calbindin (CB, rabbit polyclonal, 1:2000), vesicular glutamate transporter 1 (VGLUT1, guinea pig polyclonal, 1:1000, 1:2000), vesicular acetylcholine transporter (VACHT, goat polyclonal, 1:1000, 1:2000), and Parvalbumin (PV, mouse monoclonal, 1:1000). Several combinations of antibody mixtures were used; CB/VGLUT1, CB/VACHT, CB/PV, and CB/VGLUT1/PV (See General Methods for antibody sources and buffers). The following day, immunoreactive sites were revealed using species-specific secondary antibodies, which differed and were dependent on the primary antibody combinations used. In dual-color immunofluorescent preparations, CB-immunoreactivity was revealed using either donkey Cy3-conjugated (CB/VGLUT1 and CB/VACHT) or FITC-conjugated (CB/PV) anti-rabbit antibodies. VGLUT1-IR and VACHT-IR were revealed using donkey FITC-conjugated anti-guinea pig and anti-goat antibodies respectively. PV-immunoreactivity was revealed with donkey Cy3-conjugated anti-mouse antibodies. In triple-color immunofluorescent preparations, CB-IR was revealed with donkey Cy5-conjugated anti-

rabbit antibodies; PV with donkey Cy3-conjugated anti-mouse antibodies; and VGLUT1-IR using donkey FITC-conjugated anti-guinea pig antibodies.

In some embryonic (E16 and E18) and neonatal sections (P0, P5, and P10), primary afferents and motor axon recurrent collaterals were traced using fluorescent dextrans (fdxt; Fluorescein, F-dxt; Texas Red, TR-dxt; and Cascade Blue, CB-dxt) (see General Methods; *Dorsal root and ventral root tracing in embryonic and neonatal mouse spinal cords*). The fdxt used depended on whether the traced dorsal and ventral roots were ipsilateral or contralateral. Sections with fdxt-fills were also processed for dual and triple-color immunofluorescence using a combination of primary antibody mixtures: CB (alone), CB/VGLUT1, CB/VACHT, and CB/PV. Secondary antibody mixtures differed and depended on the fdxt used and the primary antisera mixture used.

*Percentage of late embryonic (after E16), postnatal and adult CB-IR Renshaw cells with inputs from primary afferents and/or motor axon collaterals.*

To determine the percentage of RCs contacted by either markers of primary afferents (VGLUT1, Dxt, or PV) or motor axon collaterals (VACHT), high magnification (60x1.5) confocal images were obtained from strongly labeled CB-IR cells in the first 50-100 microns from the ventral funiculus. The size of the ventral region analyzed differed depending on the age (E16-P5, 50  $\mu$ m and P10-adult, 100  $\mu$ m from the border between the ventral funiculus and the ventral horn) because of the significant increase in the size of the surrounding neuropil with age. This region contains a high density of RCs and therefore, these criteria assured that we did not include a significant number of CB-IR non-RCs in the sample. A “contacted RC” was a CB-IR cell which received at least one



contact from a fluorescently labeled varicosity on the soma or dendrite. Sample characteristics: we sampled 41 to 166 RCs from 1 to 3 mice were analyzed at each age. Similarly, 1-3 rats at each age were used and 10-71 cells analyzed (exact number of animals and cells analyzed for each age, species, and marker is summarized in Table 3).

*Confocal analysis of VGLUT1 and VAcHT densities on Calbindin-IR Renshaw cell somata and proximal dendrites.*

To analyze if convergent inputs from sensory afferents and motor axons on postnatal RCs have similar synaptic weights, as estimated by the number of contacts, we used dual-color immunofluorescence in sections from L4 and L5 spinal cord segments of both rats (Sprague-Dawley) and mice (C57/black) of each postnatal age (P0/1, P5, P10, P15, P20, and adult, i.e. >2 months) using antibodies against CB and VGLUT1 or CB and VAcHT. CB-IR RC somata and dendrites were reconstructed using *3DSpace* software and VGLUT1-IR or VAcHT-IR contacts were counted for each compartment (somata and dendrite) (See General Methods; *Imaging, Analysis, and Statistics*). The number of VGLUT1-IR or VAcHT-IR contacts was then normalized against the amount of surface sampled and a surface density of VGLUT1-IR or VAcHT-IR contacts obtained for each cell and in each cell compartment. Differences in synaptic densities were compared between P0, P5, P10, P15, P20, and adult using one-way ANOVAs for both VGLUT1-IR and VAcHT-IR contacts.

Renshaw cells are believed to lack primary afferent input; this conclusion is derived from cat spinal cord *in vivo* electrophysiological recordings. In these studies, RCs failed to respond to dorsal root volleys (Renshaw, 1946). To investigate if RCs in

the adult cat also receive inputs from primary afferents, we used dual-color immunofluorescence in sections from cat lumbar spinal cord segments using antibodies against VGLUT1 (rabbit polyclonal, 1:1000) and Gephyrin (mouse monoclonal antibody, clone 7a, 1:1000). Cat RCs do not exhibit strong CB-IR (Carr et al., 1998), but they can be identified by their large gephyrin-IR clusters (Alvarez et al., 1997). No cats were specifically prepared for this study; all cat tissue was obtained from Drs. Timothy Cope and Robert Fyffe after previous electrophysiological experiments. Adult cats were perfused with phosphate-buffered saline (PBS), followed by 4% paraformaldehyde in 0.1 M phosphate buffer, postfixed for 2-6 hours, and cryoprotected in 15% sucrose. Transverse sections were acquired from L4/L5 spinal cord segments using a freezing sliding microtome (50  $\mu$ m) and processed free-floating. Although Gephyrin-IR pattern is a good marker of cat RCs, but it only labels the somata and very proximal dendrites. Therefore, estimates of synaptic densities were only obtained from the somata using estimates of surface area from approximate ellipsoids of similar maximum and minimum diameters. The number of VGLUT1-IR contacts was then normalized against the amount of surface sampled and a surface density of VGLUT1-IR contacts obtained for each cell. Differences in synaptic densities and number of contacts were compared between cat, adult mouse, and adult rat using one-way ANOVAs. Sample characteristics: analysis of VGLUT1-IR contact density was carried out in 1-3 rats and mice at each age. Approximately 10-30 RCs were sampled per age. Analysis of VACHT-IR contact density was carried out in 1 animal at each age and 9-10 cells sampled (exact number of rats used and cells sampled for VGLUT1 and VACHT analysis shown in Table 4). Fifteen RCs were sampled from 2 adult cats in this aim.

*NeuroLucida analysis of VGLUT1-IR and VAcHt-IR densities on distal CB-IR RC dendrites.*

Only the first ~20-40  $\mu\text{m}$  (depending on age) of the dendritic tree of Renshaw cells is visible in the field of view using high magnification confocal microscopy. Moreover, decreased CB immunofluorescence with dendritic distance or in neonates also reduced the dendritic lengths that could be analyzed using the thresholding method (see General Methods; *3D reconstructions of CB-IR RCs to estimate synaptic densities of VGLUT1-IR or VAcHt-IR contacts*). To determine the distribution of VGLUT1-IR and VAcHt-IR inputs on the dendritic tree past 40 microns distance from the cell body, preparations were made to analyze the distal dendrites in NeuroLucida. Dual chromogen immunohistochemistry was performed on tissue sections of P15, P20 and adult rats. VGLUT1-IR and VAcHt-IR was revealed with silver intensification of the DAB reaction product (See General Methods; *Light Microscopy Immunohistochemistry*). The peroxidase labeling of antigenic sites for CB was developed with DAB with no silver intensification. The DAB reaction product appeared brown and DAB followed by silver intensification appeared dark brown/black.

CB-IR (DAB) RCs were reconstructed using a computer-aided neuron tracing system (NeuroLucida) and VGLUT1-IR or VAcHt-IR (DAB-silver intensification) contacts plotted on the reconstructions (See General Methods; *Imaging, Analysis, and Statistics*). The density of VGLUT1-IR or VAcHt-IR contacts was expressed as the number of contacts per 10  $\mu\text{m}$  of linear dendrite sampled in each dendritic bin. Synaptic density differences in various dendritic compartments were compared between P15, P20, and adult using one-way ANOVAs. Sample characteristics: we estimated VGLUT1-IR

contact density in 1-3 rats. Approximately 14-30 RCs were sampled. For estimations of VAcHT-IR contact density, approximately 13-16 RCs were sampled from 1 rat at each age.

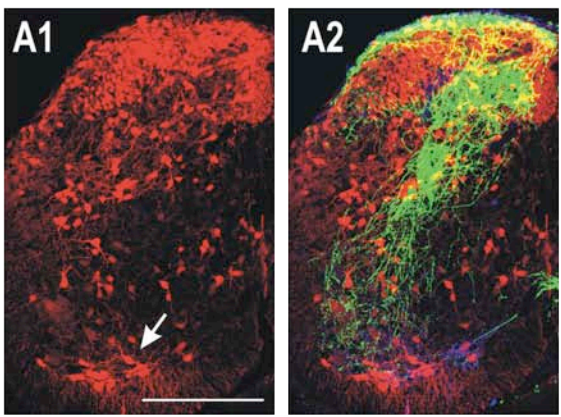
## **Results**

### *Primary afferent and motor axon synaptic markers in the developing spinal cord*

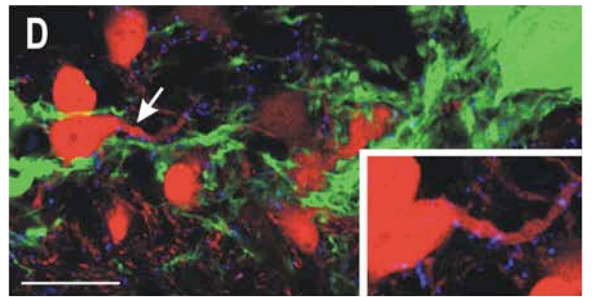
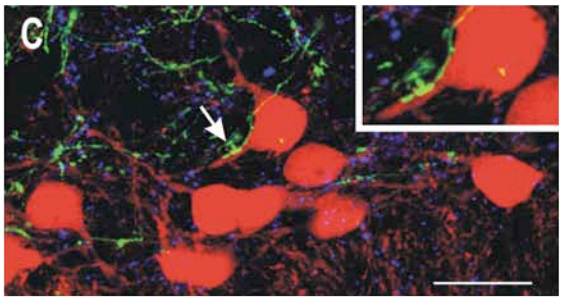
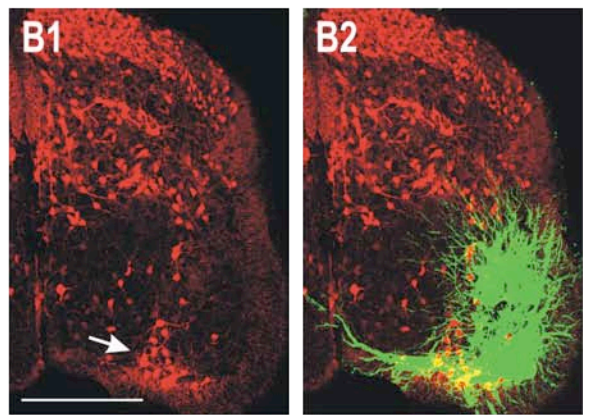
Several different anatomical methods were used to identify primary afferents and motor axon collaterals on developing RCs. Each approach was most advantageous during specific overlapping developmental periods. Therefore, conclusions are based on the best methodological combinations at different postnatal times. First we analyzed these markers and their changes/maturation with development. Tract-tracing with fluorochrome-conjugated dextrans (Fdxts) from either dorsal or ventral roots and immunolabeling with PV, VGLUT1, or VAcHT were used to analyze sensory afferent and motor axon synaptic inputs on embryonic (E16 and E18), postnatal (P0, P5, P10, P15, P20), and adult Renshaw cells. Fdxts were used to label sensory afferents in late embryonic (after E16) and early postnatal (P0, P5, and P10) spinal cords (Figure 10). Fdxt tracings were not used before E16, due to technical difficulties placing suction electrodes on the very thin and small ventral and dorsal roots. In addition, the efficiency of Fdxt tracings decreases sharply at P15, probably due to the larger size of the spinal cords and the extent of myelination. This impedes oxygenation of the cord under *in vitro* conditions and during the necessary long transport times (>16 hours). Therefore, Parvalbumin-immunoreactivity, which specifically labels sensory afferents (Arber et al., 2000), was used as an alternative marker (Figure 11). A problem with using PV as a

**Figure 10.** Sensory and motor axon inputs on embryonic and postnatal Renshaw cells. **A**, E18 mouse spinal cord showing in **A1**, CB-IR (Cy3, red) and in **A2**, superimposed dorsal sensory afferents filled with fdxt (green) and VACHT-IR (Cy5, blue). The arrow indicates a prominent group of CB-IR cells in the ventral horn that corresponds to the exit region of motor axons. Geiman et al., 2000 found that this group of cells in the rat spinal cord receives cholinergic inputs throughout development and matures in adult RCs. They are surrounded by VACHT-IR boutons also in the embryo (A2). By E18, some fdxt-filled sensory afferents extend ventrally in the RC area. **B**, Contralateral side showing CB-IR (red) and superimposed motoneurons retrogradely labeled with fdxts from the ventral root (B2; green; VACHT-IR is not shown in B2 because immunoreactivity was masked by intense fdxt labeling). There is a group of CB-IR cells in the ventral most portion of lamina VII (LVII) that is, as mentioned previously, in the area that corresponds to the exit region of motor axons (arrow). **C**, High magnification confocal image showing clear fdxt-filled sensory afferent varicosities (green) on CB-IR RCs (red). Arrow indicates cell in inset that receives inputs from sensory afferents. Arrowhead indicates a CB-IR RC that receives VACHT-IR inputs. Most Renshaw cells received VACHT-IR contacts, but only a small proportion were contacted by anterogradely labeled dorsal root axons. **D**, High magnification image shows CB-IR RCs (red) that receive VACHT-IR (blue) contacts. Retrogradely labeled motoneurons somata and processes (green) are also shown. The area marked with an arrow is enlarged in the inset. **E**, Low magnification image of a P0 mouse spinal cord immunolabeled with CB-IR (red) and superimposed with sensory afferents (left) and motoneurons and their processes (right) filled with fdxt applied to the dorsal and ventral roots respectively. The yellow boxes indicate the areas shown at higher magnification in E2 and E3. **E2**, High magnification image of retrogradely labeled motor axon recurrent collaterals and dendrites (green) and CB-IR RCs (red). Motor axon collaterals are distinguished by their non-tapering and varicose-studded fine processes branching frequently at right angles (arrows). Asterisk indicates higher magnification image of a cell (shown in inset) receiving contacts from fdxt-filled motor axons. Postnatal CB-IR RCs are contacted by motor axon recurrent collaterals. **E3**, Fdxt-filled sensory afferents contacting CB-IR RCs (white arrows; inset shows cell with asterisk at higher magnification). Not all CB-IR RCs at P0 are contacted by sensory afferents (yellow arrow). **Scale bars:** **A1-A2, B1-B2** and **E1** (in A1, B1, and E1) 200  $\mu\text{m}$ ; **C, D** and **E2-E3** (in C, D, E2, and E3) 20  $\mu\text{m}$ .

E18 Calbindin-IR + I<sup>0</sup> aff.(F-Dxt) + VChT-IR



E18 CB-IR + Ventral root (F-Dxt) + VChT-IR



P0 Calbindin-IR + Motoneuron (right side) + I<sup>0</sup> afferents (left side)

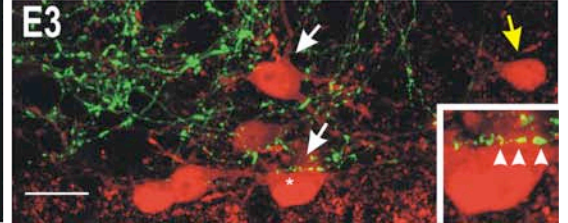
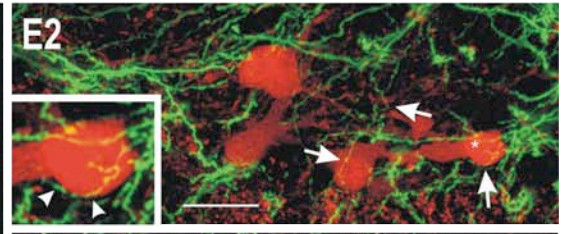
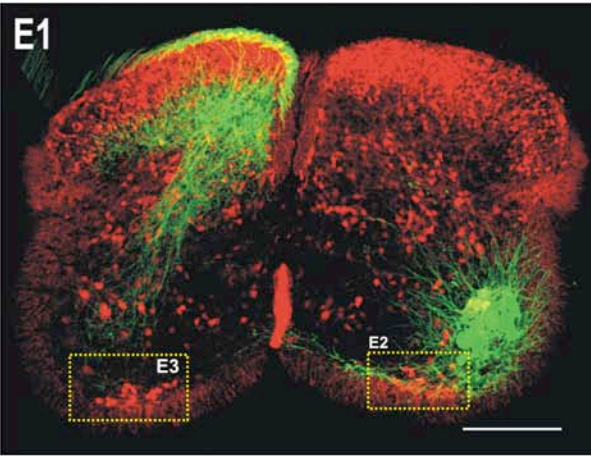
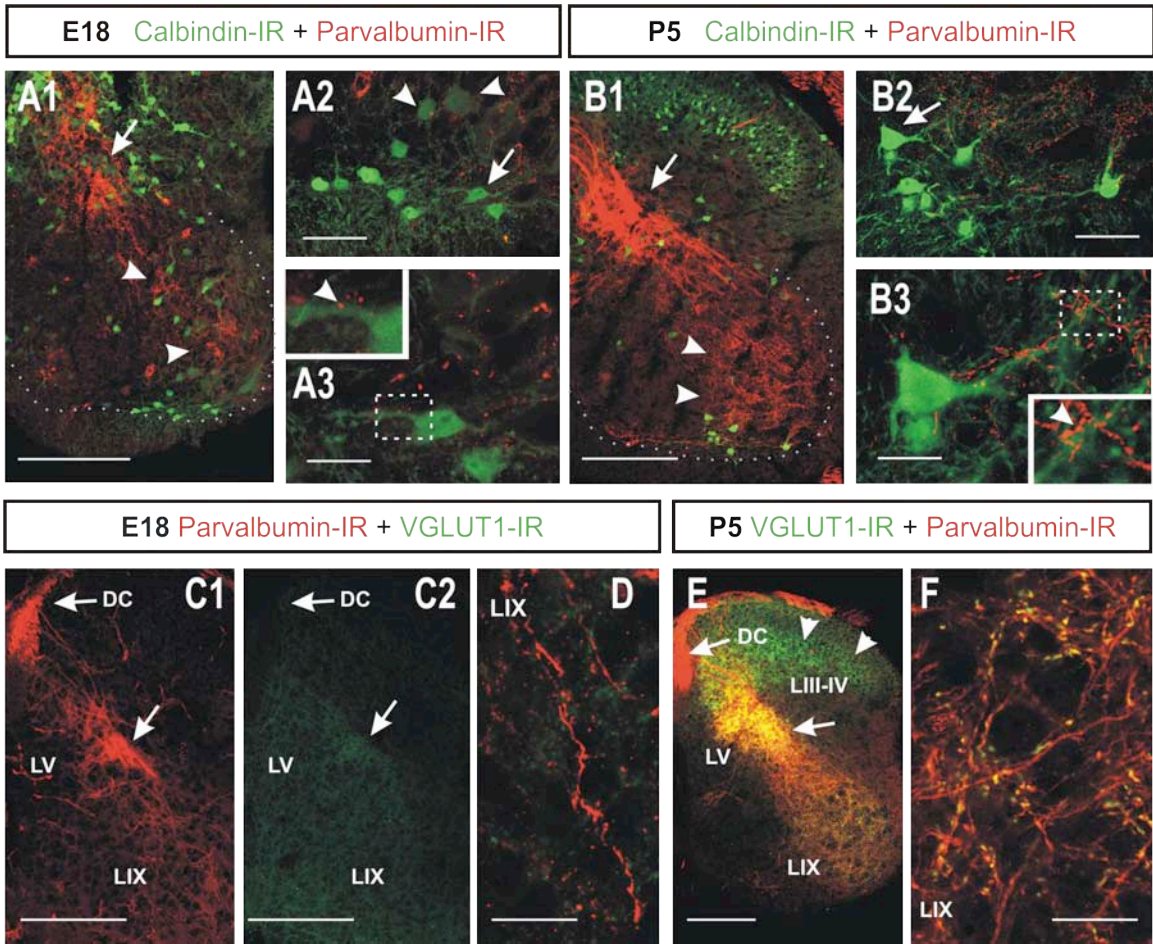


**Figure 11.** Expression of Parvalbumin in the embryonic and postnatal spinal cord. **A**, E18 mouse spinal cord dual-immunolabeled with Parvalbumin (Cy3, red) and Calbindin (FITC, green). **A1**, Low magnification image showing a dense plexus of PV-IR axons (red) located in medial lamina V (LV; arrow), from here axons extend ventrally (arrowheads). **A2**, High magnification image of the RC area. Some motoneurons (MNs) weakly express CB (green) at E18 (arrowheads), but these cells are easily distinguished from CB-IR RCs by their size. Very few PV-IR axons contact RCs at this age. In contrast, MNs are frequently contacted. Arrow indicates cell shown at higher magnification in A3. **A3**, PV-IR axon contacting a CB-IR RC. **B**, Low magnification image showing the same dual-immunolabeling as in A, but in a P5 spinal cord. **B1**, By P5, PV-IR axons have proliferated and significantly more axons are seen in the ventral horn. **B2**, High magnification image of the RC area. **B3**, Higher magnification image of the RC indicated in B2 (arrow in B2) showing several contacts from PV-IR sensory afferents. Box indicates area shown at higher magnification in inset. **C**, E18 spinal cord showing dual-immunolabeling from PV (red) and VGLUT1 (FITC, green). **C1**, Low magnification image of PV-IR axons in the embryonic spinal cord. PV-IR axons are seen in the dorsal columns (DC), LV, and lamina IX (LIX). **C2**, No VGLUT1-IR varicosities are seen in the spinal cord at E18. Only some weak and diffuse labeling was seen in LV. **D**, High magnification image of a PV-IR axon with no VGLUT1-IR. **E**, Low magnification image of a P5 spinal cord showing dual-immunolabeling of PV (red) and VGLUT1 (green). High densities of VGLUT1-immunolabeled varicosities are present in LIII-LIV (arrowheads) and in the LV and LIX. **F**, High magnification image of LIX at P5 showing co-localization of VGLUT1-IR clusters (green) and PV-IR varicosities (red). **Scale bars:** **A1**, **B1**, **C1-C2** and **E** (in A1,B1,C1,C2,E) 200  $\mu\text{m}$ ; **A2** and **B2** (in A2,B2), 50  $\mu\text{m}$ ; **A2-A3**, **B2-B3**, **D** and **F** (in A2,A3,B2,B3,D,F), 20  $\mu\text{m}$ .







marker of sensory afferents is that by P10, spinal interneurons begin to upregulate PV expression making it difficult to identify, with certainty, the origin of PV-immunolabeled axons. Therefore, Fdxs and PV are excellent markers of sensory afferents until P10.

Ideally we would like to combine labelings of primary afferent axons with a specific presynaptic marker indicating the presences of a synapse. For this purpose we used vesicular glutamate transporter isoform 1 (VGLUT1). VGLUT1-IR proved to be a specific marker of sensory afferents in postnatal developing and adult RCs. In postnatal spinal cords, bright VGLUT1-IR clusters were found in both PV-IR sensory axons and dorsal root Dxt-filled varicosities. Therefore, ventral horn synapses from sensory afferents express VGLUT1, which can be demonstrated by the lack of VGLUT1-IR inputs on RCs of *Er81<sup>(-/-)</sup>* animals (Figure 12). Interestingly, no VGLUT1-IR was detected in Dxt-filled or PV-IR sensory afferents in embryonic spinal cords, but nearly all of the labeled varicosities contained clear VGLUT1-IR clusters by P0 (Figure 11C-F). VGLUT1-immunoreactivity displayed considerable maturation during development, most likely indicative of the maturation of the presynaptic vesicle pools. VGLUT1-IR immunofluorescence inside Dxt-filled sensory afferents increased significantly from P0 to P10 [P0 =  $1638 \pm 481$  units (n = 50; average  $\pm$  SD, in arbitrary units from 24 bit images, i.e., max of 4095) and P10 =  $3399 \pm 539$  units (n = 50);  $p < 0.001$ , t-test]. Background levels remained the same ( $357 \pm 199$  units). Dxt-filled varicosities also doubled in size from P0 to P10 (P0 =  $0.71 \pm 0.33 \mu\text{m}^2$  and P10 =  $1.30 \pm 0.52 \mu\text{m}^2$  (average  $\pm$  SD;  $p < 0.001$ , t-test). Similarly, VGLUT1 immunofluorescence in PV-IR varicosities increased significantly from  $1464 \pm 382.23$  units at P0 to  $3473 \pm 295.63$  units at P10 (n = 50 clusters at each age;  $p < 0.001$ , t-test). VGLUT1-IR clusters in mice

increased significantly in size during development ( $p < 0.001$ , one-way ANOVA). VGLUT1-IR clusters more than tripled in size from  $1.10 \pm 0.43 \mu\text{m}^2$  at P0 to  $3.52 \pm 1.36 \mu\text{m}^2$  at P15 and after P15, nearly doubled at P20 (Figure 13) ( $5.08 \pm 0.96 \mu\text{m}^2$ ; average  $\pm$  SD;  $n = 50$  clusters at each age). *Post hoc* tests indicate that the increase from P0 to P15 and then to P20 were significant ( $p < 0.005$ , *post hoc* Tukey's test), but no differences were detected between P0 and P5 ( $p = 0.062$ , t-test) and P20 and adult ( $p = 0.970$ , t-test). VGLUT1-IR cluster sizes were not analyzed in neonatal rats, but no significant differences were detected between P15 ( $5.1 \pm 2.25 \mu\text{m}^2$ ), P20 ( $5.3 \pm 2.12 \mu\text{m}^2$ ), and adult ( $5.9 \pm 2.22 \mu\text{m}^2$ ;  $n = 50$  clusters at each age;  $p = 0.177$ , on-way ANOVA). At these ages VGLUT1 immunofluorescence intensity was extremely bright and the imaging system was saturated at the same acquisition parameters used to detect VGLUT1-IR punctae at P0. In conclusion, VGLUT1-IR clusters were not detectable in embryonic sensory afferents and were first detected at P0, thereafter they became bigger and brighter suggesting a significant postnatal maturation of VGLUT1-IR sensory afferent synapses up to P15. We used VGLUT1 as marker of sensory afferent synapses during postnatal development.

VACHT-IR labels motor axon collaterals specifically on RCs in the adult spinal cord (Alvarez et al., 1999). Accordingly, VACHT-IR contacts disappear on RCs in adult superoxide dismutase 1-mutant animals undergoing motor axon degeneration (FitzSimons et al., 2006) and can be retrogradely labeled from the ventral root in neonates (Figure 14; Mentis et al., 2005). Unlike VGLUT1, VACHT-IR clusters in the spinal cord are present as early as E16. Therefore, motor axons synapses (VACHT-IR

**Figure 12.** Changes in VGLUT1-IR contact density on RCs in *Er81*<sup>(-/-)</sup> knockouts. **A-B**, Low magnification confocal images of spinal cord sections from P15 *Er81*<sup>(+/+)</sup> (wild-type; A) and *Er81*<sup>(-/-)</sup> (mutant; B) animals immunolabeled with NeuN (Cy3, red) and VGLUT1 (FITC, green). In *Er81*<sup>(-/-)</sup> knockouts, primary afferents fail to make arborizations in the ventral horn (Arber et al., 2000). VGLUT1-IR is largely absent in the ventral horn of *Er81*<sup>(-/-)</sup> animals. The line above the central canal (CC) represents the border between dorsal and ventral horns (DH and VH, respectively). The dotted line delineates the border between the ventral horn and the ventral funiculus (VF). **C-D**, Higher magnifications images of the ventral horns of *Er81*<sup>(+/+)</sup> and *Er81*<sup>(-/-)</sup> animals displaying VGLUT1-IR (green) and CB-IR (Cy3, red). The dotted line indicates the border between the VH and the VF. Again, VGLUT1-IR is absent in the ventral horn of *Er81*<sup>(-/-)</sup> animals at P15. **E-G**, VGLUT1-IR bouton contacts (green) on P15 CB-IR RCs (red). These are numerous in *Er81*<sup>(+/+)</sup> animals (wild-types, E), just a few in *Er81*<sup>(+/-)</sup> heterozygotes (arrows) (F) and almost none in *Er81*<sup>(-/-)</sup> (homozygotes, G). **H-I**, Quantitative analysis of the surface density of VGLUT1-IR contacts on RCs in *Er81*<sup>(+/+)</sup>, *Er81*<sup>(+/-)</sup>, and *Er81*<sup>(-/-)</sup> P15 mice. At P15, the density of VGLUT1-IR contacts were significantly reduced in both dendrites (H) and somata (I) of *Er81*<sup>(+/-)</sup> heterozygotes and *Er81*<sup>(-/-)</sup> knockouts compared to wild type (one-way ANOVA; p<0.001). VGLUT1-IR contact density was significantly different between *Er81*<sup>(+/-)</sup> heterozygotes and *Er81*<sup>(-/-)</sup> knockouts on dendrites, where a few VGLUT1-IR contacts remain in *Er81*<sup>(+/-)</sup> heterozygotes. Therefore, VGLUT1-IR contacts on RCs are of primary afferent origin. **Scale bars:** A and B (in A), 200 μm; C and D (in C and D), 100 μm; C, D, E, F, and G (in E, F, and G), 20 μm.

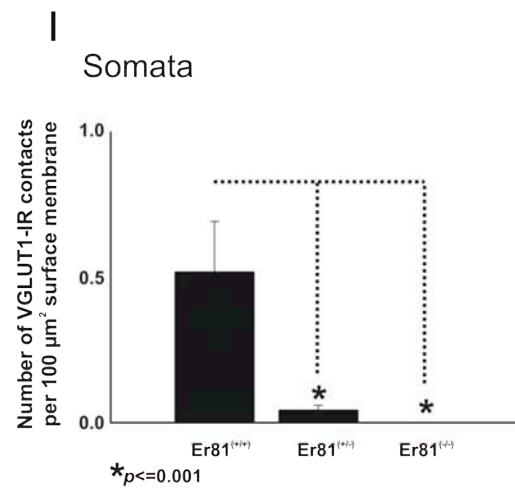
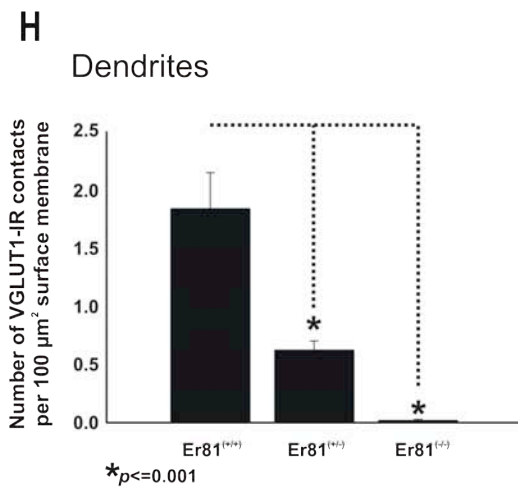
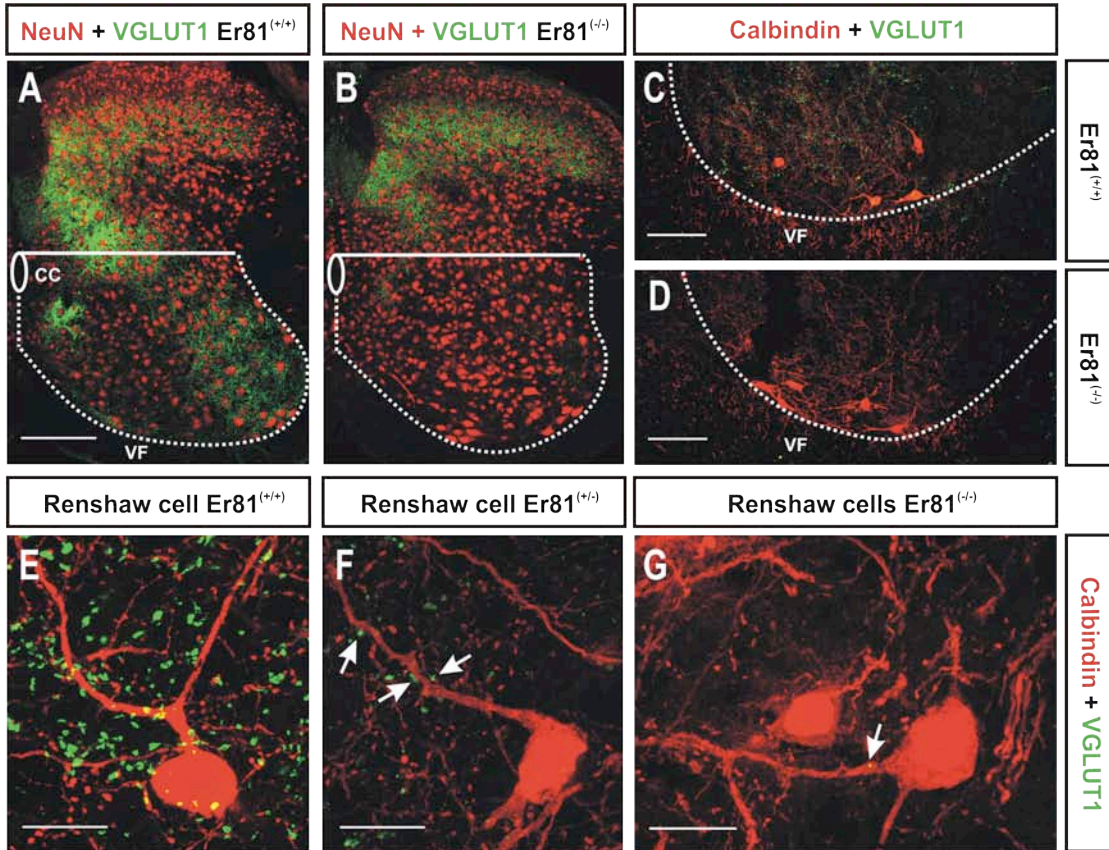


**Figure 13.** VGLUT1-IR cluster sizes in mouse and rat during postnatal development. **A**, High magnification confocal images of VGLUT1-IR clusters in Lamina IX in P0 (**A1**), P15 (**A2**), and adult (**A3**) mice. VGLUT1-IR clusters appear larger and brighter at P15 compared to P0 and adult clusters compared to P15. **B**, VGLUT1-IR clusters at P15 (**B1**), P20 (**B2**), and adult (**B3**) in rats. **C**, Size of VGLUT1-IR clusters in P0, P5, P10, P15, P20, and adult mice. VGLUT1-IR clusters increase significantly in size from P0 to P20 ( $p < 0.05$ , one-way ANOVA; no significant differences were detected between P20 and adult,  $p = 0.970$ , t test), suggesting a rapid maturation of the presynaptic machinery up to P20. **D**, VGLUT1-IR cluster size in P15, P20, and adult rats. No significant differences were detected between the three ages analyzed ( $p = 0.170$ , one-way ANOVA). **Scale bars:** **A** and **B** (in A1-A3 and B1-B3), 5  $\mu\text{m}$ .

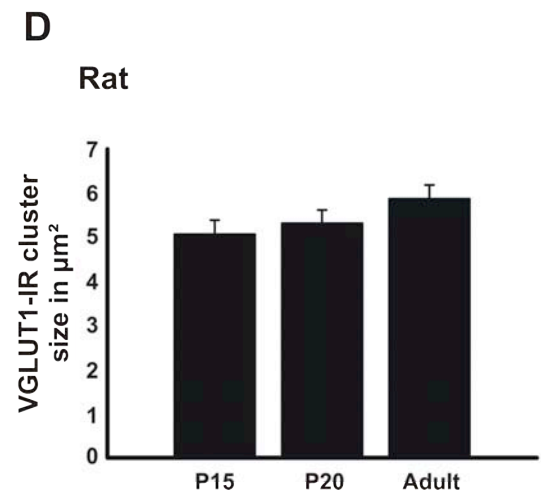
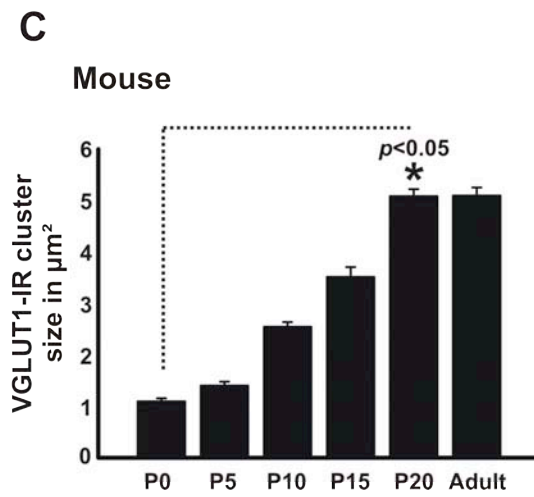
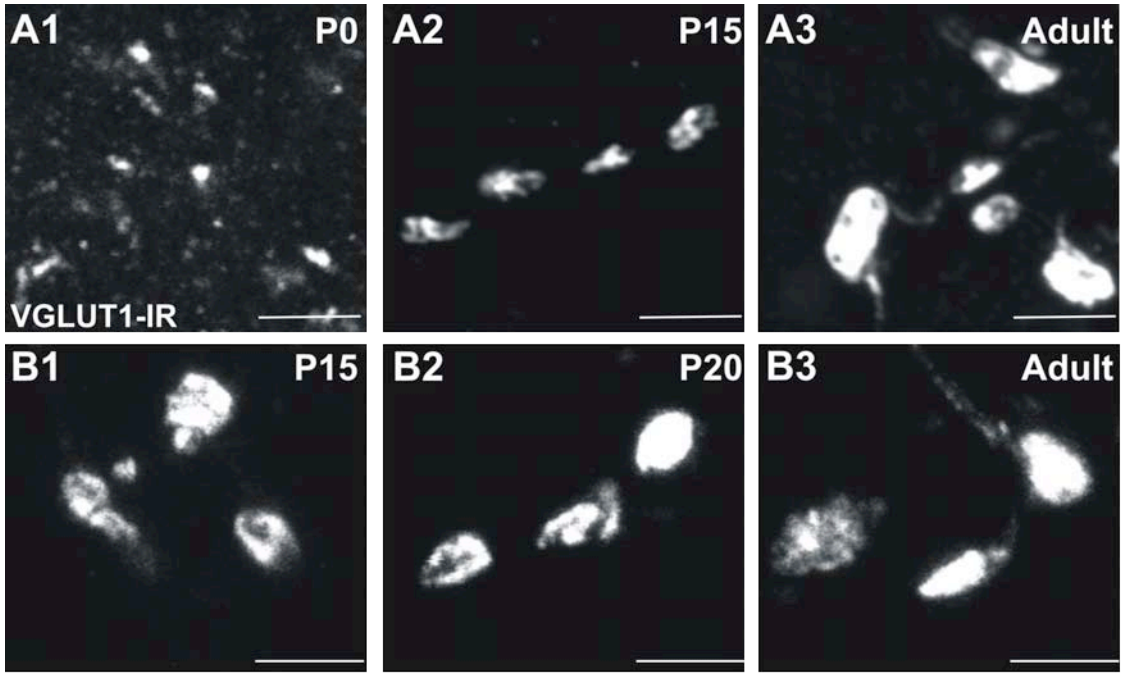
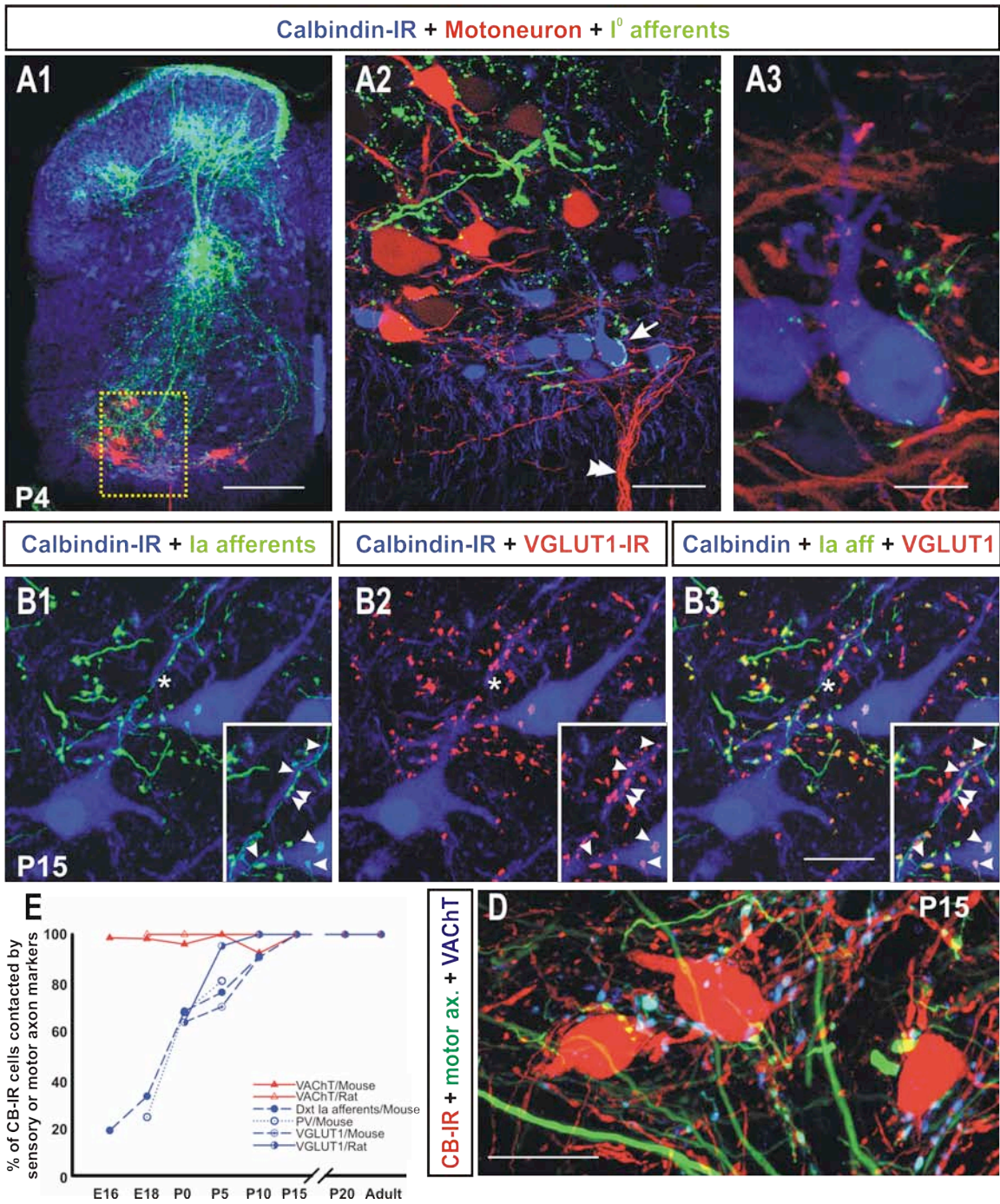


**Figure 14.** Convergence of sensory and motor axons inputs on Renshaw cells in the postnatal spinal cord. **A1**, Low magnification confocal image of a P4 spinal cord section with sensory afferent projections (FITC dextran, green) and motoneurons (MNs) and axons (Texas Red dextran, red) labeled from dorsal and ventral roots, respectively. Calbindin-IR is in blue (Cy5, blue). A group of intensely immunolabeled neurons is apparent at the ventral border of LVII (boxed area), which corresponds to the future adult Renshaw cells (Geiman et al., 2000). **A2**, Medium magnification image of the area indicated in A (box in A). MNs (red) and RCs (blue) are surrounded and contacted by primary afferent axons (green). In addition, RCs are also targeted by motor axons (red). Double arrowhead indicates the bundle of labeled motor axons exiting the spinal cord. **A3**, High magnification image of the RC indicated in B. This P4 Renshaw cell displays convergent inputs from motor axons (red, arrows) and primary afferents (arrowheads). The density of motor contacts is reduced compared to adult Renshaw cells (e.g., Alvarez et al., 1999), suggesting extensive postnatal proliferation of this input. **B**, High magnification confocal images from a P15, L5 spinal cord triple-immunolabeled to show sensory afferents (dextran-FITC), VGLUT1-IR varicosities (Cy3, red) and CB-IR RCs (blue). Sensory afferent axons at this age show varicosities that make contact with P15 RCs (B1, arrowheads in inset). The same RCs are contacted by VGLUT1-IR varicosities (B2, arrowheads in inset). Superimposition of both images shows that almost all sensory afferent varicosities in the P15 spinal cord contain VGLUT1-IR (B3, arrowheads in inset). **D**, High magnification image of P15 CB-IR RCs (red) in the area of the motor axon exit zone (labeled with dextran-FITC) and superimposed with VACHT (blue). This area contains a high density of motor axons with many varicosities. Fdxt-labeled motor axons co-localize with VACHT-IR varicosities (green plus blue) and often contact CB-IR RCs. **E**, Percentage of CB-IR cells receiving at least one contact from each of the markers used to identify dorsal and ventral root inputs. Numerical data is summarized in Table 1. In the embryo, almost all CB-IR RCs are contacted by VACHT-IR motor axons. In contrast, sensory afferent inputs are few in embryo, but spread to all RCs around P10-P15 (rat and mouse, respectively). PV = Parvalbumin. **Scale bars:** **A1** (in A1), 200  $\mu\text{m}$ ; **A2** (in A2), 40  $\mu\text{m}$ ; **B1-B3** and **D** (in B3 and D), 20  $\mu\text{m}$ ; **A3** (in A3), 10  $\mu\text{m}$ .







clusters) are present in the embryonic spinal cord before the establishment of primary afferent synapses (VGLUT1-IR clusters).

*Postnatal Renshaw cells receive convergent inputs from primary afferents and motor axon collaterals*

Next we investigated whether RCs receive convergent inputs from sensory afferents and motor axons. Almost all mouse and rat CB-IR neurons in the Renshaw cell area of E16, E18, P0, P5, P10, P15, P20, and adult spinal cords exhibited VACHT-IR contacts and/or contacts varicosities retrogradely labeled from ventral roots. Only VACHT-IR varicosities were used to estimate the number of RCs contacted by motor axons because although the retrograde labeling was excellent, only a proportion of VACHT-IR contacts were retrogradely labeled from ventral roots with any of the three fluorochrome-conjugated dxts used. A possible explanation is that many inputs entering via adjacent ventral roots are missed when labeling only one root. Also, motor axon collaterals were difficult to identify in embryonic spinal cords because the dense plexus of immature dendrites that, at this age, are thin and varicose and can be confused with axons without the aid of presynaptic markers. Therefore, reliable estimates of the number of RCs contacted by motor axons were obtained using estimates of contacts from VACHT-IR varicosities. We concluded that motor axon inputs have already spread to the whole RC population by E16 (Figure 14E). In contrast to motor axon inputs, inputs from primary afferents develop postnatally on RCs. In E16 spinal cords, only 18% of RCs (n = 53 CB-IR RCs/1 animal) were contacted by fdxt-filled sensory axons. By E18, ~24-34% of RCs were contacted by PV-IR or fdxt-filled sensory axons, respectively (PV, n =

41/1; fdxt, n = 77/2). Sensory axons express robust PV-IR at E18, but this is weaker at E16 and was not strong in all dextran filled afferent collaterals, therefore E16 estimates are based only on dxt-filled sensory axons. In neonates (P0/1), more than half of all RCs analyzed received contacts from sensory afferents with good agreement between all markers (fdxt = 68.2% (n = 90/2), PV = 67.7% (n = 49/2) and VGLUT1 = 63.6% (n = 11/1)). All CB-IR RCs analyzed were contacted by sensory axons by P10 (n = 21/2) or P15 (n = 20/2) for rat and mouse respectively. Therefore, we concluded that RCs are first contacted by motor axon inputs during the early embryonic period, and then convergent sensory axon inputs are established in late embryo and the perinatal period and spread to all RCs in the second postnatal week (numerical data summarized in Table 3).

Surprisingly, sensory axon synaptic contacts were retained by adult RCs in both rat and mouse.

*Adult Renshaw cells in cat, rats, and mice receive VGLUT1-IR inputs.*

To corroborate that the primary afferent inputs on RC are not a species specific phenomenon and restricted to rodents, we investigated cat RCs as described in the methods. Although cat RCs are much larger than mouse or rat RCs, they received a significantly larger number of VGLUT1-IR contacts per cell soma (~2 contacts per cell soma of mouse and rat, 14 contacts per cell soma for cat,  $p < 0.001$ , one-way ANOVA). The different number of VGLUT1-IR contacts is reflected in two-fold to four-fold increase in density over cat RCs compared, respectively, with mouse and rat (Figure 15). In conclusion, adult RCs in all species retain a significant number of VGLUT1-IR

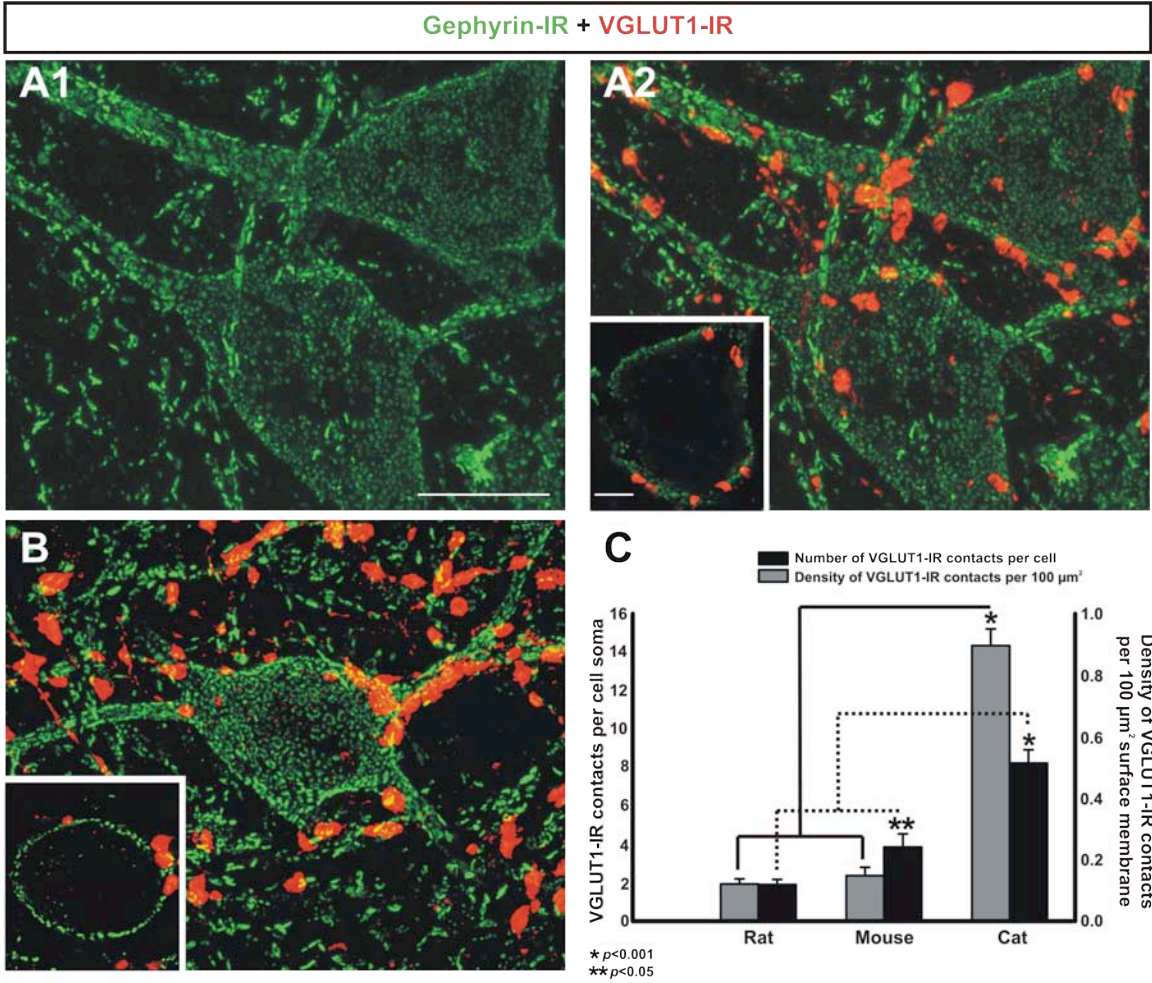
**Table 3.** Percentage of Calbindin-IR Renshaw cells contacted by different markers of sensory afferents and motor axon recurrent collaterals in mouse versus rat.

	<b>Mouse</b>				<b>Rat</b>	
<b>Age</b>	<b>Dorsal Root Dxt-filled</b>	<b>Parvalbumin</b>	<b>VGLUT1</b>	<b>VACHT</b>	<b>VGLUT1</b>	<b>VACHT</b>
<b>E16</b>	18.2% (53 cells/1) *	N.D. **	Not Present	98.6% (71 cells/1)	N.D.	N.D.
<b>E18</b>	32.9% (77 cells/2)	24.3% (41 cells/1)	Not Present	98.2% (59 cells/3)	N.D.	100% (35 cells/2)
<b>P0</b>	68.2% (90 cells/2)	67.7% (49 cells/2)	63.6% (11 cells/1)	96.6% (69 cells/1)	63.6% (11 cells/1)	100% (33 cells/1)
<b>P5</b>	76.0% (116 cells/2)	68.2% (52 cells/1)	70.0% (20 cells/2)	100% (6 cells/1)	95.2% (21 cells/2)	100% (25 cells/1)
<b>P10</b>	90.9% (75 cells/1)	N.D.	90.5% (21 cells/2)	92.3% (35 cells/3)	100% (21 cells/2)	100% (37 cells/2)
<b>P15</b>	N.D.	N.D.	100% (20 cells/2)	100% (11 cells/1)	100% (20 cells/2)	100% (27 cells/1)
<b>P20</b>	N.D.	N.D.	100% (30 cells/3)	100% (44 cells/2)	100% (30 cells/3)	100% (10 cells/1)
<b>Adult</b>	N.D.	N.D.	100% (30 cells/3)	100% (27 cells/1)	100% (30 cells/3)	100% (Alvarez et al., 1999)

\* N, Number of CB-IR RCs analyzed/Number of animals studied

\*\* N.D. = No data. The marker used was not present or suboptimal at this age

**Figure 15.** Density of VGLUT1-IR contacts on adult cat, rat, and mouse. **A**, High magnification image showing, in **A1**, surface reconstruction (23 optical planes,  $z$ -step = 0.5  $\mu\text{m}$ ) of two cat Renshaw cell somata and proximal dendrites identifiable by the high density of large, bright Gephyrin-IR clusters on their surface (FITC, green; Alvarez et al., 1997) and in **A2**, superimposed VGLUT1-IR contacts (Cy3, red). A single optical plane is shown in the inset. **B**, VGLUT1-IR contacts on Gephyrin-IR RC in the cat. **C**, Quantitative analysis of VGLUT1-IR contacts per cell soma and corresponding densities for rat, mouse, and cat Renshaw cells. Cat Renshaw cell surface area was approximated using an ellipsoid of the same long and short diameters. Cat Renshaw cells are significantly larger than rat and mouse Renshaw cells and receive a 10-fold larger number of VGLUT1-IR contacts per cell soma. Differences in number of contacts were highly significant (asterisk,  $p < 0.001$ , One-way ANOVA) between cat and rat/mouse, but not between rat and mouse. The different number of VGLUT1-IR contacts is reflected in 2 to 4-fold increase in density over cat Renshaw cells compared respectively to mouse and rat. Interestingly, significant differences ( $p < 0.05$ , asterisks) were also detected in VGLUT1-IR contact density between rat and mouse, despite similar numbers of contacts. This difference arises because distinct final sizes of adult rat and mouse Renshaw cell somata. **Scale bar:** **A** and **B** (in **A**), 20  $\mu\text{m}$ ; **insets**, 10  $\mu\text{m}$ .



sensory synapses. This conclusion is contrary to electrophysiological studies that failed to find evidence for this input.

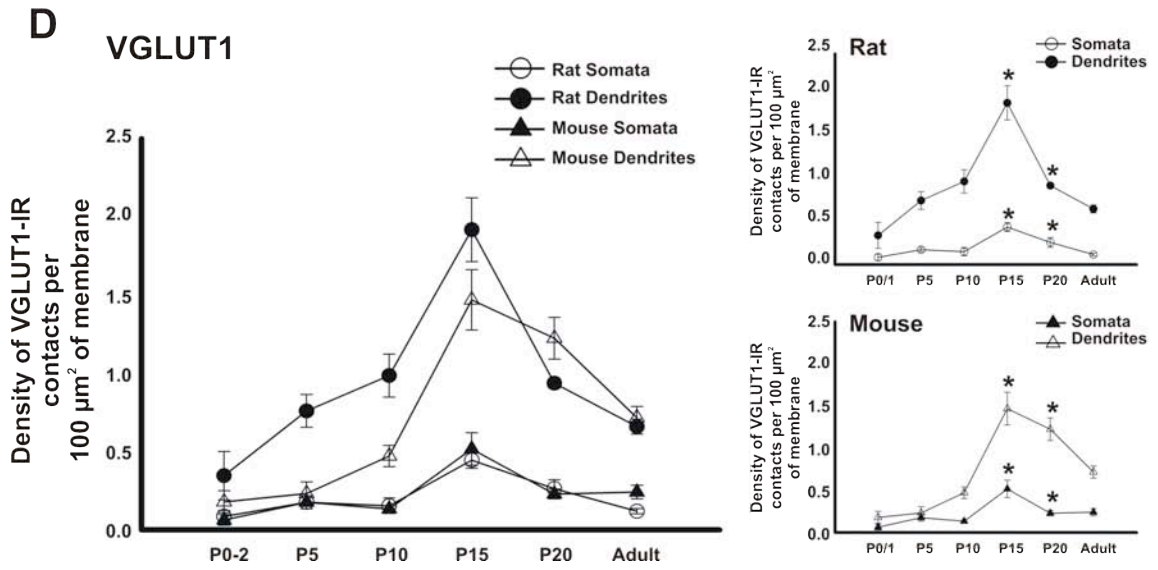
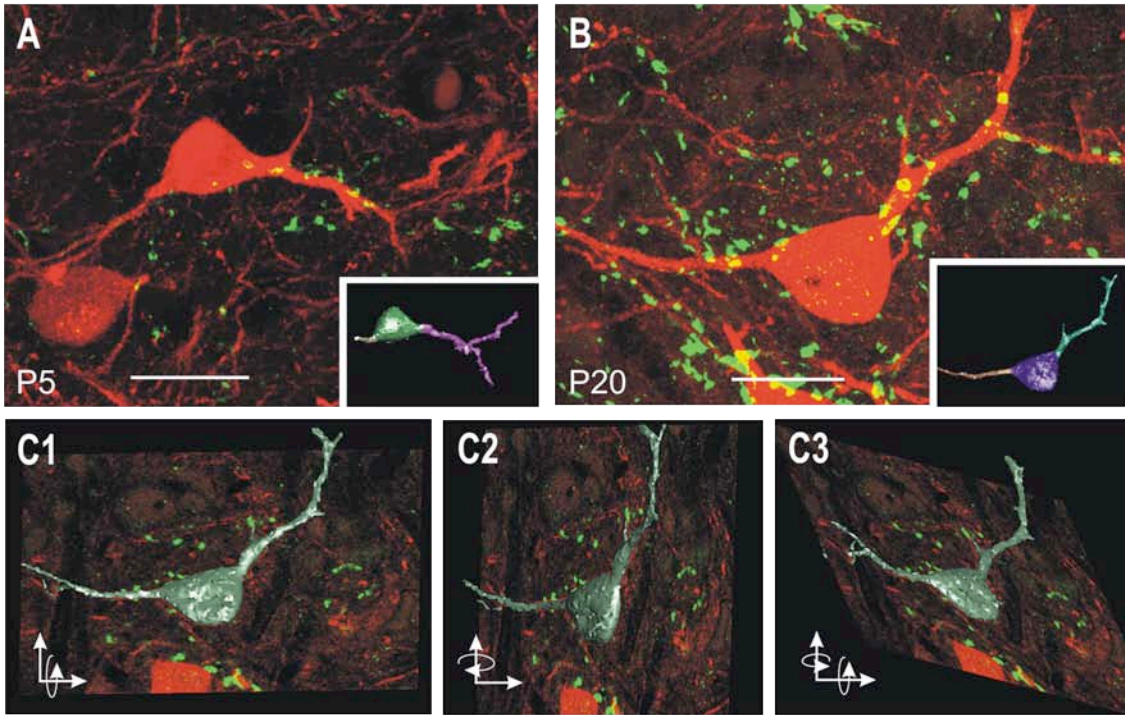
*In the early postnatal period, VGLUT1-IR and VAcHt-IR inputs proliferate on Renshaw cells, but after P15 VGLUT1-IR inputs decrease in density.*

We found that postnatal and adult RCs receive convergent inputs from primary afferents and motor axons, which contrasts with the generally accepted view that motor axons are the main source of excitatory inputs on RCs. One possibility is that each input displays different synaptic strengths in the adult. The strength of a synaptic input relies on the number of synapses, their distribution throughout the dendritic tree, and the synaptic efficacy of the individual synapses. Therefore, we investigated the number, density, and distribution of these inputs throughout development and in the adult.

Using 3D reconstructions of somata and proximal dendrites obtained from series of confocal optical sections (Figure 16), we looked at the relative densities of these inputs on postnatal RCs. For this purpose we used VGLUT1-IR as a marker of primary afferents and VAcHt-IR as a marker of motor axon collaterals in both mouse and rat of postnatal ages P0/1, P5, P10, P15, P20, and adult. The number of proximal dendritic segments analyzed ranged from one to four per cell. The relatively small field of view at the high magnification needed for “contact” identification and for CB-IR thresholding limited the maximum lengths of dendrite analyzed. The maximum dendritic lengths analyzed were also limited by age differences in dendrite immunolabeling. The average length of dendrite analyzed at P0/1 was  $26.1 \pm 1.5 \mu\text{m}$  ( $\pm\text{SEM}$ ) in rat and  $23.4 \pm 1.0 \mu\text{m}$

**Figure 16.** Development of VGLUT1-IR contacts on postnatal Renshaw cells. **A, B,** High magnification images of VGLUT1-IR (FITC, green) contacts on P5 (A) and P20 (B) CB-IR rat RCs (Cy3, red). Insets show 3D reconstructions of those same cells reconstructed using *3DSpace* software (Media Cybernetics). The analyzed regions (soma and dendrites) are color-coded. The density of VGLUT1-IR contacts in each of these regions was estimated as shown below in D. **C,** *3DSpace* 3D reconstruction of the P20 RC shown in B. The cell is shown in three different rotations. With the *3DSpace* software we scanned all optical planes containing VGLUT1-IR boutons over 3D reconstructions of the cells and the calculated number of contacts. The quantitative results are shown in D. **D,** Density of VGLUT1-IR contacts on the surface of somata and dendrites of CB-IR RCs of different ages. Overall densities increased from P0 to P15, (more rapidly after P10) and then decreased at P20. Similar results were obtained in rat and mouse spinal cords. One-way ANOVA tests indicated significant increases ( $P < 0.05$ ) from P0-P15 ages both species, and then a decrease in VGLUT1-IR contact density from P15-P20 to adult. **Scale bars:** **A** and **B** (in A and B), 20  $\mu\text{m}$ .

Calbindin-IR + VGLUT1- IR (I<sup>o</sup> afferents)





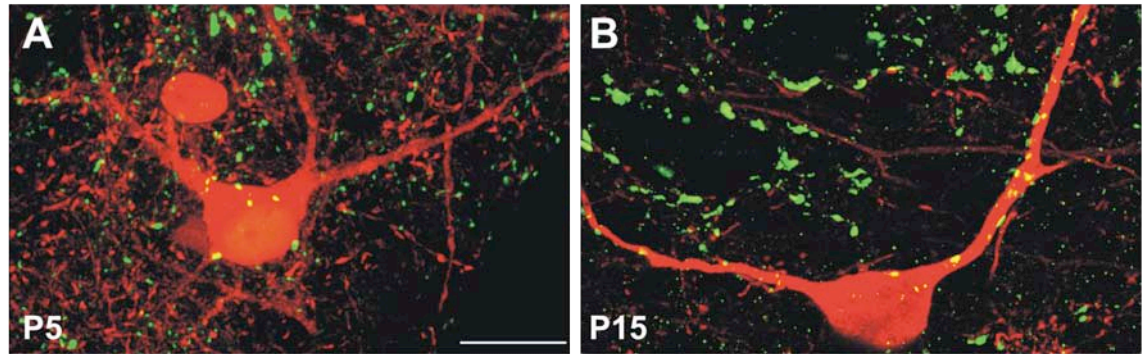
in mouse. The average dendritic length progressively increased at older ages, up to  $41.0 \pm 1.4$  and  $38.6 \pm 1.3$   $\mu\text{m}$  in adult rat and mouse RCs, respectively. The number of VGLUT1-IR and VAcHt-IR contacts per reconstructed soma or dendrite was then normalized against the total dendritic length (linear density) or total membrane surface of somata and dendrites (surface density).

More VGLUT1-IR and VAcHt-IR contacts were located on RC dendrites compared to somata, which correlated into higher density estimates on dendrites. Few VGLUT1-IR contacts were found on RC dendrites or somata at P0/1 in both rat and mouse. The density of VGLUT1-IR contacts increased significantly to P15 and then decreased in P20 and adult (Figure 16;  $p < 0.001$ , one-way ANOVA). Results were similar for both rat and mouse. ANOVA and *post hoc* analysis indicated that VGLUT1 densities at P15 were different to all other ages in both somata and dendrites ( $p < 0.05$ , *post hoc* Tukey's test). RC dendrites displayed a fivefold to sevenfold increase in VGLUT1-IR density from P0 to P15. Thereafter, VGLUT1-IR density decreased to less than half the P15 density in the adult. Although the density of VGLUT1-IR contacts decreased significantly after P15, over all the number of contacts per cell body or dendrite increased significantly from P0 (Rat soma =  $0.64 \pm 0.28$  contacts, rat dendrites =  $0.6 \pm 0.18$ ; mouse soma =  $0.4 \pm 0.2$ , mouse dendrites =  $0.54 \pm 0.22$ ) to adult (Rat soma =  $1.9 \pm 0.27$  contacts, rat dendrites =  $3.4 \pm 0.27$ ; mouse soma =  $2.4 \pm 0.25$ , mouse dendrites =  $3.97 \pm 0.28$ ) in both rat and mouse (average  $\pm$  SEM; Rat, soma  $p = 0.009$ , dendrites  $p \leq 0.001$ ; mouse, soma  $p = 0.008$ , dendrites  $p \leq 0.001$ ; t-tests) indicating a net gain of VGLUT1-IR contacts, which was reflected in generally higher synaptic densities in adult compared with P0.

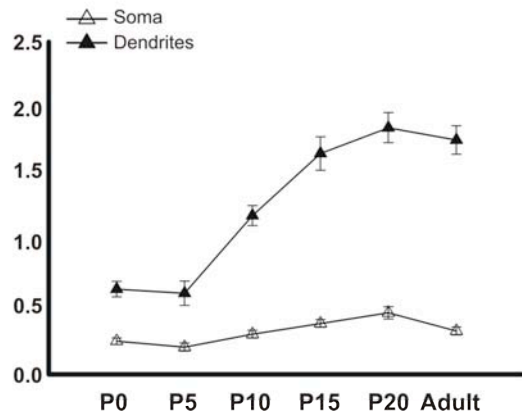
Next we investigated the density of VACHT-IR contacts on postnatal RCs in the rat. Analysis was not done in mouse because no significant species differences were observed in the density of VGLUT1-IR contacts between rat and mouse. The number of VACHT-IR contacts on RC somata and dendrites was significantly higher than VGLUT1-IR contacts at P0/1 (VACHT-IR contacts on soma =  $2.0 \pm 0.44$ , dendrites =  $1.96 \pm 0.29$ ;  $p < 0.01$ , t-test). This increased number of contacts resulted in VACHT-IR contacts being significantly denser than VGLUT1-IR contacts at P0 ( $p < 0.01$ , t test). Overall, VACHT-IR contact density increased from P0 to P15 in parallel with VGLUT1-IR contact density, but by difference to VGLUT1 contacts, the density of VACHT-IR motor axon synapses after P15 was maintained (Figure 17;  $p < 0.001$ , one-way ANOVA). *Post hoc* analysis indicates that VACHT-IR contact density increases from P5 to P15 ( $p < 0.05$ , *post hoc* Tukey's test), but no significant differences were detected between P0/P5 and P15/P20/adult ( $p > 0.05$  *post hoc* tests). The number and density of VACHT-IR contacts on adult rat Renshaw cells somata and dendrites are significantly higher than VGLUT1 ( $p \leq 0.001$ , t tests). Therefore, we concluded that the density of sensory afferent synapses on RCs first increases postnatally and then decreases after P15. In contrast the density of motor axon synapses increases in parallel during the first two postnatal weeks and it is thereafter maintained (Numerical data summarized in Table 4). One question is whether the decreases observed in VGLUT1-IR contact density are due to a decrease in the number of synapses or a redistribution of the synapses to more distal locations that could not be analyzed with confocal microscopy and the *3DSpace* software.

**Figure 17.** Density of VGLUT1-IR contacts on Renshaw cells compared to VAcHT-IR contacts. **A-B**, High magnification images of P5 (A) and P15 (B) Calbindin-IR RCs (Cy3, red) with VAcHT-IR (FITC, green) contacts. Arrowheads indicate VAcHT-IR contacts on RC dendrites. The number of VAcHT-IR contacts on RCs increases from P5 to P15, and is maintained after P15 in the adult. **C**, Density of VAcHT-IR contacts on the surface of somata and dendrites of CB-IR RCs of different ages. The density of VAcHT-IR contacts on RC somata and dendrites increases significantly from P0 to P15 and is maintained after P15 ( $p < 0.05$ , one-way ANOVA). No significant differences were detected between P15, P20, and adult (Soma,  $p = 0.068$ ; dendrites,  $p = 0.571$ , one-way ANOVA). **D**, Density of VGLUT1-IR and VAcHT-IR contacts on CB-IR RCs of different ages. The density of VGLUT1-IR and VAcHT-IR contacts on both the somata and dendrites of Renshaw cells increases significantly from P0 to P15 ( $p < 0.05$ , one-way ANOVA). The density of VGLUT1-IR contacts decreases after P15. In contrast, the density of VAcHT-IR contacts increases until P15 and then stabilizes at P20 and in the adult. **Scale bars:** A and B (in A), 20  $\mu\text{m}$ .

Calbindin-IR + VAcHt-IR (Motor axon recurrent collaterals)



**C** VAcHt-IR contacts per 100  $\mu\text{m}^2$  of surface membrane



**D** Number of contacts per 100  $\mu\text{m}^2$  of surface membrane

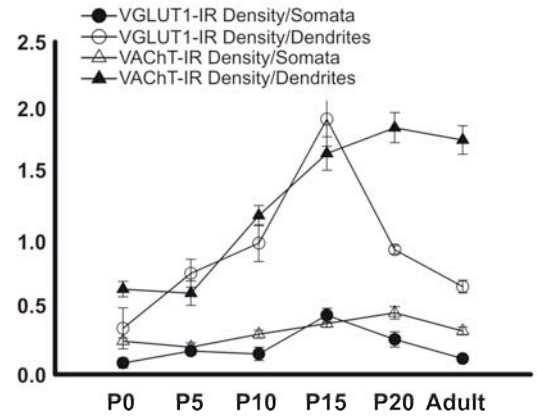


**Table 4.** Number and density (contacts per 100  $\mu\text{m}^2$ ) of VGLUT1-IR and VAcHT-IR contacts on Calbindin-IR rat Renshaw cells during postnatal development.

Age	# of VGLUT1-IR contacts ( <sup>*</sup> Soma <sup>**</sup> Dendrites)	VGLUT1-IR contact density ( <sup>*</sup> Soma <sup>**</sup> Dendrites)	N	# of VAcHT-IR contacts ( <sup>*</sup> Soma <sup>**</sup> Dendrites)	VAcHT-IR contact density ( <sup>*</sup> Soma <sup>**</sup> Dendrites)	N
P0	<sup>*</sup> 0.64 ± 0.24 <sup>**</sup> 0.61 ± 0.18	<sup>*</sup> 0.09 ± 0.09 <sup>**</sup> 0.35 ± 0.18	(13,1)	<sup>*</sup> 2.0 ± 0.44 <sup>**</sup> 1.96 ± 0.29	<sup>*</sup> 0.25 ± 0.02 <sup>**</sup> 0.64 ± 0.06	(10,1)
P5	1.75 ± 0.30 2.12 ± 0.25	0.18 ± 0.09 0.76 ± 0.19	(20,2)	2.0 ± 0.47 2.85 ± 0.47	0.20 ± 0.15 0.61 ± 0.22	(9,1)
P10	1.67 ± 0.28 3.43 ± 0.34	0.18 ± 0.09 0.99 ± 0.22	(21,2)	3.2 ± 0.57 5.44 ± 0.58	0.30 ± 0.17 1.19 ± 0.27	(10,1)
P15	4.65 ± 0.48 6.0 ± 0.39	0.44 ± 0.15 1.91 ± 0.31	(20,2)	3.8 ± 0.62 7.12 ± 0.65	0.38 ± 0.20 1.66 ± 0.31	(10,1)
P20	1.08 ± 0.03 3.86 ± 0.33	0.13 ± 0.08 0.94 ± 0.22	(30,3)	5.4 ± 0.73 12.8 ± 0.99	0.46 ± 0.22 1.85 ± 0.38	(10,1)
Adult	1.93 ± 0.26 3.38 ± 0.27	0.12 ± 0.06 0.66 ± 0.15	(30,3)	5.0 ± 0.71 10.93 ± 0.83	0.33 ± 0.18 1.76 ± 0.30	(10,1)

Data for rat only

N, Number of Renshaw Cells analyzed/Number of animals studied

We investigated the density of VGLUT1-IR and VAcHt-IR contacts on more distal segments of CB-IR RC dendrites visualized using dual-color immunoperoxidase. VGLUT1-IR and VAcHt-IR boutons were labeled with silver-intensified DAB (black) and CB-immunoreactivity with non-intensified DAB (brown) (Figure 18). Using a neuron tracing system (NeuroLucida) and Sholl analysis (Figure 18E), we studied VGLUT1-IR and VAcHt-IR synaptic densities at different distances from the cell body. We determined that VGLUT1-IR linear density on dendrites decreased from P15 to adult by 28% overall and this decrease was significant ( $p < 0.05$ , one-way ANOVA). This decrease was similarly distributed throughout the whole dendritic arbors (Figure 19). It is important to note that the decrease in VGLUT1-IR density was not accompanied by a significant decrease in the total number of contacts per cell (P15 =  $26.48 \pm 1.77$  contacts per cell compared to adult =  $23.53 \pm 1.25$ ,  $p = 0.173$ ,  $t$  test), therefore the decreased density is not explained by the removal of contacts, but by the increased size of the dendritic arbor (Total dendritic length sampled, P15 =  $204.31 \pm 14.44$   $\mu\text{m}$  and adult =  $253.48 \pm 15.98$   $\mu\text{m}$ ). In contrast, VAcHt-IR contact density remained constant in all dendritic compartments from P15 to adult ( $p > 0.05$ , one-way ANOVA). VAcHt-IR synaptic density was maintained because of a significant increase in the total number of contacts with development (P15 =  $27 \pm 2.05$  and adult =  $34.63 \pm 3.09$ ,  $p < 0.01$ ,  $t$  test) that matched the increase in dendritic length (numerical data summarized in Tables 5 and 6).

In conclusion, the motor axon VAcHt-IR synaptic input appears to proliferate and match the development of the RCs dendritic arbor. In contrast, the sensory afferent VGLUT1-IR synaptic input appears to arrest its proliferation and maturation around P15.

**Figure 18.** Brightfield preparations and NeuroLucida 3D reconstructions used to analyze VGLUT1-IR and VACHT-IR contact density on Renshaw cell distal dendritic segments. **A-D**, Calbindin-IR Renshaw cells (brown reaction product, DAB) at P15 (A,B) and in the adult (C,D) contacted by VGLUT1-IR boutons (black, silver-intensified DAB) in A and B or VACHT (also black, silver-intensified DAB) in C and D. Boxes indicate areas of RC dendrite with immunoreactive contacts shown at higher magnification in insets. Both VGLUT1-IR and VACHT-IR boutons preferentially target dendritic arbors. The number of VGLUT1-IR and VACHT-IR contacts on RCs at P15 appears similar, but VGLUT1-IR contact density is reduced in the adult. **E**, 3D reconstruction of a CB-IR RC at P15 with VGLUT1-IR contacts plotted on the reconstruction. Dotted circles represent the Sholl bins, which begin from the center of the cell soma (50  $\mu$ m bins). The black dotted circles represent the distances analyzed in this study. Although this cell has dendritic segments that extend into the 200-250 and 250-300  $\mu$ m bin (indicated by blue dotted circles), most cells analyzed did not. Therefore these bins were excluded from further analysis. **Scale bars: A-D** (in B), 50  $\mu$ m.

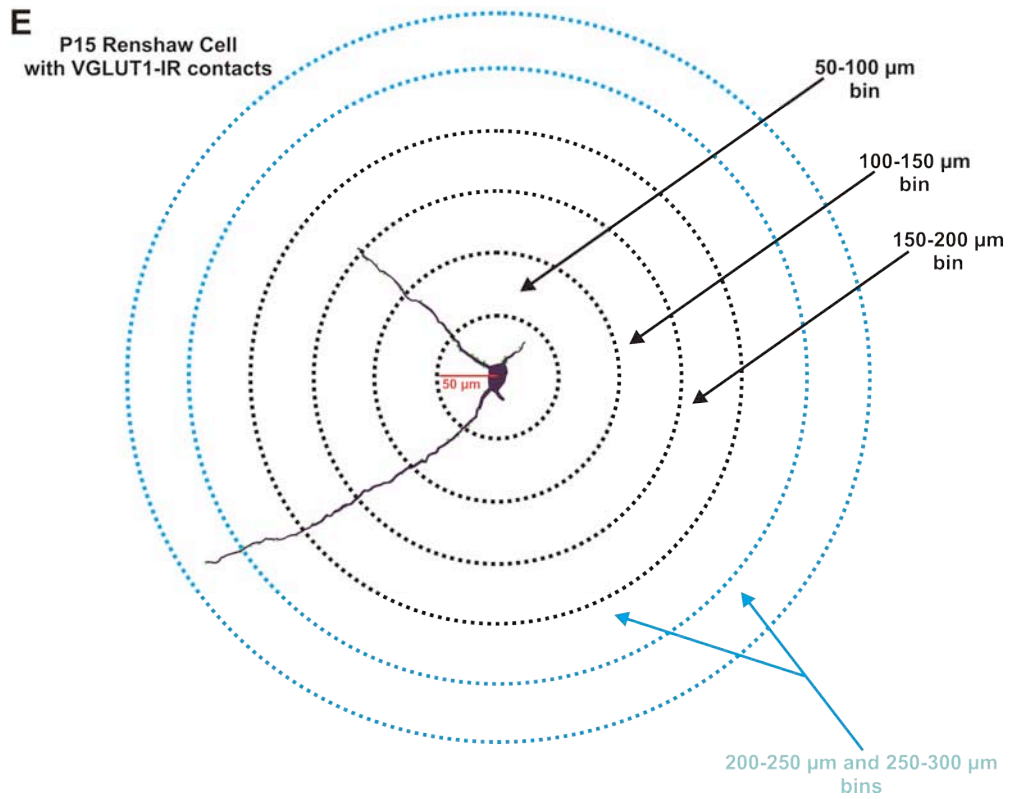
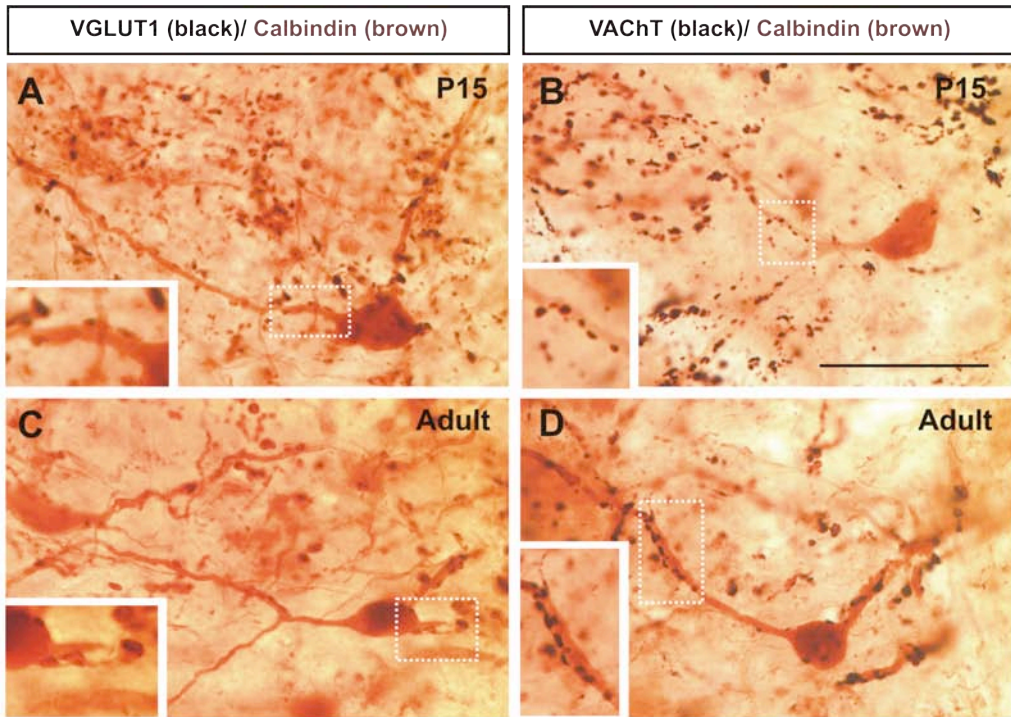




**Figure 19.** Density and distribution of VGLUT1-IR and VAcHT-IR contacts on mature Renshaw cells. **A**, Sholl analysis of VGLUT1-IR contacts on RC dendrites (per 10  $\mu\text{m}$  of linear dendrite). Numbers in parentheses indicate the number of cells that showed data in each distance bin. Too few dendrites/Renshaw cells provided data beyond 200  $\mu\text{m}$ , and therefore these bins were not analyzed further. A decrease in the number of VGLUT1-IR contacts per 10  $\mu\text{m}$  of linear dendrite was apparent in most distance bins (except for the 50 –100  $\mu\text{m}$  bin), indicating that there are no major shifts in VGLUT1-IR bouton distributions at different distances from the cell soma. **B**, Similar analyses for VAcHT-IR contacts. In contrast to VGLUT1-IR boutons, VAcHT-IR bouton density was either maintained or had a tendency to increase at P20 and adult compared with P15.

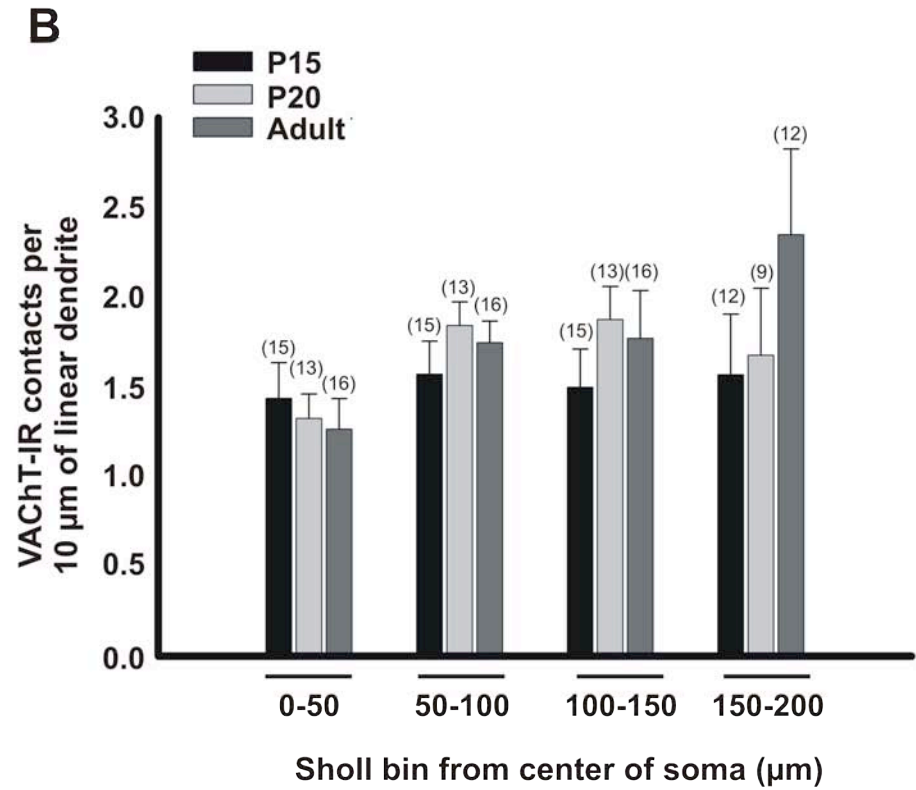
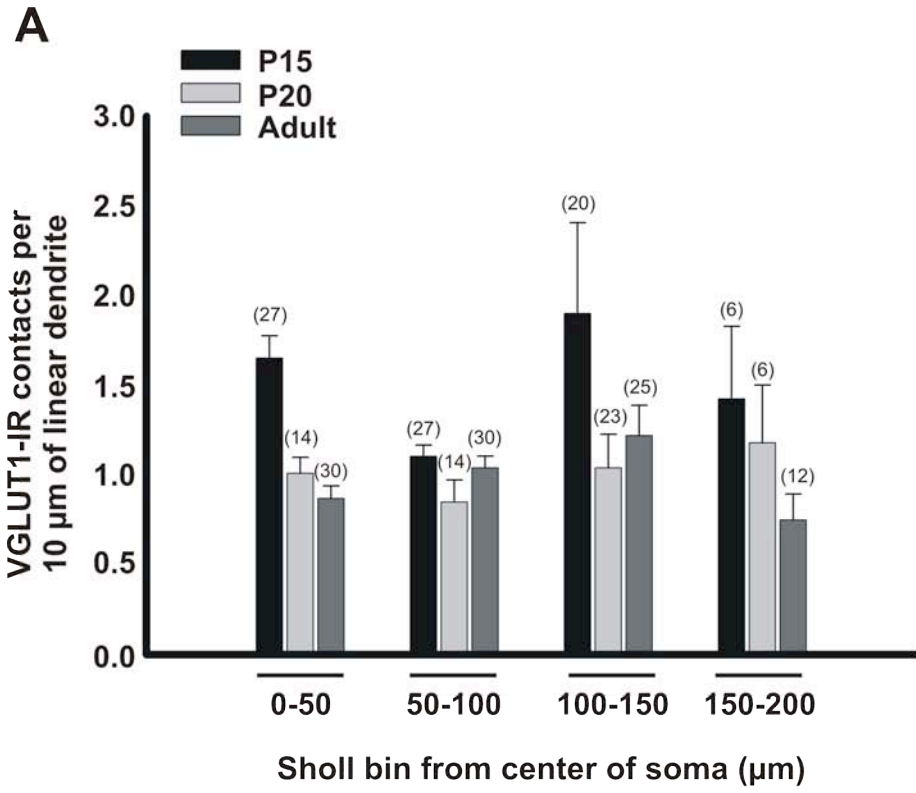


**Table 5. VGLUT1-IR bouton contact density and dendritic arbors of Renshaw cells of different ages**

	Most Distal Dendritic Point ( $\mu\text{m}$ )	Average Dendritic Length ( $\mu\text{m}$ )	Average Total Length of Dendritic Arbor ( $\mu\text{m}$ )	Average # of First-Order Dendrites	Average # of Ends	VGLUT1-IR Contacts per 10 $\mu\text{m}$ of Dendrite	Total # VGLUT1-IR contacts per cell	<i>n</i>
P15	283.90	131.60 $\pm$ 8.43	204.31 $\pm$ 14.44	2.04 $\pm$ 0.19	2.85 $\pm$ 0.24	1.34 $\pm$ 0.07	26.48 $\pm$ 1.77	27
P20	266.80	149.16 $\pm$ 13.65	210.79 $\pm$ 14.04	1.86 $\pm$ 0.21	3.00 $\pm$ 0.31	0.95 $\pm$ 0.08	19.64 $\pm$ 1.81	14
Adult	320.10	150.29 $\pm$ 9.86	253.48 $\pm$ 15.98	2.47 $\pm$ 0.29	3.43 $\pm$ 0.19	0.97 $\pm$ 0.05	23.53 $\pm$ 1.25	30

$\pm$  indicates SEM.

*n* = Number of Renshaw cells sampled

**Table 5. VACHT-IR bouton contact density and dendritic arbors of Renshaw cells of different ages**

	Most Distal Dendritic Point ( $\mu\text{m}$ )	Average Dendritic Length ( $\mu\text{m}$ )	Average Total Length of Dendritic Arbor ( $\mu\text{m}$ )	Average # of First-Order Dendrites	Average # of Ends	VACHT-IR Contacts per 10 $\mu\text{m}$ of Dendrite	Total # VACHT-IR contacts per cell	<i>n</i>
P15	187.20	122.90 $\pm$ 8.58	188.77 $\pm$ 15.56	2.00 $\pm$ 0.17	3.00 $\pm$ 0.35	1.47 $\pm$ 0.11	27.00 $\pm$ 2.05	15
P20	191.00	125.54 $\pm$ 19.45	202.69 $\pm$ 19.45	2.31 $\pm$ 0.13	3.15 $\pm$ 0.22	1.72 $\pm$ 0.18	30.92 $\pm$ 2.81	13
Adult	256.80	139.03 $\pm$ 12.28	231.88 $\pm$ 19.99	2.13 $\pm$ 0.20	3.44 $\pm$ 0.29	1.54 $\pm$ 0.08	34.63 $\pm$ 3.09	16

$\pm$  indicates SEM.

*n* = Number of Renshaw cells sampled

At this time the animal starts to display weight-bearing locomotion. This sudden stop in the formation of new synapses might reflect a process of functional de-selection of this input, by difference to the motor axons which continue to establish more synapses that likely strengthens this input.

## **Discussion**

The main findings of this aim confirm the hypothesis that embryonic and postnatal Renshaw cells receive convergent inputs from sensory afferents and motor axons recurrent collaterals. In addition, two other fundamental observations were made: 1) Motor axon inputs are already established by E16, the age at which sensory synapses arrive in the ventral horn, 2) Sensory synapses are physically retained in adult RCs, although their density decreases with development. These results suggest that there are differences in RC competence to receive and maintain inputs from motor axon recurrent collaterals, and sensory afferents compared to other ventral interneurons.

*Anatomical and electrophysiological evidence for presence of sensory afferent inputs on neonatal Renshaw cells.*

Our findings indicate that RCs receive inputs from sensory afferents and that these inputs are retained in the adult. This contrasts with previous studies that indicated that RCs lack monosynaptic inputs from sensory afferents. This conclusion was mainly derived from electrophysiological recordings in the cat spinal cord, in which dorsal root volleys failed to elicit responses in RCs (Renshaw, 1946; Curtis and Ryall, 1966). Although, when larger stimuli were applied, a response was evoked, the nature of these

responses was not addressed further and was usually considered polysynaptic. Few anatomical studies investigated whether RCs receive monosynaptic inputs from sensory afferents. In one study using electron microscopy, Lagerback and Ronnevi (1982) described synapses on cat RCs that were ultrastructurally similar to Ia afferent synapses on motoneurons in that they received axo-axonic contacts (Conradi et al., 1983; Fyffe and Light, 1984; Pierce and Mendell, 1993). However, at that time it was unknown if presynaptic axo-axonic synapses were specifically found only on primary afferent synapses. Today we know that the synapses identified by Lagerback and Ronnevi (1982) are very likely Ia afferent synapses.

We found that RCs are first contacted by sensory afferents during late embryonic development (E16-E18). Very few embryonic RCs are contacted but most (90-100%) are contacted by P10. When compared to the development of the Ia-motoneuron synaptic connection, the development of sensory afferent inputs on RCs appears to be delayed (for review, see Chen and Frank, 1999). Ia afferents enter the ventral horn around E15 (Ozaki and Snider, 1997; Chen and Frank, 1999) and by E16 a monosynaptic reflex is functional (Kudo and Yamada, 1987). Monosynaptic Ia-EPSPs can be recorded from most MNs in rodent embryos and before birth (Ziskind Conheim, 1990). The delay in establishing synapses with RCs could be due to the location of RCs in the ventralmost portion of lamina VII. MNs are located in lamina IX and extend dendrites throughout LVII and therefore the Ia axons do not have to project as ventrally to establish synapses on them. Also, because of the very ventral location of RCs, the sensory afferents identified most likely belong to Ia proprioceptors. Ia afferents are the only sensory afferents that project this ventral in the spinal cord (Brown and Fyffe, 1978 and 1979).

The lack of VGLUT1-IR in sensory afferent varicosities contacting embryonic RCs (and lack of VGLUT1-IR in the spinal cord during embryonic development) suggests a very immature synapse. It is not until P0 that the first detectable VGLUT1-IR clusters are observed and significantly mature during the first two postnatal weeks. It is possible that our detection methods are not sensitive enough to detect small amounts of VGLUT1 antibody present. Also, it is possible that there is a subtype switch from one transporter in embryo to VGLUT1 postnatally. An *in vivo* study demonstrated that parallel fibers innervating Purkinje cells in the cerebellum switch from expressing VGLUT2 to VGLUT1 during development (Miyazaki et al., 2003). Although this study looked at subtype switches during postnatal development, it is possible that a similar switch occurs in sensory afferents, but during late embryonic development. Preliminary observations suggest that VGLUT2 might be present in embryonic proprioceptive sensory primary afferents identified with PV-immunoreactivity, but further studies are necessary to prove a possible switch.

Our collaborator Dr. George Mentis attempted to discern whether the sensory afferent inputs anatomically identified on neonatal RCs were indeed functional and evoked monosynaptic EPSPs. Using an *in vitro* neonatal mouse spinal cord preparation, Dr. Mentis was able to record from RCs and ventral roots while simultaneously stimulating the dorsal roots. Dorsal roots evoked EPSPs on RCs and at stimulus strengths two times threshold for EPSPs, they consistently evoked firing (Mentis et al., 2006). The latency of RC's early response did not change when the stimulus intensity or the frequency is increased and the latency of the RC early response to dorsal root stimulation equaled that of the MN. In addition, cholinergic receptor blockers

mecamylamine, dH $\beta$ E, and atropine failed to abolish the dorsal-root evoked potential in RCs. All these observations suggest that the response is not polysynaptic, but a monosynaptic response. Furthermore, application of glutamatergic receptor antagonists (APV and CNQX) reversibly abolished the dorsal-root evoked potentials on RCs. Therefore, the anatomical sensory afferent inputs we analyzed on RCs, in the neonate, represent functional monosynaptic glutamatergic primary afferent inputs. The question is then why functional inputs from dorsal roots are not observed in adult spinal cord preparations.

#### *Postnatal development of sensory afferent synapses on Renshaw cells*

Synaptic strength corresponds to the amount of influence one neuron's firing has on another neuron's firing and can be altered at the presynaptic or the postsynaptic level (Burke, 1987). Presynaptic factors that can affect synaptic strength include the number of presynaptic boutons, the distribution of those boutons along the soma-dendritic membrane of the postsynaptic cell, and the amount of neurotransmitter released from each terminal to name a few. Postsynaptic factors include the total membrane over which synapses are distributed, the number of receptors and the efficacy with which ligands activate those receptors. Dorsal root afferent stimulation at suprathreshold levels evoked robust firing in neonatal RCs, but we demonstrated, using anatomical techniques, that the strength of the sensory afferent input on RCs likely decreases with maturation after the second postnatal week. First, the density of VGLUT1-IR inputs on RCs increases significantly from P0 to P15; but after P15, significantly decreases. We found that the decrease from P15 to P20 and in the adult is not due to a decrease in the number of



contacts or a re-distribution to more distal dendritic segments, but a failure to add synapses during development to match the growth of the dendritic arbor. Second, Ia afferent synapses on RCs could possibly be shunted by the development of strong inhibitory synapses after P10 (Geiman et al., 2000; Gonzalez-Forero and Alvarez, 2005). RCs receive an unusually high density of inhibitory synapses on their soma and proximal dendrites that have large gephyrin-IR clusters with a high density of postsynaptic receptors and display large postsynaptic currents. All of which suggest a greater inhibitory synaptic strength.

Moreover, studies from our lab using electron microscopy suggest that the synaptic machinery of VGLUT1-IR primary afferents on Renshaw cells partially regresses from P15 to adult. This conclusion is based on comparison of the size of boutons (cross-sectional area, perimeter and length of apposition with postsynaptic membrane), the number of Postsynaptic Densities (PSDs) and their lengths. Pierce and Mendell (1993) proposed that Ia synapse release properties and synaptic strength correlates with the size of the presynaptic Ia afferent bouton and postsynaptic density (PSD) apposing the Ia afferent. At P15 there were no differences in bouton size or PSD average length between VGLUT1-IR synapses contacting MNs and RCs. However, PSDs opposite to VGLUT1-IR boutons were significantly smaller and fewer over adult RCs compared to either P15 VGLUT1 synapses on RCs or adult VGLUT1 synapses on MNs (Mentis et al., 2006; Figure 20). Therefore, it appears that although the primary afferent input on RCs is not removed, part of the mechanism for “functionally” silencing might be based on partial removal of the synaptic machinery. It is possible then that the same mechanisms involved in synapse elimination also work during synaptic maturation

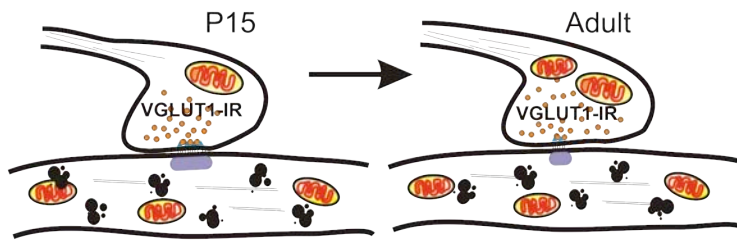
of these synapses and result in synaptic weakening. Synaptic weakening is manifested by decreases in presynaptic bouton size and is believed to be associated with the removal of postsynaptic receptors at sites of vacated or weakened synapses during synapse elimination (Lichtman and Colman, 2000; Walsh and Lichtman, 2003). If the size of Ia afferent terminals correlates with synaptic strength, then the results suggest arrested maturation and decreased synaptic efficacy of VGLUT1-IR synapses on RCs after P15 and in the adult. As mentioned previously, RCs were believed to lack sensory afferent inputs and these conclusions were based on in vivo electrophysiological recordings in the cat (Renshaw, 1946; Curtis and Ryall, 1966) where dorsal root volleys failed to elicit responses. An alternative explanation could be that there are species differences in the projection of sensory afferents onto RCs. However, we demonstrated that, similar to rodents, VGLUT1-IR boutons contact RCs in the adult cat. In fact, in the somato-dendritic regions accessible to analysis in our histological preparations, VGLUT1-IR inputs were denser in cat RCs than in rodent RCs. Therefore, it is possible that the sensory afferent inputs on cat RCs, similar to those seen on adult mouse and rat RCs, are functionally silent or weakened and subthreshold.

Based on the above information, Ricardo Zerda in our lab investigated whether primary afferent inputs on RCs become silenced by postsynaptic removal of AMPA receptors (Isaac, 2003; Voronin & Cherubini, 2004). Synapses without AMPA receptors (AMPA) are inactive, or “silent” under normal conditions. Preliminary studies in our lab demonstrated that RCs express GluR4 and GluR2 AMPA subunits postsynaptically. Using electron microscopy employing postembedding quantitative colloidal gold techniques, it was found that the number of AMPA receptors on RCs postsynaptic to

**Figure 20.** Summary of electron microscopy data of VGLUT1-IR bouton sizes and the postsynaptic densities apposing those boutons on Calbindin-IR and non-CB-IR dendrites at P15 and in the adult. **A,** The development of VGLUT1-IR boutons apposing CB-IR dendrites. No differences were detected in the average bouton size, length of the apposition and number of active zones at P15 and in the adult. In contrast, the length of the PSD decreased significantly in the adult compared to P15. **B,** Development of VGLUT1-IR boutons apposing non CB-IR dendrites. Unlike those boutons apposing CB-IR dendrites, VGLUT1-IR boutons contacting non CB-IR dendrites increased significantly in size. Also, the number of active zones and the length of the apposition increased significantly from P15 to adult. Therefore, the synaptic machinery of VGLUT1-IR Ia afferents on RCs partially regresses from P15 to adult, which may be the mechanism responsible for “functionally” silencing these inputs on RCs.

**A**

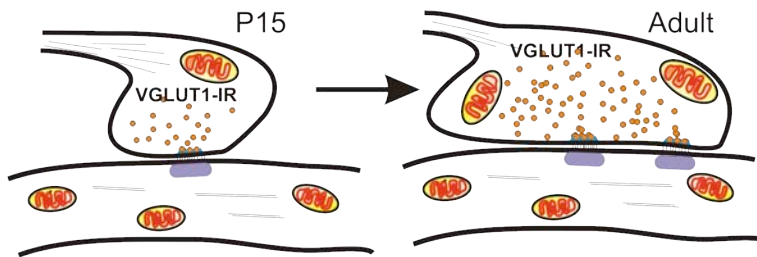
**Calbindin-IR dendrites**



- ≡ Bouton size
- ≡ APP length
- ↓ PSD / AZ length
- ≡ PSD / AZ numbers

**B**

**Non calbindin-IR dendrites**



- ↑ Bouton size
- ↑ APP length
- ≡ PSD / AZ length
- ↑ PSD / AZ numbers

Courtesy of Dr. Francisco Alvarez

VGLUT1-IR terminals decreased by more than half from P15 to adult. Therefore, it appears that the decrease in the number of AMPA receptors and the partial removal of synaptic machinery are part of a mechanism that renders sensory afferent inputs contacting RCs “functionally silent” synapses.

*Motor axon synapse development on Renshaw cells*

In contrast to sensory afferent inputs, all RCs analyzed during late embryonic development (E16-E18) received inputs from motor axon recurrent collaterals. Motor axon inputs developed in parallel to sensory afferents, but unlike those from sensory afferents, after P15, their synaptic density was maintained at P20 and in the adult. Maintenance of high synaptic density explains why motor axon inputs on RCs remain functional in the adult. Inputs from motor axons were shown to modulate the development of inhibitory synapses on RCs (Gonzalez-Forero et al., 2005). In an elaborate set of experiments, either tetanus (TeNT) or botulinum neurotoxins (BoNT-A) were injected into the gastrocnemius muscle of P5 rats in order to increase (TeNT) or decrease (BoNT-A) motor firing. They found that increasing motor firing with TeNT resulted in larger gephyrin clustering and larger inhibitory synaptic currents in RCs, whereas BoNT injections resulted in decreased motor firing and decreased gephyrin clustering in RCs. From these experiments, it was concluded that the strength of inhibitory synapses on RCs was modulated by motor axon firing as a possible mechanism to match excitatory and inhibitory input strengths during development. Therefore, it is possible that the motor axon input development strengthens inhibitory synapses, and this in turn suppresses sensory afferent inputs on RCs. A possible outcome of this process is

that the weaker inputs from sensory synapses now become unmatched to the strength of inhibitory synapses and thus functionally silenced. This would accelerate the weakening of sensory synapses if they behave in a typical Hebbian fashion. This means that synaptic inputs whose activity does not correlate with postsynaptic firing becomes further weakened and eventually partially disassembled and/or eliminated (Hebb, 1949).

By late embryonic development (later than E15), all RCs analyzed were contacted by motor axon inputs suggesting that this input is established on RCs during early embryogenesis.

#### *Diversification of V1-derived interneurons*

The present evidence suggests that final synaptic organization in RCs occurs because suppression or enhancement of certain inputs during postnatal development. The data presented in this aim raises the possibility of a “generic” V1-derived interneuron (V1-IN) with projections from both sensory and motor inputs (Figure 21). The idea of a “generic” V1-IN seems plausible because most V1-INs are located in regions of the spinal cord that are enriched in proprioceptive sensory afferents (Alvarez et al., 2005). According to this view, RCs could therefore diversify themselves from the “generic” V1-IN subclass by weakening sensory afferent inputs and strengthening those from motor axons. However we will see in aim 3 that the proposal of a “generic” V1-IN is not entirely correct.

In conclusion, we present evidence that RCs receive sensory afferent inputs during late embryonic development, which proliferates and matures until P15; after which it becomes “functionally de-selected”. We also present evidence that by E16, all

RCs receive inputs from motor axons. Motor axons inputs proliferate during postnatal development and are maintained in the adult by matching the development of the dendritic arbor.

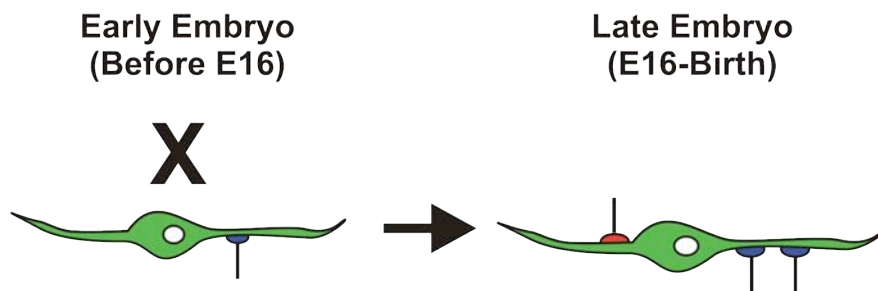
**Figure 21.** Schematic depicting developmental changes in the strength of sensory afferent (Ia afferents) and motor axon inputs on Renshaw cells. Changes can be divided into two stages; an embryonic (A) and a postnatal (B) developmental stage. **A,** Embryonic development of Ia afferents and motor axons on RCs. The embryonic developmental stage can be further divided into an early embryonic stage (before E16) and a late embryonic stage (E16-birth). During the early embryonic stage, RCs do not receive inputs from Ia afferents, but inputs from motor axons have already spread to all RCs by this stage. The first Ia afferent inputs on RCs are not observed until later embryonic stages, but even during this stage, very few RCs are contacted. **B,** Similar to the embryonic developmental stage, the postnatal development stage can be divided into an early (P0-P15) and late (P20-adult) stage. During early postnatal development, the density of Ia afferent and motor axons inputs develops in parallel. Significant differences are not detected until late postnatal development, when Ia afferent input density decreases significantly and the density of motor axons is maintained. We concluded that the decrease seen in late postnatal development is not due to a re-distribution of Ia afferent inputs to more distal locations, but a lack of adding new synapses to match the development of the RC dendritic arbor.



**A**

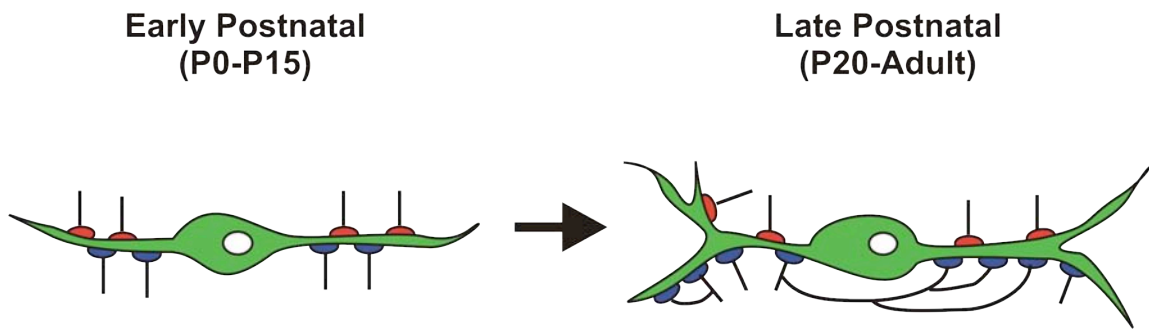
**Embryonic Development**

- Ia Proprioceptive Primary Afferents
- Motor Axons Recurrent Collaterals



**B**

**Postnatal Development**



## **CHAPTER VI**

### **Characterization of the embryonic development of the recurrent inhibitory circuit**

## Introduction

Understanding when and how spinal synaptic circuits develop is important, but unfortunately little is known about their formation. In the previous aim, we determined that approximately all Renshaw cells at E16 are contacted by motor axon collaterals, suggesting that this synaptic interaction is established very early in embryogenesis. Recent studies of E11-E12 mouse spinal cord suggest that early motoneurons' synapses target RC-like interneurons and these, through recurrent synaptic circuits, amplify motoneurons synchronous firing episodes such that waves of excitatory activity travel through the early spinal cord (Hanson & Landmesser, 2003). At this age inhibitory neurotransmitters depolarize neurons. Therefore, we investigated when RCs are first contacted by motor axon collaterals and the time course of synapse formation from RCs to motoneurons, since only when both synapses are formed the recurrent inhibitory circuit becomes closed and functional.

An exceptional study by Hanson and Landmesser (2003) characterized the circuits that they believe are responsible for the generation of episodes of spontaneous activity in the early embryonic spinal cord. Using an *in vitro* mouse spinal cord-*hindlimb* preparation, they recorded motor output from motor nerves, and demonstrated that by E12, "circuits" that utilize acetylcholine and GABA are important for the propagation of local waves of synchronous motoneuron firing episodes. Block of chemical transmission with high  $Mg^{2+}$  and low  $Ca^{2+}$  abolished the ability of MNs to elicit a local episode of activity, whereas blocking electrical transmission by the addition of carbenoxolone was not required to elicit local bursts.

Although glutamate is the main excitatory neurotransmitter in adult motor circuits, Hanson and Landmesser showed that it is not important for the generation or propagation of rhythmic episodes in the embryonic spinal cord. They found that blocking NMDA and AMPA/kainate receptors with APV and CNQX respectively had no effect on rhythmic spontaneous episodes. Since glutamatergic transmission is not important for rhythmic activity during early embryonic development, they looked at whether cholinergic transmission was important. Application of the nicotinic receptor antagonist DH $\beta$ E blocked propagating episodes, but did not affect local episodes, suggesting that DH $\beta$ E-insensitive nicotinic receptors are important for the generation of local episodes. They also investigated whether GABA and glycine could be involved in the generation of propagating rhythmic episodes. Both GABA and glycine can be excitatory during early development (Wu et al., 1992; Reichling et al., 1994; Chen et al., 1996; Owens et al., 1996). Addition of the GABA<sub>A</sub> receptor antagonists bicuculline and picrotoxin increased interepisode intervals, while GABA<sub>B</sub> receptor antagonists phaclofen and hydrosaclofen did not affect rhythmic activity; suggesting that although GABA acting via the GABA<sub>A</sub> receptor is important for excitatory drive of the local circuit, it is not required for the generation of spontaneous activity. However, application of the glycine receptor antagonist strychnine completely abolished spontaneous episodes of activity, but local episodes still occurred.

To explain this observation, Hanson and Landmesser provided a model circuit in which antidromic activation of MNs elicit local bursts of activity by activating GABAergic interneurons. It is possible that these GABAergic interneurons represent RCs because V1s are known to have axons which project rostrally short distances and

terminate on MNs (Saureissig et al., 1999). Therefore, activation of MNs will activate local GABAergic RCs which then recurrently activate MNs, ultimately amplifying and propagating episodes of spontaneous activity. Therefore, at first the recurrent circuitry between MNs and RCs is excitatory and acts to propagate episodes of spontaneous rhythmic activity. The early enhancement of MN firing and subsequent spreading of episodes of spontaneous activity are important for the development of the correct wiring of spinal motor circuits (see review Hanson et al., 2007).

Despite the impressive set of electrophysiological and pharmacological evidence in Hanson and Landmesser's study, no anatomical or physiological evidence was presented for the putative synaptic circuits proposed. To determine when both synapses (i.e., those from MNs to RCs and from RCs to MNs) are formed, we used an Hb9::gfp mouse model and analyzed early (E11.5-E13.5) and late (E15.5-E17.5) embryonic ages. Hb9 is a transcription factor expressed in MNs (Arber et al., 1999) and in Hb9::gfp mice (Wichterle et al. 2002), the MNs, their dendrites, axons and axon recurrent collaterals are fluorescently labeled. We used immunohistochemistry against Calbindin to identify a group of presumed primordial RCs. Co-localization of naked EGFP with the Vesicular acetylcholine transporter-IR (VAcHT-IR) was used to identify motor axon inputs on primordial RCs. Similarly, CB and Synaptophysin co-expression was used to identify RC inputs on EGFP labeled MNs. We analyzed when RCs are first contacted by motor axon recurrent collaterals and when MNs are first contacted by RC axons.

## **Materials & Methods**

### *Harvesting and timing embryos*

All embryos used in this aim were obtained from timed pregnant females (see General Methods; *Timed Pregnancies*). Timing pregnancies was crucial in order to be able to collect embryos at the specific developmental ages analyzed in this study. The average time of gestation of mice is relatively short (~19-21 days) and therefore significant developmental changes occur over narrow time periods. Gestational age was further confirmed by the external appearances of the embryos. All external features were confirmed using the Atlas of Mouse Development (Kaufman 2005). Embryos at the ages analyzed differed dramatically in external appearance, we outline the key features in here. By E11.5, all four limb buds (2 forelimb and 2 hindlimb) are present, but no discernable digits are seen. Before E11.5, only the forelimb buds are observed. Therefore, E11.5 embryonic ages were confirmed by the presence of all four limb buds. The gestational age of mid-to-late stage embryos (E13.5-E17.5) were easier to confirm. E13.5 limb buds are webbed, and by E15.5, clear digits are seen. Another distinguishing feature that allowed us to correctly age E13.5 embryos was the disappearance of the hump associated with the caudal hindbrain. Older embryos (E15.5 to E17.5) showed more noticeable differences. At E15.5 the developing cornea is visible because eyelids do not begin to fuse until approximately E16.0. By E17.5, no cornea is present and the eyelids are formed and closed. Probably the most distinguishing external feature of E17.5 embryos is the wrinkles and creases in the skin. Before E17.5, the skin is smoother and follows the contours of the body.

Once the embryos were sectioned, gestational age was confirmed further by the overall morphology of the spinal cord (refer to Figure 1 for schematic of general morphology of the embryonic spinal cord). At E11.5, most of the spinal cord consists of the mantle layer (future gray matter) and ventricular zone (VZ), which contains postmitotic and mitotic cells respectively. Very little mantle layer is seen in the alar (dorsal) half of the spinal cord compared to the basal (ventral) half. By E13.5, the size of the VZ has decreased dramatically whereas the overall size of the mantle layer has increased significantly, especially in the alar plate. The marginal layer (future white matter) at E13.5 is still relatively thin, but by E15.5, it has increased in size. By E15.5, very little of the VZ remains and the size of the mantle layer has increased even more, again, particularly in the alar plate. At E17.5, the morphology of the spinal cord closely resembles that at birth.

### *Tissue Preparation*

Sections from lumbar spinal cord segments of Hb9::gfp mouse of embryonic ages E11.5, E13.5, E15.5, and E17.5 were processed for dual and triple-immunofluorescence using antibodies against Calbindin D28k (CB, rabbit polyclonal, 1:2000), VACHT (goat polyclonal, 1:500), and Synaptophysin (guinea pig polyclonal, 1:1000). Similar as before, sections were incubated overnight in one of the following primary antisera mixtures: CB/EGFP, CB/VACHT/EGFP, and CB/Synaptophysin/EGFP. No antibody was used to reveal EGFP-IR because endogenous “naked” EGFP labeling was strong in all ages analyzed. Immunoreactive sites were revealed using the following secondary antibodies: CB-IR, depending on the primary antisera mixture used, was revealed with

either donkey Cy3-conjugated or Cy5-conjugated anti-rabbit antibodies. Synaptophysin-IR was revealed using donkey Cy3-conjugated anti-guinea pig antibodies. VACHT-IR was revealed using the indirect tyramide signal amplification method (See General Methods; *Tyramide signal amplification in embryonic tissues*). Briefly, following an overnight incubation in primary antibodies, sections were incubated in a species-specific biotinylated secondary antibody, then incubated in an ABC (avidin-biotin complex), and incubated in biotinylated-tyramide, which binds to the biotin in the secondary antibody. Finally, antigenic sites were visualized using a streptavidin-conjugated to Alexa 555. No amplification was necessary to reveal CB-IR or Synaptophysin-IR. Preparations were then imaged at high magnification (60X1.5 oil, N.A. 1.35) using the FV1000 confocal microscope.

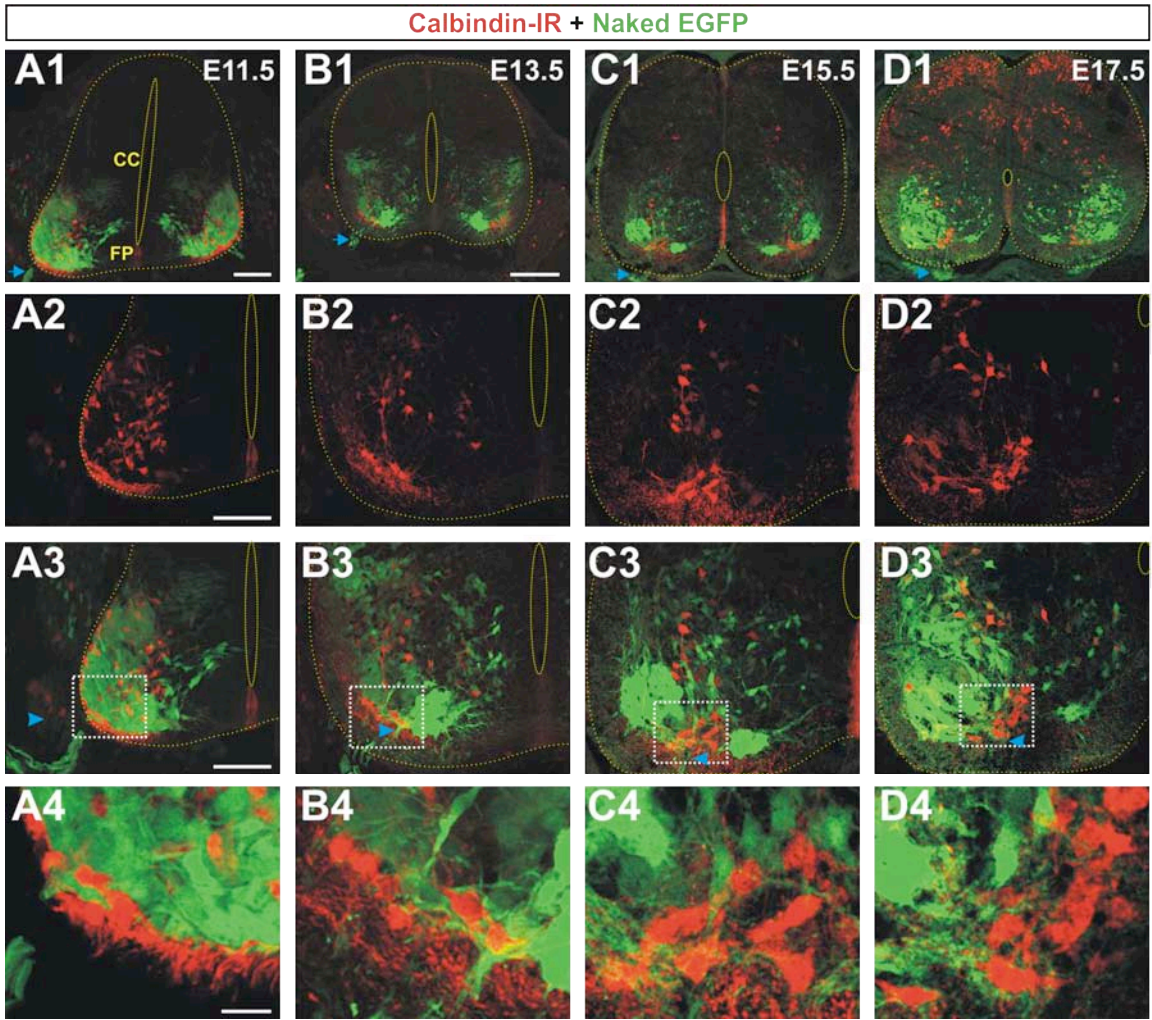
## **Results**

*Calbindin-immunoreactivity labels a population of ventrally located cells throughout embryonic development.*

The motoneurons and their collaterals are fluorescently labeled in Hb9::gfp mice, but in order to study the establishment of the recurrent inhibitory circuit (RIC) in the embryonic spinal cord, we needed a way to label RCs. Calbindin-IR is an excellent marker of RCs during late embryonic development (E16-E18), throughout postnatal development, and in the adult, but whether it labels RCs in early embryonic development was unknown. We investigated when RCs begin expressing Calbindin during embryonic development. At the earliest age studied (E11.5) a group of interneurons in the presumed ventral horn were intensely labeled with Calbindin (Figure 22). Similar to E11.5, CB-IR



**Figure 22.** Calbindin-immunoreactive cells in relation to EGFP+ motoneurons in the embryonic spinal cord. **A1-D1**, Low magnification confocal image of an Hb9::gfp embryonic mouse spinal cord at E11.5 (A1), E13.5 (B1), E15.5 (C1), and E17.5 (D1) showing Calbindin-IR (Cy3, red) and naked EGFP (green). *Hb9* is a transcription factor expressed in motoneurons (MNs) and in Hb9::gfp mice the somata, axons, and dendrites of motoneurons are fluorescently labeled. The dotted line indicates the limits of the spinal cord. Blue arrow indicates EGFP+ ventral root. CB-IR cells are present as early as E11.5 and in earlier embryonic ages (i.e., E11.5 to E15.5) CB-IR cells are seen only in the ventral horn. CB-IR is also seen in the remnants of the floorplate (FP). **A2-D2**, Same spinal cord sections shown in A1-D1, showing only CB-IR. **A3-D3**, Medium magnification image of the presumptive ventral horn at E11.5 (A3), E13.5 (B3), E15.5 (C3), and E17.5 (D3), again showing CB-IR (red) and naked EGFP (green). The box indicates the area shown at higher magnification in A4-D4. Blue arrow indicates EGFP+ ventral root. CB-IR cells are present throughout the ventral horn, but as early as E11.5, there is a prominent group of CB-IR cells that occupies the exit region of motor axons, which corresponds to the “Renshaw cell area”. This group is present throughout embryonic development. **A4-D4**, Higher magnification image of the area indicated in A3-D3, showing a prominent group of CB-IR cells near the where motor axons exit. The remainder of the analyses in this aim focused only on these intensely labeled CB-IR cells. **Scale bars:** **B1-D1** (B1); **A1, A2-D2** and **A3-D3** (in A1, A2 and A3), 100  $\mu\text{m}$ ; **A2-D2** (in A2), 100  $\mu\text{m}$ ; **A4-D4** (in A4), 20  $\mu\text{m}$



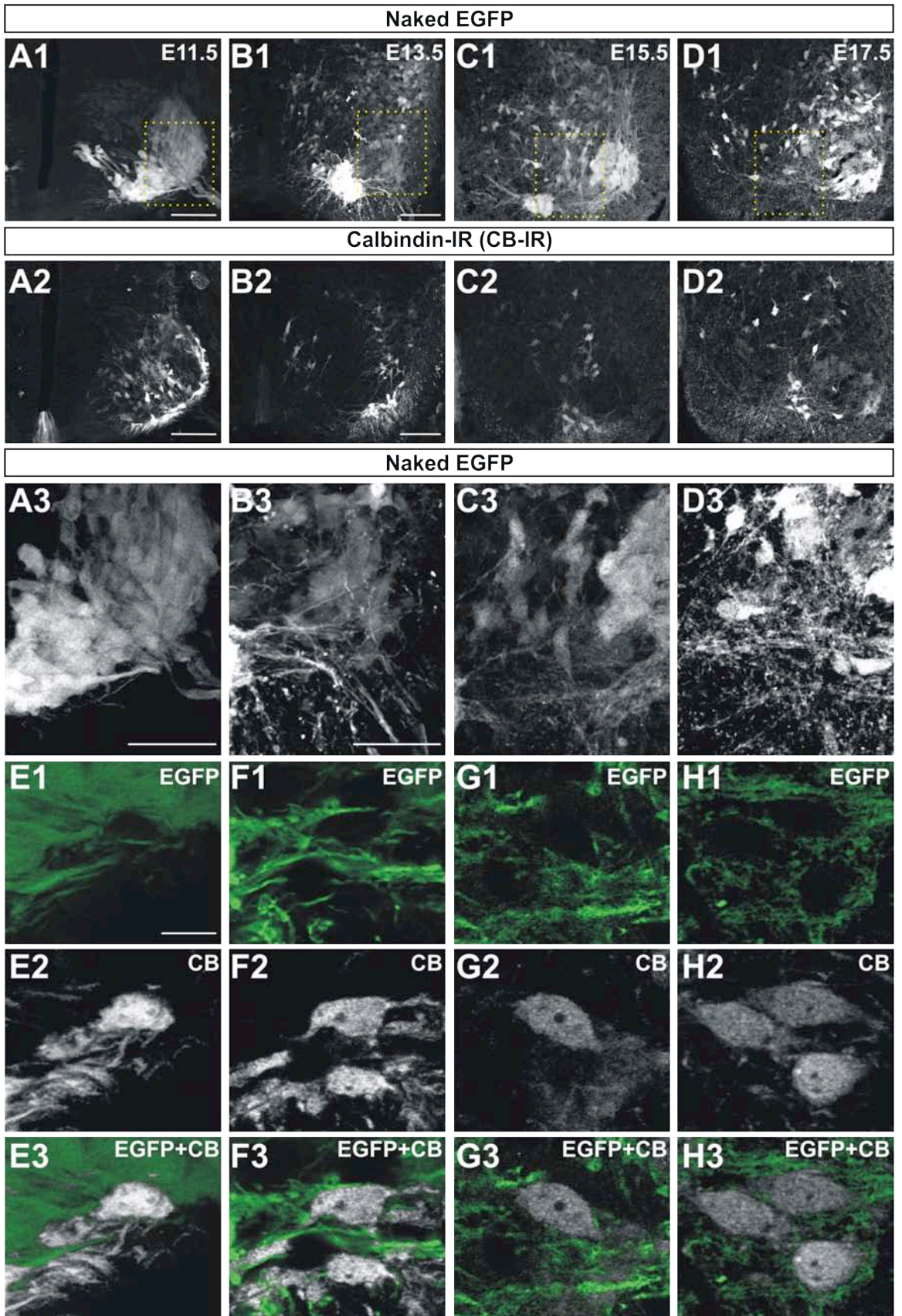
cells were seen in the ventral horn at E13.5 and none were seen in the dorsal horn. In embryonic spinal cord sections from Hb9::gfp mice, at all ages examined (E11.5, E13.5, E15.5, and E17.5), there was a definitive group of CB-IR cells that occupied the area near where a bundle of EGFP labeled motor axons exit the spinal cord. This is the area that is usually deemed the “Renshaw cell area” in the adult spinal cord. Therefore, we determined that as early as E11.5 there is a group of CB-IR cells with a similar location to that of RCs. Several other groups of CB-IR cells were seen in the ventral horn, but this study only focuses on those cells intensely immunolabeled at the apparent ventral border of lamina VII (LVII). We are currently investigating the V1-origin of these cells but these studies were hampered by the developmental regulation of the Thy1 promoter used to label V1-derived interneurons with YFP. We noted that Thy1 and therefore YFP expression upregulates postnatally and is very weak embryonically. Interestingly, RCs seem to be one of the last groups to upregulate YFP expression in this line of mice during embryonic development. Therefore, the V1 origin of this group of CB-IR cells located among exiting motor axons is now being investigated in other mouse lines encoding reporter genes regulated by alternative promoters.

*Motor axon inputs are established on CB-IR putative Renshaw cells during early embryonic development.*

By E11.5, CB-IR RCs are surrounded by EGFP+ processes, but no clear varicose contacts could be seen (Figure 23). In contrast, at E13.5, CB-IR RCs are surrounded by EGFP+ axons, but clear contacts from EGFP- labeled motor axons were observed. By

**Figure 23.** Distribution of EGFP<sup>+</sup> motor axon recurrent collaterals in the spinal cord at different embryonic ages. **A1-D1**, Low magnification images of naked EGFP (white) labeling in the spinal cord of Hb9::gfp mice at E11.5 (A1), E13.5 (B1), E15.5 (C1), and E17.7 (D1). Motoneurons (MNs) are fluorescently labeled as early as E11.5 and labeling is present throughout embryonic development. Box indicates area shown at higher magnification in A3-D3. **A2-D2**, Same spinal cord section shown in A1-D1, but showing Calbindin-IR (Cy3, white). At all ages, some MNs are CB-IR. **A3-D3**, Medium magnification images of the areas indicated in A1-D1 showing MNs, their axons, and dendrites (naked EGFP, green). At E11.5 (A3), it is hard to distinguish any EGFP<sup>+</sup> motor axons; only MN somata are clearly labeled. In contrast, by E13.5 (B3), EGFP<sup>+</sup> motor axons are seen and the density of labeled axons in this area increases at E15.5 (C3) and again at E17.5 (D3). **E1-H1**, EGFP labeling (green) in Hb9::gfp mice at E11.5 (E1), E13.5 (F1), E15.5 (G1), and E17.5 (H1). Again, no clear motor axons are seen at E11.5, but at E13.5, E15.5, and E17.5, EGFP<sup>+</sup> motor axons are clearly labeled. **E2-H2**, CB-IR (white) cells from the area that is enriched in motor axons. **E3-H3**, EGFP<sup>+</sup> contacts from motor axons on CB-IR Renshaw cells at E11.5 (E3), E13.5 (F3), E15.5 (G3), and E17.5 (H3). No clear EGFP<sup>+</sup> contacts are seen on CB-IR RCs at E11.5. In contrast, clear contacts are seen at E13.5 and the number of contacts on CB-IR RCs increases at E15.5 and again at E17.5. **Scale bars:** **A1-D1** and **A2-D2** (in A1, B1, A2, and B2), 200  $\mu$ m; **A3-D3** (in A3 and B3), 50  $\mu$ m; **E1-H1**, **E2-H2**, and **E3-H3** (in E1), 10  $\mu$ m.





E15.5 all CB-IR RCs examined had clear contacts from EGFP+ motor axons. RCs at E17.5 displayed multiple EGFP+ contacts.

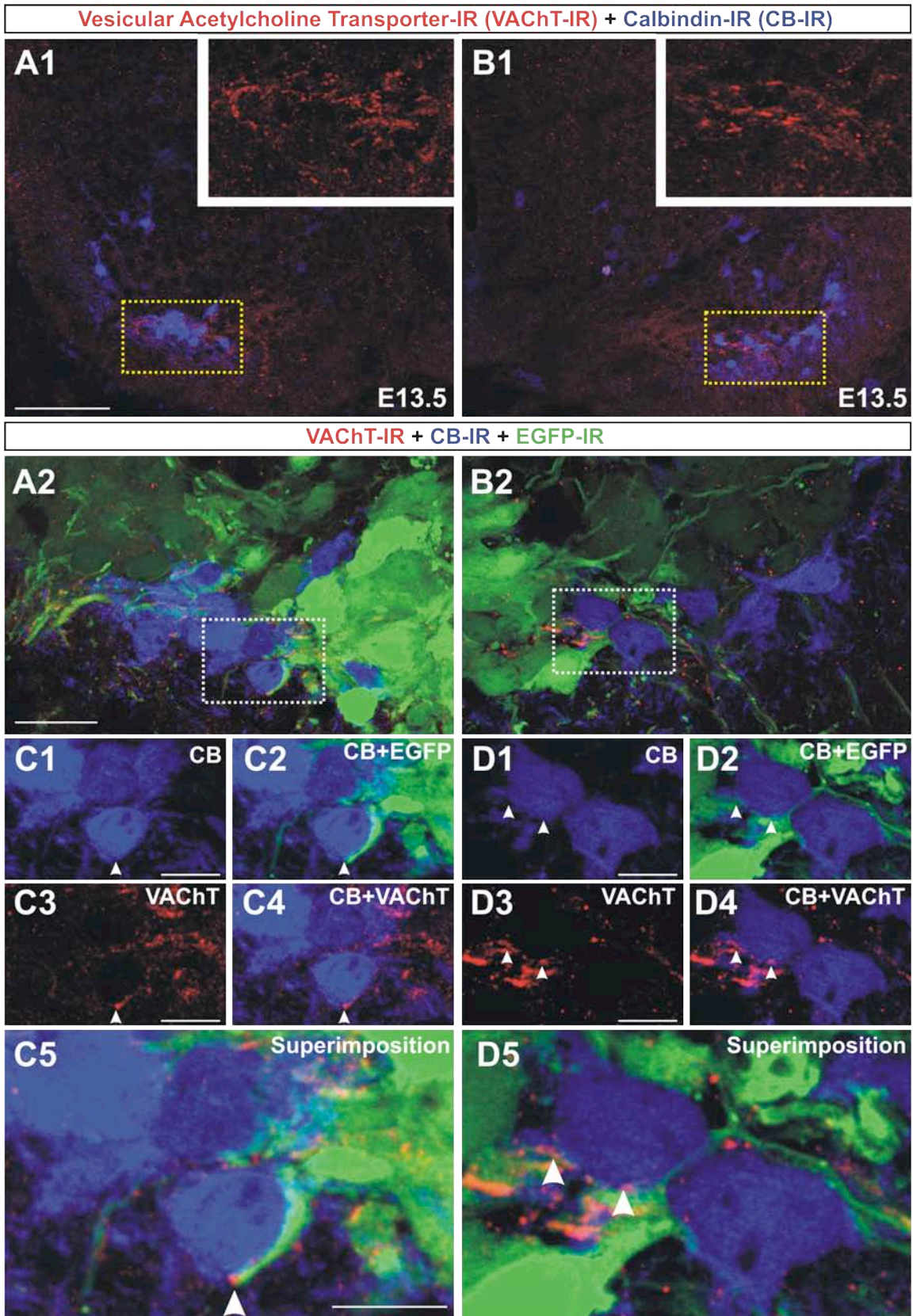
Next we investigated whether the contacts from EGFP+ motor axons represented synapses using VAcHT as a presynaptic marker. Analysis was carried out at E13.5 because at E11.5 no VAcHT-IR varicosities were seen in the ventral horn. At E11.5, VAcHT-IR was only seen diffusely distributed in the ventral root motor axons (Figure 24). Diffuse distribution of synaptic vesicle markers is the basal condition that precedes their accumulation at presynaptic sites during synapse formation (Araki et al., 2004). Therefore, these images constitute also indirect evidence for the lack of synapses. VAcHT-IR was not extensive at E13.5; most of the labeling was concentrated in the area occupied by CB-IR RCs (Figure 24). E13.5 RCs received EGFP+ contacts that were also VAcHT-IR. Interestingly, not all EGFP+ contacts on RCs co-localized with VAcHT at this point. In conclusion, it appears that RCs are contacted by motor axons very early in embryogenesis.

*Motoneurons receive inputs from Calbindin-IR Renshaw cells during late embryonic development.*

The recurrent inhibitory circuit consists of RCs receiving excitatory cholinergic inputs from motor axons and those same motoneurons receiving inhibitory inputs from RCs. To have a fully functional circuit both synapses need to be established. We therefore investigated when EGFP+ motoneurons are first contacted by CB-IR axons. At E11.5 and E13.5 many CB-IR axons were visible in the ventral funiculus, but the area in the developing ventral horn occupied by EGFP+ motoneurons was void of CB-IR

**Figure 24.** VACHT-immunoreactivity in the ventral horn during embryonic development. **A1-B1**, Hb9::gfp mouse spinal cord at E13.5 (A1 and B1) showing VACHT-IR (Cy3, red) and Calbindin-IR (Cy5, blue) in the ventral horn. Box indicates area showing VACHT-IR only in the insets and also represents the area shown at higher magnification in A2-B2. VACHT-IR at E13.5 is not extensive and is concentrated mainly in the Renshaw cell area. **A2-B2**, Medium magnification images showing VACHT-IR (red), CB-IR (blue), and naked EGFP (green). Box indicates cells shown at higher magnification in C1-C5 and D1-D5. CB-IR RCs are contacted by EGFP+ motor axons and VACHT-IR contacts. **C1-C5**, High magnification confocal images of CB-IR RCs (blue; C1, C2, and C4) that receives EGFP+ motor axon inputs (green; C2) and VACHT-IR (red; C3 and C4) inputs. White arrowheads represent contacts that are EGFP+ and VACHT-IR. Superimposition in C5. **D1-D5**, Similar to C1-C5, more CB-IR RCs that receive inputs from motor axons that are EGFP+ and VACHT-IR. **Scale bars:** **A1-B1** (in A1), 100  $\mu\text{m}$ ; **A2-B2** (in A2), 50  $\mu\text{m}$ ; **C1-C5** and **D1-D5** (in C1, C3, C5, D1, and D3), 10  $\mu\text{m}$ .







processes (Figure 25). In contrast, by E15.5 CB-IR processes are frequent in this same area. By E17.5, this area is enriched with CB-IR processes containing clear varicosities. No CB-IR contacts were detected on EGFP+ motoneurons at E11.5 and E13.5. It was not until E15.5 that the first CB-IR contacts on motoneurons were observed. It is important to note that at E15.5 not all EGFP+ motoneurons received CB-IR inputs. By E17.5, more motoneurons were seen with CB-IR contacts (again not all were contacted) each receiving a large number of contacts, possibly suggesting a proliferation of CB-IR inputs on motoneurons.

Similar to the motor axon input on RCs, we looked at the synaptic nature of the CB-IR inputs on motoneurons during late embryonic development using synaptophysin as a synaptic marker. No Synaptophysin-IR processes were seen in the ventral horn at E11.5 and E13.5, labeling was only seen in the ventral funiculus (Figure 26). By E15.5, many Synaptophysin-IR processes and a high density of punctae are present. By E17.5, the ventral horn is enriched with Synaptophysin-IR punctae. We then looked at whether any CB-IR contacts on motoneurons co-localized with Synaptophysin. As mentioned before, motoneurons at E15.5 receive few CB-IR contacts and of those contacts, very few co-localized with Synaptophysin. In contrast, motoneurons at E17.5 received many CB-IR contacts and a portion of those contacts co-localized with Synaptophysin (Figure 27). In conclusion, motoneurons are first contacted by CB-IR RCs around E15.5 and by E17.5 the synapses have matured, containing clear accumulations of presynaptic vesicles and this input has spread to many motoneurons.

**Figure 25.** Calbindin-immunoreactivity in Lamina IX of the spinal cord at different embryonic ages. **A1-D1**, Low magnification images of Hb9::gfp mice showing CB-IR in the ventral horn at E11.5 (A1), E13.5 (B1), E15.5 (C1), and E17.5 (D1). Boxes indicate areas shown at higher magnification in A3-D3. The yellow dotted line indicates the border between the ventral horn and white matter. **A2-D2**, Same sections shown in A1-D1, but showing naked EGFP labeling (white). As mentioned before, in Hb9::gfp mice, MNs, their axons and dendrites are fluorescently labeled. Boxes indicate areas showing BC-IR at higher magnification in A3-D3. **A3-D3**, Medium magnification images showing CB-IR (white) in the lamina IX (LIX) during embryonic development. At E11.5 and E13.5, the area that was largely occupied by EGFP+ motoneurons was void of CB-IR processes. In contrast, by E15.5 CB-IR processes are frequent in this same area. By E17.5, this same area is enriched with CB-IR processes containing clear varicosities. **E1-H1**, High magnification images of EGFP+ MNs (green). Note that the size of MN somata appears to increase from E11.5 to E17.5. **E2-H2**, Same area shown in E1-H1, but showing CB-IR (Cy3, red). Very little CB-IR processes are seen in the LIX at E11.5 and E13.5, but many are seen at E15.5 and E17.5. **E3-H3**, CB-IR contacts on EGFP+ MNs are seen at E15.5 and E17.5, but not at E11.5 and E13.5; suggesting that these inputs are formed in late embryo. **Scale bars:** **A1-D2** and **A2-D2** (in A1, B1, A2, and B2), 100  $\mu\text{m}$ ; **A3-D3** (in A3 and B3), 50  $\mu\text{m}$ ; **E1-H1**, **E2-H2**, and **E3-H3** (in E1), 10  $\mu\text{m}$ .

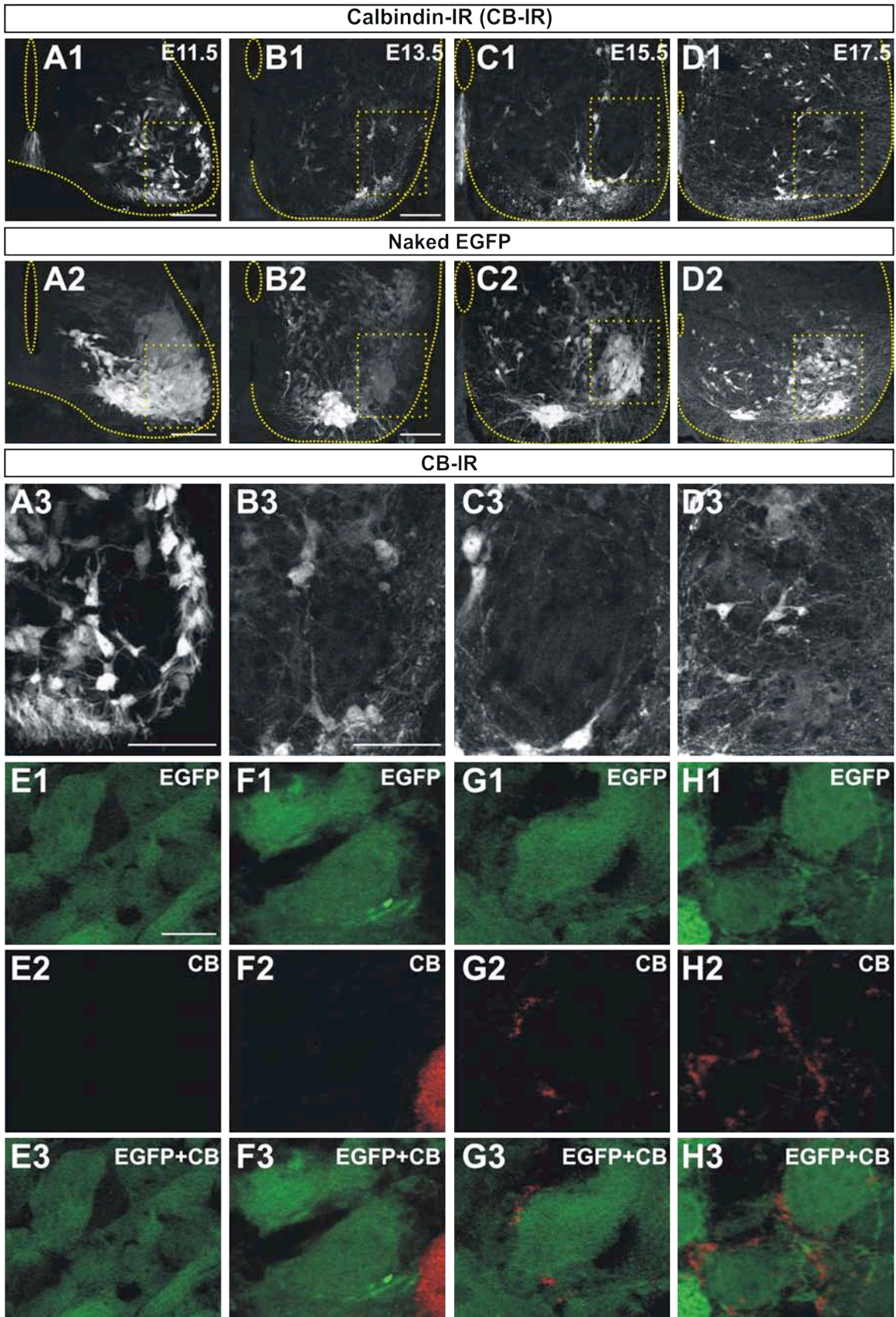


**Figure 26.** Synaptophysin-immunoreactivity in the embryonic spinal cord. **A1-D1**, Low magnification images of embryonic spinal cords at E11.5 (A1), E13.5 (B1), E15.5 (C1), and E17.5 (D1) immunolabeled with synaptophysin (white). Synaptophysin is a synaptic vesicle integral membrane protein and is present at glycinergic synaptic boutons (Dumoulin et al., 1999). Synaptophysin-IR is not seen in the gray matter (GM) of the spinal cord at E11.5, but is seen in the white matter (WM), dorsal root ganglion (DRG), ventral and dorsal roots (VR and DR, respectively). **A2-D2**, Higher magnification image showing Synaptophysin-IR (white) in the ventral horn. No Synaptophysin-IR processes are seen in the ventral horn at E11.5 and E13.5, but by E15.5 plenty of processes are seen. By E17.5, the ventral horn is enriched with Synaptophysin-IR. Therefore, further analysis was only carried out at E15.5 and E17.5. **Scale bars:** **A1-D1** (in A1), 100  $\mu\text{m}$ ; **A2-D2** (in A2), 50  $\mu\text{m}$ .

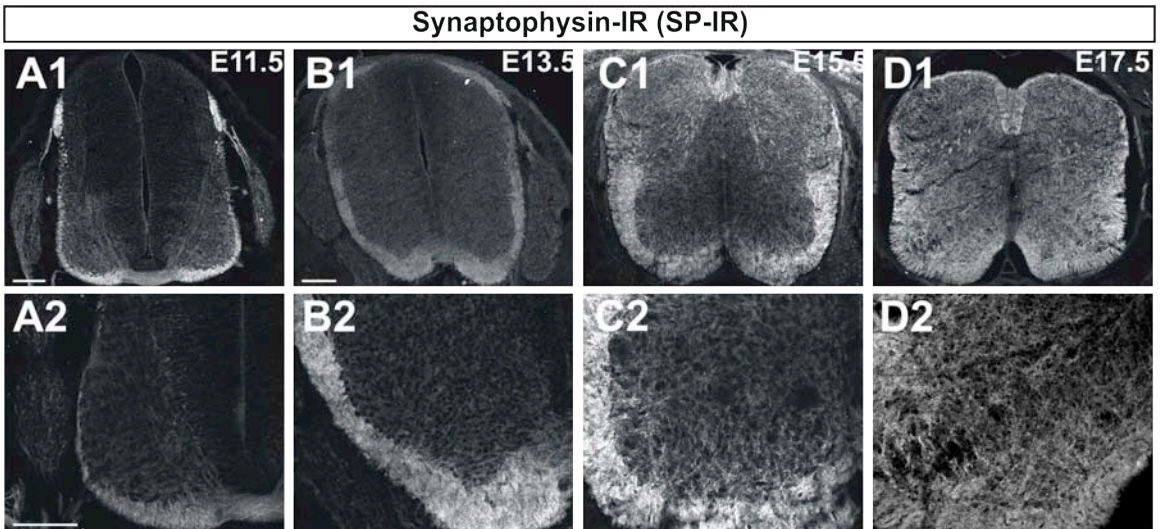
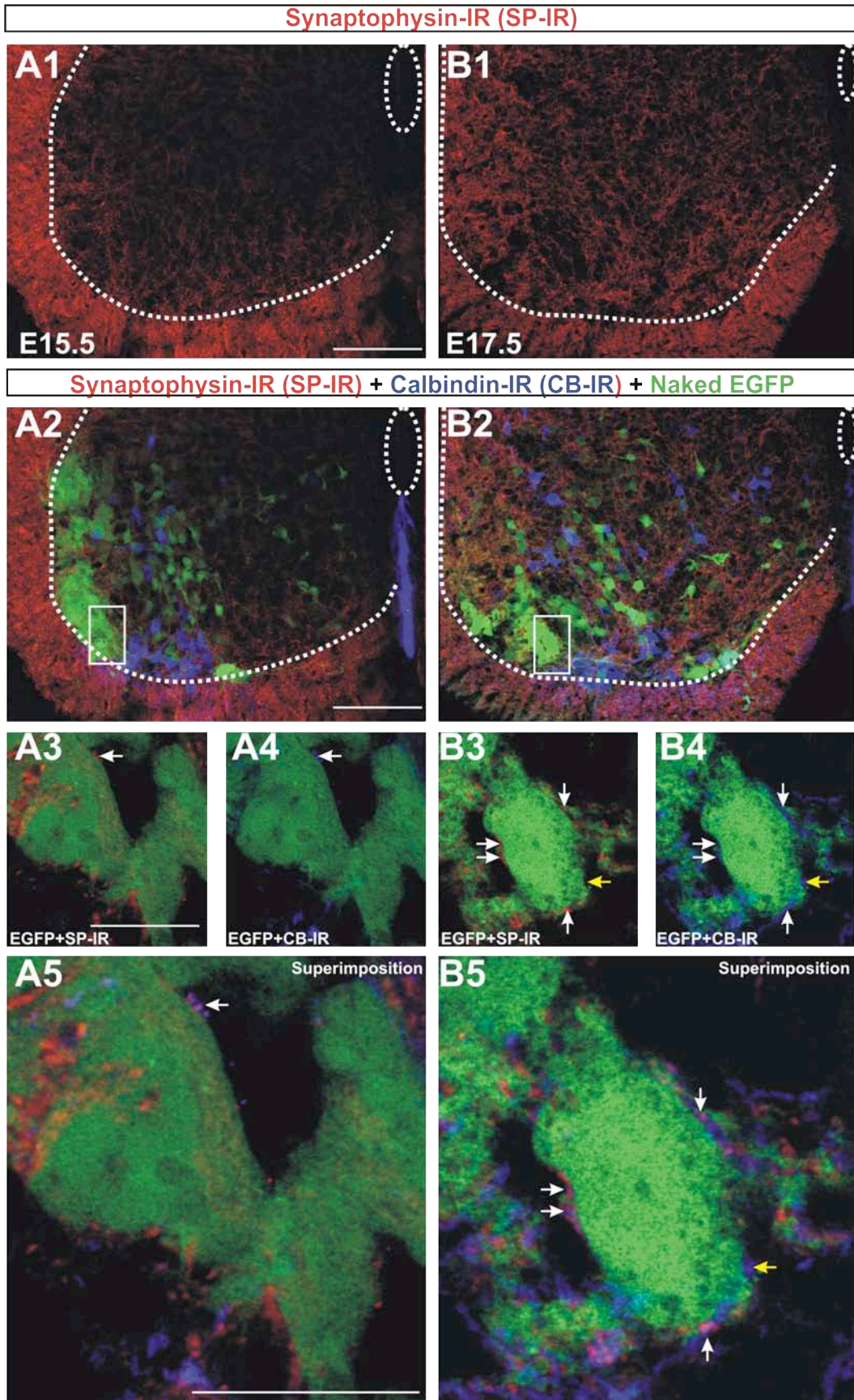


**Figure 27.** Synaptophysin-IR inputs on motoneurons during late embryonic development. **A1-B1**, Low magnification image showing an E15.5 (A1) and E17.5 (B1) ventral horn immunolabeled with Synaptophysin (Cy3, red). The dotted line indicates the border between the ventral horn and white matter. As mentioned previously, by E13.5 Synaptophysin-IR processes are present in the ventral horn and by E17.5; the ventral horn is enriched with Synaptophysin-IR. **A2-B2**, Same sections shown in A1-B1, but with Calbindin-IR (Cy5, blue) and naked EGFP (green) superimposed. The box indicates the EGFP+ motoneurons (MNs) shown at higher magnification in A3-A5 and B3-B5. **A3-A5 and B3-B5**, High magnification image of EGFP+ MNs (green; A3, A4, B3, and B4) receiving Synaptophysin-IR contacts (red; A3 and B3; white arrows) and CB-IR contacts (blue; A4 and B4). Superimposition in A5 and B5. At E17.5, more Synaptophysin-IR contacts are seen on EGFP+ MNs compared to at E15.5. There are some CB-IR contacts that are not Synaptophysin-IR (yellow arrows). **Scale bars:** **A1-B1** and **A2-B2** (in A1 and A2), 100  $\mu\text{m}$ ; **A3-A5** and **B3-B5** (in A3 and A5), 20  $\mu\text{m}$ .





## Discussion

The morphological results obtained in this aim allow us to reject the hypothesis that a recurrent inhibitory synaptic circuit is established in the early embryonic spinal cord by E12. This conclusion was based fundamentally on physiological and pharmacological data from Hanson and Landmesser. However, in the mouse spinal cord recognizable synapses between motoneurons and RC are first present at E13 and the formation of synapses from RCs onto motoneurons is delayed for another 24-48 hours. Thus the previous physiological data might represent non-synaptic interactions between developing motoneurons and interneurons.

### *Calbindin-IR as a marker of early primordial Renshaw cells*

Renshaw cells are easily identified by their CB-IR throughout postnatal development and in the adult (see aim 1; Mentis et al., 2006), but until this study it was not known whether CB-IR would be an efficient marker of embryonic RCs. We demonstrated that throughout embryonic development, there is a group of CB-IR cells that occupy the area where motor axons exit the spinal cord, suggesting that these cells represent primordial RCs. In order to determine if these CB-IR cells were V1-derived, we attempted to use two different transgenic mouse models to label V1-INs. The *En1-Cre/Thy1-YFP* mice were not useful because the *Thy1* promoter used is upregulated postnatally (Morris, 1985; Kollias et al., 1987; Caroni, 1997). Moreover, YFP expression was upregulated later in CB-IR cells in the “Renshaw cell area” compared to other V1-INs. Initial attempts to identify V1-INs using *En1-Cre/Tau-lacZ* mice, in which V1-INs are labeled with *lacZ* were unsuccessful. No *lacZ* expression was seen in the embryos



collected at two different ages (E15.5 and E17.5). Several possibilities exist for the lack of lacZ labeling: 1) Similar to the Thy1 promoter, the Tau promoter is upregulated postnatally or 2) No embryos at either age were the correct genotype, although this seems unlikely because normal Mendelian ratios are usually obtained for these animals. It is important to note that in one of the pregnant females, three of the embryos died in utero and were being reabsorbed. The female was initially pregnant with nine embryos and if three died then it is possible that those three were the genotype needed, although this seems unlikely. Therefore, whether these CB-IR cells are V1-derived needs to be studied further, possibly using a different reporter line.

#### *Timing of synapse formation between Renshaw cells and motoneurons*

In this study we demonstrated that RCs are contacted by motor axons early during embryogenesis. No contacts were seen at E11.5, but by E13.5 clear motor axon contacts that co-localized with VAcHT were seen and thus spread to many RCs by E15.5. Interestingly, this timing coincides with or shortly precedes synaptogenesis in hindlimb muscles (E14.5; Pun et al., 2002). To establish a fully functional recurrent circuit, both synapses, MN on RCs and RCs on MNs, need to be present. We determined that MNs are not contacted by CB-IR processes from RCs until E15.5 and this input spreads to most MNs by E17.5. In conclusion, both synapses are not simultaneously established. Interestingly, CB-IR axons are clearly visible in the ventral funiculus as early as E11 suggesting a waiting period before they invade the ventral horn.

Our results are inconsistent with the conclusions from Hanson and Landmesser (2003). They concluded that, by E11-E12, synaptic interactions between MNs and a RC-

like GABAergic interneurons are present and responsible for the generation and propagation of early embryonic episodes of spontaneous activity.

Xu and colleagues (2005) demonstrated also using electrophysiological recordings of motor output that a recurrent excitatory circuit is present by E8 in chick. Similar to Hanson and Landmesser, the pathway was activated by stimulating a ventral root and the response evoked recorded in the adjacent ventral root. The GABA<sub>A</sub> receptor antagonist bicuculline and nicotinic receptor antagonist mecamylamine abolished the ventral root response suggesting a circuit between a MN and a GABAergic interneuron that at this age recurrently excites motoneurons. However, the developmental stage analyzed in chicks might correspond to a later age than when it is first observed in mice.

Comparisons between embryonic ages in chick and mouse are complicated by some important differences in the timing of reaching developmental milestones. Probably the best way to establish equivalence is to compare the timing of major developmental events. For example, motoneurons are born between E2.5-E5 in chick, but not until E9-E10 in the mouse (Hollyday and Hamburger, 1977; Nornes and Carry, 1978; Briscoe et al., 1999; Pierani et al., 1999; Sander et al., 2000). Chick MNs connect to muscle between E2-E4 while in the mouse this occurs around E13-E14, moreover primary afferents connect with MNs around E5.5-E7.5 in chick (Lee et al., 1988) and E15-E16 in the mouse (Ozaki and Snider, 1997; Chen and Frank, 1999). Therefore, the period studied by Xu and colleagues likely correspond with a relatively older embryonic age in rodents. Chicks are then born by E20-E21, one day later than mice (born E19-E20), but by difference to mice their locomotor system is fully matured at this stage.

Intracellular recordings of EPSPs demonstrating connectivity between chick R-interneurons and motoneurons were obtained between E9-E11 (Wenner and O'Donovan, 1999) and this stage likely corresponds with recurrent EPSPs recorded in E18 mouse motoneurons (Sapir et al., 2004). Sapir and colleagues (2004) provided direct evidence for the presence of a functional recurrent synaptic circuit in late mouse embryos. They recorded intracellularly from MNs in E18.5 embryos after stimulating ventral roots to antidromically fire motor axon synapses on RCs. They demonstrated that stimulation of the ventral roots elicited synaptic potentials in MNs that were blocked by both curare and mecamylamine, which blocked cholinergic input to RCs. Similarly, the synaptic potentials were also blocked by glycinergic and GABAergic receptor antagonists strychnine and bicuculline, which blocked the input from RCs to MNs. Therefore, the embryonic ages at which functional synapses have been demonstrated agree well with our anatomical data; unfortunately intracellular recordings have not been performed earlier in this circuit.

Only one study characterized the onset of synaptic currents in embryonic motoneurons (Pascal de Legendre, Universite Pierre et Marie Curie, France; personal communication). In this study no glycinergic/GABAergic synaptic currents in mice motoneurons were found at E12.5 and first appeared at E13. Interestingly, synapses recognizable ultrastructurally were first described at E11 in mouse motoneurons (Vaughn et al., 1976) but the nature of these synapses could not be demonstrated.

*Open question on the generation of functional connectivity between Renshaw cells and motoneurons*

In this study we provided evidence that RCs are first contacted by MNs during early embryonic development and do not contact MNs until after a 48 hour waiting period. Why is there such a long period of time between the formation of these two connections? Furthermore, why does the anatomical data not correspond with the electrophysiological and pharmacological data? One possibility is that the early spontaneous episodes of activity are mediated via paracrine actions and these early non-synaptic interactions between MNs and RCs guide the motor axons to specific RCs. After MNs establish connections with specific RCs, these RCs will then make connections with those same MNs. Therefore, it is possible that the early episodes of spontaneous activity are non-synaptic, but they are important for establishing the correct wiring of ventral motor circuits. It is suggestive that RC contact MNs only after they have projected to periphery and segregated into pools. It is thus possible that retrograde signals from the periphery are important for the establishment of synapses from premotor interneurons. These and other important issues will need to be investigated in the future.

## **CHAPTER VII**

### **Characterization of the development of the glutamatergic primary afferents on Ia inhibitory interneurons in the postnatal spinal cord**

## Introduction

Renshaw cells (RCs) and Ia inhibitory interneurons (IaINs) derive from a common pool of embryonic interneurons (V1) and yet develop a distinct synaptic organization in the adult. Briefly, adult RCs main excitatory drive arises from motor axons, while adult IaINs receive inputs from sensory afferents and lack inputs from motoneurons. In aim 1 we found that motor axon and sensory afferent inputs converge on neonatal RCs, but sensory afferent bouton density is reduced on RCs after P15 and the input is “functionally deselected” (see Discussion of Aim 1 for more on “functional deselection”). In this study we analyzed whether postnatal V1-derived IaINs receive convergent inputs from motor axons and sensory afferents and studied their development.

IaINs mediate reciprocal inhibition of antagonist motor pools (Eccles, 1956), are located in LVII dorsomedial to LIX (Jankowska and Lindstrom, 1972; Rastad et al., 1990), and receive a dense projection from Ia sensory afferents (Alvarez et al., 2005). Unfortunately, due to the lack of histological means of identification in the neonate, the development of Ia afferents on IaINs is not known. In this aim we will address new criteria in order for IaINs to be identified throughout postnatal development.

IaINs and RCs derive from the V1 group which derives from a single set of progenitors all expressing the late transcription factor *engrailed-1* (Sapir et al., 2004; Alvarez et al., 2005). In aim 1 we discussed the possibility that Ia afferent and motor axon inputs converge on a “generic” V1-IN, which then selects or de-selects certain inputs. Fitting with this theory we proposed the possibility that RCs diversify themselves from this “generic” V1-IN subtype by strengthening inputs from motor axons and weakening those from Ia sensory afferents. Therefore, we now explored the possibility

that diversification of IaINs from the “generic” V1-IN is done by strengthening inputs from sensory afferents and complete removal of inputs from motor axons, because very few VAcHt-IR contacts are seen on IaINs at P20 (Alvarez et al., 2005).

More evidence for our proposed theory of convergent inputs in immature V1-INs comes from studies in the embryonic chick spinal cord. As mentioned previously, the R-interneuron (R-IN) is an *En1* expressing interneuron which receives monosynaptic inputs from sensory afferents and motor axon recurrent collaterals (Wenner and O’Donovan, 1999; Wenner et al., 2000). The adult synaptic connectivity of the R-IN is presently not known, but it could represent the avian equivalent of a putative mammalian V1-IN with “generic” connections.

Alternatively, it is possible that IaINs never receive convergent inputs. In this case, fundamental differences between IaINs and RCs might exist in their competence for receiving synapses from motor axons and this could be determined at very early stages, perhaps genetically specified.

V1-derived IaINs were previously identified by their Parvalbumin (PV) expression and Calbindin-IR (CB-IR) contacts from Renshaw cells. However, PV expression was only useful in identifying IaINs after P10 because at earlier ages, PV labels very few if any interneurons and only labels sensory afferents. Also PV only labels very proximal dendrites in contrast to CB immunoreactivity in RCs. Therefore, using PV as marker, it would be difficult to analyze synaptic densities in distal dendrites and throughout postnatal development. In this study, IaINs were identified in *En1*<sup>Cre/+</sup> mice crossed to a Thy1-loxP-STOP-YFP reporter mouse. In these mice, YFP is expressed in V1-derived interneurons and distributed throughout their axons and dendrites. IaINs were identified using immunohistochemistry against yellow fluorescent protein (YFP) to

identify V1-INs, IaINs were identified from the general V1-IN population as YFP-IR cells that received dense innervation from CB-IR axons. Similar to aim 1, VGLUT1-IR and VACHT-IR were used to identify sensory afferents and motor axon recurrent collaterals respectively at P5, P10, P15, P20, and in the adult. RCs were identified as YFP-IR cells that also express CB. We analyzed whether IaINs receive convergent inputs and how the density of these inputs compares to RCs in the same animals and sections. We hypothesized that during development, IaINs receive convergent inputs from motor axons and primary afferents, but they de-select the motor axon input by removal of this input. Comparisons with the information gathered on RC development will hopefully permit drawing some general principles on the diversification of subclasses of interneurons from canonical embryonic subgroups.

The results were presented in abstract form (Siembab et al., 2008).

## **Materials & Methods**

### *Tissue Preparation*

Sections from L4-L5 spinal cord segments of *En1-Cre/Thy1-YFP* mice of postnatal ages P5, P10, P15, P20, and adult were processed for triple-immunofluorescence using antibodies against Calbindin D28k (CB, rabbit polyclonal, 1:2000), Enhanced Green Fluorescent Protein (EGFP, sheep polyclonal, 1:1000), VGLUT1 (guinea pig polyclonal, 1:1000, 1:2000), and VACHT (guinea pig polyclonal, 1:1000). Yellow Fluorescent Protein-immunoreactivity (YFP-IR) was enhanced using EGFP antibodies. Sections were incubated overnight in one of the following primary antisera mixtures: CB/EGFP/VGLUT1 or CB/EGFP/VACHT (See General Methods for



antibody sources and buffers). Immunoreactive sites were revealed using the following species-specific secondary antibodies: CB-IR and EGFP-IR were revealed respectively with donkey Cy5-conjugated anti-rabbit antibodies and donkey FITC-conjugated anti-sheep antibodies (both diluted 1:50). VGLUT1-IR or VAcHt-IR, depending on the primary antisera mixture used, was revealed with donkey Cy3-conjugated anti-guinea pig antibodies (diluted 1:50). In some P10 sections, we combined YFP, CB and VGLUT1 antibodies with a mouse monoclonal antibody against Parvalbumin (PV; diluted 1:1000) to immunolabel proprioceptive sensory afferents. In these sections, CB-IR sites were revealed using a secondary antibody coupled to Streptavidin 405 (405) (Molecular Probes, Temecula, CA). Preparations that used 405 required a preincubation in a species-specific biotinylated secondary antibody (diluted 1:100, Jackson Laboratories, West Grove, PA) followed by 405-conjugated Streptavidin.

#### *Neurolucida analysis of the number and distribution of V1-derived interneurons*

The percentages and distributions of V1-derived interneurons in adult (i.e., >2 months) *En1-Cre/R26-LacZ*, *En1-Cre/Tau-LacZ*, and *En1-Cre/Thy1-YFP* mice were obtained. Free-floating sections (50  $\mu\text{m}$ ) were incubated in Neuronal Nuclear Protein (NeuN, mouse monoclonal, 1:1000),  $\beta$ -galactosidase ( $\beta$ -gal, chicken polyclonal, 1:1000), or YFP. The following primary antisera mixtures were used,  $\beta$ -gal/NeuN or YFP/NeuN. NeuN-IR was revealed with donkey Cy3-conjugated anti-mouse antibodies.  $\beta$ -gal-IR and YFP-IR was revealed with donkey FITC-conjugated anti-chicken or anti-sheep antibodies, respectively. Sections were then analyzed in Neurolucida (MicroBrightField,

Colchester, VT) under fluorescent conditions using an x 40 objective lens. The central canal was outlined and a line was drawn from the dorsal tip of the central canal straight across to the lateral border between the ventral horn and the white matter. This line is somewhat arbitrarily set, but allowed us to consistently point to a similar boundary between the dorsal and ventral horns in all the sections and animals. The ventral horn was then outlined along the border between the white matter and grey matter and the cells with the appropriate label were plotted. Only those neurons that had their nuclei fully within the section were counted. The software analysis tools allowed visualization of the distribution of counted neurons and also provided us with a tally of how many neurons were counted within each spinal cord section. Percentages of cells in the ventral horn with V1-labels were then calculated and compared across animal models using a One-way ANOVA. When comparisons were made among two animal models we used a t-test. Statistical significance was always set at  $p < 0.05$ . Sample characteristics: analysis of V1-IN numbers and distribution was carried out in 1-2 P40 animals of each transgenic mouse model (1 *En1-Cre/R26-lacZ*; 1 *En1-Cre/Tau-lacZ*; 2 *En1-Cre/Thy1-YFP*). Five to thirteen ventral horns per animal were sampled.

*Co-localization of PV immunofluorescence in VGLUT1-IR varicosities on YFP-IR IaINs and CB-IR RCs*

For quantification of PV immunofluorescence in VGLUT1-IR varicosities on YFP-IR IaINs and CB-IR RCs, VGLUT1-IR varicosities were traced in the confocal optical plane of the maximum VGLUT1 brightness and the average PV-IR intensity inside the varicosity outline measured. The outline was then left in the same x-y

coordinates and the z-axis was moved up and down 3  $\mu\text{ms}$ . In this manner, the outline was now on a region of neuropil to measure background fluorescence from surrounding neuropil. Co-localization was determined when PV immunofluorescence average intensity in the outlined VGLUT1-IR varicosity was 2 standard deviations above the average background estimate. Comparisons of the percentage of VGLUT1-IR synaptic contacts containing PV among IaINs and RCs were made using t-tests. Sample characteristics: analysis of PV and VGLUT1 co-localization was carried out in 1 P10 *En1-Cre/Thy1-YFP* mouse. 215 clusters from 5 V1-IaINs and 177 clusters from 5 RCs were measured.

*Confocal analysis of VGLUT1 and VAcHT contact densities of YFP-IR IaINs and CB-IR RCs*

In order to obtain synaptic densities on V1-IaINs and Renshaw cells throughout development we used the NeuroLucida neuron tracing software on stacks of confocal optical sections containing the cell bodies and dendrites of the neurons of interest. We analyzed approximately 10 RCs and 10 IaINs per animal (N=1 animal at P5; N=2 animals per age: P10, P15, P20, and adult). Triple-color immunofluorescent preparations were imaged with a confocal microscope at 60X1.5 magnification (oil, N.A. 1.35) and a series of confocal optical sections (z-step 0.5  $\mu\text{m}$ ) obtained throughout individual randomly sampled V1-IaINs and RCs with their cell bodies and most of their immunolabeled dendritic arbors fully contained within the field of view and thickness of the tissue sections. The stacks of images were then loaded in NeuroLucida, traced and reconstructed in 3D using the NeuroLucida neuron tracing confocal module. Synaptic

contacts were plotted on the reconstructed dendritic arbors. From these reconstructions we estimated dendritic arbor morphology, synaptic densities, and the distribution of synaptic contacts. Sholl analysis was performed in 50  $\mu\text{m}$  increments from the cell soma. Densities of contacts were obtained by plotting the number of contacts per 10  $\mu\text{m}$  of linear dendrite and compared across cell type at each age using a one-way ANOVA. Comparisons between IaINs and RCs were made using t-tests. Significance was set at  $p < 0.05$ .

Estimates of VGLUT1 and VAcHT synaptic densities on IaINs and RC somata were obtained by estimating surface area from approximate ellipsoids of similar maximum and minimum diameters. The number of VGLUT1 and VAcHT contacts was then normalized against the amount of surface to obtain a density of contacts for each cell. Differences between surface densities and the number of contacts were then compared between IaINs and RCs using t-tests. Sample characteristics: analysis of VGLUT1-IR and VAcHT-IR contact density was carried out in 1-2 *En1-Cre/Thy1-YFP* mice at each age (N=1 animal, P5; N=2 animals per age: P10, P15, P20, and adult). 8-12 IaINs and RCs were sampled per animal.

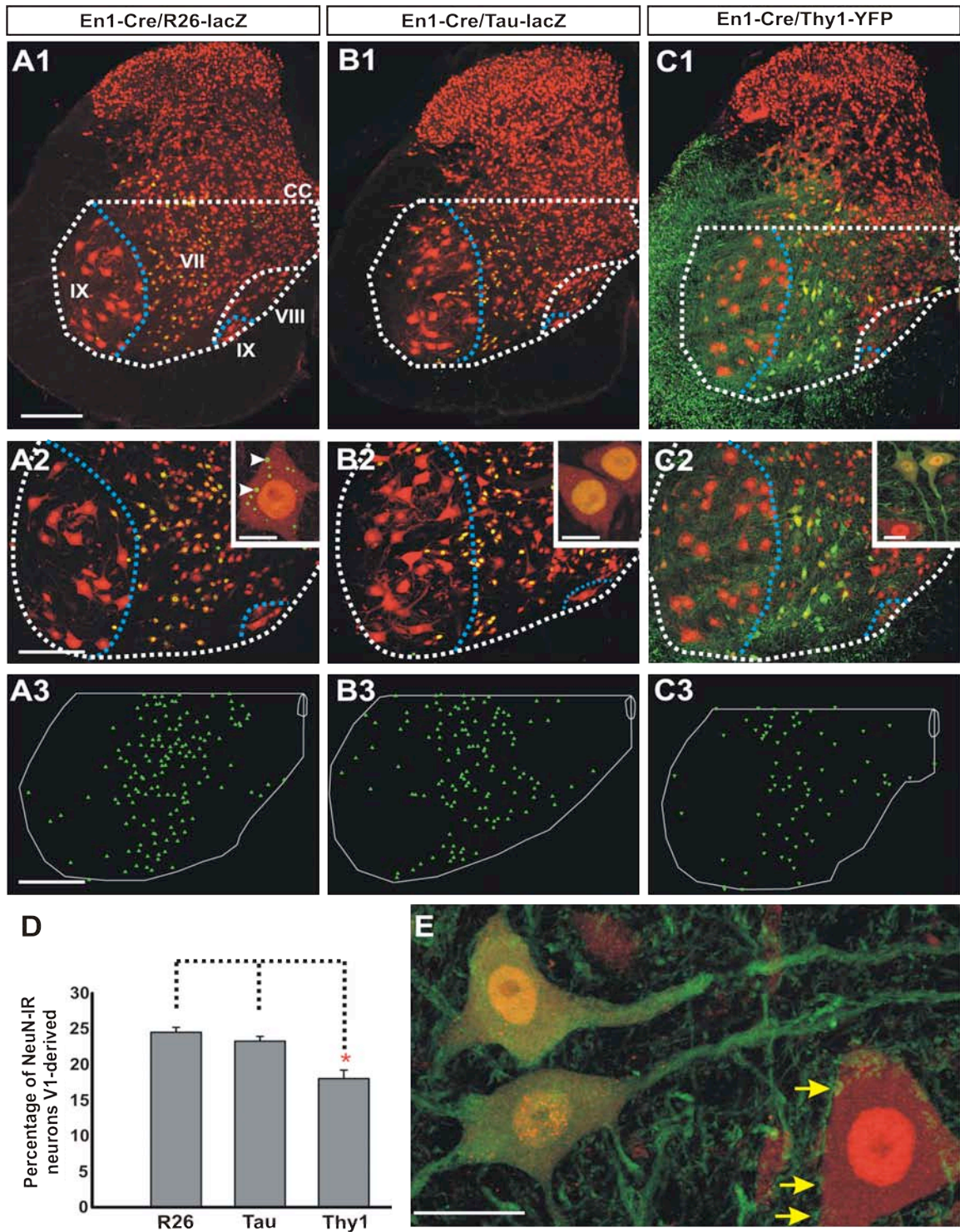
## **Results**

### *Animal models used to label V1-derived interneurons in the postnatal spinal cord*

To identify the best genetic marker for the study, we first compared labeling in three animal models designed to genetically label V1-INs in the postnatal spinal cord. Dual immunolabeling with the neuronal marker NeuN was used for laminar identification

and to estimate the proportion of ventral horn interneurons labeled in each animal (Figure 28). In *En1-Cre/R26-lacZ* and *En1-Cre/Tau-mEGFP-nls lacZ* mice,  $\beta$ -galactosidase-immunoreactivity ( $\beta$ gal-IR) was mainly restricted to the nucleus with additional labeling of small intracytoplasmic inclusions in *En1-Cre/R26-lacZ* mice (Figure 28A1,A2,B1,B2). Nuclear  $\beta$ gal-IR was more intense in *En1-Cre/Tau-mEGFP-nls lacZ* animals compared to *En1-Cre/R26-lacZ*. Additionally in *En1-Cre/Tau-mEGFP-nls lacZ* mice mEGFP was preferentially targeted to axons. The overall distribution of V1 mEGFP-IR axons (not shown) was similar to that previously described using a *En1-Cre/R26-GAP43-EGFP* reporter mouse (Alvarez et al., 2005) and to axonal labeling in *En1-Cre/Thy1-YFP* mice. YFP (revealed naked or amplified using an anti-EGFP antibody, see Methods) filled the cell bodies, dendrites, and axons of V1-derived interneurons in *En1-Cre/Thy1-YFP* mice (Figure 28C1,C2,E). In all three animal models, labeled V1-INs in the lumbar 4 and 5 segments were mostly located laterally in lamina VII (LVII) forming a dorso ventral arc surrounding lamina IX (LIX) motoneurons. In *En1-Cre/Thy1-YFP* mice V1 axons occupy the lateral and ventral funiculi and project throughout the ventral horn with lower density in lamina VIII and highest in LIX (Figure 28C1). In the *En1-Cre/Tau-mEGFP-nls lacZ* and *En1-Cre/Thy1-YFP* mice we observed some labeled interneurons in dorsal horn lamina (LI-LV, not depicted in the figure). NeuroLucida plots were used to determine the percent and locations of labeled and unlabeled ventral horn NeuN-IR interneurons with and without V1-lineage markers (Figure 28A3,B3,C3). The ventral horn dorsal boundary was arbitrarily set from the dorsal tip of the central canal. The percentage of NeuN-IR neurons with V1-lineage markers was not significantly different between *En1-Cre/R26-lacZ* ( $24.5\% \pm 1.49$ ) ( $\pm$  S.E.M.) and *En1-Cre/Tau-mEGFP-nls lacZ*

**Figure 28.** Distribution and labeling pattern of V1-derived neurons in *En1-Cre/R26-lacZ*, *En1-Cre/Tau-lacZ*, and *En1-Cre/Thy1-YFP* P40 mice. **A1,B1,C1**, Low magnification images of lumbar spinal cords immunolabeled with NeuN (Cy3) and either  $\beta$ -gal (FITC; **A1**, **B1**) or YFP (FITC; **C1**) in *En1-Cre/R26-lacZ* (**A1**), *En1-Cre/Tau-lacZ* (**B1**), and *En1-Cre/Thy1-YFP* (**C1**) P40 mice. In all three models, V1-INs are largely restricted to the ventral horn and located in lamina VII (LVII) forming an arc around the motoneurons (large NeuN-IR cells) in LIX. VI-INs and their projections are virtually excluded from LVIII and the dorsal horn. The dotted line above the central canal (CC) indicates the border between the dorsal and ventral horns. The blue line delineates the border between LIX and LVII. **A2**, **B2**, **C2**, Distribution of V1-INs in the ventral horn at higher magnification. Insets represent labeling pattern of V1-derived interneurons seen in each animal model. **A2**, In *En1-Cre/R26-lacZ* mice,  $\beta$ -gal-IR (green) is concentrated in the nucleus and in intracytoplasmic inclusions (arrowheads). **B2**, In *En1-Cre/Tau-lacZ* mice,  $\beta$ -gal-IR is concentrated in the nucleus, but intracytoplasmic inclusions are not seen. **C2**, YFP-IR (green) in *En1-Cre/Thy1-YFP* mice is seen in the somata, dendrites, and axons (labeling in lateral and ventral funiculi) of V1-derived interneurons. **A3**, **B3**, **C3**, NeuroLucida plots on the distribution and number of V1-INs in the ventral horn of *En1-Cre/R26-lacZ* (**A3**), *En1-Cre/Tau-lacZ* (**B3**), and *En1-Cre/Thy1-YFP* (**C3**) mice. NeuroLucida plots were used to determine the percentage of NeuN-IR cells with V1 lineage markers ( $\beta$ -gal or YFP). NeuN plots are not shown for clarity. **D**, Percentage of V1-derived interneurons in the ventral horn of all three mouse models. Error bars indicate S.E.M. V1-INs make up approximately 23-25% of all NeuN-IR cells in the ventral horn of *En1-Cre/R26-lacZ* and *Tau-lacZ* mice. However, in *En1-Cre/Thy1-YFP* mice, V1-derived interneurons make up only 16% of all NeuN-IR cells in the ventral horn. Differences between the percentage of NeuN-IR cells that contained V1 lineage markers was significant between *En1-Cre/R26-lacZ* and *Tau-lacZ* mice when compared to *En1-Cre/Thy1-YFP* mice (asterisk;  $p < 0.05$ , one-way ANOVA), but not between *En1-Cre/R26-lacZ* and *Tau-lacZ* mice ( $p = 0.203$  t-test). **E**, Inset in **C2** at higher magnification to show extent of labeling in *En1-Cre/Thy1-YFP* mice. Arrows indicate EGFP-IR axons contacting a large NeuN-IR cell (presumably a motoneuron). Scale bars; **A**, **B**, **C** series, (in **A1**, **A2**, and **A3**) 100  $\mu$ m; **Inset in C2** and **E**, 20  $\mu$ m; **Insets in A2** and **B2**, 10  $\mu$ m.



(23.3%  $\pm$  1.45) ( $p=0.203$ , t-test) (Figure 28D). In *En1-Cre/Thy1-YFP* mice, only 18%  $\pm$  1.23 of NeuN-IR cells expressed YFP and this was significantly different compared to the other two lines ( $p<0.001$ , One-way ANOVA,  $p<0.05$ , *post-hoc* Dunn's tests). Therefore, only 73.6% of all V1-derived interneurons were labeled in *En1-Cre/Thy1-YFP* mice.

In summary, the cell bodies, dendrites and axons of most V1-INs are best labeled in *En1-Cre/Thy1-YFP* mice. Because of its optimal visualization of somatic and dendritic surfaces we used this model to analyze postnatal development of synaptic connectivity. However, some expression mosaicism was noted and this prevents us from claiming that the whole population of V1-derived Ia inhibitory interneurons (IaINs) and Renshaw cells (RCs) were labeled in *En1-Cre/Thy1-YFP* mice.

*Criteria for Renshaw cell and V1-derived Ia inhibitory interneuron identification in En1-Cre/Thy1-YFP mice.*

Renshaw cells were identified in *En1-Cre/Thy1-YFP* mice by their ventral location in the “Renshaw cell area”, their relatively intense CB-IR throughout development and V1-derivation (see Alvarez and Fyffe, 2007 for a critical review of these criteria; also see aim 1).

Regarding IaINs, unfortunately PV is not expressed in V1-INs until late in postnatal development and PV labeling of V1-IN dendrites is less efficient than YFP. Therefore, in this study, V1-derived IaINs (V1-IaINs) were recognized as YFP interneurons receiving a dense pericellular basket innervation from RC axons identified



by their V1-origin (YFP-IR) and CB-immunoreactivity (Figure 29). Although it is likely that not all IaINs are densely innervated with pericellular CB-IR baskets, these criteria allow unambiguous detection of a population of V1-IaINs to compare synaptic input development with V1-RCs. These cells can be identified from P1 and by P15 many (25%) YFP V1-INs with pericellular baskets had upregulated PV-immunoreactivity.

However we found that not all PV-IR IaINs identified using these criteria are V1-derived. In P15 *En1-Cre/Thy1-YFP* lower lumbar segments (L4-L5) only 59% of 187 PV-IR cells with CB-IR contacts expressed YFP. As mentioned earlier we expect  $\frac{3}{4}$  of V1-INs labeled in *En1-Cre/Thy1-YFP* mice. Therefore we repeated this analysis in *En1-Cre/Tau-mEGFP-nlslacZ* mice and also compared upper lumbar levels (L2-L3), with lower lumbar levels (L4-L5) (Figure 30). While 68% of PV-IR cells receiving RC inputs (n=667) were V1-derived ( $\beta$ gal-IR) in L4-L5, significantly fewer (49%, n=671 p<0.01 t-test) were V1-derived in L2-L3 segments. PV-IR cells in lower lumbar levels (L4-L5) are largely V1-derived, whereas 50% of those occupying upper lumbar levels (L2-L3) are non-V1-derived.

In summary, IaINs consist of various populations with differing embryonic origins. The groups of IaINs we focus on here are lower lumbar V1-derived IaINs that can be recognized by pericellular baskets of V1 CB-IR axons and that when mature express parvalbumin. Other populations of IaINs, either non-V1-derived or V1-derived but with a lesser RC input are undetected by our criteria.

**Figure 29.** Histochemical identification of V1-IaINs in *En1-Cre/Thy1-YFP* mice. **A1**, Low magnification image of the ventral horn of an *En1-Cre/Thy1-YFP* P15 mouse spinal cord showing, CB-IR (Cy5, blue) and YFP-IR (FITC, green). The dotted white line indicates the border between the ventral horn and white matter. Box indicates the YFP-IR cell shown at higher magnification in A2 and A3. **A2, A3**, High magnification of an YFP-IR V1-IN (green) which receives a dense innervation from CB-IR axons (blue). These criteria were used to identify V1-IaINs throughout this study. **B**, Low magnification confocal images of an *En1-Cre/Thy1-YFP* P15 ventral horn labeled with Parvalbumin (PV-IR; Cy3, red) and CB (Cy5, blue). Previously, IaINs were identified as PV-IR cells with a dense innervation from CB-IR Renshaw cells. Since PV-IR is limited in the extent of staining (labeling largely seen in the soma and proximal dendrites) and in the ages in which it can be used as a reliable marker of IaINs; V1-derived IaINs in this study were identified as YFP-IR cells with a dense innervation from CB-IR axons from V1-derived Renshaw cells. Box indicates PV-IR cell shown at higher magnification in B2 and B3. **B2**, High magnification image of a PV-IR (red; B1) cell with CB-IR (blue; B1-B2) contacts. Box indicates area shown in inset. Inset, Higher magnification images showing CB-IR contacts. **B3**, Superimposed CB-IR and YFP-IR (FITC, green) on a PV-IR cell. Inset, higher magnification image showing co-localization between YFP and CB-IR contacts on a V1-IaIN verifying that the CB-IR contacts on V1-IaINs are from V1-INs. Scale bars; **A1 and B1** (in A1 and B1), 100  $\mu\text{m}$ ; **A2, A3, B2, and B3**, (in A2 and B2) 20  $\mu\text{m}$ .

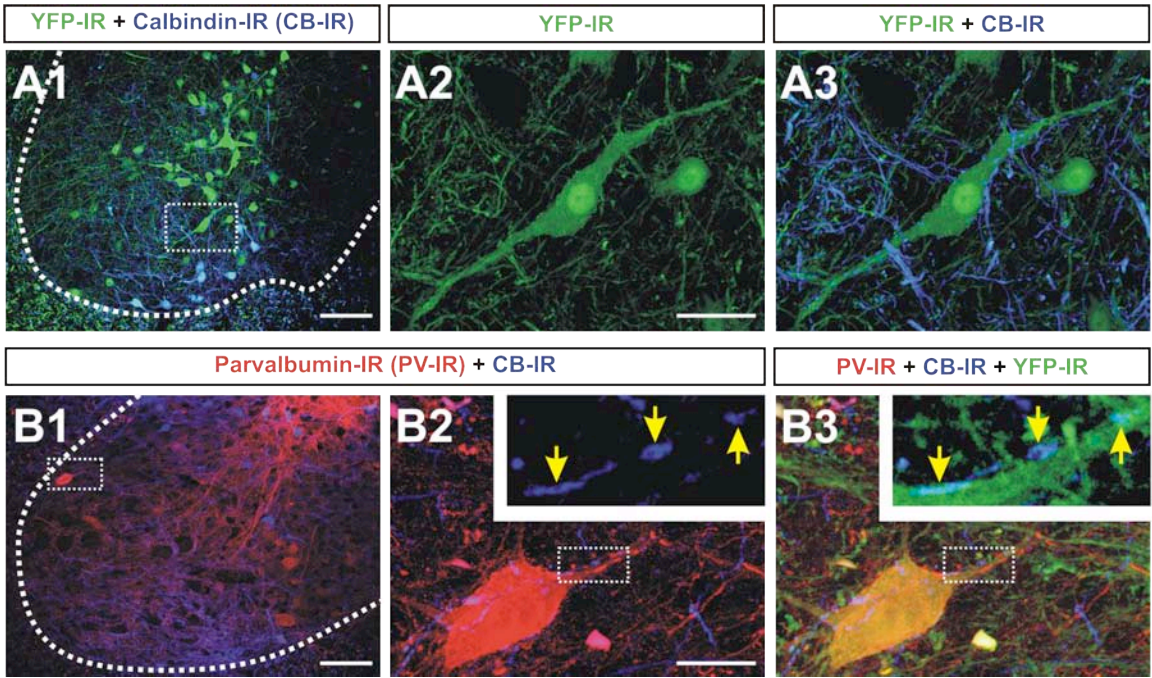
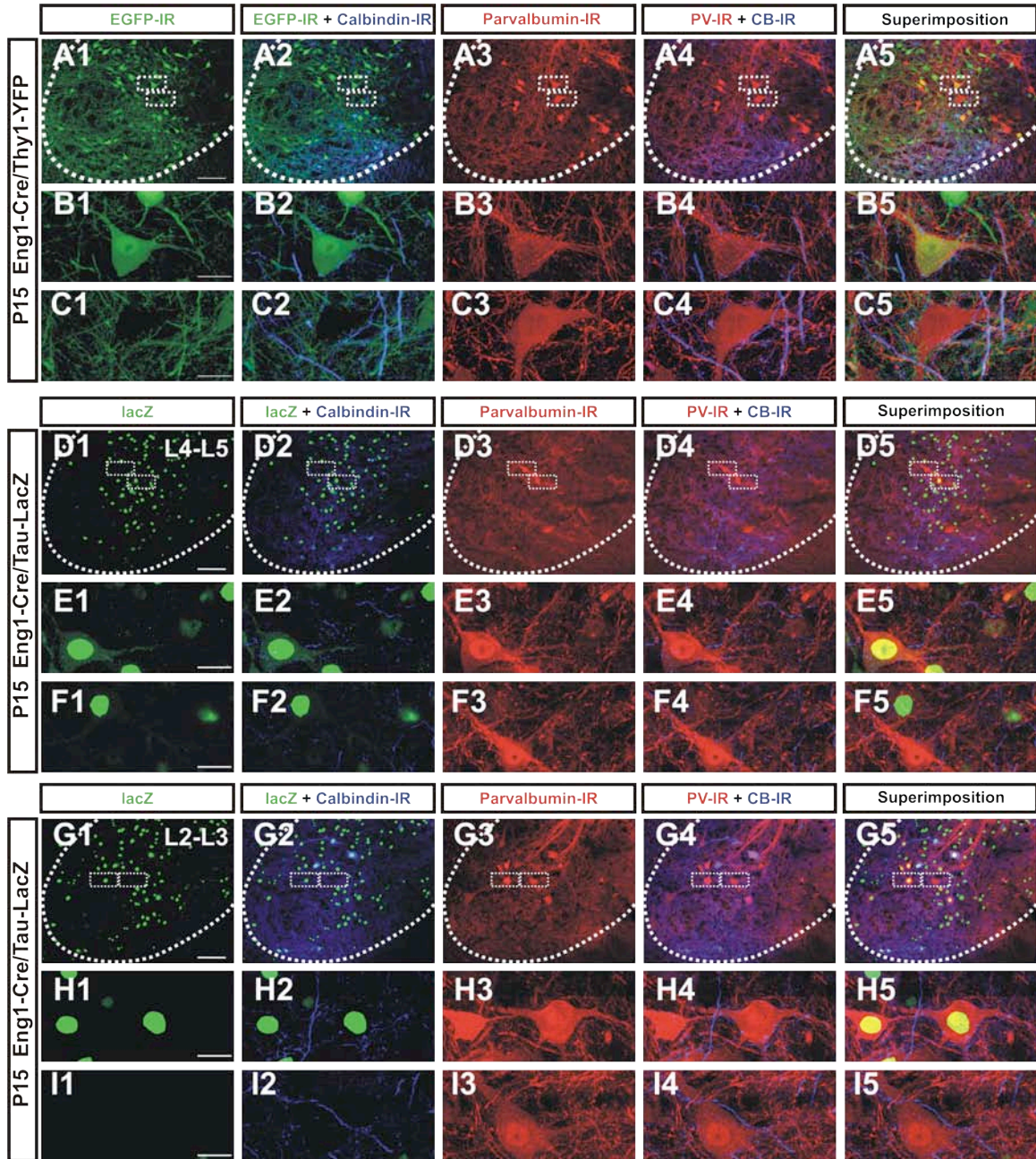


**Figure 30.** Lineage of Parvalbumin-IR IaINs. **A**, Low magnification confocal images of a P15 ventral horn section from an *En1-Cre/Thy1-YFP* mouse spinal cord immunolabeled for YFP (FITC, green) (A1 and A2), Calbindin (Cy5, blue) (A2 and A4), and Parvalbumin (Cy3, red) (A3 and A4). Superimposition in A5. The dotted line indicates the border between the ventral horn and the white matter. Boxes indicate areas shown at higher magnification in B and C. **B, C**, Higher magnification images of the areas indicated in A showing YFP-IR (green; B1, B2, C1, and C2), CB-IR (blue; B2, B4, C2, and C4), and PV-IR (red; B3, B4, C3, and C4). Superimposition in B5 and C5. The cell in the B series represents a PV-IR cell, receiving a dense innervation from CB-IR axons, which is also YFP-IR. The PV-IR cell shown in the C series also receives a dense innervation from CB-IR V1-derived axons, but it is not YFP-IR. Therefore, not all PV-IR cells in *En1-Cre/Thy1-YFP* P15 mice are YFP-IR. The reporter label indicates V1-derived. **D**, Low magnification images of a ventral horn section from lumbar segments L4 and L5 of an *En1-Cre/Tau-lacZ* P15 mouse showing  $\beta$ -gal-IR (FITC, green) (D1 and D2), Calbindin-IR (Cy5, blue) (D2 and D4), and Parvalbumin-IR (Cy3, red) (D3 and D4). Superimposition in D5. Boxes indicate cells shown at higher magnification in E and F series. **E, F**, High magnification confocal images of  $\beta$ -gal-IR (green; E1, E2, F1, and F2), CB-IR (blue; E2, E4, F2, and F4), and PV-IR (red; E3, E4, F3, and F4). Superimposition in E5 and F5. The cell in the E series is a PV-IR cell with a dense innervation from CB-IR Renshaw cell axons, which is LacZ<sup>+</sup>. The F series shows a PV-IR, which also receives inputs from CB-IR axons, but it is not LacZ<sup>+</sup>. In lumbar segments L4 and L5, there are twice as many PV-IR cells that are LacZ<sup>+</sup> compared to those PV-IR cells that are not LacZ<sup>+</sup> ( $p < 0.001$ , t-test). **G**, Low magnification confocal images of a ventral horn section from lumbar segments L2 and L3 of a P15 *En1-Cre/Tau-lacZ* mouse spinal cord immunolabeled for  $\beta$ -gal (FITC, green) (G1 and G2), CB (Cy5, blue) (G2 and G4), and PV (Cy3, red) (G3 and G4). Superimposition in G5. **H, I**, High magnification confocal images of PV-IR (H3, H4, I3, and I4) cells receiving a dense innervation from CB-IR RC axons (H4 and I4), which are (H5) or are not (I5) LacZ<sup>+</sup>. There were no significant differences in the percentage of PV-IR cells in L2 and L3 that are LacZ<sup>+</sup> and those that are not LacZ<sup>+</sup> ( $p = 0.397$ , t-test). When compared to L4 and L5, there are significantly more PV-IR cells in L2 and L3 that are not LacZ<sup>+</sup> ( $p < 0.001$ , t-test). Scale bars; **A, D, and G series** (in A1, D1, and G1), 100  $\mu\text{m}$ ; **B, C, E, F, H, and I series** (in B1, C1, E1, F1, H1, and I1), 20  $\mu\text{m}$ .



*Validation of VGLUT1-IR synaptic contacts to analyze proprioceptive sensory inputs on V1-derived Ia inhibitory interneurons and Renshaw cells.*

Of the three known isoforms of VGLUTs, VGLUT1 is a synaptic marker for large primary sensory afferents (Todd et al., 2003; Oliveira et al., 2003; Alvarez et al., 2004). VGLUT1-IR was therefore used to identify proprioceptive sensory afferent synapses on developing V1-derived IaINs and RCs in *En1-Cre/Thy1-YFP* mice. Most ventral horn VGLUT1-IR boutons are likely originated from proprioceptors since they are anterogradely labeled from dorsal roots, contain parvalbumin immunoreactivity, most disappear after dorsal rhizotomies and they are largely deleted in the ventral horns of *Er81<sup>(-/-)</sup>* animals which lack ventral horn proprioceptive axons (Alvarez et al., 2004; Mentis et al., 2006). Some ventral horn VGLUT1-IR synapses might however originate from the corticospinal tract (CST) (Alvarez et al., 2004; Persson et al., 2006). Moreover, *Er81* is also expressed by CST neurons (Yoneshima et al., 2006), and it is possible that anomalies in CST VGLUT1-IR boutons are also present in *Er81<sup>(-/-)</sup>* animals. Alternative unknown descending projections could also contribute VGLUT1-IR synapses in the ventral horn. To confirm that VGLUT1-IR contacts on V1-IaINs and RCs originate from sensory afferents we analyzed their co-localization with parvalbumin, which specifically labels sensory afferents in neonatal spinal cords (Arber et al., 2000). To diminish confounding effects from interneuron parvalbumin axons we performed the analysis at P10 (Figure 31). Co-localization of PV inside VGLUT1-IR clusters was determined as PV-immunofluorescence intensity 2 standard deviations above background. At P10, 82% and 85% of VGLUT1-IR contacts respectively on RCs (n = 177 contacts) and V1-IaINs (n = 215) contained PV. This small difference was not significant (p=0.586, t-test).



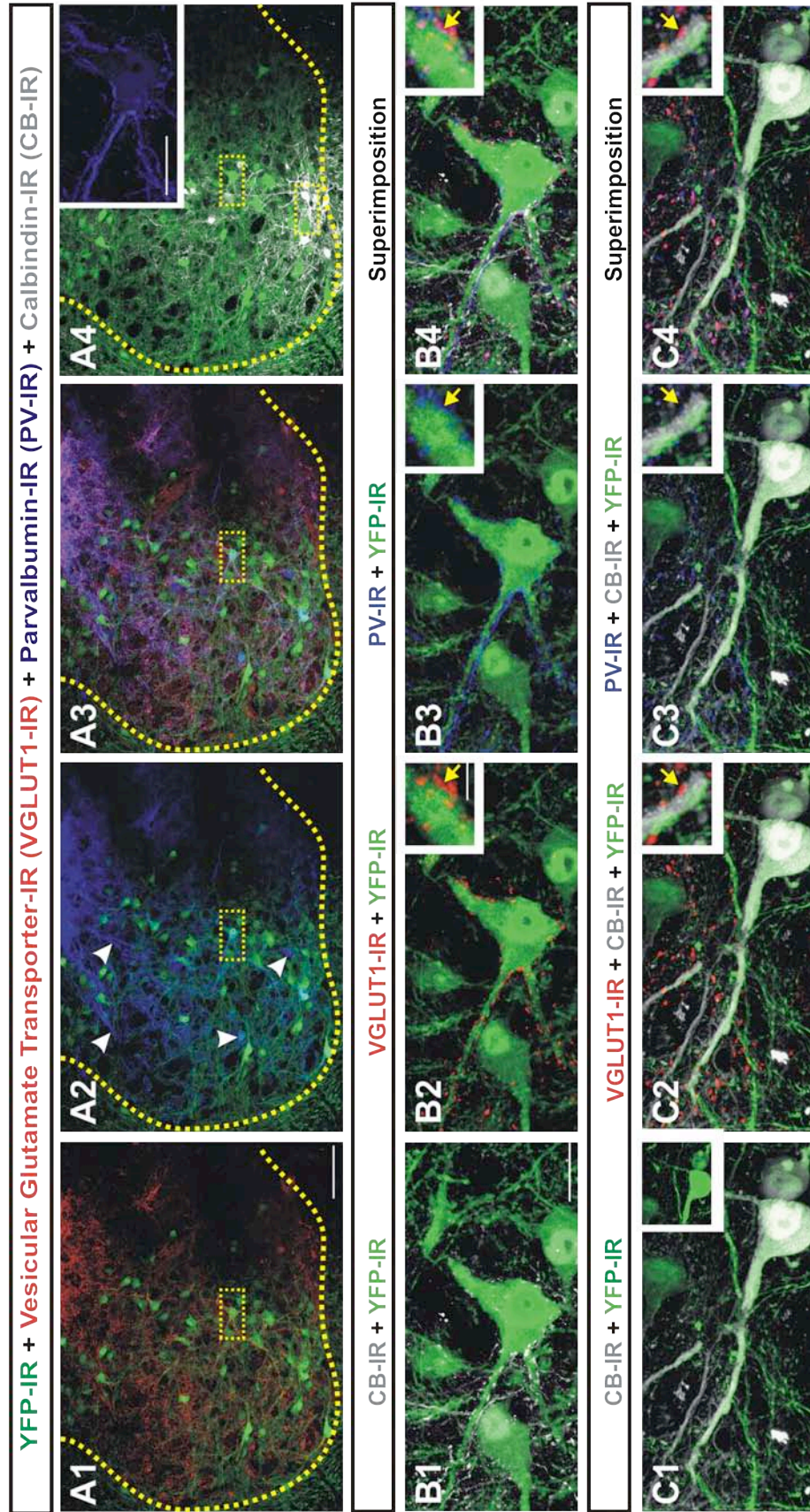
Similarly no differences were detected on average PV immunofluorescence intensity inside P10 VGLUT1-IR contacts on each cell type ( $1701.69 \pm 591.61$  on V1-IaINs and  $1600.73 \pm 707.27$  on RCs; average  $\pm$  SD, arbitrary units from 24 bit images). Several alternative explanations can be raised to explain the remaining 15-18% of boutons that were PV negative. They might originate from alternative sources or they might suggest PV underdetection because our stringent criteria for PV-IR (92% were labeled at 1 SD above background) or might represent primary afferents boutons that started to downregulate their PV-content (primary afferents synaptic boutons in the ventral horn downregulate PV with development). These alternative possibilities were not pursued further. We can conclude however that the large majority of VGLUT1-IR synaptic inputs on V1-IaINs and RCs originate from proprioceptive sensory afferents.

*VGLUT1-IR input strength on V1-derived IaINs is higher than on V1-derived RCs during postnatal development.*

Because most VGLUT1-IR contacts target dendrites, VGLUT1 synaptic densities were analyzed using NeuroLucida-based reconstructions of YFP-labeled dendritic trees from approximately 20 V1-IaINs and 20 V1-RCs sampled in two *En1-Cre/Thy1-YFP* mice at each different age (P10, P15, P20 and adult or P40; at P5 only 10 cells of each type were analyzed in one animal, examples in Figure 32). No differences were found between cells sampled from different animals. Therefore cells of the same type and age from the two different animals were pooled together (cells from each animal represent approximately 50% of the total sample). Synaptic densities were calculated as VGLUT1-

**Figure 31.** Origin of proprioceptive sensory afferents on V1-derived Ia inhibitory interneurons and V1-derived Renshaw cells in *En1-cre/Thyl-YFP* mice. **A**, Low magnification images of a ventral horn section from *En1-Cre/Thyl-YFP* P10 mouse immunolabeled for YFP (FITC, Green) (A1), VGLUT1 (Cy3, Red) (A2), Parvalbumin (PV; Cy5, Blue) (A3), and Calbindin (CB; 405, White) (A4). At P10, PV-IR is strong in proprioceptive sensory afferents and labels few interneuron cell bodies (arrowheads; A2). Inset in A4 shows that the V1-cell shown at high magnification in B is PV-IR. Boxes indicate areas of high magnification shown in B and C. The dotted line indicates the border between the ventral horn and the white matter. **B1, B2, B3, B4**, High magnification confocal images of an YFP-IR (green) V1-IaIN that receives inputs from V1-derived CB-IR axons (white; B1). Yellow arrows represent contacts that are VGLUT1-IR (B2) and PV-IR (B3). Superimposition in B4. Asterisks in B3, B4, and B5 indicate insets showing, at higher magnification, VGLUT1-IR contacts co-localized with PV. **C1, C2, C3, C4**, High magnification images of an YFP-IR and CB-IR V1-derived Renshaw cell. Yellow arrows represent contacts on RCs that are VGLUT1 (C2) and PV-IR (C3). Superimposition in C4. 82-85% of all VGLUT1-IR contacts on RCs and IaINs, respectively, co-localized with PV-IR. Scale bars; **A series** (in A1), 100  $\mu\text{m}$ ; **B and C series and inset in A4** (in B1, C1, and A4), 20  $\mu\text{m}$ ; **Insets in B and C series** (in B1 and C1), 10  $\mu\text{m}$ .





IR contacts per 10  $\mu\text{m}$  of linear dendrite. At P5 V1-IaINs already displayed a larger number of VGLUT1-IR contacts compared to RCs. Moreover, VGLUT1-IR contacts on V1-IaINs significantly increased during development ( $p < 0.001$ , one-way ANOVA, Figure 33C, Table 7). *Post hoc* tests indicated that the increases in density from P10 to P15 were significant ( $p < 0.05$ , *post hoc* Dunn's test). No differences were detected between P15, P20 and adult ( $p = 0.488$ , one-way ANOVA). Estimation of VGLUT1-IR contact density on developing YFP and CB-labeled RC dendrites sampled in parallel to V1-IaINs replicated our previous findings on CB-IR RCs (Aim 1 and Mentis et al., 2006). VGLUT1-IR contact density significantly increased from P5 to P15 and then significantly decreased in P20 and adult ( $p < 0.001$ , one-way ANOVA; VGLUT1-IR density at P15 was significantly higher than in all other ages  $p < 0.05$ , *post hoc* Dunn's test). When compared to V1-IaINs, VGLUT1-IR density in RC dendrites was always significantly lower (P5  $p = 0.005$ ; P10  $p = < 0.001$ ; P15  $p = 0.024$ ; P20  $p = < 0.001$ ; P40  $p = < 0.001$ , t-tests) (Figure 33C, Table 7). A significant number of VGLUT1-IR contacts target the somata of IaINs (20% of all contacts sampled), but not RCs (5% or less of all contacts sampled), therefore differences in contact density and number were even more exaggerated when comparing the cell bodies of adult (P40) V1-IaINs and RCs (Figure 33D, Table 8).

The possibility that differences exist in the proximo-distal distributions of VGLUT1-IR boutons on IaIN dendrites was investigated using Sholl analyses. The dendritic arbor was divided in three compartments (0-50  $\mu\text{m}$ , 50-100  $\mu\text{m}$  and 100-150  $\mu\text{m}$ ) that were well visualized with YFP labeling in the majority of cells. With distance there was a tendency towards decreasing densities in V1-IaINs and increasing densities in

RCs, however differences in contact density at different dendritic distances were not significant in any of the two cell types ( $p>0.05$ , one-way ANOVA, Figure 33E). At each distance bin VGLUT1-IR contact density on V1-IaINs is always significantly higher when compared to RCs ( $p<0.001$ , t-tests). The percentage of VGLUT1-IR boutons sampled in each cell was consistently higher in the proximal regions of the dendrite compared to the soma and distal dendrite compartment. However a higher percentage of VGLUT1-IR boutons were located in the first 50  $\mu\text{m}$  of dendrite and cell body (70 %) on V1-IaINs compared to RCs (52 %). Also interestingly, mature VGLUT1-IR contacts on V1-IaIN dendrites and somata were significantly larger than those contacting RCs ( $4.5\pm 1.7$  and  $4.0\pm 1.3 \mu\text{m}^2$ , respectively; average  $\pm$  SD;  $p=0.003$ , t-test). This analysis was conducted at P15, a postnatal time at which VGLUT1-IR cluster growth and immunofluorescence intensity plateaus (Aim 1 and Mentis et al., 2006).

In summary, VGLUT1-IR input density increases in V1-IaINs and RCs from P5 to P15, however V1-IaINs receive a higher density of contacts than RCs at any postnatal age. In addition, VGLUT1-IR contact density is maintained on developing V1-IaINs after P15, by contrast, VGLUT1-IR contact density decreases on RCs after P15. Finally in the mature spinal cord the larger size and more proximal locations of VGLUT1-IR contacts on IaINs suggest a higher input strength on these cells compared to RCs.

*VACHT-IR bouton density on V1-derived IaINs is lower than on Renshaw cells of all ages and preferentially target the cell soma and initial segment of primary dendrites.*

Vesicular Acetylcholine Transporter (VACHT), which packages acetylcholine into synaptic vesicles for exocytosis, is an effective synaptic marker of motor axons in the

**Figure 32.** Development of VGLUT1-immunoreactive contacts on V1-derived Ia inhibitory interneurons and V1-derived Renshaw cells in postnatal *En1-Cre/Thy1-YFP* mice. **A1, B1, C1**, Low magnification images of VGLUT1-IR (CY3, Red), YFP-IR (FITC, Green), and Calbindin-immunoreactivity (CB-IR; CY5, Blue) in the ventral horn at P5 (A1), P15 (B1), and P40 (C1) in *En1-Cre/Thy1-YFP* mice. Yellow dotted line indicates border between the ventral horn and the white matter. Boxes indicate areas shown at higher magnification in A2-A3, B2-B3, and C2-C3. **A2, B2, C2**, High magnification confocal images showing that at P5 (A2), P15 (B2), and P40 (C2), YFP-IR V1-derived Ia inhibitory interneurons (green) with a dense innervation from V1-derived CB-IR Renshaw cell axons (blue) receive VGLUT1-IR contacts (red). Arrowheads indicate VGLUT1-IR contacts on V1-IaIN dendrites and cell bodies. The number of VGLUT1-IR contacts on V1-IaINs increases from P5 to P15. Insets indicate, at higher magnification, VGLUT1-IR contacts on V1-IaIN somata and dendrites. **A3, B3, C3**, VGLUT1-IR contacts on V1-derived Renshaw cells that are both CB-IR and YFP-IR at P5 (A3), P15 (B3), and P40 (C3). Arrowheads indicate VGLUT1-IR contacts on RC dendrites. There are fewer contacts on RCs at P5 and P40 compared to P15. Insets show VGLUT1-IR contacts on RC dendrites. Scale bars; **A1, B1, and C1**, (in A1) 100  $\mu\text{m}$ ; **A2-A3, B2-B3, and C2-C3**, (in A2) 20  $\mu\text{m}$ ; **Insets**, 10  $\mu\text{m}$ .

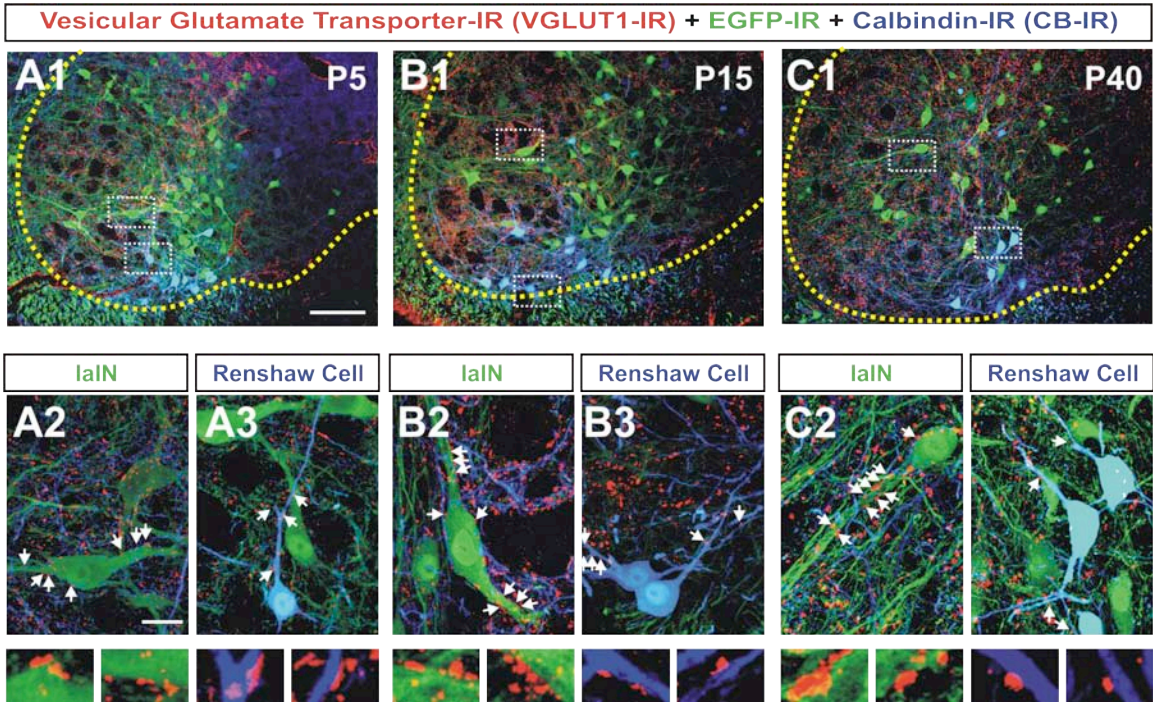
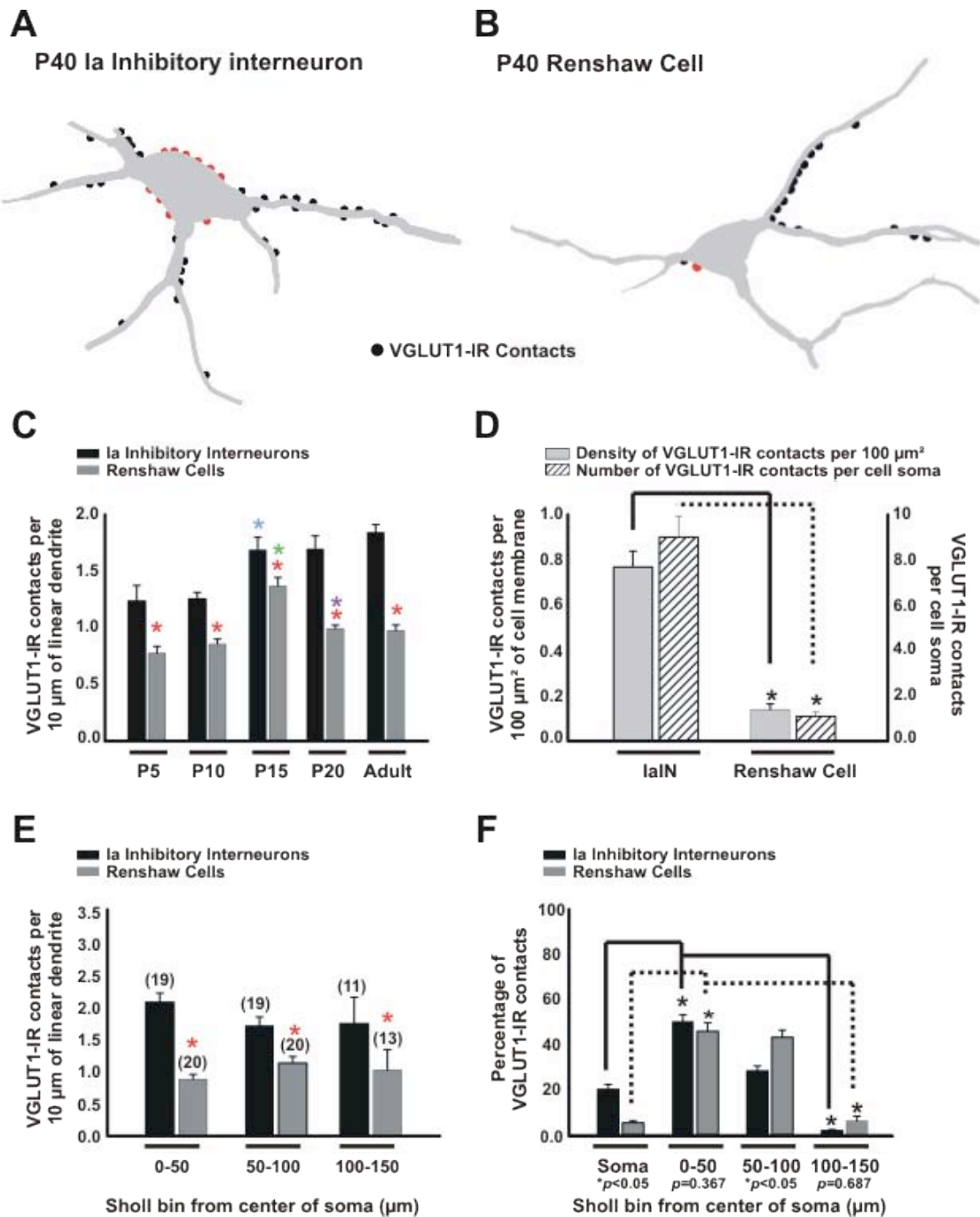




**Figure 33.** Density and distribution of VGLUT1-IR contacts on V1-derived IaINs compared to Renshaw cells. **A,B**, 3D reconstruction of a V1-derived Ia inhibitory interneuron (A) and Renshaw cell (B) from a P40 *En1-Cre/Thy1-YFP* mouse reconstructed in NeuroLucida using the confocal module. VGLUT1-IR contacts are plotted on the dendrites (black dots) and soma (red dots). Densities of contacts are calculated as plotting the number of contacts per 10  $\mu\text{m}$  of linear dendrite. **C**, Quantitative analysis of the linear density of VGLUT1-IR contacts on V1-IaINs and CB-IR RCs in *En1-Cre/Thy1-YFP* mice of P5, P10, P15, P20, and adult (P40) ages. V1-IaINs display statistically significant increases in VGLUT1-IR contact density from P10 to P15 (blue asterisk,  $p=0.05$ , one-way ANOVA). VGLUT1-IR contact density on V1-IaINs are maintained after P15 and no significant differences were found between P15, P20, and adult ( $p=0.488$ , one-way ANOVA). VGLUT1-IR input density on CB-IR Renshaw cells increases significantly from P5 to P15 (green asterisk;  $p<0.05$ , one-way ANOVA) and the decrease at P20 is also significant (purple asterisk;  $p<0.05$ , one-way ANOVA). No significant differences are seen between P20 and adult ( $p=0.715$ , t-test). At all ages, VGLUT1-IR contact density on V1-IaINs is always significantly higher when compared to RCs (red asterisks, P5  $p=0.005$ ; P10  $p<0.001$ ; P15  $p=0.024$ ; P20  $p<0.001$ ; P40  $p<0.001$ , t-tests). **D**, VGLUT1-IR contacts per 100  $\mu\text{m}^2$  of cell membrane and total number of VGLUT1-IR contacts per cell soma on V1-IaINs and RCs at P40. The density of VGLUT1-IR contacts on the cell soma of V1-IaINs was always significantly greater than that on RCs (one asterisk;  $p<0.001$ , t-test). This difference was due to there being significantly more VGLUT1-IR contacts on V1-IaIN cell somas compared to RCs (two asterisks;  $p<0.001$ , t-test). **E**, Sholl analysis of VGLUT1-IR contacts (per 10  $\mu\text{m}$  of linear dendrite). Numbers in parentheses indicate the number of cells that showed data in each distance bin. There were no significant differences in the distribution of VGLUT1-IR contacts among V1-IaINs ( $p=0.318$ , one-way ANOVA). RCs also showed no significant differences in the distribution of VGLUT1-IR contacts ( $p=0.336$ , one-way ANOVA). At all distance bins, the density of VGLUT1-IR contacts on IaINs is always significantly higher when compared to RCs ( $p<0.05$ , one-way ANOVA). **F**, Percentage of VGLUT1-IR contacts on the soma and in each 50  $\mu\text{m}$  bin in V1-IaINs and RCs. Most VGLUT1-IR contacts on V1-IaINs are distributed between the soma and in the first 100  $\mu\text{m}$  of linear dendrite. Significantly more VGLUT1-IR contacts were seen in the first 50  $\mu\text{m}$  of dendrite compared to the soma and the other dendritic bins of V1-IaINs (one asterisk;  $p<0.05$ , one-way ANOVA). Similar to V1-IaINs, most VGLUT1-IR contacts on RCs are in the first 100  $\mu\text{m}$  of linear dendrite, but unlike V1-IaINs, RC somas do not receive a large percentage of VGLUT1-IR contacts. There are significantly more VGLUT1-IR contacts in the first 100  $\mu\text{m}$  of RC dendrite compared to the soma and the last 100-150  $\mu\text{m}$  of RC dendrite (two asterisks;  $p<0.05$ , one-way ANOVA). No significant differences were seen between the 0-50 and 50-100  $\mu\text{m}$  dendritic bins ( $p=0.590$ , one-way ANOVA). P-values in parentheses below graph indicate any significant differences in the percentage of contacts on the soma and in each bin between V1-IaINs and RCs.



ventral horn (Alvarez et al., 1997). Indeed, VAcHT-IR contacts on RCs can be retrogradely labeled from ventral roots and disappear in adult superoxide dismutase 1-mutant animals undergoing motor axon degeneration (FitzSimons et al., 2006). Few VAcHT-IR contacts were seen on V1-IaIN dendrites at P20 (Alvarez et al. 2005), therefore we analyzed the possibility that this input was removed from V1-IaINs postnatally (Figure 34). However VAcHT-IR contacts were sparse on the dendrites of V1-IaINs of any age and their density was always much lower than on RCs (P5-P40,  $p < 0.001$ , t-tests paired comparison at each age) (Figure 35, Table 7). In addition, VAcHT-IR contact density on V1-IaIN dendrites significantly decreased by a third from P5 to P15 ( $p < 0.05$ , one-way ANOVA; Table 7). After P15 VAcHT-IR contact density on V1-IaIN dendrites was relatively stable and no significant differences were found between P15, P20, and adult ( $p = 0.316$ , one-way ANOVA). In contrast, VAcHT-IR contact density on RC dendrites increased significantly from P5 to P20 ( $p < 0.05$ , one-way ANOVA) and then it was maintained after P20.

Surprisingly, the somata of V1-IaINs receive a four-fold larger number of VAcHT-IR contacts compared to RCs ( $p < 0.001$ , t-test). Approximately 44% of all VAcHT-IR contacts targeted the cell body of IaINs. V1-IaIN somata are larger than RC somata, nevertheless these larger number of boutons represent a significant two-fold increase in VAcHT-IR contact density on V1-IaINs compared to RCs ( $p < 0.01$ , t-test)(Figure 35D). No significant differences were found in the density of VAcHT-IR contacts on different dendritic compartments of V1-IaINs or RCs, although at each compartment density was much lower on IaINs (Figure 35E). Similar to VGLUT1, most VAcHT-IR contacts on RCs (~89%) were located within the first 100  $\mu\text{m}$  of dendrite



analyzed and very few on RC somata (~4.6%). VAcHT-IR contacts on V1-IaINs were distributed differently and also different to VGLUT1 contact distributions in these same cells (Figure 35). Most VAcHT-IR contacts were located on the soma and together with the first dendritic compartment (first 50  $\mu\text{m}$ ) they account for the vast majority of contacts (~82%). Other than one V1-IaIN with one VAcHT-IR contact, no contacts were found beyond 100  $\mu\text{m}$  on the dendrite. Therefore, when compared to RCs, VAcHT-IR contacts on V1-IaINs are preferentially located on the soma and the initial stem of the primary dendrites.

The average size of VAcHT-IR contacts on V1-IaINs was less than half compared to those contacting RCs ( $1.5 \pm 0.4$  and  $3.4 \pm 1.9 \mu\text{m}^2$ , respectively;  $p < 0.001$ , t-test) (Figure 34). Previously spinal cord VAcHT-IR labeled synapses of different size were predicted to have different sources (Alvarez et al., 1999). To investigate if VAcHT-IR terminals on V1-IaINs were of motor axon origin Cascade Blue fluorescent dextran was applied to the L5 ventral root of one P7 *En1-Cre/Thy1-YFP* mouse and the percentages of retrogradely labeled VAcHT-IR boutons on V1-IaINs and CB-IR RCs was estimated (Figure 36). The large majority of VAcHT-IR boutons on CB-IR RCs (80.2%,  $n = 190$  boutons) contained retrograde labeling, however only 6.9% of VAcHT-IR boutons ( $n = 162$ ) on V1-IaINs were labeled.

In summary, V1-IaINs do not receive a significant VAcHT-IR input on their distal dendrites at any time during development. However, surprisingly their somata and most proximal dendrites are the specific targets of a VAcHT-IR input (numerical data summarized in Tables 7 & 8). These synapses are at relatively high density but are small in size and are not originated from cholinergic motor axons. In conclusion, the origins

**Figure 34.** Development of VAcHT-immunoreactive contacts on V1-derived Ia inhibitory interneurons and Renshaw cells in postnatal *En1-Cre/Thy1-YFP* mice. **A1,B1,C1**, *En1-Cre/Thy1-YFP* mouse spinal cords at P5 (A1), P15 (B1), and P40 (C1) showing Calbindin-immunoreactivity (CB-IR; Cy5, blue), YFP-IR (FITC, green) and VAcHT-IR (CY3, Red) in the ventral horn. Yellow dotted line indicates border between the ventral horn and the white matter. Boxes indicate areas shown at higher magnification in A2-A3, B2-B3, and C2-C3. **A2,B2,C2**, Higher magnification confocal images showing CB-IR axons (blue) contacting YFP-IR V1-derived Ia inhibitory interneurons (V1-IaINs) (green) at P5 (A2), P15 (B2), and P40 (C2) that receive VAcHT-IR inputs (red). Arrows indicate VAcHT-IR contacts on V1-IaIN dendrites and cell bodies. The number of VAcHT-IR contacts on V1-IaINs decreases from P5 to P15. Insets show, at higher magnification, VAcHT-IR contacts on V1-IaIN somata and dendrites. **A3, B3, C3**, Calbindin and YFP-IR Renshaw cells at P5 (A3), P15 (B3), and P40 (C3) that receive VAcHT-IR contacts. Arrows indicate VAcHT-IR contacts on RC dendrites. Most VAcHT-IR contacts on RCs are on the dendrites. There are more VAcHT-IR contacts on RCs at P40 than at P5. Insets indicate, at higher magnification, VAcHT-IR contacts on RC dendrites. **D1**, Low magnification image of VAcHT-IR (Cy3, red), YFP-IR (FITC, green), and Calbindin-IR (CB-IR; Cy5, blue) in the ventral horn of a P15 *En1-Cre/Thy1-YFP* mouse spinal cord. Boxes indicate areas of high magnification shown in D2 and D3. **D2**, High magnification image of VAcHT-IR contacts (red) on an YFP-IR V1-IaIN (green) that also receives a dense innervation from CB-IR RC dendrites (blue). Arrowheads indicate VAcHT-IR contacts on V1-IaINs. VAcHT-IR inputs on V1-IaINs are located proximally and often on the cell body. **D3**, High magnification image of VAcHT-IR contacts on a CB-IR RC that is also YFP-IR, indicating that it is V1-derived. Arrowheads point to VAcHT-IR contacts on RC dendrites. **E**, Size of VAcHT-IR contacts on soma and dendrites of V1-IaINs compared to RCs. VAcHT-IR contacts on V1-IaINs are significantly smaller than those on RCs ( $p < 0.001$ , t-test). Therefore it appears that the VAcHT-IR contacts on V1-IaINs are possibly from a different source than those on RCs. Scale bars; **A1, B1, C1, and D1**, (in A1 and D1) 100  $\mu\text{m}$ ; **A2-A3, B2-B3, C2-C3, and D2-D3**, (in A2 and D2) 20  $\mu\text{m}$ ; **Insets**, 10  $\mu\text{m}$ .

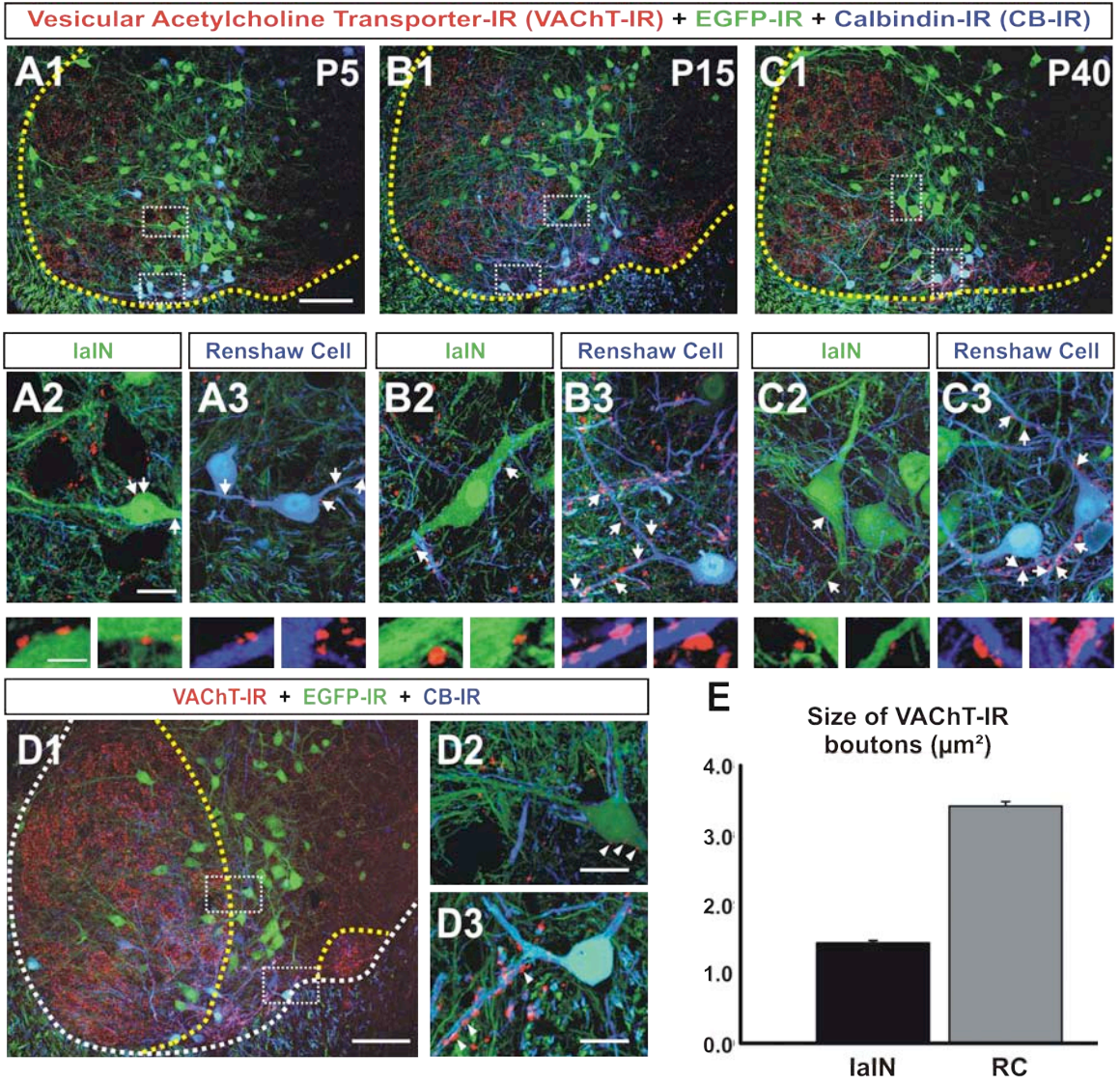


**Figure 35.** Density and distribution of VACHT-IR contacts on V1-derived IaINs compared to Renshaw cells. **A, B,** Neurolucida 3D reconstruction of a V1-IaIN (A) and Renshaw cell (B) from a P40 *En1-Cre/Thy1-YFP* with VACHT-IR contacts plotted on the dendrites (black dots) and soma (red dots) of the reconstruction. **C,** VACHT-IR contacts per 10  $\mu\text{m}$  of linear dendrite of V1-IaINs and CB-IR RCs in *En1-Cre/Thy1-YFP* mice of P5, P10, P15, P20, and adult ages. V1-IaINs display statistically significant decreases in VACHT-IR contact density from P5 to P15 (blue asterisk,  $p < 0.05$ , one-way ANOVA). No significant differences were seen between P5 and P10 ( $p = 0.283$ , one-way ANOVA). VACHT-IR contact density on V1-IaINs decreases slightly after P15 but no significant differences were found between P15, P20, and adult ( $p = 0.316$ , one-way ANOVA). VACHT-IR input density on CB-IR Renshaw cells increases significantly from P5 to P20 (green asterisk,  $p < 0.05$ , one-way ANOVA) and is maintained after P20 with no significant differences between P20 and adult ( $p = 0.052$ , one-way ANOVA). At all ages, VACHT-IR contact density on V1-IaINs is significantly less when compared to RCs (red asterisks, P5-P40  $p < 0.001$ , t-tests). **D,** Quantitative data of VACHT-IR contacts per cell soma and their corresponding densities over V1-IaINs and RCs at P40. V1-IaIN somas are larger than RCs and they receive three-fold more VACHT-IR contacts compared to RCs (two asterisks;  $p < 0.001$ , t-test). This difference in the number of VACHT-IR contacts correlates into a significant two-fold increase in surface density between V1-IaINs and RCs (one asterisk;  $p < 0.001$ , t-test). **E,** Sholl analysis of VACHT-IR contacts on the dendrites of V1-derived IaINs compared to CB-IR RCs in *En1-Cre/Thy1-YFP* mice at P40. Sholl analysis is estimated in 50  $\mu\text{m}$  bins of increasing distance from the center of the cell body. V1-IaINs displayed significant differences in the distribution of VACHT-IR contacts ( $p < 0.05$ , one-way ANOVA). There were no significant differences detected in the distribution of VACHT-IR contacts on RC dendrites at P40 ( $p = 0.113$ , one-way ANOVA). VACHT-IR contact density on RC dendrites was always significantly higher when compared to V1-IaINs ( $p < 0.05$ , one-way ANOVA). **F,** Percentage of VACHT-IR contacts in each Sholl bin (50  $\mu\text{m}$  increments from center of cell soma) in V1-IaINs and RCs at P40. In contrast to VGLUT1-IR contacts, VACHT-IR contacts on V1-IaINs are largely restricted to the soma and the first 50  $\mu\text{m}$  bin. No significant differences were seen in the percentage of VACHT-IR contacts on the soma and the first 50  $\mu\text{m}$  ( $p = 0.134$ , t-test), but there were significantly less VACHT-IR contacts in the 50-100 and 100-150  $\mu\text{m}$  dendritic bins (one asterisk;  $p < 0.05$ , one-way ANOVA). Similar to VGLUT1-IR contacts, most VACHT-IR contacts were in the first 100  $\mu\text{m}$  of RC dendrite. There are significantly more VACHT-IR contacts in the first 100  $\mu\text{m}$  of RC dendrite compared to the soma and the last 100-150  $\mu\text{m}$  of RC dendrite (two asterisks;  $p < 0.05$ , one-way ANOVA).

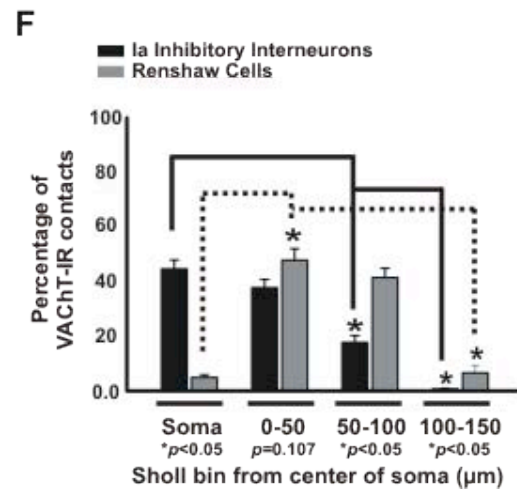
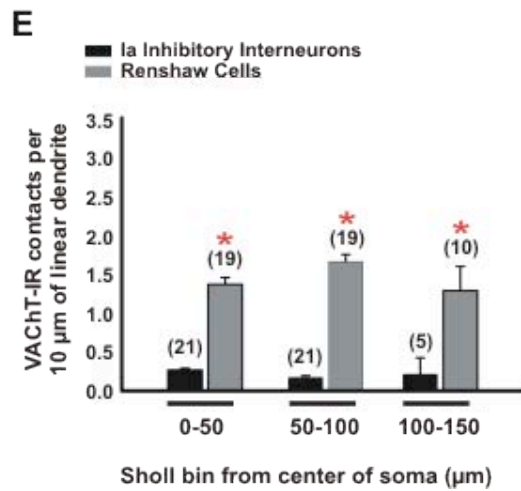
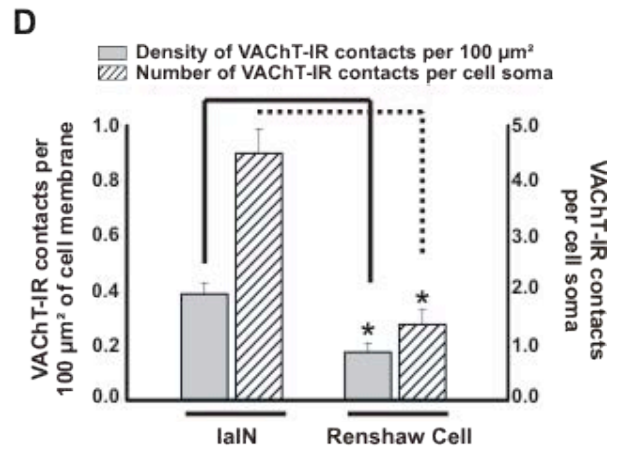
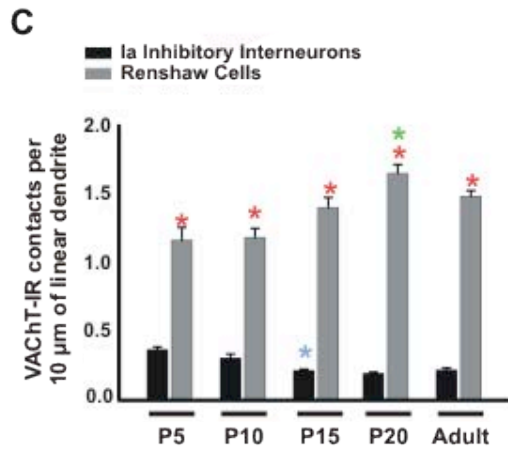
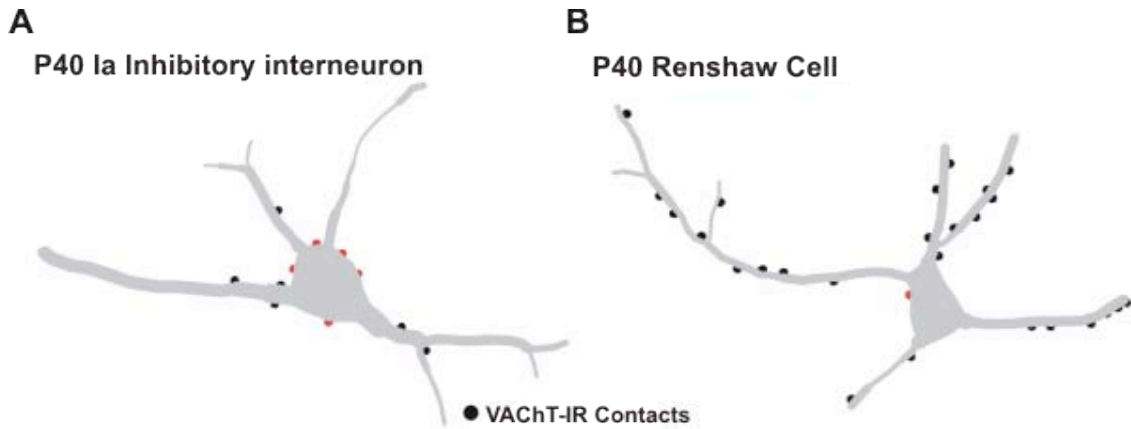


**Figure 36.** Origin of VChT-IR boutons on V1-derived Ia inhibitory interneurons compared to Renshaw cells. **A**, P7 *En1-Cre/Thy1-YFP* spinal cord showing retrogradely labeled motoneurons and motor axon recurrent collaterals (Cascade blue dextran, blue)(A1-A4) superimposed with VChT (Cy3, red)(A2 and A4), naked YFP (Naked YFP, green)(A3-A4), and Calbindin (405, white)(A3 and A4). **A5**, Superimposition of all. Box with one asterisk indicates area shown in the insets in A3 and A4 demonstrating that the CB-IR cells shown in B are YFP-IR and that same area contains VChT-IR. Box with one asterisk is shown at higher magnification in the B and D series and represents the area which is populated with Renshaw cells. Box with two asterisks is shown at higher magnification in the C series and represents the area enriched with V1-IaINs. Yellow dotted line indicates the border between the ventral horn and white matter. **B**, Cells labeled with YFP (green) (B3-B4) that are CB-IR (white) (B3-B4) and contacted by retrogradely labeled motor axon recurrent collaterals (blue) (B1-B3) and VChT-IR boutons (red) (B2 and B4). Superimposition in **B5**. Insets represent VChT-IR boutons that contain retrograde labeling (yellow arrowheads). Most VChT-IR boutons on CB-IR RCs contain retrograde labeling. White arrows demonstrate that not all retrogradely labeled recurrent collaterals contain VChT. **C**, V1-IaIN labeled with YFP with CB-IR axons (C3-C4) showing retrogradely labeled motor axon collaterals (C3) and VChT-IR boutons (C4). **C5**, Superimposition of all. In contrast to CB-IR RCs, few VChT-IR boutons on V1-IaINs contained retrograde labeling from ventral roots. **D**, Non-CB-IR cell that is labeled with YFP in the area populated with CB-IR RCs which receives a dense innervation from CB-IR axons. **E**, Percentage of VChT-IR boutons on V1-IaINs and CB-IR RCs with retrograde labeling from ventral roots in *En1-Cre/Thy1-YFP* mice. There was a significant difference in the percentage of VChT-IR boutons with retrograde labeling on V1-IaINs (6.2%) compared to RCs (93.8%) ( $p < 0.05$ , one-way ANOVA). The main source of VChT-IR contacts on RCs, and not V1-IaINs, appears to originate from motor axon recurrent collaterals. Scale bars; **A series**, (in A1) 100  $\mu\text{m}$ ; **B, C, and D series**, (in B1) 20  $\mu\text{m}$ ; **Insets**, (in B1) 10  $\mu\text{m}$ .



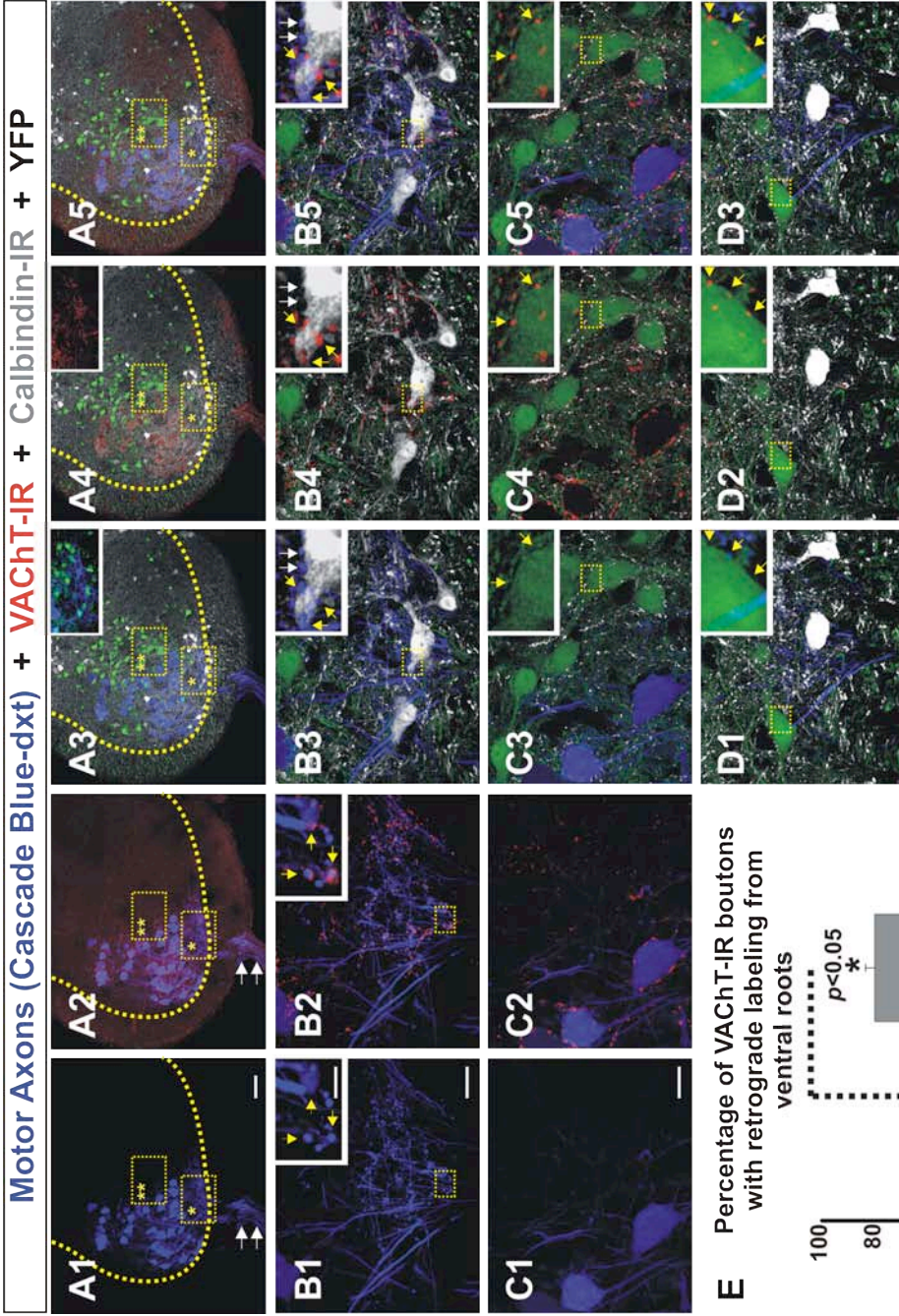


**Table 7.** Density of VGLUT1-IR and VAcHt-IR contacts per 10  $\mu\text{m}$  of linear dendrite of Ia inhibitory interneurons and Renshaw cells during postnatal development.

	<b>Ia Inhibitory Interneurons</b>		<b>Renshaw Cells</b>	
<b>Age</b>	<b>VGLUT1-IR contact density</b>	<b>VAcHt-IR contact density</b>	<b>VGLUT1-IR contact density</b>	<b>VAcHt-IR contact density</b>
<b>P5</b>	1.23 $\pm$ 0.35	0.37 $\pm$ 0.18	0.77 $\pm$ 0.06	1.17 $\pm$ 0.09
<b>P10</b>	1.26 $\pm$ 0.25	0.31 $\pm$ 0.12	0.86 $\pm$ 0.05	1.19 $\pm$ 0.07
<b>P15</b>	1.69 $\pm$ 0.29	0.22 $\pm$ 0.10	1.37 $\pm$ 0.07	1.46 $\pm$ 0.07
<b>P20</b>	1.70 $\pm$ 0.29	0.20 $\pm$ 0.10	0.99 $\pm$ 0.03	1.65 $\pm$ 0.06
<b>Adult</b>	1.84 $\pm$ 0.31	0.22 $\pm$ 0.10	0.98 $\pm$ 0.05	1.45 $\pm$ 0.04

$\pm$  SEM.



**Table 8.** Density and number of VGLUT1-IR and VAcHt-IR contacts on the somata of Ia inhibitory interneurons compared to Renshaw cells at P15 and in the adult.

<b>Ia Inhibitory Interneurons</b>						
	<b>VGLUT1-IR Contact Density</b>	<b># of VGLUT1-IR Contacts</b>	<b>% of VGLUT1-IR Contacts</b>	<b>VAcHt-IR Contact Density</b>	<b># of VAcHt-IR Contacts</b>	<b>% of VAcHt-IR Contacts</b>
<b>P15</b>	* 0.82 ± 0.20	9.35 ± 0.69	** 18.61 ± 1.38	0.40 ± 0.14	4.10 ± 0.41	44.51 ± 3.45
<b>Adult</b>	0.80 ± 0.21	9.47 ± 0.71	19.99 ± 2.20	0.36 ± 0.13	4.29 ± 0.45	44.47 ± 3.32
<b>Renshaw Cells</b>						
	<b>VGLUT1-IR Contact Density</b>	<b># of VGLUT1-IR Contacts</b>	<b>% of VGLUT1-IR Contacts</b>	<b>VAcHt-IR Contact Density</b>	<b># of VAcHt-IR Contacts</b>	<b>% of VAcHt-IR Contacts</b>
<b>P15</b>	0.13 ± 0.08	1.00 ± 0.23	2.82 ± 0.39	0.15 ± 0.09	1.10 ± 0.23	3.38 ± 0.41
<b>Adult</b>	0.15 ± 0.09	1.15 ± 0.24	5.11 ± 0.51	0.18 ± 0.10	1.42 ± 0.27	4.61 ± 0.19

± SEM.

\* VGLUT1-IR/VAcHt-IR contacts per 100 μm<sup>2</sup> of cell membrane

\*\* Percentage of VGLUT1-IR/VAcHt-IR contacts on the somata of IaINs and RCs

and organization of cholinergic synapses on V1-IaINs and RCs is dramatically different. The differences are already apparent in neonates and are maintained in the adult.

## **Discussion**

The results allow us to reject our hypothesis that IaINs receive convergent inputs from motor axons and sensory afferents during postnatal development. Neonatal IaINs did not receive motor axon inputs and VChT-IR synapses on this cell type have a different origin. Sensory inputs develop in parallel in IaIN and RCs during early postnatal development. However there are also clear differences in density, location, and more importantly maintenance of high densities in the adult. These results suggest fundamental differences between IaINs and RCs in their competence for receiving and maintaining motor and Ia afferent inputs and argue against the existence of convergent inputs in all V1 cell during development.

### *Postnatal V1-derived Ia inhibitory interneurons*

Ia inhibitory interneurons (IaINs) were previously identified by their Parvalbumin (PV) expression, CB-IR contacts from Renshaw cells (Alvarez et al., 2005), and their location in the mid and ventral LVII of the ventral horn (Jankowska and Lindstrom, 1972; Rastad et al., 1990). However, these criteria restricted IaIN identification only until after P10, because before P10 PV labels very few if any interneurons and only labels sensory afferents (Smith et al., 2005). Therefore, no studies to date have addressed the development of the synaptic connectivity of IaINs, probably due to a lack of reliable markers for their identification before P10. Here we characterized a transgenic animal

model that allowed the identification of IaINs (and other V1-derived interneurons) throughout postnatal development and in the adult. *En1-Cre/Thy1-YFP* mice provided us with a useful tool to identify IaINs because not only were we able to label the cells, but extensive dendritic and axonal labeling allowed us to analyze synaptic densities on distal dendritic segments. Although not all V1-derived interneurons were labeled in *En1-Cre/Thy1-YFP* mice, because a certain mosaicism of expression of YFP, these mice allowed for the visualization of definitive groups of cells that could be consistently followed through the different postnatal ages analyzed.

As mentioned above, IaINs were previously identified as cells that are densely innervated by strong Renshaw cell inputs manifested anatomically as baskets of CB-IR axons that were also V1-derived (YFP-labeled). No other interneurons, with the exception of other RCs, are known to be targeted by strong CB-IR RCs inputs, but whether neonatal IaINs can be identified by presence of these inputs had not been analyzed until now. Here we demonstrated that a population of YFP-IR cells receiving dense baskets of CB-IR axons can be identified from P1 and that a large proportion of these cells had up-regulated PV-IR by P15. These anatomical data agree with physiological evidence for the presence of recurrent inhibition of IaINs as early as one week after birth (P7; Wang et al., 2008). Stimulation of the L3-4 ventral roots reduced the amplitude of the inhibitory postsynaptic potentials (IPSPs) elicited by activation of IaINs at P7. The reduction in IPSP amplitude in P7 mice was similar to those recorded from mature IaINs in adult cats after stimulation of L5-6 ventral roots (Hultborn et al., 1971). From these experiments, it was concluded that recurrent inhibition of IaINs was present in mice and well-developed as early as one week after birth.

In the Wang et al. study, deleting the transcription factor Pax6, which is required for V1-IN development, did not disturb the development of reciprocal inhibition (Wang et al., 2008). In *Pax6*<sup>(-/-)</sup> knockouts, stimulating the quadriceps nerve at E18 and P0 results in a hyperpolarizing synaptic potential in posterior biceps-semitendinosus (PBSt) motoneurons. These results are similar to wild-type animals. Wang and colleagues postulated that this result could be due to IaINs being selectively spared in *Pax6* knockouts or that there are different subsets of IaINs, being that not all IaINs are V1-derived. Similarly, Gosgnach et al (2006) failed to abolish flexor-extensor alternation in fictive locomotor rhythms by genetically silencing V1-INs postnatally. Here we provided anatomical evidence supporting the theory that not all IaINs are V1-derived and that lumbar IaINs are a heterogeneous population and originate from more than one type of embryonic precursor. We can only speculate as to the origins of non-V1-derived IaINs, but one class in particular stands out. V2 interneurons (V2-INs) express the transcription factor *Lhx3* and in the adult give rise to an excitatory and an inhibitory population of interneurons that have ipsilateral projections and contact motoneurons similar to V1-INs (Al-Mosawie et al., 2007; Lundfald et al., 2007). Excitatory V2-INs express *Chx10* (V2a) and inhibitory V2s express *Gata2/3* (V2b). V2-derived interneurons are located in ventral lamina VII and receive primary afferent inputs. V2b-INs establish glycinergic boutons apposing motoneurons (Al-Mosawie et al., 2007). The similarities between V2b-INs and V1-INs raise the possibility that the heterogeneous population of IaINs originate from these two precursors. Moreover, flexor-extensor alternations in locomotor rhythms evoked pharmacologically in the in vitro mouse spinal cord are fully abolished when V1-INs and V2b-INs are silenced (Martyn Goulding, personal communication).

#### *Postnatal development of sensory afferent inputs on IaINs*

We found that similar to RCs, the density of sensory afferent inputs on V1-derived IaINs, increases significantly during neonatal and early postnatal development.

In contrast to RCs, sensory afferent synaptic density on IaINs is maintained after P15 and in the adult. Moreover, at all ages analyzed, there were significantly more sensory afferent inputs on IaINs compared to RCs and these inputs were more proximally located. Increased synaptic density should, in essence, result in increased synaptic efficacy (or strength). Therefore, the sensory afferent input that IaINs receives seems stronger than those contacting RCs at all developmental stages. In addition, IaINs, compared to RCs, receive significantly more sensory afferent inputs on their somata. Location of synapses is important. For example, if synapses are located on the soma of one cell and farther away on another, then assuming equal densities, the EPSPs evoked would be larger and faster in the cell with the synapses on the soma. If our prediction that those Ia-EPSPs on IaINs are of larger amplitude and faster rise time than on RCs, it would suggest that the proximal regions of somato-dendritic membrane on IaINs have specializations that favor the establishment of stronger sensory inputs compared to RCs. In this sense, the specialization of V1-INs into distinct subclasses with distinct inputs is not only dependent on competence to establish synapses, but also on their bias to form them in different numbers and with different distributions on dendrites and somata.

#### *Postnatal IaINs lack motor axon inputs*

Our findings indicate that V1-derived IaINs do not receive inputs from motor axons during development. Although IaINs do receive VAcHT-IR inputs, the size of these inputs suggest that these inputs derive from another cholinergic source. VAcHT-IR labels not only inputs from motor axon collaterals, but also those from spinal cholinergic interneurons and the C-terminals on motoneurons (Alvarez et al., 1999). These inputs are

generally distinguished by size categories. Large VAcHT-IR boutons located in lamina IX and contacting motoneurons cell bodies are C-terminals whose origin are most likely from a group of interneurons located near the central canal (McLaughlin, 1972; Crone et al., 2008; Zagoraiou et al., 2008). VAcHT-IR boutons densely populating ventral lamina VII are smaller than C-terminals and originate from motor axon recurrent collaterals and contact Renshaw cells. Many of these VAcHT-IR boutons on RCs are retrogradely labeled with fluorescent dextrans from the ventral root (see also Mentis et al., 2005). Finally, other VAcHT-IR contacts found throughout ventral LVII contacting non-RC interneurons are smaller than C-terminals and motor axons collaterals and believed to originate from spinal cholinergic interneurons. The VAcHT-IR boutons contacting IaINs were significantly smaller than those contacting RCs and were not retrogradely labeled from the ventral root. Wang et al. (2008) found that stimulation of L3 and L4 ventral roots at P3 evoked a synaptic potential in PBSt MNs but with latencies longer than expected from a disynaptic reciprocal inhibitory pathway. Wang and colleagues concluded that these latencies represented a trisynaptic linkage (ie, L3/4 MNs → RCs → IaINs → PBSt MNs) and that IaINs do not receive inputs from motor axons. Therefore, the present anatomical study and a recent electrophysiological analysis strongly suggest that neonatal IaINs do not receive inputs from motor axons. Given that cholinergic systems in the spinal cord do not originate in descending pathways from higher brain centers (Sherriff et al., 1991; Vanderhorst and Ulfhake, 2006), VAcHT-IR contacts on IaINs must originate from spinal interneurons. The exact spinal interneurons that establish VAcHT-IR synapses on IaINs needs to be further investigated.

Our findings in this aim focused on the postnatal development of the synaptic connectivity of postnatally identified IaINs and we did not address the synaptic connectivity of embryonic IaINs. Whether IaINs receive motor axon inputs during embryonic development remains to be explored. Initial attempts to identify IaINs in embryonic *En1-Cre/Thy1-YFP* mice were unsuccessful. Labeling of V1-INs was weak and only a few somata were labeled. Moreover, labeling appeared to be restricted to axons and dendrites (unpublished observations). Weak embryonic labeling of V1-INs is likely due to developmental regulation of the Thy1 promoter. It is known that, in neurons, the Thy1 promoter becomes most active postnatally (Morris, 1985; Kollias et al., 1987; Caroni, 1997). Labeling of IaINs in embryo therefore necessitates a different reporter line to cross with *En1<sup>Cre/+</sup>* mice. Unfortunately, other lines available in lab do not label dendrites. Although, as of present, we cannot reliably identify IaINs in embryonic spinal cords, we can speculate what their synaptic connectivity may be. In mice, the specific Ia-MN and Ia-IaIN connections mediating reciprocal inhibition are already present at birth (Wang et al., 2008). Therefore, it appears that the Ia-MN and Ia-IaIN connections are established simultaneously before birth. As explained in aim 1, Ia afferent projections invade the ventral horn in late embryo (older than E15). However, in aim 2 we showed that motor axons establish synapses in the spinal cord in very early embryos. Motoneurons are born (become postmitotic) between E9 and E10 and have motor axon collaterals by E11 which is around the same time that V1-INs are born. Interestingly, at embryonic stages E11-E16, several interneuron populations are contacted by motor axons, contributing to the spontaneous rhythmic activity of early motor circuits (Hanson and Landmesser, 2003). Therefore, it is possible that motor axons innervate

more than RCs in early embryo. It is also possible that IaINs never receive inputs from motor axons and only receive excitatory inputs from interneurons in early and late embryo and from sensory afferents only in late embryo. One problem is what criteria should be used to recognize “primordial IaINs” before they receive the synaptic inputs we use to characterize them. In the future, alternative markers will need to be developed to conduct these analyses.

#### *Evidence against a “generic” V1-derived interneuron*

In aim1 we presented the idea that all V1-INs derive from a “generic” V1-IN that gives rise to different classes of V1-INs by differential development of synaptic inputs. The data presented in aim 1 demonstrated that RCs receive convergent inputs from sensory afferents and motor axons, but only the input from motor axons is strengthened while the sensory afferent input is likely weakened. In this aim we presented data arguing against a “generic” connectivity from motor axons and sensory afferents on V1-INs. Postnatal IaINs never receive motor axon inputs. Studies from our lab using BrdU pulse-labeling demonstrated that different classes of V1-INs are born at different times (Benito-Gonzalez et al., 2008). RCs are the first born V1-INs (born between E9.5-E10.5, with most born at E9.5), whereas IaINs are born between E10.5 and E12.5 with most being born around E10.5. Since RCs are born around the same time when MNs extend motor axons, it seems likely that motor axons are biased toward RCs. The lack of motor axon input on IaINs and their later birthdate suggest that there are fundamental differences between IaINs and RCs in their mechanisms of differentiation and these might include differential competence for receiving synapses from motor axons.



In conclusion, we present evidence that IaINs do not receive inputs from motor axons during postnatal development. We also present evidence that sensory afferent inputs on IaINs proliferate during postnatal development and are maintained in the adult. Although IaINs and RCs share this primary afferent input, the anatomical analysis presented suggests that there are fundamental differences in the organization of this input between both cells.

## **CHAPTER VIII**

### **Role of primary afferents in the specification of excitatory synaptic inputs on mature Renshaw cells**

## Introduction

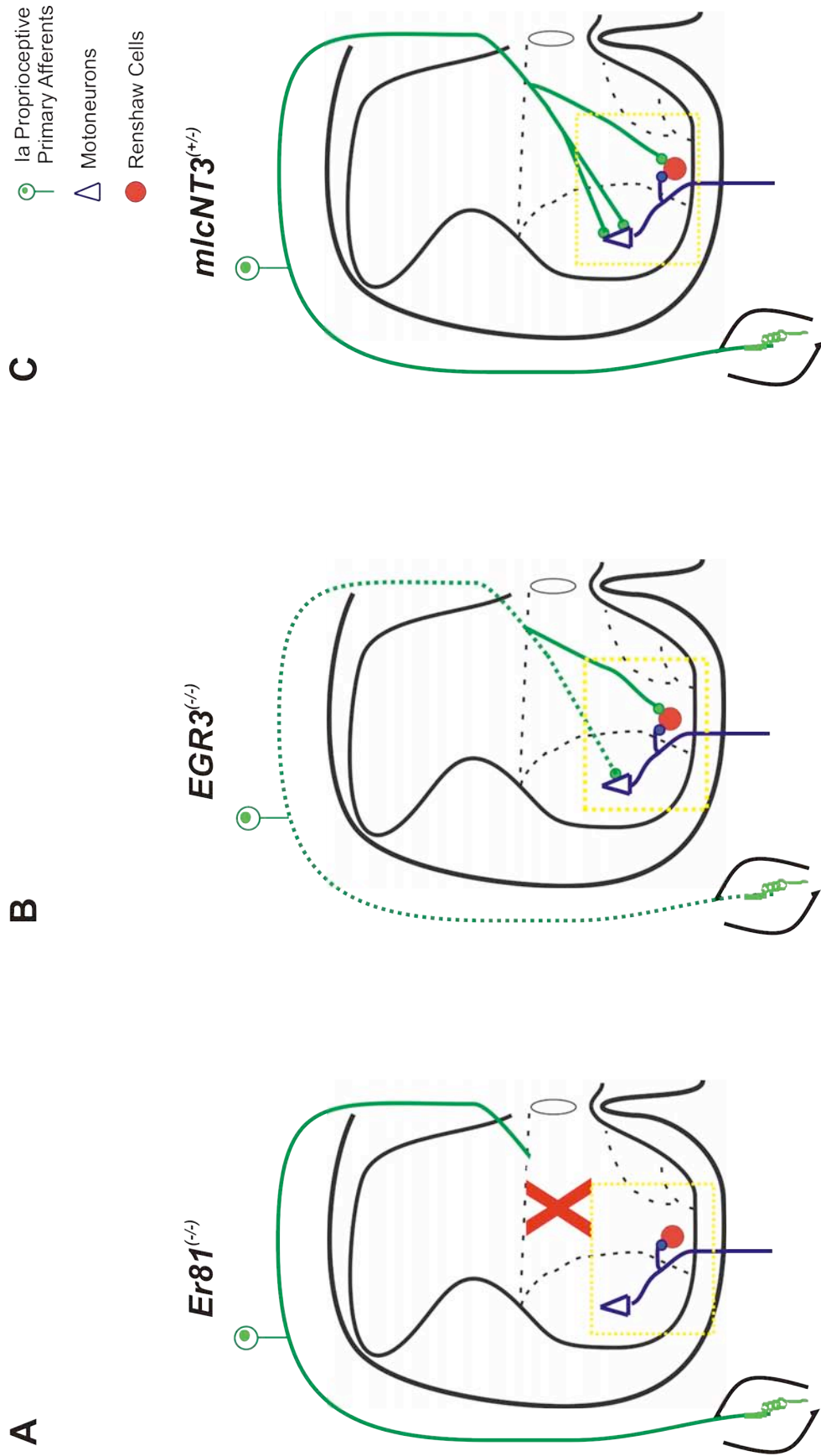
The mechanisms that underlie synaptic selection on ventral interneurons are completely unknown. Input selection through synaptic competition has been amply demonstrated when the postsynaptic targets are unique and singly innervated, for example in climbing fibers on Purkinje cells (Ito, 1984) and at the neuromuscular junction (reviewed in Sanes and Lichtman, 1999, 2001). Less is known how diverse inputs are selected or de-selected on most central neurons that are multi-innervated by a variety of inputs from different sources. In this aim we tested the novel hypothesis that a similar competition process might operate heterosynaptically to select specific excitatory inputs and adjust their densities on RCs. In other words, we examined whether alterations in the number of sensory synapses on RCs could change synaptic densities of other inputs on RCs. If this was the case we could argue that the transient sensory inputs on RCs might have a role in shaping the synaptic organization of RCs (see aim 1 Discussion). Therefore we looked at whether there is an interaction between the motor axon collaterals and the primary afferent inputs on Renshaw cells (RCs) using three transgenic mice models, one without primary afferent projection onto the ventral horn and Renshaw cell area (*Er81*), one with a progressive weakening of primary afferent projections after birth (*EGR3*), and one with an excess of primary afferent synapses in these regions (*mlcNT3*) (Figure 37).

Past research using these transgenic animal models has focused on the monosynaptic stretch reflex. Simply put, the monosynaptic stretch reflex is elicited when a muscle is stretched, and the Ia spindle afferents fire. The Ia spindle afferents make monosynaptic, excitatory synapses on the alpha motoneurons ( $\alpha$ MNs) that innervate the

same muscle (homonymous muscle). Monosynaptic connections between homonymous  $\alpha$ MNs and Ia spindle afferents are stronger than those monosynaptic connections with synergistic heteronymous muscles (Eccles et al., 1957; Frank & Westerfield, 1983; Lichtman et al., 1984). No research has addressed whether alterations in primary afferent input in the ventral horn affects the synaptic connectivity between Ia afferents and ventral horn interneurons. Similarly, no studies investigated whether the strength of the Ia afferent input influences the development of other excitatory inputs (i.e., inputs from motor axons or spinal interneurons).

Er81 is a member of the *ETS* (E twenty-six Transformation specific) domain family of transcription factors and is expressed in all proprioceptive neurons and regulates the growth of Ia afferents into the ventral horn. *Er81*<sup>(-/-)</sup> knockout animals display severe deficits in motor coordination and these deficits are due to a failure of muscle afferents to establish arborizations in the ventral horn (Arber et al., 2000). As a result, *Er81*<sup>(-/-)</sup> knockout animals die in the third or fourth postnatal week. Afferents fail to project to and make monosynaptic connections with motoneurons in the absence of Er81 (Arber et al., 2000). Connectivity between motoneurons and sensory afferents was tested by stimulating the dorsal root while examining the synaptic response of MNs extracellularly recorded from the ventral roots. Dorsal root stimulation failed to elicit action potentials in *Er81*<sup>(-/-)</sup> MNs and the amplitude of the monosynaptic response was significantly reduced. Therefore, it was concluded that the monosynaptic connections between MNs and sensory afferents were severely altered in *Er81*<sup>(-/-)</sup> mice. Confocal analysis of primary afferent bouton density on MNs, using VGLUT1-IR as a marker of primary afferents, demonstrated that MNs from *Er81*<sup>(-/-)</sup> mutants had virtually no

**Figure 37.** Mouse models exhibiting alterations in primary afferent inputs into the ventral horn. **A**, Synaptic connectivity in the ventral horn of *Er81*<sup>(-/-)</sup> knockouts. In *Er81*<sup>(-/-)</sup> animals Ia afferents do not enter the ventral horn (indicated by the red “X”). Motoneurons (MNs) in *Er81*<sup>(-/-)</sup> knockouts do not receive inputs from Ia afferents (Smith et al., 2007). In this aim we investigated whether the density of motor axon recurrent collaterals, immunolabeled with VACHT, are affected by deletion of primary afferents. **B**, Effects of altering primary afferent inputs on RC synaptic connectivity in *EGR3*<sup>(-/-)</sup> knockouts. In *EGR3*<sup>(-/-)</sup> mice, Ia afferents project to the ventral horn but the number of synapses is reduced (Smith et al., 2007) and functionally weaker (Chen et al., 2002). Previous studies indicate that the density of primary afferent input, labeled with VGLUT1, on MNs is reduced in *EGR3*<sup>(-/-)</sup> mice, but it is not known whether VGLUT1-IR or other excitatory input densities on RCs is altered in these animals. **C**, In *mlcNT3*<sup>(+/-)</sup> mice, an excess of NT3 prevents normal cell death of Ia afferents and enhances the formation of central synapses from proprioceptive sensory axons (Smith et al., 2007) these also being functionally stronger (Wang et al., 2007). Here we investigated whether RCs also receive an excess of VGLUT1-IR inputs and whether the density of other excitatory inputs are also affected.



VGLUT1-IR inputs (95-99% depletion) (Smith et al., 2007), essentially corroborating electrophysiological data. Therefore, the monosynaptic connections between MNs and sensory afferents are altered in the absence of Er81, but no studies have focused on whether deletion of sensory afferents in the ventral horn affects the development/maturation of other excitatory synaptic connections on MNs or interneurons.

EGR3, or *early growth response gene 3*, is a member of the zinc finger family of transcription factors and is expressed in developing intrafusal muscle fibers being essential for development of muscle spindles (Tourtellotte et al., 2001). Adult mice deficient in EGR3 (*EGR3<sup>-/-</sup>*) lack muscle spindles and have a profound gait ataxia (Tourtellotte & Milbrandt, 1998). No differences in the number of sensory DRG neurons were seen, but significant reductions in the number of large diameter (>5  $\mu\text{m}$ ) myelinated fibers in the dorsal root were observed. Large diameter axons correspond to those Ia afferents that innervate muscle spindles (Duchen & Scaravilli, 1977). Recent evidence suggests that EGR3 is also important for the development and maintenance of the monosynaptic connections between MNs and primary afferents (Chen et al., 2002). In *EGR3<sup>-/-</sup>* knockouts, primary afferents form and make arborizations in the ventral horn, but postnatally, as muscle spindles begin to degenerate, the central synapse between MNs and primary afferents weakens (Chen et al., 2002), possibly due to the failure of mutant spindles to produce NT3 (neurotrophin -3). Injection of NT3 into the hindlimbs of *EGR3<sup>-/-</sup>* mice restored the synaptic connectivity between sensory neuron and MNs, emphasizing the importance of muscle spindle-derived NT3 in the maintenance of functional synaptic connections. Smith and colleagues (2007) found that VGLUT1-IR

contact density decreased by 48% in *EGR3*<sup>(-/-)</sup> knockouts when compared to wild-type controls.

Neurotrophin-3 (NT3) is part of the nerve growth factor-related family of molecules (Thoenen, 1991) and play an important role during development, including differentiation and survival of sensory and motoneurons as well as proliferation of proprioceptive axons (Hory-Lee et al., 1993; Lindsay, 1996; Coppola et al., 2001; Zhou et al., 2003). NT3 is expressed in muscle spindles (Copravay et al., 1994), dorsal root ganglion (DRG) (Schechterson & Bothwell, 1992), and motoneurons (Ernfors et al., 1992). NT3 has been shown to be important for Ia afferent arborization in the ventral horn.

NT3 is believed to play a role not only in the formation of Ia afferent-MN connections but also their long-term maintenance and maturation (Taylor et al., 2001). To study long-term effects of high NT3 expression, transgenic mice over expressing NT3 in perinatal, postnatal, and adult skeletal muscle were developed using the myosin light chain promoter (*mlcNT3*<sup>(+/-)</sup>) to constitutively express NT3 in muscle from embryo to adult. These mice exhibited a loss of synaptic specificity between MNs and sensory neurons in *mlcNT3*<sup>(+/-)</sup> mice (Wang et al., 2007). Stimulation of the quadriceps and adductor muscle nerves led to an increased response in L5 MNs in *mlcNT3*<sup>(+/-)</sup> mice. Normally, L5 MNs receive very little input from afferents deriving from the quadriceps and adductor muscles. It is important to note that the “correct” muscle afferents provided stronger inputs to MNs also. Wang and colleagues suggested that there was no increase in anatomical projections in *mlcNT3*<sup>(+/-)</sup> mice compared to wild-types. However, these results are in contrast to Smith et al. (2007), who found that the density of VGLUT1-IR boutons on MNs, in *mlcNT3*<sup>(+/-)</sup> mice compared to age-matched wild-type controls,



increased by 84% at P5 and nearly a 205% increase was seen at P21. Differences could be due to the segmental level analyzed, and/or differences in the anatomical and analytical techniques used in each study. Wang and colleagues labeled primary afferents in lumbar segment 3 (L3) using anterograde tracings with fluorescent dextrans and the density of projections was assessed by comparing the percentage of pixels above threshold in the ventral horn. Smith and colleagues used VGLUT1-IR as a marker of primary afferents in L4-L5 and the number of VGLUT1-IR contacts per cell soma was counted on MNs as well as within 100  $\mu\text{m}^2$  areas in the surrounding neuropil. In conclusion, *mlcNT3*<sup>(+/-)</sup> animals show an increase in the Ia projections and synapses on MNs with some loss of specificity. Similar to the other two transgenic mouse models, no research has assessed whether any other excitatory inputs on MNs or interneurons are affected by changes in primary afferent strength.

In order to determine whether altering primary afferent strength in the ventral horn affects the strength of other excitatory inputs on RCs, we used immunohistochemistry against Calbindin to identify Renshaw cells, Vesicular glutamate transporter-immunoreactivity (VGLUT1-IR) to identify primary afferents, Vesicular acetylcholine transporter-IR (VAcHT-IR) to identify motor axon recurrent collaterals, and Vesicular glutamate transporter isoform 2-IR (VGLUT2-IR) to label inputs from excitatory spinal interneurons in *Er81*<sup>(-/-)</sup>, *EGR3*<sup>(-/-)</sup>, and *mlcNT3*<sup>(+/-)</sup> animals at P15, P20, and adult (>P40) postnatal ages. We analyzed whether these differences in input strength modified the de-selection or maturation of Ia afferent inputs on RCs during late postnatal development (after P15) and whether they influence the organization of other excitatory inputs converging in the same cells, i.e., those from motoneurons or excitatory

interneurons. We hypothesized that alterations in the number of sensory synapses on RCs will change the synaptic densities of other excitatory inputs on RCs.

The results were presented in abstract form (Siembab et al., 2007).

## **Materials and Methods**

### *Tissue preparation*

Sections from L4 and L5 spinal cord segments of *Er81<sup>(-/-)</sup>*, *EGR3<sup>(-/-)</sup>*, *mlcNT3<sup>(+/-)</sup>*, and wild-type littermates of P15, P20, and adult postnatal ages were processed for dual or triple-color immunofluorescence using antibodies against CB (rabbit polyclonal, 1:2000; 1:5000), VGLUT1 (guinea pig polyclonal, 1:1000, 1:2000), and VACHT (goat polyclonal, 1:1000, 1:2000). Data from Courtney Smith in our laboratory indicated that the number of CB-IR RCs per ventral horn in all three animal models at P20 was unchanged (WT =  $6.4 \pm 0.5$  and *mlcNT3* =  $7.5 \pm 0.7$ , not significant,  $p = 0.230$ , *t* test; WT =  $9.9 \pm 0.5$  and *Er81<sup>(-/-)</sup>* =  $9.0 \pm 0.4$  (average number of CB-IR cells per ventral horn  $\pm$  SEM.), not significant,  $p = 0.190$ , *t* test; WT =  $6.9 \pm 0.7$  and *EGR3<sup>(-/-)</sup>* =  $8.4 \pm 0.5$ , not significant  $p = 0.070$ , *t* test). Therefore the animal genotype does not affect the criteria for recognition of RCs for these analyses.

Spinal cord sections were incubated overnight in one of the following primary antisera mixtures: CB/VACHT, CB/VGLUT1, or CB/VACHT/VGLUT1 (See General Methods for antibody sources and buffers). The following day, immunoreactive sites were revealed using species-specific secondary antibodies. Secondary antibody combinations differed and depended on the primary antisera mixture used. CB and VGLUT1-immunoreactivity were revealed respectively with donkey Cy3-conjugated

anti-rabbit antibodies and donkey FITC-conjugated anti-guinea pig antibodies (both diluted 1:50). Similarly, CB and VAcHT-IR were revealed with donkey Cy3-conjugated anti-rabbit antibodies and donkey FITC-conjugated anti-goat antibodies. In triple-fluorescent preparations; CB, VGLUT1, and VAcHT-IR were revealed respectively with donkey Cy3-conjugated anti-rabbit antibodies, donkey FITC-conjugated anti-guinea pig antibodies, and donkey Cy5-conjugated anti-goat antibodies. Renshaw cells were identified as neurons with strong CB-IR in the ventral most portion of LVII.

We also investigated whether the density of excitatory inputs from spinal interneurons was affected by alterations in primary afferent inputs. Dual-color immunofluorescence was performed in sections from *Er81*<sup>(-/-)</sup>, *EGR3*<sup>(-/-)</sup>, and *mlcNT3*<sup>(+/-)</sup> mice at P20, with antibodies against CB and Vesicular Glutamate Transporter isoform 2 (VGLUT2, guinea pig polyclonal, 1:1000). VGLUT2-IR is a good marker of synaptic inputs from spinal interneurons (Todd et al., 2003). CB and VGLUT2-IR were revealed with donkey Cy3-conjugated anti-rabbit antibodies and donkey FITC-conjugated anti-guinea pig antibodies respectively.

#### *Confocal analysis of VGLUT1-IR and VAcHT-IR synaptic densities on CB-IR RCs*

VGLUT1-IR and VAcHT-IR densities were obtained by reconstructing CB-IR RCs using the NeuroLucida neuron tracing confocal module. Briefly, low magnification (20x) confocal images of dual or triple-immunofluorescent preparations were obtained and RCs were randomly sampled for higher magnification (60x) scans. Only those RCs with extensive CB-IR dendritic labeling were chosen for further analysis. The selected RCs were then imaged at high magnification (60x oil immersion digitally zoomed 1.5x,

N.A., 1.35) and series of confocal optical sections (z-step 0.5  $\mu\text{m}$ ) were obtained throughout individual randomly sampled RCs with their cell bodies and most of their immunolabeled dendritic arbors fully contained within the field of view and thickness of the tissue sections. The stacks of images were loaded in Neurolucida and the cells were reconstructed in 3D from the confocal stacks using the neuron tracing confocal module as explained below. VGLUT1-IR and VAcHT-IR contacts were then plotted on the reconstructed dendritic arbors. From these reconstructions we estimated dendritic arbor morphology and VGLUT1-IR and VAcHT-IR synaptic densities and their distribution. Densities of contacts were obtained by plotting the number of contacts per 10  $\mu\text{m}$  of linear dendrite. We did not detect significant differences among estimates obtained from Renshaw cells sampled from wild type spinal cords from the different lines. Therefore one single pooled value was used as a control wild type Renshaw cell average at each age.

Similar to analysis mentioned above, the density of VGLUT2-IR contacts on P20 *Er81*<sup>(-/-)</sup>, *EGR3*<sup>(-/-)</sup>, *mlcNT3*<sup>(+/-)</sup>, and wild-type CB-IR RCs were obtained by reconstructing the RCs in Neurolucida. VGLUT2-IR contacts were plotted on the reconstruction and linear densities obtained and compared.

Sample characteristics: we sampled 21-66 RCs at each age analyzed from 2-5 wild-type, *Er81*<sup>(-/-)</sup>, *EGR3*<sup>(-/-)</sup>, or *mlcNT3*<sup>(+/-)</sup> animals (exact number of animals and cells analyzed for each age, animal, and marker are summarized in Tables 9 and 10)

### *Statistical Analysis*

Values are reported as the average number of contacts per 10  $\mu\text{m}$  of linear dendrite  $\pm$  S.E.M. Linear densities across genotypes were compared using a one-way ANOVA. Significance was set at  $p < 0.05$ . If significant differences existed, then multiple comparisons were done using *post hoc* tests with a level of significance of  $p < 0.05$ . Densities estimated for the different genotypes were compared to the age-matched control wild type pooled average using t-tests.

### **Results**

*VGLUT1-IR density on Renshaw cells decreases in  $EGR3^{(-/-)}$  mice and increases in  $mlcNT3^{(+/-)}$  mice. There were no VGLUT1-IR contacts on Renshaw cells in  $Er81^{(-/-)}$  mice.*

As mentioned in Aims 1 and 3, the density of VGLUT1-IR and VAcHT-IR contacts on RCs increases until P15 and, thereafter, VGLUT1-IR synaptic density decreases, whereas VAcHT-IR synaptic density is maintained. We investigated whether there were any differences in VGLUT1-IR contact density on P15, P20, and adult RCs in  $Er81^{(-/-)}$ ,  $EGR3^{(-/-)}$ , and  $mlcNT3^{(+/-)}$  mice. First we investigated whether the absence or weakening of primary afferent inputs into the ventral horn affected the density of VGLUT1-IR contacts on RCs. RCs from P15 and P20  $Er81^{(-/-)}$  knockouts had no VGLUT1-IR contacts (Figure 38). Similar to previous reports, VGLUT1-IR in the ventral horn was noticeably reduced in  $EGR3^{(-/-)}$  mice at all ages analyzed (Figure 38) (Smith et al., 2007). RCs from P15  $EGR3^{(-/-)}$  knockouts showed a significant 29% decrease in the density of VGLUT1-IR contacts compared to age-matched wild-type controls (Figure 39, 40) (WT =  $1.35 \pm 0.05$  VGLUT1-IR contacts per 10  $\mu\text{m}$  of dendrites

(n = 5 animals, 57 RCs) and  $EGR3^{(-/-)} = 0.95 \pm 0.03$  (n = 3 animals, 37 RCs),  $p = < 0.001$ ,  $t$  test). P20 RCs in  $EGR3^{(-/-)}$  mutants showed a significant 14% decrease in VGLUT1-IR contact density compared to controls (Figure 39, 40)(WT =  $0.98 \pm 0.03$  (n = 5, 66 RCs) and  $EGR3^{(-/-)} = 0.83 \pm 0.04$  (n = 3, 32 RCs),  $p = 0.009$ ,  $t$  test), while P40 RCs displayed a 29% decrease (WT =  $0.98 \pm 0.03$  (n = 4, 35 RCs) and  $EGR3^{(-/-)} = 0.7 \pm 0.04$  (n = 3, 31 RCs),  $p = < 0.001$ ,  $t$  test). VGLUT1-IR contact density decreased significantly overall from P15 to adult in  $EGR3^{(-/-)}$  animals ( $p < 0.001$ , one-way ANOVA). *Post hoc* tests indicated that the decrease from P15 to P20 and from P20 to adult were significant ( $p < 0.05$ , *post hoc* Tukey's test). Therefore, the density of VGLUT1-IR contacts on P15 and mature (P20 and adult) RCs decreases with development as in WT after P15, but at all ages,  $EGR3^{(-/-)}$  animals display significantly less VGLUT1-IR contacts than WTs (summarized in Table 9).

Next we investigated whether the density of VGLUT1-IR contacts on RCs was affected in animals that display an excess of primary afferent input in the ventral horn. Previous reports have been in disagreement as to whether there are any changes in the density of primary afferent projections in  $mlcNT3^{(+/-)}$  mice. Chen et al., 2007 reported that there were no significant changes in the density of filled afferents, whereas Smith et al., 2007 reported that there was an increase in VGLUT1-IR primary afferents in  $mlcNT3^{(+/-)}$  mice. Our findings indicate that there is an increase in VGLUT1-IR in the ventral horn (Figure 38). Although we did not quantify the density of VGLUT1-IR in the ventral horn of  $mlcNT3^{(+/-)}$  and wild-type controls in this study, differences were noticeable. In  $mlcNT3$  animals the number of VGLUT1-IR primary afferent inputs on

**Figure 38.** VGLUT1-immunoreactivity in the ventral horn of wild-type (**A**), *EGR3*<sup>(-/-)</sup> (**B**), *mlcNT3*<sup>(+/-)</sup> (**C**), and *Er81*<sup>(-/-)</sup> (**D**) mice at P15, P20 and in the adult. **A-D**, Low magnification images of VGLUT1-IR in the ventral horn at P15, P20, and adult in control, *EGR3*<sup>(-/-)</sup>, *mlcNT3*<sup>(+/-)</sup>, and *Er81*<sup>(-/-)</sup> animals. The dotted line indicates the border between the ventral horn and white matter. The blue line delineates the border between lamina IX (LIX) and lamina VII (LVII). VGLUT1-IR density in the ventral horn decreased in *EGR3*<sup>(-/-)</sup> mice (**B**) at all ages analyzed and in contrast, increased in *mlcNT3*<sup>(+/-)</sup> animals (**C**). VGLUT1-IR in the ventral horn of *Er81*<sup>(-/-)</sup> mice at P15 (**D1**) or P20 (**D2**) was largely depleted. These results are similar to previous reports (Smith et al., 2007; Mentis et al., 2006). Changes in VGLUT1-IR were most noticeable in LIX. **Scale bars:** **A1-A3**, **B1-B3**, **C1-C3**, and **D1-D2** (in A1), 100  $\mu$ m.

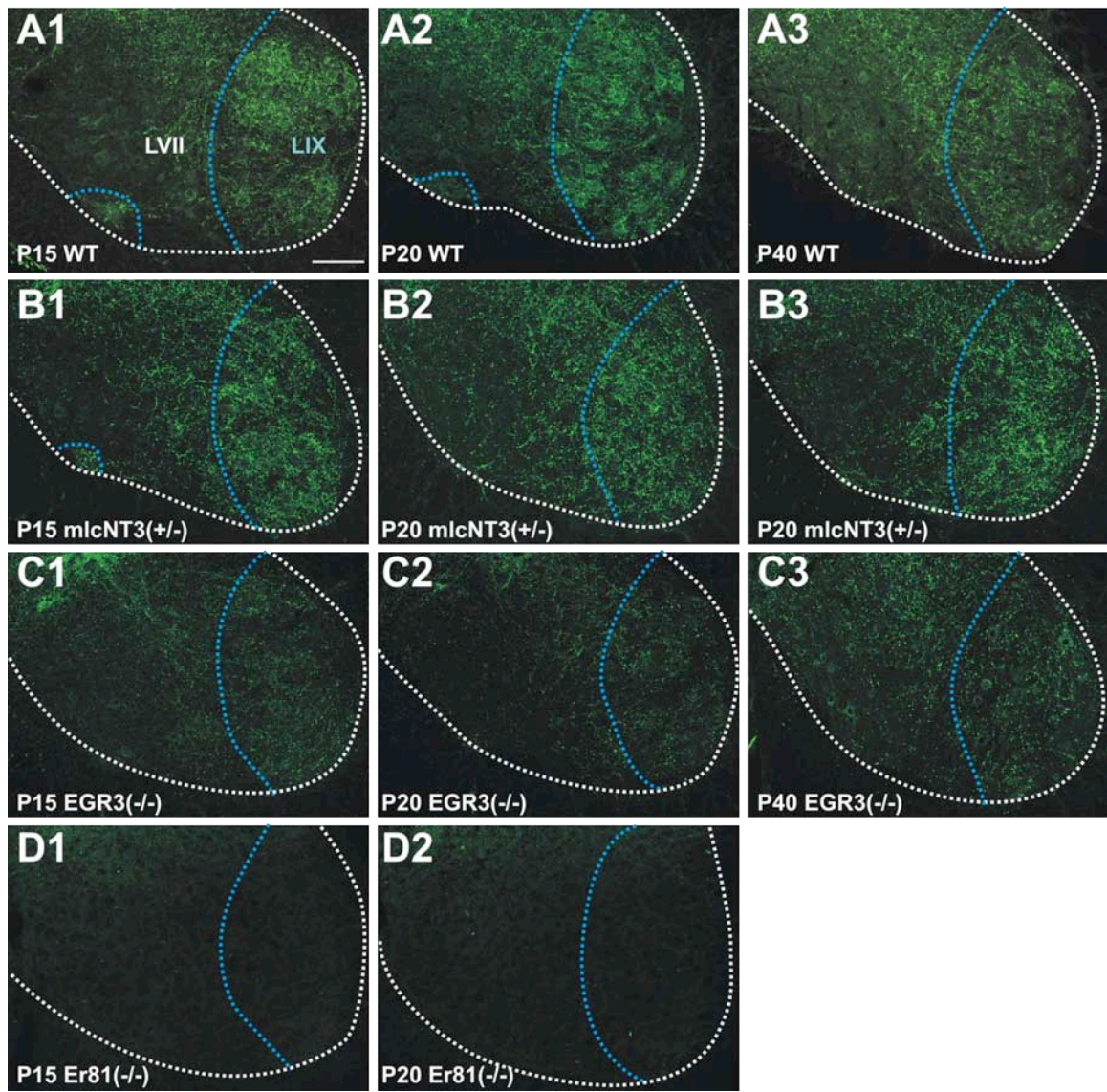




**Figure 39.** Density of VGLUT1-immunoreactive contacts on Renshaw cells in the ventral horn of control, *EGR3*<sup>(-/-)</sup>, and *mlcNT3*<sup>(+/-)</sup> P20 mice. **A1, B1, C1**, Low magnification images of VGLUT1-IR (FITC, green) in the ventral horn at P20 in control, *EGR3*<sup>(-/-)</sup> and *mlcNT3*<sup>(+/-)</sup> animals. VGLUT1-IR density in the ventral horn decreased in *EGR3*<sup>(-/-)</sup> and increased in *mlcNT3*<sup>(+/-)</sup>. The dotted line indicates the border between the ventral horn and the white matter. **A2, B2, C2**, Superimposed VGLUT1-IR (green) and CB-IR (Cy3, red) in the same field shown in A1, B1, and C1. Box indicates area of high magnification shown in A3, B3, and C3. **A3, B3, C3**, High magnification images of VGLUT1-IR on P20 CB-IR RCs. Arrowheads indicate VGLUT1-IR contacts on RC dendrites. There are fewer contacts on RCs in *EGR3*<sup>(-/-)</sup> mice compared to control. In contrast, *mlcNT3*<sup>(+/-)</sup> mice have more contacts from Ia afferents when compared to the control. **Scale bars:** A1-A2, B1-B2, and C1-C2 (in A1), 100  $\mu$ m; A3, B3, and C3 (in A3), 20  $\mu$ m.

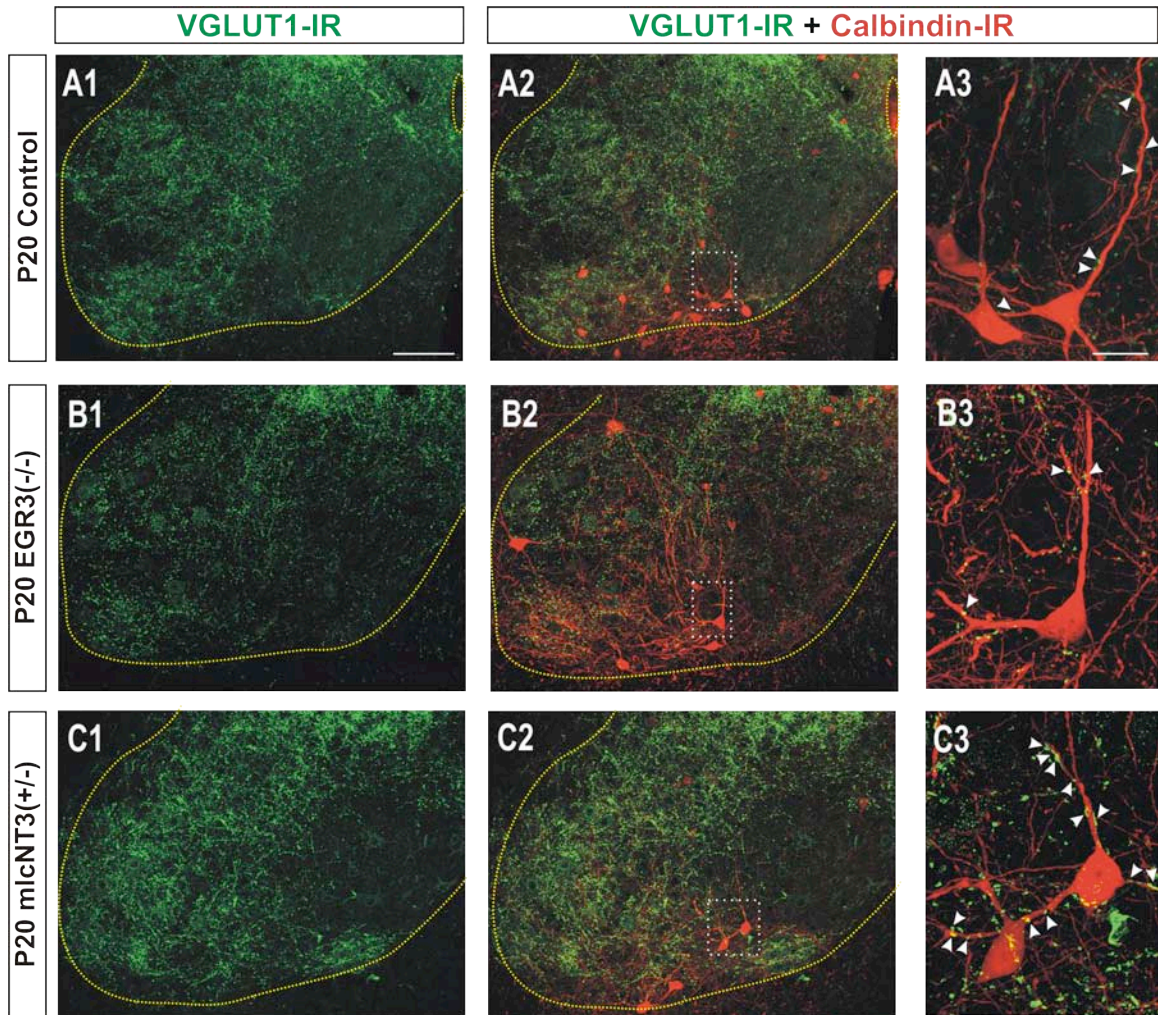
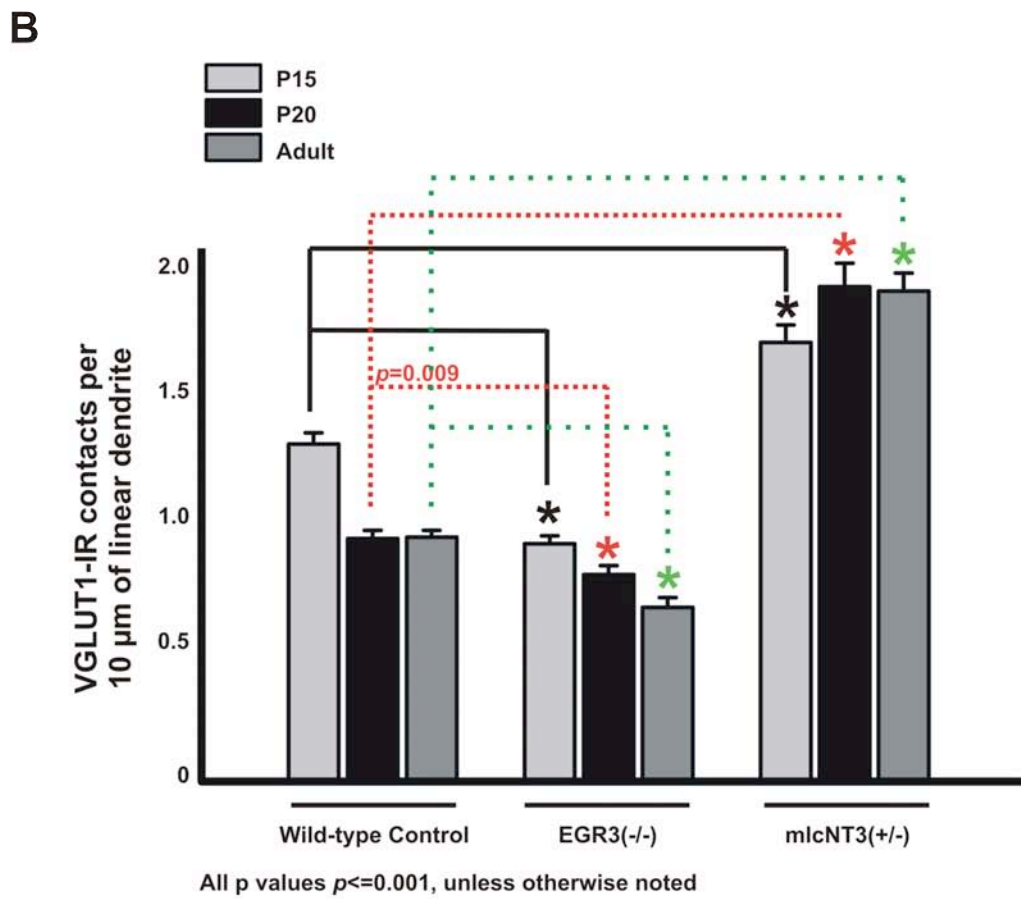
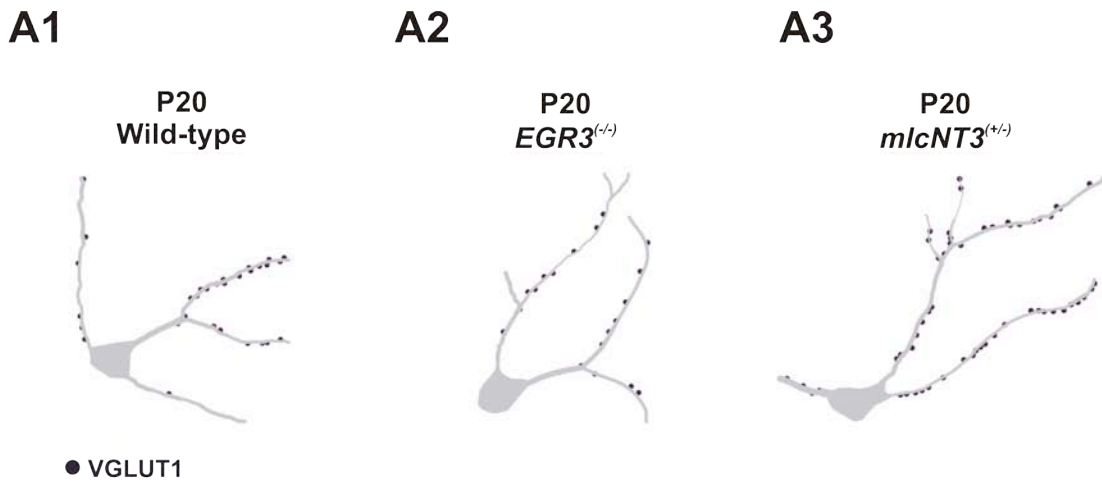


**Figure 40.** Density of VGLUT1-IR contacts on mature Renshaw cells in *EGR3*<sup>(-/-)</sup> and *mlcNT3*<sup>(+/-)</sup> mice compared to wild-type controls. **A**, 3D reconstruction of RCs from P20 wild-type (**A1**), *EGR3*<sup>(-/-)</sup> (**A2**), and *mlcNT3*<sup>(+/-)</sup> (**A3**) mice reconstructed in NeuroLucida using the confocal module with VGLUT1-IR contacts plotted on the reconstruction. **B**, VGLUT1-IR contacts per 10  $\mu\text{m}$  of linear dendrite of CB-IR RCs in control, *EGR3*<sup>(-/-)</sup>, and *mlcNT3*<sup>(+/-)</sup> mice of P15, P20, and adult postnatal ages. Control animals show densities and changes with maturation similar to those reported in Mentis et al., 2006 and Aim 1 and 3. In both control and *EGR3*<sup>(-/-)</sup> animals, RCs display statistically significant decreases in VGLUT1-IR contact density from P15 to adult ( $p \leq 0.001$ , one-way ANOVA). RCs in *EGR3*<sup>(-/-)</sup> animals display statistically significant decreases (asterisks; t-tests) in VGLUT1-IR contact density (~30% decrease in adult) compared to age-matched controls. In contrast, VGLUT1-IR contact density increased significantly from P15 to adult in *mlcNT3*<sup>(+/-)</sup> mice ( $p = 0.041$ , one-way ANOVA). In mature *mlcNT3*<sup>(+/-)</sup> mice (P20 and adult), VGLUT1-IR contact density on RCs more than doubled compared to WTs (asterisks; 114% increase). VGLUT1-IR synaptic density on RCs is influenced by changes in primary afferent strength. There are fewer contacts from primary afferents on RCs in *EGR3*<sup>(-/-)</sup> mice compared to control animals. In contrast, *mlcNT3*<sup>(+/-)</sup> mice have more contacts from primary afferents compared to control animals.



RCs was increased and maintained from P15 to adult (Figure 39,40). P15 RCs from *mlcNT3* animals showed a significant 28% increase in the density of VGLUT1-IR contacts compared to age-matched wild-types (WT =  $1.35 \pm 0.05$  (n = 5, 57 RCs) and *mlcNT3*<sup>(+/-)</sup> =  $1.76 \pm 0.07$  (n = 3, 40 RCs),  $p < 0.001$ , *t* test) (Figure 40). At P20, RCs display more than double (114% increase) the density of VGLUT1-IR contacts compared to age-matched wild-type controls (WT =  $0.98 \pm 0.03$  (n = 5, 66) and *mlcNT3*<sup>(+/-)</sup> =  $1.99 \pm 0.09$  (n = 3, 26 RCs), significant,  $p < 0.001$ , *t* test). Adult RCs also displayed a significant increase (99%) in VGLUT1-IR contact density compared to wild-types (WT =  $0.98 \pm 0.03$  (n = 4, 35 RCs) and *mlcNT3*<sup>(+/-)</sup> =  $1.97 \pm 0.1$  (n = 3, 24 RCs),  $p < 0.001$ , *t* test). These estimates result from maintenance (or even perhaps small increase) of VGLUT1-IR densities from P15 to adult animals while in wild-types the VGLUT1 input decreased in density (Figure 40). VGLUT1-IR contact densities significantly increased (13% increase) from P15 to adult ( $p < 0.001$ , one-way ANOVA). *Post hoc* tests indicated that the increase in density from P15 to P20 was significant ( $p < 0.05$ , *post hoc* Dunn's test), but no differences were detected between P20 and adult (P20 =  $1.99 \pm 0.09$  and adult =  $1.97 \pm 0.1$ ,  $p = 0.908$ , *t* test). In contrast, densities were reduced by 33% from P15 to P20 in wild-type controls (summarized in Table 9) (P15 =  $1.35 \pm 0.045$  and P20 =  $0.98 \pm 0.03$ , significant,  $p = 0.001$ , *t* test), which is in agreement with the normal age-dependent reduction in VGLUT1-IR densities already described in aims 1 and 3 in two independent samples of RCs

**Table 9.** VGLUT1-IR contact densities of Renshaw cells from P15, P20, and adult wild-type, *Er81*<sup>(-/-)</sup>, *EGR3*<sup>(-/-)</sup>, and *mlcNT3*<sup>(+/-)</sup> mice.

Animal Model	Changes in VGLUT1-IR in Ventral Horn	VGLUT1-IR contacts per 10 $\mu$ m of dendrite	Percent change compared to WT	P Value (*, significant) t test	Total # of VGLUT1 contacts per cell	N (# animals, # RCs)
Wild-type	N/A	1.35 $\pm$ 0.05	N/A	N/A	26.72 $\pm$ 0.68	5, 57 RCs
<i>Er81</i> <sup>(-/-)</sup>	No VGLUT1-IR in VH	N/A	N/A	N/A	N/A	N/A
<i>EGR3</i> <sup>(-/-)</sup>	↓	0.95 $\pm$ 0.03	29% ↓	* <i>p</i> < 0.001	21.08 $\pm$ 0.75	3, 37 RCs
<i>mlcNT3</i> <sup>(+/-)</sup>	↑	1.76 $\pm$ 0.07	28% ↑	* <i>p</i> < 0.001	39.83 $\pm$ 0.99	3, 40 RCs
<b>P20</b>						
Wild-type	N/A	0.98 $\pm$ 0.03	N/A	N/A	18.54 $\pm$ 0.53	5, 66 RCs
<i>Er81</i> <sup>(-/-)</sup>	No VGLUT1-IR in VH	N/A	N/A	N/A	N/A	N/A
<i>EGR3</i> <sup>(-/-)</sup>	↓	0.83 $\pm$ 0.04	14% ↓	* <i>p</i> = 0.009	16.81 $\pm$ 0.72	3, 32 RCs
<i>mlcNT3</i> <sup>(+/-)</sup>	↑	1.99 $\pm$ 0.09	114% ↑	* <i>p</i> < 0.001	35.89 $\pm$ 1.01	3, 26 RCs
<b>Adult</b>						
Wild-type	N/A	0.98 $\pm$ 0.03	N/A	N/A	20.18 $\pm$ 0.68	4, 35 RCs
<i>Er81</i> <sup>(-/-)</sup>	N/A	N/A	N/A	N/A	N/A	N/A
<i>EGR3</i> <sup>(-/-)</sup>	↓	0.70 $\pm$ 0.04	29% ↓	* <i>p</i> < 0.001	14.35 $\pm$ 0.68	3, 31 RCs
<i>mlcNT3</i> <sup>(+/-)</sup>	↑	1.97 $\pm$ 0.10	99% ↑	* <i>p</i> < 0.001	37.24 $\pm$ 1.06	3, 24 RCs

N/A = Not applicable or No data available

*VACHT-IR density on Renshaw cells increases in  $Er8I^{(-/-)}$  and  $EGR3^{(-/-)}$  mice and decreases in  $mlcNT3^{(+/-)}$  mice.*

Next we studied whether VACHT-IR contact density on RCs is altered in animals with altered strength of the VGLUT1 input. The ventral horn of  $Er8I^{(-/-)}$  knockouts showed marked increases in VACHT-IR (Figure 41). As mentioned above, RCs from  $Er8I^{(-/-)}$  knockouts had no VGLUT1-IR contacts, but RCs at P15 showed a 70% increase in the density of VACHT-IR contacts (Figure 42,43) that was statistically significant compared to age-matched wild-type controls (WT =  $1.45 \pm 0.043$  contacts per  $10 \mu\text{m}$  of dendrites (n = 5, 57 RCs) and  $Er8I^{(-/-)}$  =  $2.44 \pm 0.09$  (n = 3, 31 RCs),  $p < 0.001$ ,  $t$  test). There was only a 23% increase in VACHT-IR contact density at P20 compared to WT, although this increase was still significant (WT =  $1.67 \pm 0.05$  (n = 5, 66 RCs) and  $Er8I^{(-/-)}$  =  $2.06 \pm 0.08$  (n = 3, 37 RCs),  $p < 0.001$ ,  $t$ -test). VACHT-IR contact density on RCs significantly decreased from P15 to P20 ( $p = 0.002$ ,  $t$  test). Analyses were not carried out in adult  $Er8I^{(-/-)}$  animals because of the high mortality rate after the first three postnatal weeks.

Similar to  $Er8I^{(-/-)}$  animals, VACHT-IR staining was increased in LIX and the RC area of  $EGR3^{(-/-)}$  animals compared to wild-types (Figure 41). RCs from  $EGR3^{(-/-)}$  animals displayed significant increases in VACHT-IR contact density at P15 (Figure 42,43) (21% increase; WT =  $1.45 \pm 0.04$  (n = 5, 57 RCs) and  $EGR3^{(-/-)}$  =  $1.76 \pm 0.06$  (n = 3, 37 RCs),  $p < 0.001$ ,  $t$  test) and P20 (18% increase; WT =  $1.67 \pm 0.05$  (n = 5, 66 RCs) and  $EGR3^{(-/-)}$  =  $1.97 \pm 0.1$  (n = 3, 24 RCs),  $p < 0.001$ ,  $t$  test). RCs at P40 showed a 40% increase compared to wild-type (WT =  $1.54 \pm 0.09$  (n = 2, 24 RCs) and  $EGR3^{(-/-)}$  =  $2.14 \pm 0.06$  (n = 3, 31 RCs),  $p < 0.001$ ,  $t$  test).

**Figure 41.** VAcHt-IR in the ventral horn of wild-type, *EGR3*<sup>(-/-)</sup>, *mlcNT3*<sup>(+/-)</sup>, and *Er81*<sup>(-/-)</sup> mice at P15, P20, and in the adult. **A-D**, Low magnification confocal images of VAcHt-IR in the ventral horn at P15, P20, and adult in control, *EGR3*<sup>(-/-)</sup>, *mlcNT3*<sup>(+/-)</sup>, and *Er81*<sup>(-/-)</sup> animals. The dotted line indicates the border between the ventral horn and white matter. The blue line delineates the border between lamina IX (LIX) and lamina VII (LVII). VAcHt-IR in the ventral horn is largely reduced in LIX in *mlcNT3*<sup>(+/-)</sup> mice (**A**) at all ages analyzed. In contrast, VAcHt-IR is increased in LIX and the RC area of mature *EGR3*<sup>(-/-)</sup> (**B**) and *Er81*<sup>(-/-)</sup> (**C**) mice. **Scale bars: A1-A3, B1-B3, C1-C3 and D1-D2** (in A1), 100  $\mu$ m.



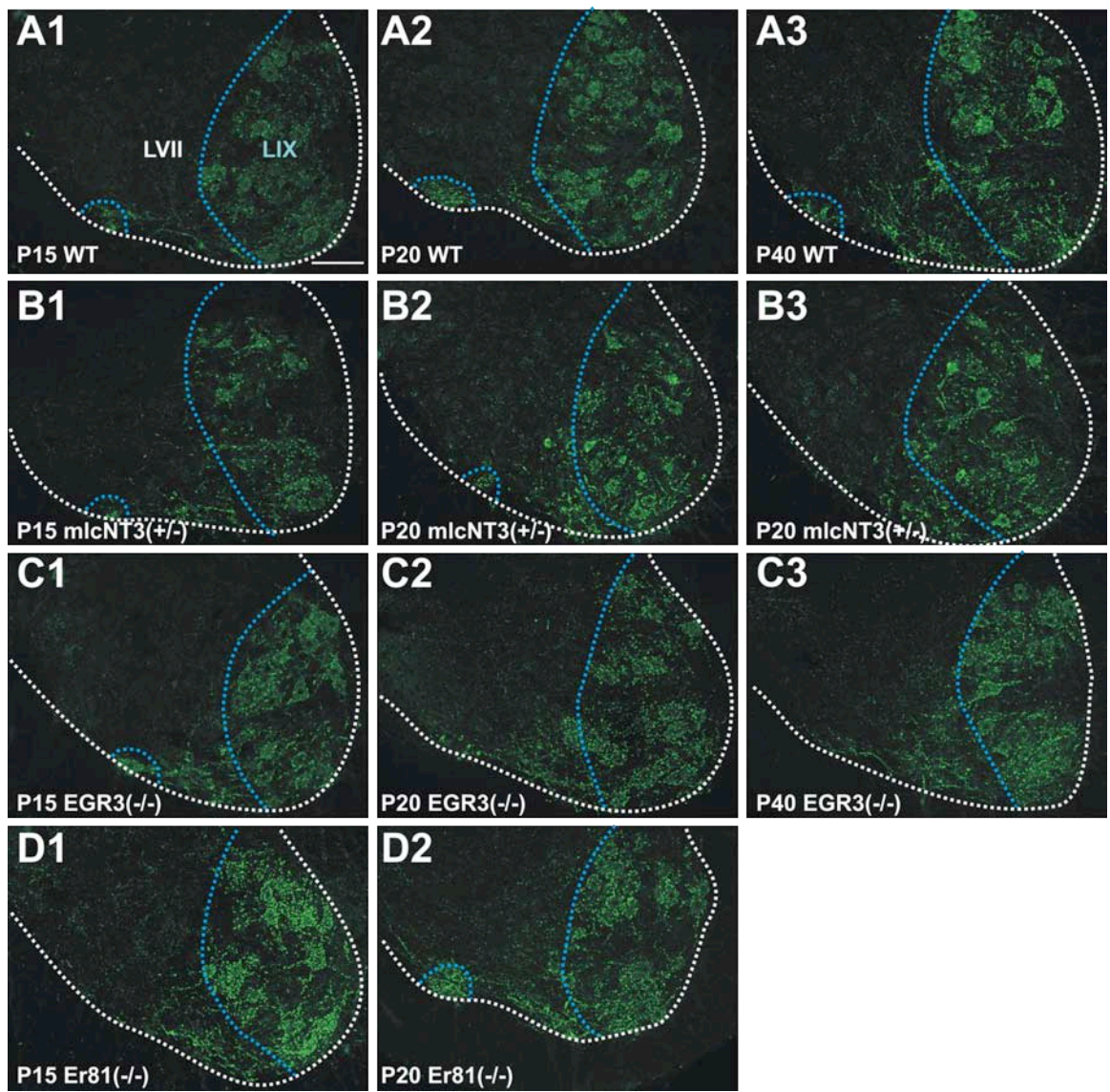


**Figure 42.** Density of VACHT-immunoreactive contacts on Renshaw cells in the ventral horn of control, *Er81*<sup>(-/-)</sup> *EGR3*<sup>(-/-)</sup>, and *mlcNT3*<sup>(+/-)</sup> P20 mice. **A1, B1, C1, D1,** Low magnification images of VACHT-immunoreactivity (VACHT-IR) in the ventral horn at P20 in control, *Er81*<sup>(-/-)</sup>, *EGR3*<sup>(-/-)</sup>, and *mlcNT3*<sup>(+/-)</sup> animals. VACHT-IR staining is increased in LIX and in the RC area of *EGR3*<sup>(-/-)</sup> and *Er81*<sup>(-/-)</sup> mice compared to controls. The dotted line indicates the border between the ventral horn and white matter. **A2, B2, C2, D2,** Superimposed VACHT-IR (green) and CB-IR (CY3, red) in the same field shown in A1, B1, C1, and D1. Box indicates area of high magnification shown in A3, B3, C3, and D3. **A3, B3, C3, D3,** High magnification images of VACHT-IR contacts on P20 CB-IR RCs. Arrowheads indicate VACHT-IR contacts on RC dendrites. There is a greater density of VACHT-IR contacts on RCs in *Er81*<sup>(-/-)</sup> and *EGR3*<sup>(-/-)</sup> mice compared to control animals. In contrast, RCs in *mlcNT3*<sup>(+/-)</sup> mice have less VACHT-IR contacts compared to the control. **Scale bars: A1-A2, B1-B2, C1-C2 and D1-D2** (in A1), 100  $\mu\text{m}$ ; **A3, B3, C3 and D3** (in A3), 20  $\mu\text{m}$ .

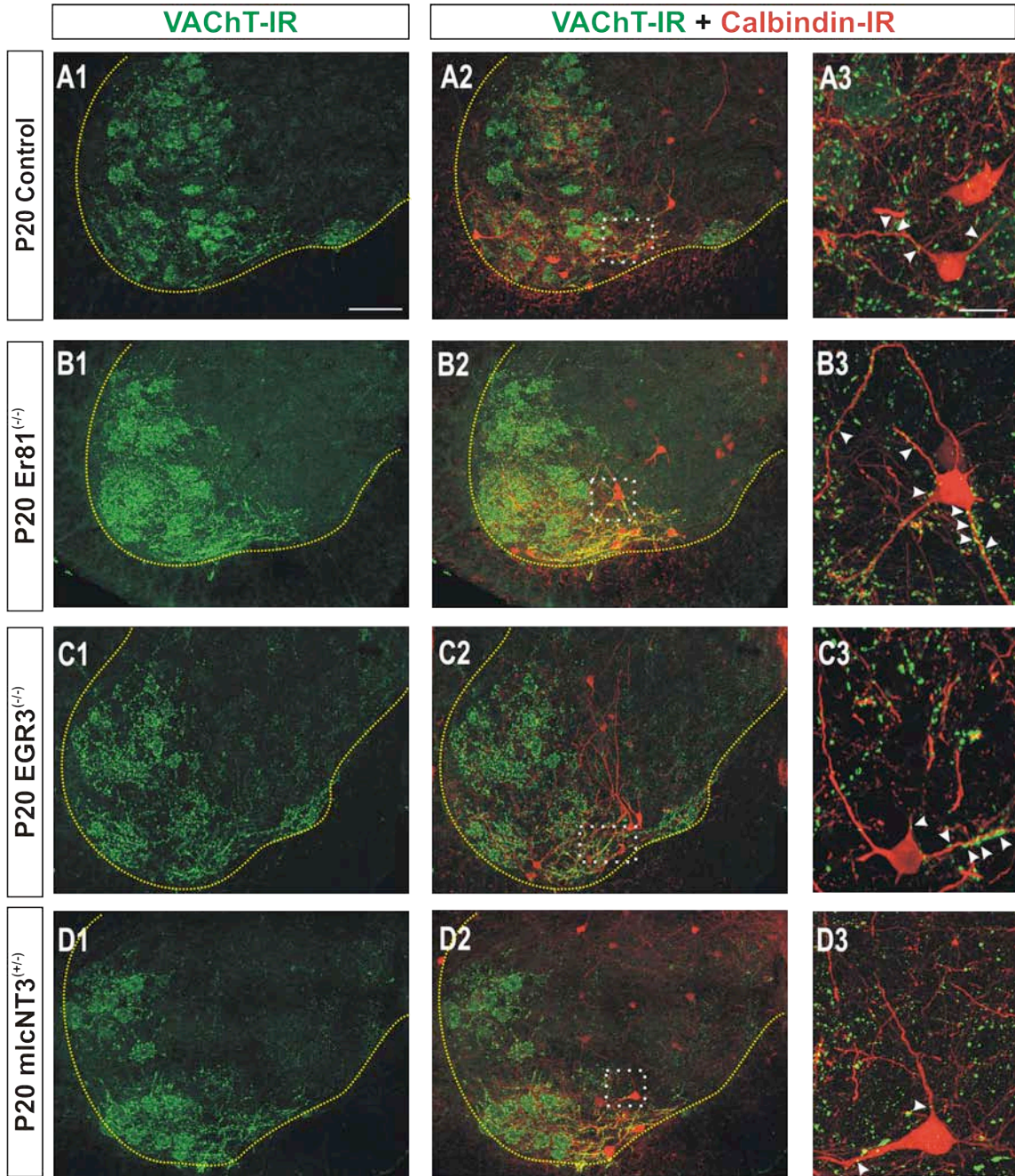
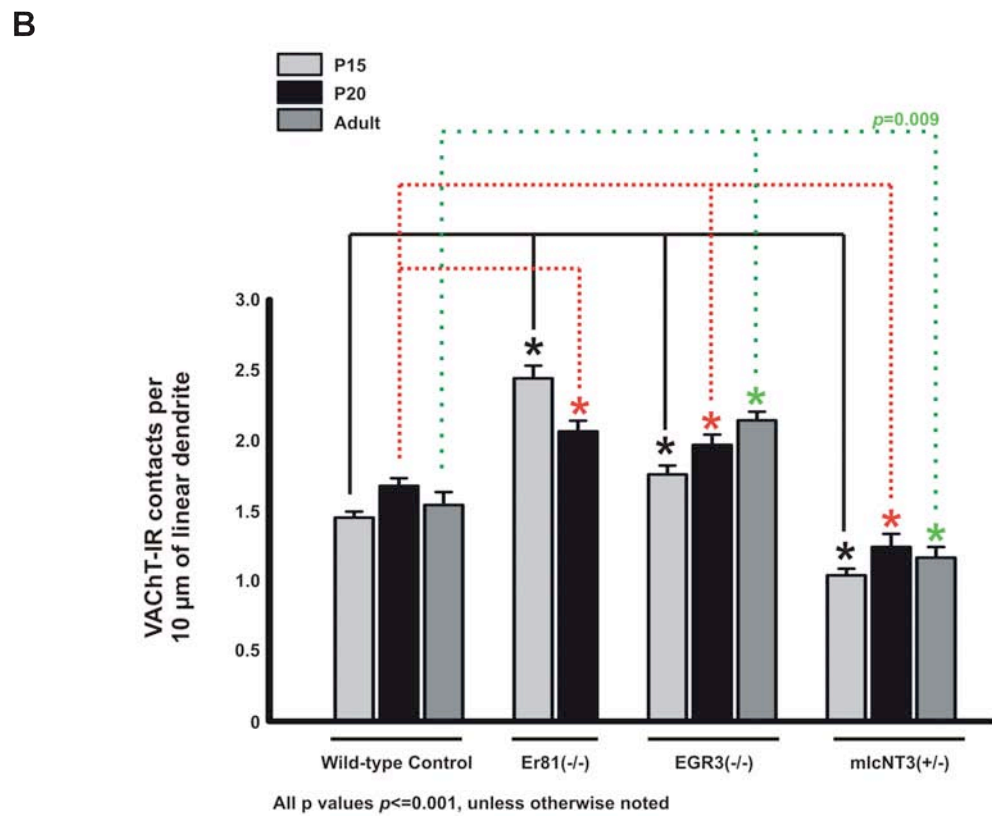
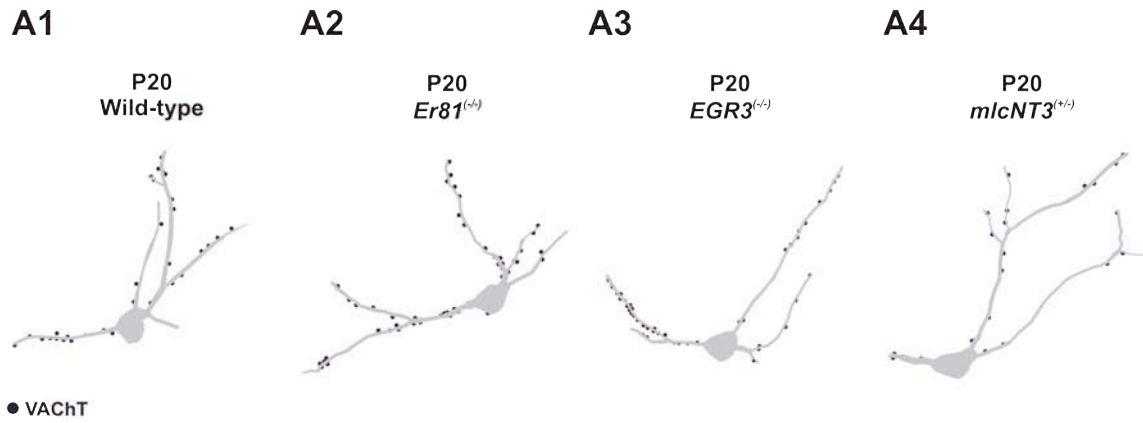


**Figure 43.** VACHT-IR contacts per 10  $\mu\text{m}$  of linear dendrite of CB-IR RCs in control, *Er81*<sup>(-/-)</sup>, *EGR3*<sup>(-/-)</sup>, and *mlcNT3*<sup>(+/-)</sup> mice of P15, P20, and adult postnatal ages. **A**, 3D reconstruction of RCs from P20 wild-type (**A1**), *Er81*<sup>(-/-)</sup> (**A2**), *EGR3*<sup>(-/-)</sup> (**A3**), and *mlcNT3*<sup>(+/-)</sup> (**A4**) mice reconstructed in NeuroLucida with VACHT-IR contacts plotted on the reconstruction. **B**, Density of VACHT-IR contacts per 10  $\mu\text{m}$  of linear RC dendrite in *Er81*<sup>(-/-)</sup>, *EGR3*<sup>(-/-)</sup>, and *mlcNT3*<sup>(+/-)</sup> compared to age-matched wild-type controls. Wild-type controls animals showed changes in VACHT-IR contact density similar to those reported in Mentis et al., 2006 and Aims 1 and 3. VACHT-IR contact density increased significantly from P15 to adult ( $p=0.020$ , one-way ANOVA), there were no significant differences between P20 and adult ( $p=0.724$ , t-test). RCs from *Er81*<sup>(-/-)</sup> animals showed a significant decrease in VACHT-IR contact density from P15 to P20 ( $p=0.002$ , t-test). Compared to wild-type controls, the density of VACHT-IR contacts increased significantly for both P15 and P20 (P15 and P20,  $p\leq 0.001$ , t-test). VACHT-IR contact density on RCs from *EGR3*<sup>(-/-)</sup> mice increased from P15 to adult ( $p=0.001$ , one-way ANOVA). At all ages analyzed, VACHT-IR contact density in *EGR3*<sup>(-/-)</sup> animals increased significantly compared to age-matched wild-type controls ( $p\leq 0.001$ , t-tests). In contrast, VACHT-IR contact densities in *mlcNT3*<sup>(+/-)</sup> displayed significant decreases compared to control animals (P15 and P20,  $p\leq 0.001$ , t-tests; adult,  $p=0.009$ , t-test). There is a greater density of VACHT-IR contacts on RCs in *Er81*<sup>(-/-)</sup> and *EGR3*<sup>(-/-)</sup> mice compared to control animals. In contrast, RCs in *mlcNT3*<sup>(+/-)</sup> mice have less VACHT-IR contacts than control. Therefore primary afferent strength affects the density of VACHT-IR contacts on RCs.





Overall, VACHT-IR contact density increased significantly from P15 to adult ( $p < 0.001$ , one-way ANOVA). In conclusion, there is a greater density of VACHT-IR contacts on RCs in *Er81*<sup>(-/-)</sup> and *EGR3*<sup>(-/-)</sup> mice compared to control animals (Figure 43; summarized in Table 10); suggesting that decreasing primary afferent inputs results in a significant increase in VACHT-IR inputs on RCs.

Next we investigated whether increasing primary afferent inputs in the ventral horn affects the density of VACHT-IR contacts on RCs using the *mlcNT3*<sup>(+/-)</sup> mice. In contrast to VACHT-IR staining seen in *Er81*<sup>(-/-)</sup> and *EGR3*<sup>(-/-)</sup> mice, VACHT-IR staining in *mlcNT3*<sup>(+/-)</sup> mice appeared to be decreased, particularly in LIX (Figure 41). In *mlcNT3*<sup>(+/-)</sup> animals displaying an increased VGLUT1-IR input showed an overall significant decrease in the density of VACHT-IR contacts compared to age-matched wild-type controls (Figure 42,43). RCs at P15 exhibited a 30% decrease in VACHT-IR contact density (WT =  $1.45 \pm 0.04$  (n = 5, 57 RCs) and *mlcNT3*<sup>(+/-)</sup> =  $1.04 \pm 0.05$  (n = 3, 40 RCs),  $p = < 0.001$ , *t* test). There was a slight increase in VACHT-IR contact density in P20 and adult *mlcNT3*<sup>(+/-)</sup> animals compared to P15, but this increase was not significant (P20 =  $1.24 \pm 0.09$  (n = 3, 21 RCs) and adult =  $1.16 \pm 0.1$  (n = 3, 24 RCs),  $p = 0.169$ , one-way ANOVA) and densities at each of these ages was always significantly less than with age-matched WT. Therefore it appears that alterations in primary afferent input strength affects the density of VACHT-IR contacts on RCs (summarized in Table 10).

*Excitatory glutamatergic inputs from spinal interneurons on Renshaw cells are not influenced by the strength of primary afferents.*

Since the density of excitatory inputs from motor axons is influenced by the strength of primary afferents, we looked at whether there was a change in the density of other excitatory inputs also converging on RCs. We analyzed inputs for spinal cord interneurons using VGLUT2-IR as a marker (Figure 44). The density of VGLUT2-IR contacts on WT RCs at P20 was greater than that of VGLUT1-IR or VACHT-IR contacts from primary afferents and motor axon collaterals, respectively. Interestingly, there was no significant difference in the density of VGLUT2-IR contacts on RCs in *Er81<sup>-/-</sup>*, *EGR3<sup>-/-</sup>*, and *mlcNT3<sup>+/-</sup>* compared to WT animals (Figure 44) (WT =  $3.11 \pm 0.53$  (n = 1 animal, 11 RCs), *Er81<sup>-/-</sup>* =  $3.09 \pm 0.59$  (n=1, 9 RCs), *EGR3<sup>-/-</sup>* =  $3.07 \pm 0.53$  (n=1, 11 RCs), *mlcNT3<sup>+/-</sup>* =  $3.08 \pm 0.47$  (n=1, 14 RCs);  $p = 0.997$ , one-way ANOVA). Therefore it appears that only inputs from motor axons are affected by alterations in primary afferents.

## **Discussion**

The main findings in this aim include: 1) Altering primary afferent input in the ventral horn affects the density of VGLUT1-IR contacts on RCs; 2) The density of VACHT-IR inputs are altered opposite to VGLUT1. Decreasing primary afferent input in the ventral horn results in an increase in VACHT-IR contact strength, while increasing primary afferent strength results in a decrease in VACHT-IR strength; 3) Excitatory inputs from spinal interneurons on RCs are not affected by changes in primary afferent

**Table 10.** VAcHT-IR contact densities of Renshaw cells from P15, P20, and adult wild-type, *Er81*<sup>(-/-)</sup>, *EGR3*<sup>(-/-)</sup>, and *mlcNT3*<sup>(+/-)</sup> mice.

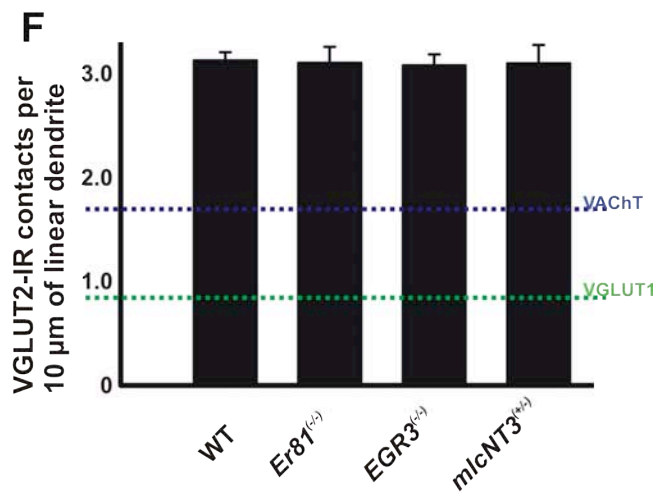
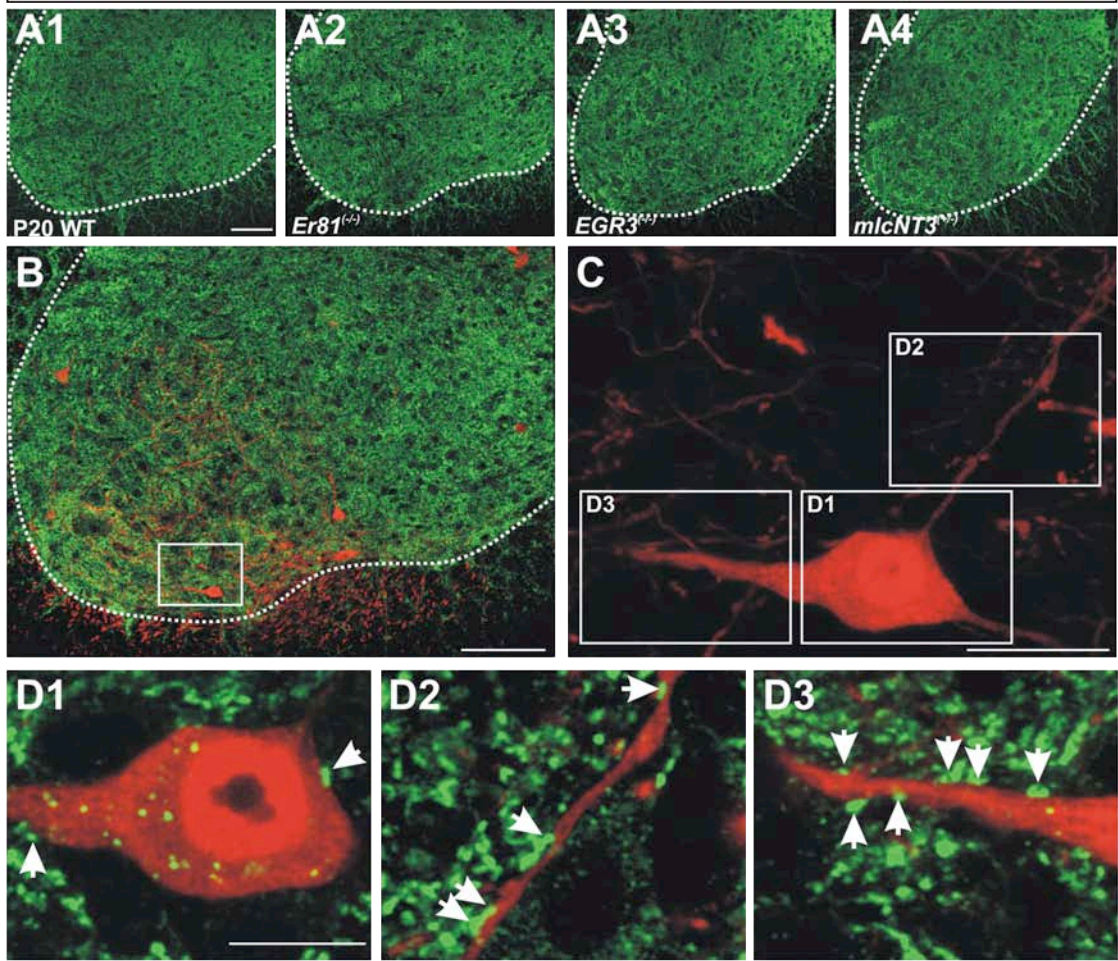
Animal Model	Changes in VAcHT-IR in Ventral Horn	VAcHT-IR contacts per 10 $\mu$ m of dendrite	Percent change compared to WT	P Value (*, significant) t test	Total # of VAcHT contacts per cell	N (# animals, # RCs)
Wild-type	N/A	1.45 $\pm$ 0.04	N/A	N/A	28.05 $\pm$ 0.71	5, 57 RCs
<i>Er81</i> <sup>(-/-)</sup>	↑	2.44 $\pm$ 0.09	70% ↑	* <i>p</i> < 0.001	47.97 $\pm$ 1.24	3, 31 RCs
<i>EGR3</i> <sup>(-/-)</sup>	↑	1.76 $\pm$ 0.06	21% ↑	* <i>p</i> < 0.001	37.81 $\pm$ 1.01	3, 37 RCs
<i>mlcNT3</i> <sup>(+/-)</sup>	↓	1.04 $\pm$ 0.05	30% ↓	* <i>p</i> < 0.001	23.75 $\pm$ 0.77	3, 40 RCs
<b>P20</b>						
Wild-type	N/A	1.67 $\pm$ 0.05	N/A	N/A	30.52 $\pm$ 1.21	5, 66 RCs
<i>Er81</i> <sup>(-/-)</sup>	↑	2.06 $\pm$ 0.08	23% ↑	* <i>p</i> < 0.001	38.92 $\pm$ 1.03	3, 37 RCs
<i>EGR3</i> <sup>(-/-)</sup>	↑	1.97 $\pm$ 0.10	18% ↑	* <i>p</i> < 0.001	38.09 $\pm$ 1.06	3, 34 RCs
<i>mlcNT3</i> <sup>(+/-)</sup>	↓	1.24 $\pm$ 0.09	27% ↓	* <i>p</i> < 0.001	22.08 $\pm$ 0.87	3, 21 RCs
<b>Adult</b>						
Wild-type	N/A	1.54 $\pm$ 0.09	N/A	N/A	30.52 $\pm$ 1.21	2, 24 RCs
<i>Er81</i> <sup>(-/-)</sup>	N/A	N/A	N/A	N/A	N/A	N/A
<i>EGR3</i> <sup>(-/-)</sup>	↑	2.14 $\pm$ 0.06	39% ↑	* <i>p</i> < 0.001	41.61 $\pm$ 1.16	3, 31 RCs
<i>mlcNT3</i> <sup>(+/-)</sup>	↓	1.16 $\pm$ 0.10	23% ↓	* <i>p</i> < 0.001	21.48 $\pm$ 0.81	3, 24 RCs

N/A = Not applicable or No data available



**Figure 44.** Density of VGLUT2-IR contacts in wild-type, *Er81*<sup>(-/-)</sup>, *EGR3*<sup>(-/-)</sup> and *mlcNT3*<sup>(+/-)</sup> mice at P20. **A**, VGLUT2-IR (FITC, green) in the ventral horn of wild-type (A1), *Er81*<sup>(-/-)</sup> (A2), *EGR3*<sup>(-/-)</sup> (A3), and *mlcNT3*<sup>(+/-)</sup> (A4) mice at P20. Dotted line represents the border between the ventral horn and the white matter. There does not appear to be any differences in VGLUT2-IR in the ventral horn of all three transgenic animals compared to wild-type controls. **B**, Low magnification confocal image of the ventral horn of a P20 *Er81*<sup>(-/-)</sup> spinal cord immunolabeled for CB (Cy3, red) and VGLUT2 (green). The box indicates the cell shown at higher magnification in C. **C**, High magnification image of the CB-IR RC selected in B. Boxes indicate the areas shown at higher magnification in D1-D3. **D**, High magnification images of VGLUT2-IR contacts (green) on the soma (D1) and dendrites (D2-D3) of a P20 CB-IR RC (red). Arrowheads indicate VGLUT2-IR contacts. VGLUT2-IR contacts were located on the soma and whole dendritic arbor analyzed. **E**, Neurolucida 3D reconstruction of a RC from a P20 *Er81*<sup>(-/-)</sup> knockout with VGLUT2-IR contacts plotted on the reconstruction. **F**, Density of VGLUT2-IR contacts per 10  $\mu\text{m}$  of linear CB-IR RC dendrites in P20 animals. There were no significant differences in the density of VGLUT2-IR contacts in *Er81*<sup>(-/-)</sup>, *EGR3*<sup>(-/-)</sup>, and *mlcNT3*<sup>(+/-)</sup> compared to control animals ( $p=0.997$ , one-way ANOVA). The blue line represents the density of VACHT-IR contacts on P20 RCs from wild-type controls and the green line represents the density VGLUT1-IR contacts. The density of VGLUT2-IR contacts on RCs at P20 was greater than that of VGLUT1-IR or VACHT-IR. **Scale bars: A1-A4 and B** (in A1 and B), 100  $\mu\text{m}$ ; **C**, 20  $\mu\text{m}$ ; **D1-D3** (in D1), 10  $\mu\text{m}$ .

Vesicular Glutamate Transporter 2 (VGLUT2-IR) + CB-IR



input. These results suggest that there is a specific interaction between motor axons and primary afferents throughout development.

During development and in mature neurons, excitatory synaptic input strength is controlled by two different activity-dependent mechanisms, homeostatic and Hebbian synaptic plasticity. Both are discussed below to best interpret our findings. In addition, it is also possible that competition between Ia afferents and motor axons is activity-independent and a molecular model is proposed that could explain this observation. All these mechanistic explanations are highly speculative at this point and will need further work to be validated.

#### *Homeostatic Plasticity*

Neural activity is modulated so that neurons do not become hyperactive or hypoactive. Homeostatic plasticity (HSP) is the ability of a neuron to maintain a steady state of activity relative to the activity of the network. It is believed that a neuron maintains a steady state of activity, in part by altering the synaptic strength of its inputs. HSP works as a negative feedback mechanism. In other words, excitatory synapses are weakened by overactivation of the neuron, while inhibitory synapses are strengthened (Turrigiano & Nelson, 2004; Burrone & Murthy, 2003; Davis, 2006). HSP is believed to work as a global mechanism where all synapses on a neuron are equally affected, so that the synaptic strengths are proportionally scaled up or down. A global signal will affect all synapses in a neuron and synapses will change in unison. If one major excitatory input, like primary afferents, is strengthened that could then decrease the strength of all other excitatory inputs. HSP mechanisms fail to explain the changes in density of motor

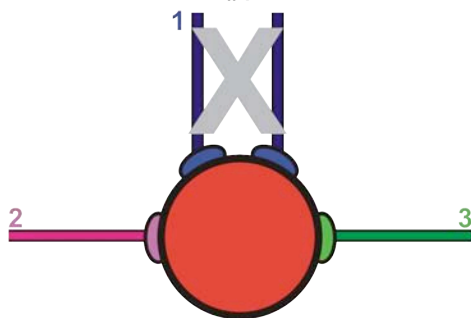
axon synapses seen in this aim because not all excitatory inputs were equally affected. In this aim only those inputs from motor axons, and not those from excitatory spinal interneurons, were affected by changes in primary afferent input in the ventral horn (Figure 45). Therefore, we rule out the possibility that the changes in synaptic strength described here arise via some form of homeostatic synaptic plasticity.

### *Hebbian Synaptic Plasticity*

Hebbian theory of synaptic plasticity differs greatly from homeostatic plasticity and was postulated in 1949 by Donald Hebb. In Hebbian synapses, increased synaptic strength results from the association of the presynaptic terminal activity with postsynaptic cell firing within a narrow time-window (Hebb, 1949). Hebbian theory is a positive feedback mechanism that strengthens synapses capable of modulating postsynaptic actions while ineffective synapses are weakened or eliminated. It is often summarized as “cells that fire together, wire together.” Hebbian synaptic plasticity is competitive because only the synaptic inputs best correlated with postsynaptic firing are maintained. It is possible that motor axons and primary afferents compete during development to modulate MN firing in a Hebbian-like mode. During normal development, motor axons are generally strengthened because the tight coupling between MNs and RCs firing. In contrast, primary afferent inputs are functionally weakened. In the case of the *Er81*<sup>(-/-)</sup> and *EGR3*<sup>(-/-)</sup> mice, where primary afferent input in the ventral horn is further weakened, motor axon synapses could proliferate because of weaker competition from primary afferents. In contrast, in *mlcNT3*<sup>(+/-)</sup> mice, the increase in primary afferent input results in significantly less inputs from motor axons. A Hebbian theory of plasticity seems

**Figure 45.** Model of homeostatic plasticity (HSP) mechanisms in a mature cell. The cell depicted here, under normal conditions, receives three excitatory inputs (#1, 2, and 3). Upon complete removal of input #1 (indicated by 'X'), since HSP mechanisms refer to uniform changes in synaptic strength, we would expect to see changes in the synaptic densities of both input #2 and 3 to maintain a homeostatic number of excitatory synapses. In this aim, we found that removing one input (here input #1) does not affect both inputs #2 and 3. Only one of these inputs (input #3) is affected and alters its synaptic strength upon complete removal of input #1. Input #2 remains unchanged.

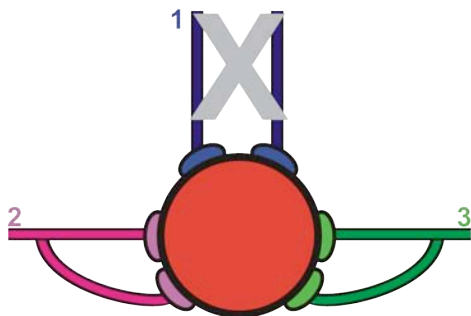
Removal of  
excitatory input  
#1



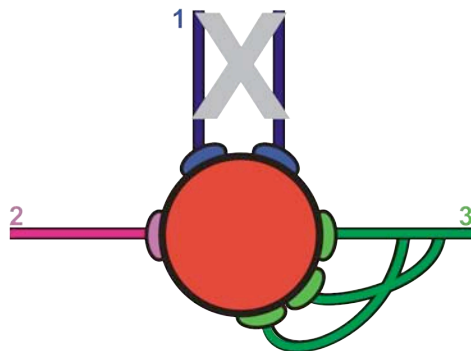
Expected



Actual



Changes in  
Synaptic Density  
of Inputs  
# 2 and 3



Changes in  
Synaptic Density  
of only  
Input #3

plausible but it also raises several questions: 1) is the increased strength of motor axon inputs on RCs observed in *Er81<sup>(-/-)</sup>* and *EGR3<sup>(-/-)</sup>* mice a result of specific preexisting motor axon connections sprouting new terminals, or 2) is increased motor axon input density the result of RCs receiving inputs from a larger number of MNs, perhaps resulting in a loss of specificity? Loss of specificity means that RCs receive correct inputs from homonymous and synergist MNs, but also receive inputs from MNs innervating antagonistic muscles (Figure 46).

*Activity-independent mechanisms: molecular hypothesis*

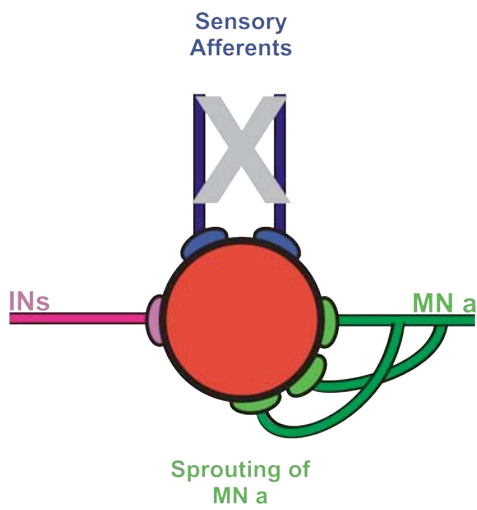
Formation of neural circuits requires that appropriate synaptic connections be made and that the appropriate presynaptic and postsynaptic plasma membranes be brought together. Thereafter, specific signaling results in the induction of a pre- and postsynaptic apparatus. A wealth of studies indicates that these interactions are mainly mediated by neurexins (NRXs) and their binding partner neuroligins (NLs; reviewed in Literature Review). There are four NL genes and three NRX genes in mouse, but numerous isoforms exist generated by alternative splicing. Two transcripts per NRX genes are generated ( $\alpha$  and  $\beta$  NRXs). The specific interactions adjust the number of synapses formed independently for different inputs. For example, NL-1 interactions are responsible for excitatory synapses and NL-2 for inhibitory synapses (Varoqueaux et al., 2004). NL-1 specifically binds  $\beta$ -neurexins ( $\beta$ -NRX) and NL-2 binds both  $\alpha$ -neurexins ( $\alpha$ -NRX) and  $\beta$ -NRXs, but  $\beta$ -NRX that bind NL-2 are different isoforms than the one that binds NL-1 (Figure 47; Missler et al., 2003).

**Figure 46.** Schematic depicting a Hebbian plasticity mechanism upon complete removal of one excitatory input. Upon removal of primary afferent inputs on RCs, the density of motor axon inputs increases, but the inputs from spinal interneurons remain unchanged. Therefore, it appears that there is an interaction between primary afferents and motor axons throughout development. **A,** Increased motor axon input density on RCs could be explained by changes in the synaptic strength of the motor axons inputs. In other words, there is an increase in the number of synapses from MN a. **B,** In contrast, RCs may now receive inappropriate connections from MN b, which do not usually contact that RC. If this were the case, then there would be a loss of specificity of the connections from motor axons on RCs.



A

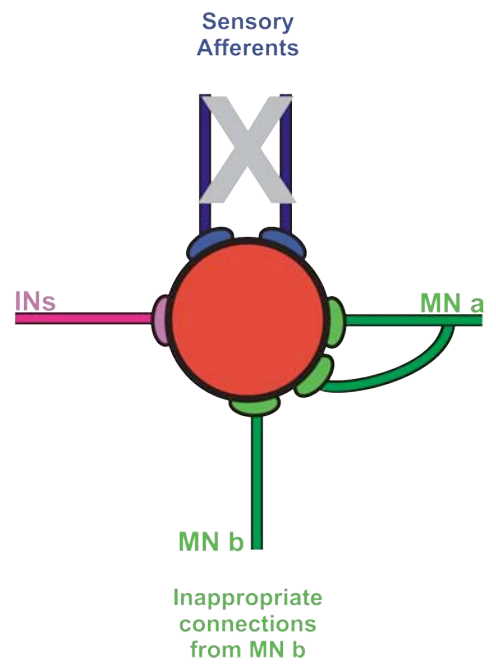
Change in synaptic strength  
(# of synapses)



OR


B

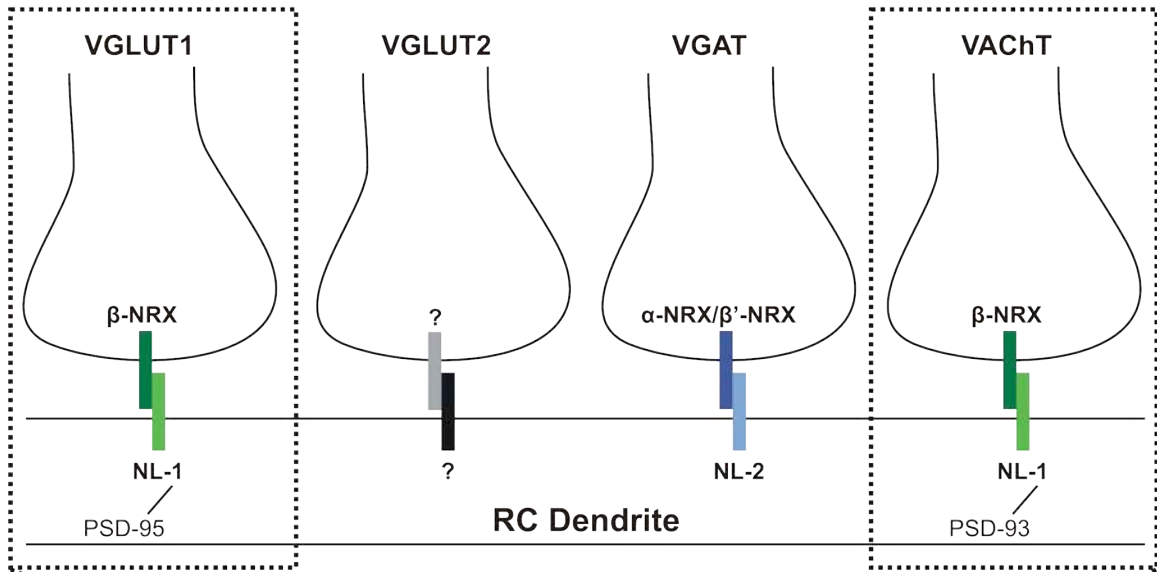
Loss of Specificity



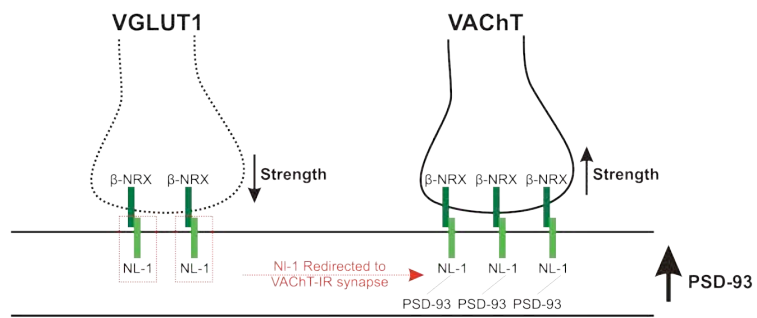
However, there are also examples of competition for NLs that heterosynaptically affect synaptic densities. As mentioned above, NL-1 interacts with postsynaptic scaffolding protein PSD-95 at glutamatergic synapses. Several studies have demonstrated that overexpression of PSD-95 in cultured hippocampal neurons leads to redirecting of all available NLs (including NL-2) to excitatory synapses such that, for example, GABAergic synapses are found at lower densities (Levinson et al., 2005). From these studies, we can hypothesize that the specific interaction between motor axons and sensory afferents synapse number could occur via a similar mechanism of redirecting NLs from one synapse type to another. For this hypothesis to be correct, it is necessary that: cholinergic synapse formation, similar to glutamatergic synapses, are dependent on the same isoforms of NL-1 and  $\beta$ -NRX. The specific NL and NRX isoforms of cholinergic synapses are not yet known. By difference to glutamatergic synapses, central cholinergic synapses express PSD-93 (Parker et al., 2004). Therefore, we can hypothesize that during normal development PSD-93 expression at cholinergic synapses increases, leading to a recruitment of NL-1 away from glutamatergic synapses ultimately reducing sensory afferent input and strengthening inputs from motor axons. In *Er81<sup>(-/-)</sup>* and *EGR3<sup>(-/-)</sup>* mice, the further weakening of primary afferents synapses could redirect the now available NL-1 in RCs, resulting in more motor axon synapses formed. In contrast, in *mlcNT3<sup>(+/-)</sup>* mice, an excess of sensory synapses and accumulation of postsynaptic PSD-95 could result in a redirection of NL-1 away from cholinergic synapses, decreasing the density of motor axon synapses.

**Figure 47.** Molecular hypothesis of activity-independent input selection on mature Renshaw cells in *Er81*<sup>(-/-)</sup>, *EGR3*<sup>(-/-)</sup> and *mlcNT3*<sup>(+/-)</sup> mice. Neuroligin-1 (NL-1) and its binding partner  $\beta$ -neurexin ( $\beta$ -NRX) are found at glutamatergic synapses (VGLUT1 synapses; the NL/NRX combination at VGLUT1-IR synapses is presently unknown). Inhibitory synapses (VGAT synapses) have neuroligin-2 (NL-2) and a combination of  $\alpha$ - and  $\beta$ -neurexins (note that the  $\beta$ -NRX found at inhibitory synapses is a different isoform and is represented as  $\beta^{\gamma}$ -NRX). The NL/NRX combination at cholinergic synapses is unknown, but here we are assuming that the same complement of NL/NRXs found at VGLUT1 synapses are also found at VACHT synapses. There are different scaffolding proteins associated with glutamatergic and cholinergic synapses. Postsynaptic density protein-95 and -93 (PSD-95 and PSD-93) are associated with glutamatergic and cholinergic synapses respectively. In *Er81*<sup>(-/-)</sup> and *EGR3*<sup>(-/-)</sup> animals, weakening of sensory afferents and accumulation of PSD-93 at cholinergic synapses, results in more NL-1 being redirected away from VGLUT1 synapses to VACHT synapses. Therefore, a further decrease in the density of sensory afferent inputs and an exacerbated increase in motor axon input density are observed. In *mlcNT3*<sup>(+/-)</sup> animals, the excess of sensory afferent inputs and the accumulation of PSD-95, could result in NL-1 being redirected from VACHT synapses to VGLUT1 synapses, decreasing the density of motor axon synapses.

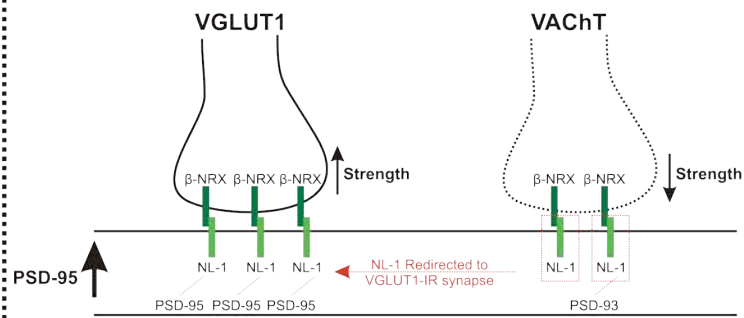
 Presynaptic Terminal  
 NL Neurologin (1 or 2)  
 NRX Neurexin (α or β)  
 PSD Postsynaptic Density Protein (93 or 95)



*Er81<sup>(-/-)</sup> and EGR3<sup>(-/-)</sup>*



*mlcNT3<sup>(+/-)</sup>*



*Activity-dependent molecular mechanism for synaptic strengthening*

A further alternative mechanism can be proposed. It has been suggested that excitatory synapse maturation is dependent on neuregulin (NRGs) and its receptors, ErbBs (Falls, 2003; Yarden and Sliwkowski, 2001). More specifically, neuregulin-1 (NRG-1) and its receptor ErbB4 have been implicated in excitatory synapse development. Intracellular signaling pathways are activated by NRG binding to ErbB receptors, which are receptor tyrosine kinases. Activation of ErbB receptors via NRGs mediates several cellular responses including: apoptosis, migration, differentiation, adhesion, and stimulation or inhibition of proliferation. Several studies have found that one ErbB receptor in particular, ErbB4, is found in the postsynaptic density (PSD) of excitatory synapses and interacts with PSD-95, a scaffolding protein of glutamatergic synapses (Garcia et al., 2000; Huang et al., 2000). Li and colleagues (2007) demonstrated that the NRG/ErbB4 signaling pathway is required for activity dependent AMPA receptor incorporation and stabilization at glutamatergic synapses in cultured hippocampal neurons. They also found that if activity at these synapses is inhibited, there is a corresponding decrease in ErbB4 in the PSDs. They concluded that the NRG/ErbB4 signaling pathway is activated by synaptic activity, which leads to a recruitment and stabilization of ErbB4 receptors in synapses. Moreover, stabilization of ErbB4 at PSDs stabilizes AMPA receptors permitting synaptic plasticity and maturation. From these conclusions we can hypothesize that, under normal wild-type conditions, motor axon synapses on RCs could be strengthened and mature by activity-dependent activation of NRG/ErbB signaling pathways, ultimately leading to stabilization of motor axon postsynaptic receptors. In contrast, decreased activity of sensory afferent synapses

results in decreased signaling. Competition of motor axon synapses and primary afferents for ErbB might provide a molecular substrate for a possible interaction between these two inputs during development. ErbBs accumulate at motor axon synapses, but are removed from sensory synapses leading to fewer AMPA receptors being incorporated during late postnatal development, this mechanism is exacerbated in *Er81*<sup>(-/-)</sup> and *EGR3*<sup>(-/-)</sup> mice. Moreover, the activity of sensory afferent inputs on RCs might increase in *mlcNT3*<sup>(+/-)</sup> mice, thus leading to incorporation of ErbB4 at PSDs and ultimately incorporation of more AMPA receptors and stabilization of these receptors at the expense of motor axon synapse stabilization.

Above we proposed separate activity-independent and activity-dependent mechanisms to explain the interaction between motor axon and sensory afferent inputs on RCs, but more likely, several of these mechanisms could work in concert. During normal development, it is possible that motor axon inputs are stabilized and proliferate because of increased activity. Increased activity leads to aggregation of ErbB receptors at PSDs, which then may increase PSD-93 expression, ultimately leading to recruitment of NL-1 from sensory afferent synapses. Motor axon inputs are strengthened by increased aggregation of ErbB receptors at PSDs, which activate signaling cascades that not only lead to increased incorporation of motor axon postsynaptic receptors, but also proliferation of this input. In contrast, in *mlcNT3*<sup>(+/-)</sup> mice, sensory afferent activity may increase and, similar to wild-type mice, ErbB receptors aggregate and increase PSD-95 expression. Increased PSD-95 expression may then recruit NL-1 from cholinergic synapses, strengthening sensory afferent inputs on RCs.

In conclusion, we present evidence that interactions exist between sensory afferent strength and motor axon input density on RCs, but not with other excitatory inputs, suggesting that early sensory afferent inputs contribute to shape the organization of motor synapses on RCs. We propose a number of mechanistic models that could explain this interaction.

## **CHAPTER IX**

### **Conclusions**



In this thesis, we hypothesized that the common genetic background of adult Renshaw cells (RCs) and Ia inhibitory interneurons (IaINs) makes them competent to receive convergent inputs from motor axons and Ia proprioceptive primary afferents, but that each input is differentially matured by each interneuron type during development in a cell-type specific manner. Here we determined that:

1. Renshaw cells receive convergent inputs from motor axons and Ia afferents, both inputs develop in parallel until after the second postnatal week; after which the motor input is maintained and the input from Ia afferents is “functionally de-selected”,
2. Synapses between RCs and motoneurons (MNs) are first present at E13, but there is a 24-48 hour delay before the formation of synapses from RCs onto MNs,
3. Neonatal Ia inhibitory interneurons do not receive motor axon inputs. Ia afferent inputs develop in parallel in IaINs and RCs during early postnatal development, but Ia afferent synaptic density on IaINs is always higher than on RCs and is maintained after P15 and in the adult, and
4. Altering Ia afferent strength in the ventral horn affects the strength of sensory afferent and motor axon inputs on RCs, but not other excitatory inputs, suggesting that there is an interaction between motor axons and Ia afferents throughout development.

From these findings, some general conclusions may be drawn. First, RCs and IaINs do not diversify from a “generic” V1-IN by the loss/weakening or gain/strengthening of specific inputs. RCs are a unique subtype of the V1 class because they are the only known V1-INs that are competent to receive convergent inputs from both Ia afferents and motor axons. Moreover, we demonstrate that the overall synaptic organization of motor axons inputs on RCs appears to be shaped by the presence of early sensory afferent inputs. IaINs were unique in the density, location, and maintenance of

sensory afferent inputs in the adult. Finally, we find little evidence for the convergence of motor axons and sensory synapses on neonatal IaINs, suggesting that there are fundamental differences between IaINs and RCs in their competence for receiving synapses from motor axons and that this is determined at very early stages, and is perhaps genetically specified.

**CHAPTER X**  
**BIBLIOGRAPHY**

- Al-Mosawie A, Wilson JM, Brownstone RM (2007) Heterogeneity of V2-derived interneurons in the adult mouse spinal cord. *Eur J Neurosci* 26:3003-3015.
- Alvarez FJ, Dewey DE, Harrington DA, Fyffe RE (1997) Cell-type specific organization of glycine receptor clusters in the mammalian spinal cord. *J Comp Neurol* 379:150-170.
- Alvarez FJ, Dewey DE, McMillin P, Fyffe RE (1999) Distribution of cholinergic contacts on Renshaw cells in the rat spinal cord: a light microscopic study. *J Physiol* 515 (Pt 3):787-797.
- Alvarez FJ, Villalba RM, Zerda R, Schneider SP (2004) Vesicular glutamate transporters in the spinal cord, with special reference to sensory primary afferent synapses. *J Comp Neurol* 472:257-280.
- Alvarez FJ, Jonas PC, Sapir T, Hartley R, Berrocal MC, Geiman EJ, Todd AJ, Goulding M (2005) Postnatal phenotype and localization of spinal cord V1 derived interneurons. *J Comp Neurol* 493:177-192.
- Alvarez FJ, Fyffe RE (2007) The continuing case for the Renshaw cell. *J Physiol* 584:31-45.
- Araki T, Eccles JC, Ito M (1960) Correlation of the inhibitory post-synaptic potential of motoneurons with the latency and time course of inhibition of monosynaptic reflexes. *J Physiol* 154:354-377.
- Araki S, Kawano A, Seldon HL, Shepherd RK, Funasaka S, Clark GM (2000) Effects of intracochlear factors on spiral ganglion cells and auditory brain stem response after long-term electrical stimulation in deafened kittens. *Otolaryngol Head Neck Surg* 122:425-433.
- Arber S, Ladle DR, Lin JH, Frank E, Jessell TM (2000) ETS gene Er81 controls the formation of functional connections between group Ia sensory afferents and motor neurons. *Cell* 101:485-498.
- Arvidsson U, Ulfhake B, Cullheim S, Ramirez V, Shupliakov O, Hokfelt T (1992) Distribution of calbindin D28k-like immunoreactivity (LI) in the monkey ventral horn: do Renshaw cells contain calbindin D28k-LI? *J Neurosci* 12:718-728.
- Balice-Gordon RJ, Lichtman JW (1993) In vivo observations of pre- and postsynaptic changes during the transition from multiple to single innervation at developing neuromuscular junctions. *J Neurosci* 13:834-855.
- Balice-Gordon RJ, Lichtman JW (1994) Long-term synapse loss induced by focal blockade of postsynaptic receptors. *Nature* 372:519-524.

- Battye R, Stevens A, Jacobs JR (1999) Axon repulsion from the midline of the *Drosophila* CNS requires slit function. *Development* 126:2475-2481.
- Benito-Gonzalez A, Berrocal MC, Goulding M, Alvarez FJ (2008) Renshaw cells are V1-derived neurons with a very early birthdate. Program No. 374.8. *2008 Abstract Viewer/Itinerary Planner*. Washington, DC: Society for Neuroscience, 2008. Online.
- Benson DL, Tanaka H (1998) N-cadherin redistribution during synaptogenesis in hippocampal neurons. *J Neurosci* 18:6892-6904.
- Bosc DG, Goueli BS, Janknecht R (2001) HER2/Neu-mediated activation of the ETS transcription factor ER81 and its target gene MMP-1. *Oncogene*;20:6215-6224.
- Bresler T, Shapira M, Boeckers T, Dresbach T, Futter M, Garner CC, Rosenblum K, Gundelfinger ED, Ziv NE (2004) Postsynaptic density assembly is fundamentally different from presynaptic active zone assembly. *J Neurosci* 24:1507-1520.
- Briscoe J, Sussel L, Serup P, Hartigan-O'Connor D, Jessell TM, Rubenstein JL, Ericson J (1999) Homeobox gene Nkx2.2 and specification of neuronal identity by graded Sonic hedgehog signaling. *Nature* 398:622-627.
- Briscoe J, Ericson J (1999) The specification of neuronal identity by graded Sonic Hedgehog signaling. *Semin Cell Dev Biol* 10:353-362.
- Briscoe J, Pierani A, Jessell TM, Ericson J (2000) A homeodomain protein code specifies progenitor cell identity and neuronal fate in the ventral neural tube. *Cell* 101:435-445.
- Brose K, Bland KS, Wang KH, Arnott D, Henzel W, Goodman CS, Tessier-Lavigne M, Kidd T (1999) Slit proteins bind Robo receptors and have an evolutionarily conserved role in repulsive axon guidance. *Cell* 96:795-806.
- Brown MC, Jansen JK, Van Essen D (1976) Polyneuronal innervation of skeletal muscle in new-born rats and its elimination during maturation. *J Physiol* 261:387-422.
- Brown AG, Fyffe RE (1978) The morphology of group Ia afferent fibre collaterals in the spinal cord of the cat. *J Physiol* 274:111-127.
- Brown AG, Fyffe RE (1979) The morphology of group Ib afferent fibre collaterals in the spinal cord of the cat. *J Physiol* 296:215-226.
- Buchert M, Schneider S, Meskenaite V, Adams MT, Canaani E, Baechi T, Moelling K, Hovens CM (1999) The junction-associated protein AF-6 interacts and clusters with specific Eph receptor tyrosine kinases at specialized sites of cell-cell contact in the brain. *J Cell Biol* 144:361-371.

- Buffelli M, Burgess RW, Feng G, Lobe CG, Lichtman JW, Sanes JR (2003) Genetic evidence that relative synaptic efficacy biases the outcome of synaptic competition. *Nature* 424:430-434.
- Bui TV, Cushing S, Dewey D, Fyffe RE, Rose PK (2003) Comparison of the morphological and electrotonic properties of Renshaw cells, Ia inhibitory interneurons, and motoneurons in the cat. *J Neurophysiol* 90:2900-2918.
- Burke RE, Fedina L, Lundberg A (1971) Spatial synaptic distribution of recurrent and group Ia inhibitory systems in cat spinal motoneurons. *J Physiol* 214:305-326.
- Burrill JD, Moran L, Goulding MD, Saueressig H (1997) PAX2 is expressed in multiple spinal cord interneurons, including a population of EN1+ interneurons that require PAX6 for their development. *Development* 124:4493-4503.
- Burrone J, Murthy VN (2003) Synaptic gain control and homeostasis. *Curr Opin Neurobiol* 13:560-567.
- Busetto G, Buffelli M, Tognana E, Bellico F, Cangiano A (2000) Hebbian mechanisms revealed by electrical stimulation at developing rat neuromuscular junctions. *J Neurosci* 20:685-695.
- Caroni P (1997) Overexpression of growth-associated proteins in the neurons of adult transgenic mice. *J Neurosci Methods* 71:3-9.
- Carr PA, Alvarez FJ, Leman EA, Fyffe RE (1998) Calbindin D28k expression in immunohistochemically identified Renshaw cells. *Neuroreport* 9:2657-2661.
- Charron F, Tessier-Lavigne M (2005) Novel brain wiring functions for classical morphogens: a role as graded positional cues in axon guidance. *Development* 132:2251-2262.
- Chen G, Trombley PQ, van den Pol AN (1996) Excitatory actions of GABA in developing rat hypothalamic neurones. *J Physiol* 494 ( Pt 2):451-464.
- Chen HH, Frank E (1999) Development and specification of muscle sensory neurons. *Curr Opin Neurobiol* 9:405-409.
- Chen HH, Tourtellotte WG, Frank E (2002) Muscle spindle-derived neurotrophin 3 regulates synaptic connectivity between muscle sensory and motor neurons. *J Neurosci* 22:3512-3519.
- Cheng HJ, Bagri A, Yaron A, Stein E, Pleasure SJ, Tessier-Lavigne M (2001) Plexin-A3 mediates semaphorin signaling and regulates the development of hippocampal axonal projections. *Neuron* 32:249-263.

- Chin, L.S., Li, L., Ferreira, A., Kosik, K.A., and Greengard, P. (1995) Impairment of axonal development and of synaptogenesis in hippocampal neurons of synapsin-I deficient mice. *Proc. Natl. Acad. Sci. USA* 92, 9230–9234.
- Colamarino SA, Tessier-Lavigne M (1995) The role of the floor plate in axon guidance. *Annu Rev Neurosci* 18:497-529.
- Conradi S, Cullheim S, Gollvik L, Kellerth JO (1983) Electron microscopic observations on the synaptic contacts of group Ia muscle spindle afferents in the cat lumbosacral spinal cord. *Brain Res* 265:31-39.
- Coppola V, Kucera J, Palko ME, Martinez-De Velasco J, Lyons WE, Fritsch B, Tessarollo L (2001) Dissection of NT3 functions in vivo by gene replacement strategy. *Development* 128:4315-4327.
- Copray JC, Brouwer N (1994) Selective expression of neurotrophin-3 messenger RNA in muscle spindles of the rat. *Neuroscience* 63:1125-1135.
- Crepel F, Mariani J, Delhay-Bouchaud N (1976) Evidence for a multiple innervation of Purkinje cells by climbing fibers in the immature rat cerebellum. *J Neurobiol* 7:567-578.
- Crepel F, Dhanjal SS, Sears TA (1982) Effect of glutamate, aspartate and related derivatives on cerebellar purkinje cell dendrites in the rat: an in vitro study. *J Physiol* 329:297-317.
- Crone SA, Quinlan KA, Zagoraoui L, Droho S, Restrepo CE, Lundfald L, Endo T, Setlak J, Jessell TM, Kiehn O, Sharma K (2008) Genetic ablation of V2a ipsilateral interneurons disrupts left-right locomotor coordination in mammalian spinal cord. *Neuron* 60:70-83.
- Cullheim S, Ulfhake B (1982) Evidence for a postnatal elimination of terminal arborizations and synaptic boutons of recurrent motor axon collaterals in the cat. *Brain Res* 281:234-237.
- Culotti JG, Merz DC (1998) DCC and netrins. *Curr Opin Cell Biol* 10:609-613.
- Curtis DR (1959) Pharmacological investigations upon inhibition of spinal motoneurons. *J Physiol* 145:175-192.
- Curtis DR, Ryall RW (1966) The synaptic excitation of Renshaw cells. *Exp Brain Res* 2:81-96.
- Curtis DR, Ryall RW (1966) The acetylcholine receptors of Renshaw cells. *Exp Brain Res* 2:66-80.

- Dalva MB, Takasu MA, Lin MZ, Shamah SM, Hu L, Gale NW, Greenberg ME (2000) EphB receptors interact with NMDA receptors and regulate excitatory synapse formation. *Cell* 103:945-956.
- Davis GW (2006) Homeostatic control of neural activity: from phenomenology to molecular design. *Annu Rev Neurosci* 29:307-323.
- Dean C, Scholl FG, Choih J, DeMaria S, Berger J, Isacoff E, Scheiffele P (2003) Neurexin mediates the assembly of presynaptic terminals. *Nat Neurosci* 6:708-716.
- Dickson BJ (2002) Molecular mechanisms of axon guidance. *Science* 298:1959-1964.
- Dourado M, Sargent PB (2002) Properties of nicotinic receptors underlying Renshaw cell excitation by alpha-motor neurons in neonatal rat spinal cord. *J Neurophysiol* 87:3117-3125.
- Duchen LW, Scaravilli F (1977) Quantitative and electron microscopic studies of sensory ganglion cells of the Sprawling mouse. *J Neurocytol* 6:465-481.
- Eccles JC, Fatt P, Koketsu K (1954) Cholinergic and inhibitory synapses in a pathway from motor-axon collaterals to motoneurons. *J Physiol* 126:524-562.
- Eccles JC, Fatt P, Landgren S (1956) Central pathway for direct inhibitory action of impulses in largest afferent nerve fibres to muscle. *J Neurophysiol* 19:75-98.
- Eccles JC, Eccles RM, Lundberg A (1957) The convergence of monosynaptic excitatory afferents on to many different species of alpha motoneurons. *J Physiol* 137:22-50.
- Eccles JC, Llinas R, Sasaki K (1966) The excitatory synaptic action of climbing fibres on the purkinje cells of the cerebellum. *J Physiol* 182:268-296.
- Ericson J, Rashbass P, Schedl A, Brenner-Morton S, Kawakami A, van Heyningen V, Jessell TM, Briscoe J (1997) Pax6 controls progenitor cell identity and neuronal fate in response to graded Shh signaling. *Cell* 90:169-180.
- Ericson J, Briscoe J, Rashbass P, van Heyningen V, Jessell TM (1997) Graded sonic hedgehog signaling and the specification of cell fate in the ventral neural tube. *Cold Spring Harb Symp Quant Biol* 62:451-466.
- Ernfors P, Merlio JP, Persson H (1992) Cells Expressing mRNA for Neurotrophins and their Receptors During Embryonic Rat Development. *Eur J Neurosci* 4:1140-1158.



- Fallah Z, Clowry GJ (1999) The effect of a peripheral nerve lesion on calbindin D28k immunoreactivity in the cervical ventral horn of developing and adult rats. *Exp Neurol* 156:111-120.
- Falls DL (2003) Neuregulins: functions, forms, and signaling strategies. *Exp Cell Res* 284:14-30.
- Fannon AM, Colman DR (1996) A model for central synaptic junctional complex formation based on the differential adhesive specificities of the cadherins. *Neuron* 17:423-434.
- Fannon AM, Colman DR (1996) A model for central synaptic junctional complex formation based on the differential adhesive specificities of the cadherins. *Neuron* 17:423-434.
- Feng G; Mellor RH; Bernstein M; Keller-Peck C; Nguyen QT; Wallace M; Nerbonne JM; Lichtman JW; Sanes JR. 2000. Imaging neuronal subsets in transgenic mice expressing multiple spectral variants of GFP. *Neuron* 28(1):41-51.
- FitzSimons EM, Van Zundert B, Constantine-Paton M, Brown, Jr, RH, Alvarez FJ (2006) Alterations in the Renshaw cell recurrent inhibitory circuit in the G93A SOD1 mouse model of ALS. Program No. 678.9. *2006 Abstract Viewer/Itinerary Planner*. Atlanta, GA: Society for Neuroscience, Online.
- Frank E, Westerfield M (1983) Development of sensory-motor synapses in the spinal cord of the frog. *J Physiol* 343:593-610.
- Frank E, Wenner P (1993) Environmental specification of neuronal connectivity. *Neuron* 10:779-785.
- Fredette BJ, Ranscht B (1994) T-cadherin expression delineates specific regions of the developing motor axon-hindlimb projection pathway. *J Neurosci* 14:7331-7346.
- Friedman HV, Bresler T, Garner CC, Ziv NE (2000) Assembly of new individual excitatory synapses: time course and temporal order of synaptic molecule recruitment. *Neuron* 27:57-69.
- Fyffe RE, Light AR (1984) The ultrastructure of group Ia afferent fiber synapses in the lumbosacral spinal cord of the cat. *Brain Res* 300:201-209.
- Fyffe RE (1990) Evidence for separate morphological classes of Renshaw cells in the cat's spinal cord. *Brain Res* 536:301-304.
- Fyffe RE (1991) Spatial distribution of recurrent inhibitory synapses on spinal motoneurons in the cat. *J Neurophysiol* 65:1134-1149.

- Fyffe RE (1991) Glycine-like immunoreactivity in synaptic boutons of identified inhibitory interneurons in the mammalian spinal cord. *Brain Res* 547:175-179.
- Garcia RA, Vasudevan K, Buonanno A (2000) The neuregulin receptor ErbB-4 interacts with PDZ-containing proteins at neuronal synapses. *Proc Natl Acad Sci U S A* 97:3596-3601.
- Geiman EJ, Knox MC, Alvarez FJ (2000) Postnatal maturation of gephyrin/glycine receptor clusters on developing Renshaw cells. *J Comp Neurol* 426:130-142.
- Geiman EJ, Zheng W, Fritschy JM, Alvarez FJ (2002) Glycine and GABA(A) receptor subunits on Renshaw cells: relationship with presynaptic neurotransmitters and postsynaptic gephyrin clusters. *J Comp Neurol* 444:275-289.
- Goda Y, Davis GW (2003) Mechanisms of synapse assembly and disassembly. *Neuron* 40:243-264.
- Gonzalez-Forero D, Alvarez FJ (2005) Differential postnatal maturation of GABAA, glycine receptor, and mixed synaptic currents in Renshaw cells and ventral spinal interneurons. *J Neurosci* 25:2010-2023.
- Gonzalez-Forero D, Pastor AM, Geiman EJ, Benitez-Temino B, Alvarez FJ (2005) Regulation of gephyrin cluster size and inhibitory synaptic currents on Renshaw cells by motor axon excitatory inputs. *J Neurosci* 25:417-429.
- Gosgnach S, Lanuza GM, Butt SJ, Saueressig H, Zhang Y, Velasquez T, Riethmacher D, Callaway EM, Kiehn O, Goulding M (2006) V1 spinal neurons regulate the speed of vertebrate locomotor outputs. *Nature* 440:215-219.
- Goulding M, Lanuza G, Sapir T, Narayan S (2002) The formation of sensorimotor circuits. *Curr Opin Neurobiol* 12:508-515.
- Graf ER, Zhang X, Jin SX, Linhoff MW, Craig AM (2004) Neurexins induce differentiation of GABA and glutamate postsynaptic specializations via neuroligins. *Cell* 119:1013-1026.
- Gumbiner BM (2005) Regulation of cadherin-mediated adhesion in morphogenesis. *Nat Rev Mol Cell Biol* 6:622-634.
- Hall AC, Lucas FR, Salinas PC (2000) Axonal remodeling and synaptic differentiation in the cerebellum is regulated by WNT-7a signaling. *Cell* 100:525-535.
- Hamos JE, Van Horn SC, Raczkowski D, Sherman SM (1987) Synaptic circuits involving an individual retinogeniculate axon in the cat. *J Comp Neurol* 259:165-192.

- Hanson MG, Landmesser LT (2003) Characterization of the circuits that generate spontaneous episodes of activity in the early embryonic mouse spinal cord. *J Neurosci* 23:587-600.
- Hanson MG, Milner LD, Landmesser LT (2007) Spontaneous rhythmic activity in early chick spinal cord influences distinct motor axon pathfinding decisions. *Brain Res Rev.* 2008 Jan;57(1):77-85.
- Hargrave M, Karunaratne A, Cox L, Wood S, Koopman P, Yamada T (2000) The HMG box transcription factor gene *Sox14* marks a novel subset of ventral interneurons and is regulated by sonic hedgehog. *Dev Biol* 219:142-153.
- Harrison, R.G. (1910) The outgrowth of the nerve fibre as a mode of protoplasmic movement, *J. Exp. Zool.*, 9, 787-846.
- Hashimoto K, Ichikawa R, Takechi H, Inoue Y, Aiba A, Sakimura K, Mishina M, Hashikawa T, Konnerth A, Watanabe M, Kano M (2001) Roles of glutamate receptor delta 2 subunit (*GluRdelta 2*) and metabotropic glutamate receptor subtype 1 (*mGluR1*) in climbing fiber synapse elimination during postnatal cerebellar development. *J Neurosci* 21:9701-9712.
- Hebb DO (1949), *The organization of behavior*, New York: Wiley
- Higashijima S, Masino MA, Mandel G, Fetcho JR (2004) *Engrailed-1* expression marks a primitive class of inhibitory spinal interneuron. *J Neurosci* 24:5827-5839.
- Hippenmeyer S, Shneider NA, Birchmeier C, Burden SJ, Jessell TM, Arber S (2002) A role for neuregulin1 signaling in muscle spindle differentiation. *Neuron*;36(6):1035-49
- Hippenmeyer S, Vrieseling E, Sigrist M, Portmann T, Laengle C, Ladle DR, Arber S (2005) A developmental switch in the response of DRG neurons to ETS transcription factor signaling. *PLoS Biol* 3:e159.
- Hirai H, Pang Z, Bao D, Miyazaki T, Li L, Miura E, Parris J, Rong Y, Watanabe M, Yuzaki M, Morgan JI (2005) *Cbln1* is essential for synaptic integrity and plasticity in the cerebellum. *Nat Neurosci* 8:1534-1541.
- Hollyday M and Hamburger V (1977) An autoradiographic study of the formation of the lateral motor column in chick embryo. *Brain Res.* 132:197-208.
- Hory-Lee F, Russell M, Lindsay RM, Frank E (1993) Neurotrophin 3 supports the survival of developing muscle sensory neurons in culture. *Proc Natl Acad Sci U S A* 90:2613-2617.

- Huang YZ, Won S, Ali DW, Wang Q, Tanowitz M, Du QS, Pelkey KA, Yang DJ, Xiong WC, Salter MW, Mei L (2000) Regulation of neuregulin signaling by PSD-95 interacting with ErbB4 at CNS synapses. *Neuron* 26:443-455.
- Hultborn H, Jankowska E, Lindstrom S (1968) Recurrent inhibition from motor axon collaterals in interneurons monosynaptically activated from Ia afferents. *Brain Res* 9:367-369.
- Hultborn H, Jankowska E, Lindstrom S (1968) Inhibition in IA inhibitory pathway by impulses in recurrent motor axon collaterals. *Life Sci* 7:337-339.
- Hultborn H, Udo M (1970) Recurrent depression from motor axon collaterals of supraspinal inhibitory effects in motoneurons. *Acta Physiol Scand* 80:12A.
- Hultborn H, Jankowska E, Lindstrom S, Roberts W (1971) Neuronal pathway of the recurrent facilitation of motoneurons. *J Physiol* 218:495-514.
- Hultborn H, Jankowska E, Lindstrom S (1971) Relative contribution from different nerves to recurrent depression of Ia IPSPs in motoneurons. *J Physiol* 215:637-664.
- Hultborn H, Jankowska E, Lindstrom S (1971) Recurrent inhibition from motor axon collaterals of transmission in the Ia inhibitory pathway to motoneurons. *J Physiol* 215:591-612.
- Hultborn H, Jankowska E, Lindstrom S (1971) Recurrent inhibition of interneurons monosynaptically activated from group Ia afferents. *J Physiol* 215:613-636.
- Hultborn H, Udo M (1972) Convergence in the reciprocal Ia inhibitory pathway of excitation from descending pathways and inhibition from motor axon collaterals. *Acta Physiol Scand* 84:95-108.
- Hultborn H, Illert M, Santini M (1976) Convergence on interneurons mediating the reciprocal Ia inhibition of motoneurons. I. Disynaptic Ia inhibition of Ia inhibitory interneurons. *Acta Physiol Scand* 96:193-201.
- Ichikawa R, Miyazaki T, Kano M, Hashikawa T, Tatsumi H, Sakimura K, Mishina M, Inoue Y, Watanabe M (2002) Distal extension of climbing fiber territory and multiple innervation caused by aberrant wiring to adjacent spiny branchlets in cerebellar Purkinje cells lacking glutamate receptor delta 2. *J Neurosci* 22:8487-8503.
- Issack PS, DiCesare PE (2003) Recent advances toward the clinical application of bone morphogenetic proteins in bone and cartilage repair. *Am J Orthop* 32:429-436.

- Ito M (1984) The modifiable neuronal network of the cerebellum. *Jpn J Physiol* 34:781-792.
- Jacob J, Hacker A, Guthrie S (2001) Mechanisms and molecules in motor neuron specification and axon pathfinding. *Bioessays* 23:582-595.
- Jankowska E, Jukes MG, Lund S, Lundberg A (1967) The effect of DOPA on the spinal cord. 5. Reciprocal organization of pathways transmitting excitatory action to alpha motoneurons of flexors and extensors. *Acta Physiol Scand* 70:369-388.
- Jankowska E, Lindstrom S (1970) Morphological identification of physiologically defined neurones in the cat spinal cord. *Brain Res* 20:323-326.
- Jankowska E, Lindstrom S (1970) Intracellular staining of physiologically identified interneurons in the cat spinal cord. *Acta Physiol Scand* 79:4A-5A.
- Jankowska E, Roberts W (1971) Function of single interneurons established by their monosynaptic inhibitory effects on motoneurons. *Acta Physiol Scand* 82:24A-25A.
- Jankowska E, Lindstrom S (1971) Morphological identification of Renshaw cells. *Acta Physiol Scand* 81:428-430.
- Jankowska E, Roberts WJ (1972) Synaptic actions of single interneurons mediating reciprocal Ia inhibition of motoneurons. *J Physiol* 222:623-642.
- Jankowska E, Roberts WJ (1972) An electrophysiological demonstration of the axonal projections of single spinal interneurons in the cat. *J Physiol* 222:597-622.
- Jankowska E, Lindstrom S (1972) Morphology of interneurons mediating Ia reciprocal inhibition of motoneurons in the spinal cord of the cat. *J Physiol* 226:805-823.
- Jankowska E (2001) Spinal interneuronal systems: identification, multifunctional character and reconfigurations in mammals. *J Physiol* 533:31-40.
- Jessell TM (2000) Neuronal specification in the spinal cord: inductive signals and transcriptional codes. *Nat Rev Genet* 1:20-29.
- Jontes JD, Smith SJ (2000) Filopodia, spines, and the generation of synaptic diversity. *Neuron* 27:11-14.
- Kano M, Hashimoto K, Chen C, Abeliovich A, Aiba A, Kurihara H, Watanabe M, Inoue Y, Tonegawa S (1995) Impaired synapse elimination during cerebellar development in PKC gamma mutant mice. *Cell* 83:1223-1231.

- Kano M, Hashimoto K, Kurihara H, Watanabe M, Inoue Y, Aiba A, Tonegawa S (1997) Persistent multiple climbing fiber innervation of cerebellar Purkinje cells in mice lacking mGluR1. *Neuron* 18:71-79.
- Kano M, Hashimoto K, Watanabe M, Kurihara H, Offermanns S, Jiang H, Wu Y, Jun K, Shin HS, Inoue Y, Simon MI, Wu D (1998) Phospholipase cbeta4 is specifically involved in climbing fiber synapse elimination in the developing cerebellum. *Proc Natl Acad Sci U S A* 95:15724-15729.
- Karunaratne A, Hargrave M, Poh A, Yamada T (2002) GATA proteins identify a novel ventral interneuron subclass in the developing chick spinal cord. *Dev Biol* 249:30-43.
- Kaufmann M.H. (2005) *The atlas of mouse development*. Academic Press Ltd., London, United Kingdom.
- Katz LC, Shatz CJ (1996) Synaptic activity and the construction of cortical circuits. *Science* 274:1133-1138.
- Kennedy TE, Serafini T, de la Torre JR, Tessier-Lavigne M (1994) Netrins are diffusible chemotropic factors for commissural axons in the embryonic spinal cord. *Cell* 78:425-435.
- Kneussel M, Betz H (2000) Receptors, gephyrin and gephyrin-associated proteins: novel insights into the assembly of inhibitory postsynaptic membrane specializations. *J Physiol* 525 Pt 1:1-9.
- Kollias G, Spanopoulou E, Grosveld F, Ritter M, Beech J, Morris R (1987) Differential regulation of a Thy-1 gene in transgenic mice. *Proc Natl Acad Sci U S A* 84:1492-1496.
- Krylova O, Herreros J, Cleverley KE, Ehler E, Henriquez JP, Hughes SM, Salinas PC (2002) WNT-3, expressed by motoneurons, regulates terminal arborization of neurotrophin-3-responsive spinal sensory neurons. *Neuron*. Sep 12;35(6):1043-56.
- Kullander K, Butt SJ, Le Bret JM, Lundfald L, Restrepo CE, Rydstrom A, Klein R, Kiehn O (2003) Role of EphA4 and EphrinB3 in local neuronal circuits that control walking. *Science* 299:1889-1892.
- Lagerback PA, Ronnevi LO (1982) An ultrastructural study of serially sectioned Renshaw cells. II. Synaptic types. *Brain Res* 246:181-192.
- Lagerback PA, Kellerth JO (1985) Light microscopic observations on cat Renshaw cells after intracellular staining with horseradish peroxidase. I. The axonal systems. *J Comp Neurol* 240:359-367.

- Lanuza GM, Gosgnach S, Pierani A, Jessell TM, Goulding M (2004) Genetic identification of spinal interneurons that coordinate left-right locomotor activity necessary for walking movements. *Neuron* 42:375-386.
- Lee, AM., Koebe, Al., O'Donovan, M. J. (1988). The development of sensorimotor synaptic connections in the lumbosacral cord of the chick embryo. *Journal of Neuroscience* 8:2530-2543.
- Lee SK, Pfaff SL (2001) Transcriptional networks regulating neuronal identity in the developing spinal cord. *Nat Neurosci* 4 Suppl:1183-1191.
- Levinson JN, El-Husseini A (2005) Building excitatory and inhibitory synapses: balancing neuroligin partnerships. *Neuron* 48:171-174.
- Li HS, Chen JH, Wu W, Fagaly T, Zhou L, Yuan W, Dupuis S, Jiang ZH, Nash W, Gick C, Ornitz DM, Wu JY, Rao Y (1999) Vertebrate slit, a secreted ligand for the transmembrane protein roundabout, is a repellent for olfactory bulb axons. *Cell* 96:807-818.
- Li WC, Higashijima S, Parry DM, Roberts A, Soffe SR (2004) Primitive roles for inhibitory interneurons in developing frog spinal cord. *J Neurosci* 24:5840-5848.
- Li B, Woo RS, Mei L, Malinow R (2007) The neuregulin-1 receptor erbB4 controls glutamatergic synapse maturation and plasticity. *Neuron* 54:583-597.
- Lichtman JW, Frank E (1984) Physiological evidence for specificity of synaptic connections between individual sensory and motor neurons in the brachial spinal cord of the bullfrog. *J Neurosci* 4:1745-1753.
- Lichtman JW, Colman H (2000) Synapse elimination and indelible memory. *Neuron* 25:269-278.
- Liem KF, Jr., Jessell TM, Briscoe J (2000) Regulation of the neural patterning activity of sonic hedgehog by secreted BMP inhibitors expressed by notochord and somites. *Development* 127:4855-4866.
- Lindsay RM (1996) Role of neurotrophins and trk receptors in the development and maintenance of sensory neurons: an overview. *Philos Trans R Soc Lond B Biol Sci* 351:365-373.
- Lloyd DPC (1941) A direct central inhibitory action of dromically conducted impulses. *J. Neurophysiol.*, 4:184-190.
- Lohof AM, Delhaye-Bouchaud N, Mariani J (1996) Synapse elimination in the central nervous system: functional significance and cellular mechanisms. *Rev Neurosci* 7:85-101.

- Lomeli H, Sprengel R, Laurie DJ, Kohr G, Herb A, Seeburg PH, Wisden W (1993) The rat delta-1 and delta-2 subunits extend the excitatory amino acid receptor family. *FEBS Lett* 315:318-322.
- Lucas FR, Salinas PC (1997) WNT-7a induces axonal remodeling and increases synapsin I levels in cerebellar neurons. *Dev Biol* 192:31-44.
- Lundfald L, Restrepo CE, Butt SJ, Peng CY, Droho S, Endo T, Zeilhofer HU, Sharma K, Kiehn O (2007) Phenotype of V2-derived interneurons and their relationship to the axon guidance molecule EphA4 in the developing mouse spinal cord. *Eur J Neurosci* 26:2989-3002.
- Mariani J, Crepel F, Mikoshiba K, Changeux JP, Sotelo C (1977) Anatomical, physiological and biochemical studies of the cerebellum from Reeler mutant mouse. *Philos Trans R Soc Lond B Biol Sci* 281:1-28.
- Matise MP, Joyner AL (1997) Expression patterns of developmental control genes in normal and *Engrailed-1* mutant mouse spinal cord reveal early diversity in developing interneurons. *J Neurosci* 17:7805-7816.
- McLaughlin BJ (1972) Propriospinal and supraspinal projections to the motor nuclei in the cat spinal cord. *J Comp Neurol* 144:475-500.
- Mentis GZ, Alvarez FJ, Bonnot A, Richards DS, Gonzalez-Forero D, Zerda R, O'Donovan MJ (2005) Noncholinergic excitatory actions of motoneurons in the neonatal mammalian spinal cord. *Proc Natl Acad Sci U S A* 102:7344-7349.
- Mentis GZ, Siembab VC, Zerda R, O'Donovan MJ, Alvarez FJ (2004) Murine Renshaw cells receive monosynaptic input from sensory afferents. Program No. 838.6. *2004 Abstract Viewer/Itinerary Planner*. Washington, DC: Society for Neuroscience, 2004. Online.
- Mentis GZ, Siembab VC, Zerda R, O'Donovan MJ, Alvarez FJ (2006) Primary afferent synapses on developing and adult Renshaw cells. *J Neurosci* 26:13297-13310.
- Missler M (2003) Synaptic cell adhesion goes functional. *Trends Neurosci* 26:176-178.
- Miyazaki T, Fukaya M, Shimizu H, Watanabe M (2003) Subtype switching of vesicular glutamate transporters at parallel fibre-Purkinje cell synapses in developing mouse cerebellum. *Eur J Neurosci* 17:2563-2572.
- Miyazaki T, Hashimoto K, Shin HS, Kano M, Watanabe M (2004) P/Q-type Ca<sup>2+</sup> channel  $\alpha 1A$  regulates synaptic competition on developing cerebellar Purkinje cells. *J Neurosci* 24:1734-1743.



- Moran-Rivard L, Kagawa T, Saueressig H, Gross MK, Burrill J, Goulding M (2001) *Evx1* is a postmitotic determinant of v0 interneuron identity in the spinal cord. *Neuron* 29:385-399.
- Morris R (1985) *Thy-1* in developing nervous tissue. *Dev Neurosci* 7:133-160.
- Nollet F, Kools P, van Roy F (2000) Phylogenetic analysis of the cadherin superfamily allows identification of six major subfamilies besides several solitary members. *J Mol Biol* 299:551-572.
- Nornes HO, Carry M.(1978). Neurogenesis in spinal cord of mouse: an autoradiographic analysis. *Brain Res.* 1978 Dec 22;159(1):1-6.
- O'Brien RA, Ostberg AJ, Vrbova G (1978) Observations on the elimination of polyneuronal innervation in developing mammalian skeletal muscle. *J Physiol* 282:571-582.
- O'Brien RJ, Xu D, Petralia RS, Steward O, Huganir RL, Worley P (1999) Synaptic clustering of AMPA receptors by the extracellular immediate-early gene product *Narp*. *Neuron* 23:309-323.
- O'Donovan MJ, Bonnot A, Wenner P, Mentis GZ (2005) Calcium imaging of network function in the developing spinal cord. *Cell Calcium* 37:443-450.
- O'Hagan RC, Hassell JA (1998) The PEA3 Ets transcription factor is a downstream target of the HER2/Neu receptor tyrosine kinase. *Oncogene*;16:301–310.
- Okabe S, Urushido T, Konno D, Okado H, Sobue K (2001) Rapid redistribution of the postsynaptic density protein PSD-Zip45 (Homer 1c) and its differential regulation by NMDA receptors and calcium channels. *J Neurosci* 21:9561-9571.
- Oliveira AL, Hydling F, Olsson E, Shi T, Edwards RH, Fujiyama F, Kaneko T, Hokfelt T, Cullheim S, Meister B (2003) Cellular localization of three vesicular glutamate transporter mRNAs and proteins in rat spinal cord and dorsal root ganglia. *Synapse* 50:117-129.
- Owens DF, Boyce LH, Davis MB, Kriegstein AR (1996) Excitatory GABA responses in embryonic and neonatal cortical slices demonstrated by gramicidin perforated-patch recordings and calcium imaging. *J Neurosci* 16:6414-6423.
- Ozaki S, Snider WD (1997) Initial trajectories of sensory axons toward laminar targets in the developing mouse spinal cord. *J Comp Neurol* 380:215-229.
- Palay SL, Billings-Gagliardi S, Chan-Palay V (1974) Neuronal perikarya with dispersed, single ribosomes in the visual cortex of *Macaca mulatta*. *J Cell Biol* 63:1074-1089.

- Parker MJ, Zhao S, Brecht DS, Sanes JR, Feng G (2004) PSD93 regulates synaptic stability at neuronal cholinergic synapses. *J Neurosci* 24:378-388.
- Peiper A (1966) [The development of upright locomotion]. *Wien Med Wochenschr* 116:750-751.
- Peng CY, Yajima H, Burns CE, Zon LI, Sisodia SS, Pfaff SL, Sharma K (2007) Notch and MAML signaling drives Scl-dependent interneuron diversity in the spinal cord. *Neuron* 53:813-827.
- Persson S, Boulland JL, Aspling M, Larsson M, Fremeau RT Jr, Edwards RH, Storm-Mathisen J, Chaudhry FA, Broman J (2006) Distribution of vesicular glutamate transporters 1 and 2 in the rat spinal cord, with a note on the spinocervical tract. *J Comp Neurol* 497:683-701.
- Pierani A, Brenner-Morton S, Chiang C, Jessell TM (1999) A sonic hedgehog-independent, retinoid-activated pathway of neurogenesis in the ventral spinal cord. *Cell* 97:903-915.
- Pierani A, Moran-Rivard L, Sunshine MJ, Littman DR, Goulding M, Jessell TM (2001) Control of interneuron fate in the developing spinal cord by the progenitor homeodomain protein Dbx1. *Neuron* 29:367-384.
- Pierce JP, Mendell LM (1993) Quantitative ultrastructure of Ia boutons in the ventral horn: scaling and positional relationships. *J Neurosci* 13:4748-4763.
- Pierrot-Deseilligny E, Burke D (2005). *The circuitry of the human spinal cord: Its role in motor control and movement disorders*. Cambridge, UK; New York: Cambridge University Press, 2005.
- Poh A, Karunaratne A, Kolle G, Huang N, Smith E, Starkey J, Wen D, Wilson I, Yamada T, Hargrave M (2002) Patterning of the vertebrate ventral spinal cord. *Int J Dev Biol* 46:597-608.
- Price SR, Briscoe J (2004) The generation and diversification of spinal motor neurons: signals and responses. *Mech Dev* 121:1103-1115.
- Pun S, Sigrist M, Santos AF, Ruegg MA, Sanes JR, Jessell TM, Arber S, Caroni P (2002) An intrinsic distinction in neuromuscular junction assembly and maintenance in different skeletal muscles. *Neuron* 34:357-370.
- Puro DG, Woodward DJ (1977) The climbing fiber system in the Weaver mutant. *Brain Res* 129:141-146.
- Ramon y Cajal S (1890) Histology of the nervous system. *Anat. Anz.*, 5: 609-613.

- Rashid T, Upton AL, Blentic A, Ciossek T, Knöll B, Thompson ID, Drescher U (2005) Opposing gradients of ephrin-As and EphA7 in the superior colliculus are essential for topographic mapping in the mammalian visual system. *Neuron* 47:57–69
- Rastad J, Gad P, Jankowska E, McCrea D, Westman J (1990) Light microscopical study of dendrites and perikarya of interneurons mediating reciprocal inhibition of cat lumbar alpha-motoneurons. *Anat Embryol (Berl)* 181:381-388.
- Reichling DB, Kyrozis A, Wang J, MacDermott AB (1994) Mechanisms of GABA and glycine depolarization-induced calcium transients in rat dorsal horn neurons. *J Physiol* 476:411-421.
- Remahl S, Hildebrand C (1985) Myelinated non-axonal neuronal elements in the feline olfactory bulb lack sites with a nodal structural differentiation. *Brain Res* 325:1-11.
- Renshaw B (1941). Influence of discharge of motoneurons upon excitation of neighbouring motoneurons. *J. Neurophysiol.* 4, 167-183.
- Renshaw B (1946) Central effects of centripetal impulses in axons of spinal ventral roots. *J Neurophysiol* 9:191-204.
- Roche KW, Standley S, McCallum J, Dune Ly C, Ehlers MD, Wenthold RJ (2001) Molecular determinants of NMDA receptor internalization. *Nat Neurosci* 4:794-802.
- Rosahl, T.W., Spillane, D., Missler, M., Herz, J., Selig, D.K., Wolff, J.R., Hammer, R.E., Malenka, R.C., and Sudhof, T.C. (1995). Essential functions of synapsins I and II in synaptic vesicle regulation. *Nature* 375, 488–493.
- Ryall RW (1970) Renshaw cell mediated inhibition of Renshaw cells: patterns of excitation and inhibition from impulses in motor axon collaterals. *J Neurophysiol* 33:257-270.
- Ryall RW, Piercey MF (1971) Excitation and inhibition of Renshaw cells by impulses in peripheral afferent nerve fibers. *J Neurophysiol* 34:242-251.
- Ryall RW (1981) Patterns of recurrent excitation and mutual inhibition of cat Renshaw cells. *J Physiol* 316:439-452.
- Salinas PC, Price SR (2005) Cadherins and catenins in synapse development. *Curr Opin Neurobiol* 15:73-80.

- Sander M, Paydar S, Ericson J, Briscoe J, Berber E, German M, Jessell TM, Rubenstein JL (2000) Ventral neural patterning by Nkx homeobox genes: Nkx6.1 controls somatic motor neuron and ventral interneuron fates. *Genes Dev* 14:2134-2139.
- Sanes JR, Lichtman JW (1999) Development of the vertebrate neuromuscular junction. *Annu Rev Neurosci* 22:389-442.
- Sanes JR, Lichtman JW (2001) Induction, assembly, maturation and maintenance of a postsynaptic apparatus. *Nat Rev Neurosci* 2:791-805.
- Sanna PP, Celio MR, Bloom FE, Rende M (1993) Presumptive Renshaw cells contain decreased calbindin during recovery from sciatic nerve lesions. *Proc Natl Acad Sci U S A* 90:3048-3052.
- Sapir T, Geiman EJ, Wang Z, Velasquez T, Mitsui S, Yoshihara Y, Frank E, Alvarez FJ, Goulding M (2004) Pax6 and engrailed 1 regulate two distinct aspects of Renshaw cell development. *J Neurosci* 24:1255-1264.
- Sara Y, Biederer T, Atasoy D, Chubykin A, Mozhayeva MG, Sudhof TC, Kavalali ET (2005) Selective capability of SynCAM and neuroligin for functional synapse assembly. *J Neurosci* 25:260-270.
- Sassoe-Pognetto M, Wassle H, Grunert U (1994) Glycinergic synapses in the rod pathway of the rat retina: cone bipolar cells express the alpha 1 subunit of the glycine receptor. *J Neurosci* 14:5131-5146.
- Saueressig H, Burrill J, Goulding M (1999) Engrailed-1 and netrin-1 regulate axon pathfinding by association interneurons that project to motor neurons. *Development* 126:4201-4212.
- Schechterson LC, Bothwell M (1992) Novel roles for neurotrophins are suggested by BDNF and NT-3 mRNA expression in developing neurons. *Neuron* 9:449-463.
- Scheiffele P, Fan J, Choih J, Fetter R, Serafini T (2000) Neuroligin expressed in nonneuronal cells triggers presynaptic development in contacting axons. *Cell* 101:657-669.
- Schneider SP, Fyffe RE (1992) Involvement of GABA and glycine in recurrent inhibition of spinal motoneurons. *J Neurophysiol* 68:397-406.
- Serafini T, Kennedy TE, Galko MJ, Mirzayan C, Jessell TM, Tessier-Lavigne M (1994) The netrins define a family of axon outgrowth-promoting proteins homologous to *C. elegans* UNC-6. *Cell* 78:409-424.

- Shepherd TG, Kockeritz L, Szrajber MR, Muller WJ, Has-sell JA (2001) The *pea3* subfamily ets genes are required for HER2/Neu-mediated mammary oncogenesis. *Curr. Biol* ;11:1739–1748.
- Sherrington CS (1897) On the Question whether any Fibres of the Mammalian Dorsal (Afferent) Spinal Root are of Intraspinal Origin. *J Physiol* 21:209-212.
- Sherrington CS (1906) Observations on the scratch-reflex in the spinal dog. *J Physiol* 34:1-50.
- Shirasaki R, Pfaff SL (2002) Transcriptional codes and the control of neuronal identity. *Annu Rev Neurosci* 25:251-281.
- Smith CA, Siembab VC, Berrocal MC, Goulding M, Alvarez FJ (2005) Postnatal Diversification of V1-Derived Interneurons Program No. 603.15. *2005 Abstract Viewer/Itinerary Planner*. Washington, DC: Society for Neuroscience, 2005. Online.
- Smith CA, Shneider NA, Berrocal MC, Alvarez FJ (2007) Influence of sensory afferents and motoneurons on the developmental regulation of Calbindin and Parvalbumin expression in spinal interneurons. Program No. 132.22. *2007 Abstract Viewer/Itinerary Planner*. San Diego, CA: Society for Neuroscience, 2007. Online.
- Smith E, Hargrave M, Yamada T, Begley CG, Little MH (2002) Coexpression of SCL and GATA3 in the V2 interneurons of the developing mouse spinal cord. *Dev Dyn* 224:231-237.
- Song S, Miller KD, Abbott LF (2000) Competitive Hebbian learning through spike-timing-dependent synaptic plasticity. *Nat Neurosci* 3:919-926.
- Soriano P (1999) Generalized lacZ expression with the ROSA26 Cre reporter strain. *Nat Genet* 21:70-71.
- Speidel CC (1941). Adjustments of nerve endings. *Harvey Lectures* 36:126-158.
- Sretavan DW, Shatz CJ (1986) Prenatal development of retinal ganglion cell axons: segregation into eye-specific layers within the cat's lateral geniculate nucleus. *J Neurosci* 6:234-251.
- Sur M, Weller RE, Sherman SM (1984) Development of X- and Y-cell retinogeniculate terminations in kittens. *Nature* 310:246-249.
- Suzuki H, Yanagisawa M, Yoshioka K, Hosoki R, Otsuka M (1997) Enzymatic inactivation of enkephalin neurotransmitters in the spinal cord of the neonatal rat. *Neurosci Res* 28:261-267.

- Sweeney C, Fambrough D, Huard C, Diamonti AJ, Lander ES, Cantley LC, Carraway KL 3<sup>rd</sup> (2001) Growth factor-specific signaling pathway stimulation and gene expression mediated by ErbB receptors. *J. Biol. Chem*;276:22685–22698.
- Takayama C, Nakagawa S, Watanabe M, Mishina M, Inoue Y (1995) Light- and electron-microscopic localization of the glutamate receptor channel delta 2 subunit in the mouse Purkinje cell. *Neurosci Lett* 188:89-92.
- Takeichi M, Uemura T, Iwai Y, Uchida N, Inoue T, Tanaka T, Suzuki SC (1997) Cadherins in brain patterning and neural network formation. *Cold Spring Harb Symp Quant Biol* 62:505-510.
- Tamagnone L, Artigiani S, Chen H, He Z, Ming GI, Song H, Chedotal A, Winberg ML, Goodman CS, Poo M, Tessier-Lavigne M, Comoglio PM (1999) Plexins are a large family of receptors for transmembrane, secreted, and GPI-anchored semaphorins in vertebrates. *Cell* 99:71-80.
- Tanaka H, Shan W, Phillips GR, Arndt K, Bozdagi O, Shapiro L, Huntley GW, Benson DL, Colman DR (2000) Molecular modification of N-cadherin in response to synaptic activity. *Neuron* 25:93-107.
- Taylor MD, Vancura R, Patterson CL, Williams JM, Riekhof JT, Wright DE (2001) Postnatal regulation of limb proprioception by muscle-derived neurotrophin-3. *J Comp Neurol* 432:244-258.
- Tessier-Lavigne M, Goodman CS (1996) The molecular biology of axon guidance. *Science* 274:1123-1133.
- Thelen E, Fisher DM, Ridley-Johnson R, Griffin NJ (1982) Effects of body build and arousal on newborn infant stepping. *Dev Psychobiol* 15:447-453.
- Thoenen H, Zafra F, Hengerer B, Lindholm D (1991) The synthesis of nerve growth factor and brain-derived neurotrophic factor in hippocampal and cortical neurons is regulated by specific transmitter systems. *Ann N Y Acad Sci* 640:86-90.
- Thomas RC, Wilson VJ (1965) Precise localization of Renshaw cells with a new marking technique. *Nature* 206:211-213.
- Todd AJ, Hughes DI, Polgar E, Nagy GG, Mackie M, Ottersen OP, Maxwell DJ (2003) The expression of vesicular glutamate transporters VGLUT1 and VGLUT2 in neurochemically defined axonal populations in the rat spinal cord with emphasis on the dorsal horn. *Eur J Neurosci* 17:13-27.
- Torres R, Firestein BL, Dong H, Staudinger J, Olson EN, Huganir RL, Brecht DS, Gale NW, Yancopoulos GD (1998) PDZ proteins bind, cluster, and synaptically colocalize with Eph receptors and their ephrin ligands. *Neuron* 21:1453-1463.

- Tourtellotte WG, Milbrandt J (1998) Sensory ataxia and muscle spindle agenesis in mice lacking the transcription factor *Egr3*. *Nat Genet* 20:87-91.
- Tourtellotte WG, Keller-Peck C, Milbrandt J, Kucera J (2001) The transcription factor *Egr3* modulates sensory axon-myotube interactions during muscle spindle morphogenesis. *Dev Biol* 232:388-399.
- Tsui CC, Copeland NG, Gilbert DJ, Jenkins NA, Barnes C, Worley PF (1996) *Narp*, a novel member of the pentraxin family, promotes neurite outgrowth and is dynamically regulated by neuronal activity. *J Neurosci* 16:2463-2478.
- Turrigiano GG, Nelson SB (2004) Homeostatic plasticity in the developing nervous system. *Nat Rev Neurosci* 5:97-107.
- Uchida N, Honjo Y, Johnson KR, Wheelock MJ, Takeichi M (1996) The catenin/cadherin adhesion system is localized in synaptic junctions bordering transmitter release zones. *J Cell Biol* 135:767-779.
- Vallstedt A, Muhr J, Pattyn A, Pierani A, Mendelsohn M, Sander M, Jessell TM, Ericson J (2001) Different levels of repressor activity assign redundant and specific roles to *Nkx6* genes in motor neuron and interneuron specification. *Neuron* 31:743-755.
- Van Keulen L (1981) Autogenetic recurrent inhibition of individual spinal motoneurons of the cat. *Neurosci Lett* 21:297-300.
- VanderHorst VG, Ulfhake B (2006) The organization of the brainstem and spinal cord of the mouse: relationships between monoaminergic, cholinergic, and spinal projection systems. *J Chem Neuroanat* 31:2-36.
- Varoqueaux F, Jamain S, Brose N (2004) *Neurologin 2* is exclusively localized to inhibitory synapses. *Eur J Cell Biol* 83:449-456.
- Vaughn JE, Henrikson CK (1976) Surface specializations of neurites in embryonic mouse spinal cord. *Brain Res* 110:431-445.
- Voronin LL, Cherubini E (2004) 'Deaf, mute and whispering' silent synapses: their role in synaptic plasticity. *J Physiol* 557:3-12.
- Walsh MK, Lichtman JW (2003) In vivo time-lapse imaging of synaptic takeover associated with naturally occurring synapse elimination. *Neuron* 37:67-73.
- Wang G, Scott SA (1999) Independent development of sensory and motor innervation patterns in embryonic chick hindlimbs. *Dev Biol* 208:324-336.
- Wang Z, Li L, Goulding M, Frank E (2008) Early postnatal development of reciprocal Ia inhibition in the murine spinal cord. *J Neurophysiol* 100:185-196.

- Wang Z, Li LY, Taylor MD, Wright DE, Frank E (2007) Prenatal exposure to elevated NT3 disrupts synaptic selectivity in the spinal cord. *J Neurosci. Apr* 4;27(14):3686-94.
- Wasserman RH, Taylor AN, Kallfelz FA (1966) Vitamin D and transfer of plasma calcium to intestinal lumen in chicks and rats. *Am J Physiol* 211:419-423.
- Watanabe M (2008) Molecular mechanisms governing competitive synaptic wiring in cerebellar Purkinje cells. *Tohoku J Exp Med* 214:175-190.
- Wenner P, O'Donovan MJ (1999) Identification of an interneuronal population that mediates recurrent inhibition of motoneurons in the developing chick spinal cord. *J Neurosci* 19:7557-7567.
- Wenner P, O'Donovan MJ, Matisse MP (2000) Topographical and physiological characterization of interneurons that express engrailed-1 in the embryonic chick spinal cord. *J Neurophysiol* 84:2651-2657.
- Wenner P, O'Donovan MJ (2001) Mechanisms that initiate spontaneous network activity in the developing chick spinal cord. *J Neurophysiol* 86:1481-1498.
- Wichterle H, Lieberam I, Porter JA, Jessell TM (2002) Directed differentiation of embryonic stem cells into motor neurons. *Cell* 110:385-397.
- Wiesel TN, Hubel DH (1963) Effects of Visual Deprivation on Morphology and Physiology of Cells in the Cats Lateral Geniculate Body. *J Neurophysiol* 26:978-993.
- Wilkinson DG (2001) Multiple roles of EPH receptors and ephrins in neural development. *Nat Rev Neurosci* 2:155-164.
- Wright DE, Williams JM, McDonald JT, Carlsten JA, Taylor MD (2002) Muscle-derived neurotrophin-3 reduces injury-induced proprioceptive degeneration in neonatal mice. *J Neurobiol* 50:198-208.
- Wu WL, Ziskind-Conhaim L, Sweet MA (1992) Early development of glycine- and GABA-mediated synapses in rat spinal cord. *J Neurosci* 12:3935-3945.
- Xu H, Whelan PJ, Wenner P (2005) Development of an inhibitory interneuronal circuit in the embryonic spinal cord. *J Neurophysiol* 93:2922-2933.
- Yagi T, Takeichi M (2000) Cadherin superfamily genes: functions, genomic organization, and neurologic diversity. *Genes Dev* 14:1169-1180.
- Yarden Y, Sliwkowski MX (2001) Untangling the ErbB signaling network. *Nat Rev Mol Cell Biol* 2:127-137.



- Yoneshima H, Yamasaki S, Voelker CC, Molnar Z, Christophe E, Audinat E, Takemoto M, Nishiwaki M, Tsuji S, Fujita I, Yamamoto N (2006) Er81 is expressed in a subpopulation of layer 5 neurons in rodent and primate neocortices. *Neuroscience* 137:401-412.
- Yoshida Y, Han B, Mendelsohn M, Jessell TM (2006) PlexinA1 signaling directs the segregation of proprioceptive sensory axons in the developing spinal cord. *Neuron* 52:775-788.
- Zagoraiou L, Miles GB, Akay T, Martin JF, Brownstone RM, Jessell TM (2008). Genetic identification and manipulation of spinal cholinergic interneurons. 2<sup>nd</sup> Society for Neuroscience Satellite Symposium on Motor Systems. Washington, DC: Society for Neuroscience, 2008.
- Zhang Y, Narayan S, Geiman E, Lanuza GM, Velasquez T, Shanks B, Akay T, Dyck J, Pearson K, Gosgnach S, Fan CM, Goulding M (2008) V3 spinal neurons establish a robust and balanced locomotor rhythm during walking. *Neuron* 60:84-96.
- Zhou Y, Yamamoto M, Engel JD (2000) GATA2 is required for the generation of V2 interneurons. *Development* 127:3829-3838.
- Zhou L, Baumgartner BJ, Hill-Felberg SJ, McGowen LR, Shine HD (2003) Neurotrophin-3 expressed in situ induces axonal plasticity in the adult injured spinal cord. *J Neurosci* 23:1424-1431.
- Zhuang B, Sockanathan S (2006) Dorsal-ventral patterning: a view from the top. *Curr Opin Neurobiol* 16:20-24.
- Ziskind-Conhaim (1990) NMDA receptors mediate poly- and monosynaptic potentials in motoneurons of rat embryos. *J Neurosci* Jan;10(1):125-35.